Design and analysis of AC machines for traction purposes.

Coles, Philip Charles

Award date:
1984

Awarding institution:
University of Bath

DESIGN AND ANALYSIS OF AC MACHINES

FOR TRACTION PURPOSES

submitted by

Philip Charles Coles B. Sc.

for the degree of Ph. D.
of the University of Bath

1984

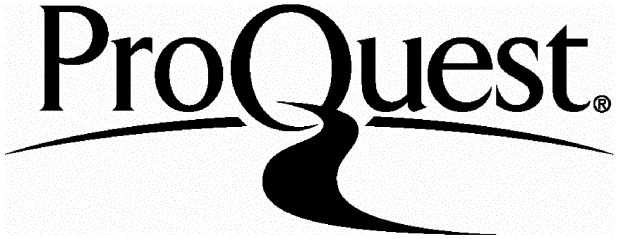

ABSTRACT

Interest is continually being shown in the replacement of variable speed DC machines with an equivalent inverter fed AC machine. This is as true in the field of highly rated machines for traction use, as in the field of smaller industrial drives.

In the following work, a general design method is presented that is suitable for the design of induction, and slip ring synchronous machines of the round rotor or salient pole type. The method is based upon machine models that employ surface quantities. This type of model clearly displays the interaction between flux and current, and is readily adaptable for design use, as the amount of detail required is kept to a minimum.

Several designs are presented for induction and synchronous machines that satisfy the requirements of a traction motor for use in a high speed locomotive. Performance predictions, based on sinusoidal supply considerations and operating under two commonly used control schemes are shown. The traction motors satisfy the main overall requirement for a minimum size and weight design.

In practice the AC traction motors would be supplied by a variable frequency inverter. In view of this, an analysis of the performance of the most suitable induction and synchronous motor designs is presented, when each is being supplied with an inverter of the preferred type. Two inverters are considered, one of the constant voltage type, and one of the constant current type. Computer models are used to predict the machine

voltage, current and torque waveforms when both inverters are operated in the 120 degree conduction mode.

Experimental results are shown, to verify the computer model of the current source inverter. A 5KVA laboratory squirrel cage induction machine is used for this purpose, in conjunction with a force measuring platform that enables the steady state torque pulsations to be recorded.

ACKNOWLEDGEMENTS

The author wishes to sincerely thank his supervisor, Dr. M.J. Balchin, for his help and encouragement during the many discussions that were had throughout the course of the work described in this thesis.

The author also wishes to thank Professor J.F. Eastham for making available the wide range of school facilities, and Mrs. A. Balchin for her help in preparing the thesis.

Finally, the financial support of the Science and Engineering Research Council and GEC Traction is gratefully acknowledged.

INDEX

LIST OF SYMBOLS

ELECTRICAL AND MAGNETIC

$\hat{B}$	maximum core flux density	T
B_g	RMS air-gap flux density	T
ρ_C	conductor resistivity	ΩM
ρ_S	conductor surface resistance	Ω
ℓ_s	surface leakage inductance	H
ℓ_m	surface magnetising inductance	H
R	phase resistance	Ω
L	phase leakage inductance	H
L_m	phase magnetising inductance	H
β	slot width/slot pitch	
γ	coil pitch/pole pitch	
α	pole arc/pole pitch	
z	series conductors per slot	
q	slots per pole phase	
λ	specific permeance	
K	conductor current density	A/mm^2
J	surface current density	A/M
V	terminal voltage	V
E	electric field strength	V/M
P	conductor loss	W
P_C	core loss	W
P_{OUT}	output power	W
T	torque	Nm
δ_T	torque angle	degrees
ω	supply angular frequency	rad/sec
ω_R	angular frequency of rotor currents	rad/sec
σ	slip	pu
Re	indicates the complex real part	

Final subscript S or R denotes stator or rotor quantity.

*	indicates the complex conjugate	
e	instantaneous electric field strength	V/m
b	instantaneous magnetic flux density	T
j	instantaneous surface current density	A/m
M	magneto-motive force	AT
I	RMS phase current	A
Q	total number of slots	
f	supply frequency	Hz
f_2	rotor frequency	Hz

DIMENSIONS

τ	slot pitch
τ_p	pole pitch
τ_c	coil pitch
τ_a	pole arc
g	air gap length
d	slot depth
w	slot width
w_t	tooth width
w_l	slot opening (semi-closed slots)
w_p	pole width (salient rotor)
ℓ_{oh}	slot conductor overhang
A_s	slot area
w_v	cooling vent width
τ_v	vent pitch
d_c	stator core depth
d_o	stator core outside diameter
θ	angle between core and end winding conductor for diamond-ended coils
D_{er}	mean diameter of squirrel cage end ring
A_{er}	cross-sectional area of end ring
t_{er}	thickness of end ring
w_{er}	width of end ring
ℓ_{mt}	mean length of coil turn
w_c	core length
θ_p	half pole angle (salient rotor)
m	conductor mass
m_i	iron mass
A	air gap surface area

CONSTANTS and FACTORS

p	number of pole pairs
k_w	winding factor
k_p	coil pitch factor
k_{xt}, k_{xco}	slot permeance correction factors
k_{sc}	squirrel-cage end ring permeance correction factor
k_{endR}	surface resistance end factor
k_{endL}	surface inductance end factor
k_{pF}	slot packing factor
k_i	iron packing factor
k_g	tooth flux fringing factor
k_v	vent flux fringing factor
k_{VL}	vent flux fringing factor for slot leakage
n_v	number of vents
K_c, x, z	constants for core loss calculation
δ	conductor density
δ_i	iron density
δ_{er}	squirrel cage end ring density
k_d	distribution factor
μ_o	magnetic constant $4\pi \times 10^{-7}$ H/m

List of principal symbols used in the analysis of the voltage and current source inverter

Induction machine

R_S	stator phase resistance	Ω
l_S	stator phase leakage inductance	H
$R_{R'}$	referred rotor phase resistance	Ω
$l_{R'}$	referred rotor phase leakage inductance	H
L_m	magnetising inductance	H

Synchronous machine

R_S	stator phase resistance	Ω
l_S	stator phase leakage inductance	H
$R_{F'}$	referred field winding resistance	Ω
$l_{F'}$	referred field winding leakage inductance	H
L_{md}	direct axis magnetising inductance	H
L_{mq}	quadrature axis magnetising inductance	H
v_{aS}, v_{bS}, v_{cS}	machine phase voltages	V
i_{aS}, i_{bS}, i_{cS}	machine phase currents	A
$i_{aR'}, i_{bR'}, i_{cR'}$	referred rotor currents (induction machine)	A
$i_{F'}$	referred field winding currents (synchronous machine)	A
p	pole pairs	
ω_R	steady rotor angular velocity	rad/sec
θ	angular position of rotor	degree
T_e	electro-magnetic torque	Nm
δ_T	torque angle	degree

γ	phase displacement between the fundamental component of the machine phase current and the commutation point t_o	degree
V_s	DC source voltage	V
I_{dc}	DC link current	A
R_{dc}, L_{dc}	DC link resistance and inductance	Ω, H
C	inverter capacitance value	F
C_{eq}	equivalent capacitance value used in inverter model	F

CHAPTER 1

GENERAL INTRODUCTION

The design of electrical machines can be broadly classified into two distinct areas, namely, design analysis and design synthesis. Design analysis techniques determine the machine performance from a knowledge of the machine parameters. These parameters are defined initially and remain unchanged throughout the execution of the method. Design synthesis, encompasses those methods in which the physical characteristics of the machine are determined from a desired performance specification.

The majority of the early problems to be attempted in the field of machine design by computer, were of the design analysis type. In these cases the computer served as an aid to the designer, by enabling larger calculations using more accurate methods to be performed. The first paper of this type appeared in 1954,[1] with the advent of the first mainframe computers. The computer evaluated the machine performance from the initial estimates of the independant variables, and then in the light of the results the designer intervened and modifed those estimates until the required performance was obtained. The speed at which a suitable design was found depended to a large extent upon the skill and experience of the design engineer.

The theme of iterative design analysis was continued by Veinott,[2] but with the addition of an extra loop in which the cost effectiveness of the design was assessed. This method produced a machine design that not only fulfilled the performance criteria but also met an overall economic requirement. An attempt to integrate the two design methods was made by the same author, in the area of small induction motor design in 1960.[3] As the core plate laminations of the small induction motor were standardised, the main independant variables were the effective turns per phase of the winding and the effective core length. The performance

objectives of the design could then be realised by a fixed step variation of the independant variables. This method represented a partial synthesis approach to the problem, and has been sucessfully employed by other authors.[4,5,6] for both induction and synchronous machines.

Progress in the more problematic area of design synthesis has been slow. Only in the field of transformer design, where the number of variables involved is considerably less than for electrical machines have full descriptions of a design synthesis approach been given.[7,8] The ideal method of designing any system would be by the direct inversion of a set of equations connecting the independant and dependant variables. If this were possible the performance requirements such as the output power, torque, speed and voltage could be specified and the inverted equations evaluated to obtain the necessary machine dimensions. In practice the equations would be underdefined as there are many more dimensions to be solved for, than there are input specifications. The problem can be eased slightly by adding an overall requirement that the solution obtained must represent a minimum cost or minimum weight design.

As an approach to the direct method of solution Middendorf,[9] derives an equation relating the performance characteristics of an induction motor to the rotor size. Although, whilst this relationship considers such quantities as the pull out torque, starting torque and current, it does not include what must be one of the most important performance criteria, the power factor.

As a direct analytical inversion of the design equations is not possible, an iterative approach to the problem has to be adopted. However as the design of electrical machines contains a high degree of discreteness, any iterative technique must be able to work within this limitation. Typical discrete variables are the standard conductor and slot sizes, numbers of

slots and conductors, which must have an integer value, and frame size, for which a limited number may have to cover a wide range of output powers. A paper presented by Chalmers and Bennington,[10] describes a method for the design of large squirrel cage induction machines, in which both design analysis and design synthesis methods are used in conjunction with iterative techniques, to produce an economical convergence scheme.

Despite the absence of progress in the field of design synthesis, work has continued in the allied theoretical study of design optimisation, disregarding fixed sizes and discontinuities.[11,12]

In the following work, a general design method is presented that is suitable for the design of induction and slip-ring synchronous machines of the round rotor or salient pole type. The design techniques presented in Chapter 2 fall broadly into the class of design analysis, but retain some elements of a design synthesis approach.

The method is based upon machine models that employ surface quantities. This type of model displays clearly the interaction between flux and current, and is readily adaptable for design use as the amount of detail required is kept to a minimum. The geometrical and electrical characteristics of the machine are evaluated with the minimum of computational effort and without the need to specify a large number of input variables. This obviously requires some reduction of the machine parameters, if the design process is to remain as concise as possible. To this end the dimensions of the magnetic circuit and the formulae for the calculation of the machine resistances, inductances and masses have been simplified, but only where it is felt to be beneficial in the area of reducing the number of input variables to be specified.

The search for an optimum design is not considered in this work, but as the simplified machine design equations use the minimum number of variables, they are in a form that is readily adaptable to some sort of sensitivity analysis.

The DC motor, in traction applications, has been developed over recent years to a high level of sophistication. This motor has an excellent overload capability, immunity to line voltage variations, and provides good torque sharing when driving wheels of different diameters. In the past 20 years the specific output has been increased by approximately 70 %, this increase being largely due to the use of improved insulating materials and higher working temperatures.[13] Increases in motor output however, are limited by constraints on the commutator performance. Removal of the commutator removes the limit on high speed operation, and assuming equal current and flux densities, significantly shortens the length of the machine, and gives a considerable reduction in weight. A reduction in machine length and weight enables mechanical changes to be made that are advantageous in traction applications. For example a smaller gearwheel diameter may be used, due to the reduced gear centre distance, enabling the vehicle height to be lowered. Any weight reduction will contribute to improving the ride quality of the bogie due to a reduced track loading. Alternatively it will mean that higher operational speeds are possible without increasing the track loading.

The railway enviroment is harsh for bogie mounted components. The steel wheel - rail system imposes high vibrational forces, and dynamic loading of the traction motor can reach 50 g. All these factors render the DC motor commutator and brushgear vulnerable to wear. This increases the frequency at which they must be inspected, with a consequent increase in maintenance costs.

The use of AC motor-inverter drives in traction applications has grown steadily, and results of some European systems [14,15,16,17,18,19,20] have been reported. Early AC electrification made use of 3-phase induction machines, but only as substantially fixed speed machines with pole change windings. This approach suited heavy locomotive work and provided useful regenerative braking, but for light weight high speed applications, the greater flexibility offered by a variable speed drive is required.

The work of Chapter 3 considers a specific application of the design method. Designs are presented for induction and slip ring synchronous machines that satisfy the requirements of a traction motor for use in a high speed diesel electric locomotive. The proposed designs represent an alternative to the DC traction motor and mechanical transmission in present use. The AC traction motor is intended to be mounted between the wheelset and provide a variable speed drive through a reduction gearbox.

As the relative sizes of the machine and power supplies are very much dependant on the way in which the system is controlled, two commonly used schemes are considered. The performance of the resulting designs is compared on a sinusoidal basis and their suitability for this particular traction application is assessed.

As the traction motor designs of Chapter 3 are based upon sinusoidal supply considerations, there is a need to determine their performance when being supplied with an inverter of the appropriate type. In Chapter 4 computer models are presented, that enable the steady state performance of induction and round rotor or salient pole machines to be predicted, whilst being fed from either a voltage or current source inverter, operating in the 120 degree conduction mode.

In force commutated inverters the thyristor conduction periods are well defined, and can range from fractions of a degree in pulse width modulated inverters, to 180 degrees of the output period in square wave inverters. For a voltage source inverter operating in the 180 degree conduction mode, three thyristors are gated on at any instant. The commutation of one thyristor and the firing of its complementary thyristor in the same leg occur at the same time. This produces a precisely defined output voltage waveform and ensures continuous phase currents. The gate firing pulses have to be applied almost simultaneously to top and bottom leg thyristors making the logic design relatively complex. Several techniques have been presented for the analysis of the 180 degree square wave inverter, with the assumption that the motor is supplied from a known voltage waveform.[21,22,23]

For voltage source inverters operating in the 120 degree conduction mode the inverter thyristors are permitted to conduct for 120 degrees of the output period. As only two devices are conducting at the same time, a 60 degree gap exists between the commutation of one thyristor and the turning on of its complementary device in the same leg. This considerably simplifies the gate pulse information, but can lead to discontinuous phase currents in high power factor loads, due to the disconnection of one of the machine phases during this period. During the period for which the phase current is zero the machine back emf appears at the output terminals of the inverter. The magnitude and duration of this voltage is a function of the load. Owing to the varying topology of the inverter circuit, the analysis is not straightforward. Lipo and Turnbull[24] have developed a method of utilising state variable analysis for the prediction of steady state waveforms for 120 and 180 degree inverters feeding constant speed low power induction machines. A tensor method presented by Al-Nimma and Williams[25] investigates the transient and steady state performance characteristics of an induction motor for both 120 and 180 degree inverter

conduction modes.

Lockwood[26] utilised an analogue computer model which again predicted the transient and steady state performance, but for a much larger 200KVA traction system using tubular axle induction motors.

The concept of the current source inverter was described by Ward[27] in 1964. In the current source inverter, the dc link current is held constant and by switching the inverter thyristors at the required rate the machine speed is continuously variable. As one of the main operating characteristics of the current source inverter is the generation of voltage spikes of several times the load terminal voltage, the application of such inverters to induction motor drives had to wait for the development of high voltage thyristors. The first general commercial description of an induction motor drive using the current source inverter was given by Phillips,[28] in 1972. If commutation of the machine current is considered to be instantaneous the current waveform is rectangular, in 120 degree blocks. The analysis of the induction motor operating on quasi-square currents is discussed in detail,[23,29] and for the synchronous motor.[30] In practice the commutation of current in the inverter is not instantaneous. During commutation, the machine resistance and inductance form a part of the commutation circuit together with the commutation capacitor, and hence the variation of current follows a damped sinusoid.

A more detailed analysis of the commutation process and a derivation of a series equivalent circuit for the induction motor was presented by Farrer and Miskin.[31] However approximations were made in their work by neglecting the stator resistance and assuming the machine back emf to be constant during the commutation interval.

An exact model of the current source inverter is presented in Chapter 4 which accurately reflects the way in which a current source would be

derived in practice. No assumptions are made about the machine back emf during commutation, and the effect of the DC link inductance is taken into account by considering the inverter to be fed from an ideal voltage source.

Because of the inherent switching symmetry in both the voltage and current source inverters, it is necessary to consider only one sixth of a cycle of inverter operation. A complete solution may then constructed from the steady state 60 degree values.

The performance equations for the induction machine are derived in terms of the actual machine voltages and currents without resorting to a two axis transformation. All the induction machine variables are related to a coordinate system that is fixed in the stator, and thus the dependancy of the matrix coefficients on the rotor position is removed. This reduces the amount of computing effort required to obtain a steady state solution, as the stator and rotor currents are at the same frequency, and enables the inverter - machine equations to be set up with relative ease.
Performance predictions are presented for what is felt to be the two most suitable designs for use in a high speed passenger train application. Current, voltage and torque waveforms are given, and a comparison is made between the harmonic torques present for each motor-inverter combination at normal operating levels.

In conclusion, experimental results are presented in Chapter 5 to verify the current source model. A 5KVA laboratory squirrel cage induction machine is used for this purpose. The stator frame of this machine is isolated from the rotor assembly and is supported on a force measuring platform. This enables dynamic measurements of the rotor shaft torque pulsations to be recorded. Inverter voltage and current waveforms are also shown.

CHAPTER 2

THE DESIGN OF INDUCTION AND SYNCHRONOUS MACHINES BASED ON A SURFACE EQUIVALENT MODEL

2.1 Introduction

The general machine design techniques presented in this chapter are applicable to squirrel-cage induction machines, and slip-ring synchronous machines of the round-rotor or salient pole type.

The design method is based upon machine models that employ 'surface quantities'. This type of model has the advantage of displaying clearly the interaction between flux and current, whilst enabling the amount of detail to be kept to a minimum. Maximum permissible values of stator and rotor conductor current density and core flux density are specified as inputs to the design process, their values being chosen according to heat dissipation and saturation levels. The machine windings are represented by thin sheets of conductors on the air gap surfaces of the stator and rotor members. Machine resistance and leakage inductance effects are incorporated into the model by giving the winding conductor sheets suitable values of surface resistance or inductance. The induction machine may then be readily represented by a conventional equivalent circuit in which surface quantities are used.

As the resultant air gap flux density of the synchronous machine is due to separate stator and rotor components, the relationship between current and flux density in this case is more easily displayed on space and time phasor diagrams.

In view of the large number of dimensions and other variables involved, some reduction of the machine formulae is necessary if the design process is to remain as concise as possible. To this end the dimensions of the magnetic circuit and the machine resistances, inductances and masses have been simplified wherever possible. In each case an exact expression is derived

and then with the use of appropriate simplifying assumptions, a reduced form is obtained that is more suitable for use in the design process.

It will be shown that for a given pole number, and assuming an equal flux density in all parts of the magnetic circuit, the stator cross-section can be completely defined by the choice of three variables. These are the outside diameter, the slot depth, and the ratio of slot width to slot pitch.

Having defined a suitable stator cross-section, consideration may then be made of the maximum stator surface current loadings attainable by that cross-section, for a specified conductor current density.

In the case of the induction machine, the air-gap length is specified as an input to the design process and thus enables the rotor geometry to be defined when the stator cross-section is known. The performance of the induction machine design is then determined, for a given core length, by the maximum permissible stator and rotor surface current loadings for an appropriate machine geometry.

For the synchronous machine, the stator cross-section is defined in the same way as the induction machine, for maximum permissible current and flux loadings. An iterative process is then adopted to find, initially, an air gap length that gives a stator component of air gap flux density that is equal to or below the maximum air gap flux density allowable, i.e. no rotor component of air gap flux. The air gap length is then increased in steps until the condition is reached for which there is insufficient rotor conductor area remaining, to support the required value of rotor surface current loading, at a specified maximum rotor conductor density, to set up the required rotor component of air gap flux.

In order to demonstrate the general design method and to form a bridge between this and the next chapter, one design for each machine type is shown. These machine designs are rated at traction levels and satisfy the requirements of a motor for use in a high speed diesel electric locomotive. The full specification of a machine for use in this application is described in more detail in Chapter 3.

2.2 Machine models and equivalent circuits

2.2.1 The induction machine

The model of a two-pole induction machine with a uniform air gap is shown in cross section in Fig. 2.1. The stator and rotor are represented by unslotted members of a homogeneous material that has a high value of both resistivity and permeability. The distribution of the conductors around the cylindrical surfaces is such that when the normal phase currents are flowing, only the fundamental component of the mmf produced by the actual winding is given. The effect of resistance and leakage inductance are modelled by giving the winding conductor sheets suitable values of surface resistance and inductance.

As the model of Fig. 2.1 is assumed to be a representative section of the actual machine, a two-dimensional analysis is appropriate. A relationship between the airgap flux density and the winding surface currents can be obtained by recalling Ampere's Law in the form,

$$\int H d\ell = \int_S J ds \qquad (2.1)$$

For the path shown in Fig. 2.1, assuming only radial gap flux and an air-gap length that is small in comparison to its mean radius; and $\mu_R \to \infty$, $\rho \to \infty$

$$-\frac{g}{\mu_o}\frac{\partial b_g}{\partial y} = j_S - j_R \qquad (2.2)$$

If each of the variables in equation (2.2) is represented by a number of the form

$$a = \mathrm{Re}\left[\sqrt{2}\,A e^{j\left[\omega t - \frac{\pi y}{\tau_p}\right]}\right]$$

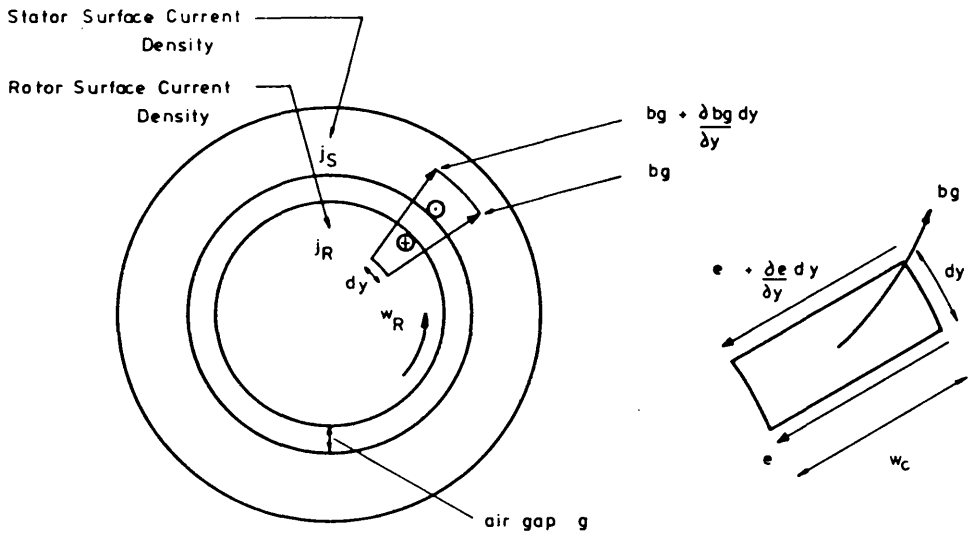

Fig 2.1 Machine Surface Model

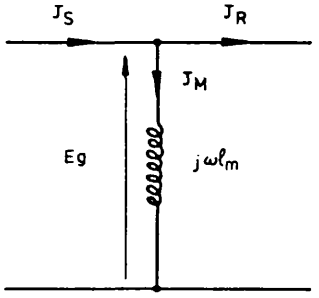

Fig 2.2 Surface Equivalent Circuit for Air Gap

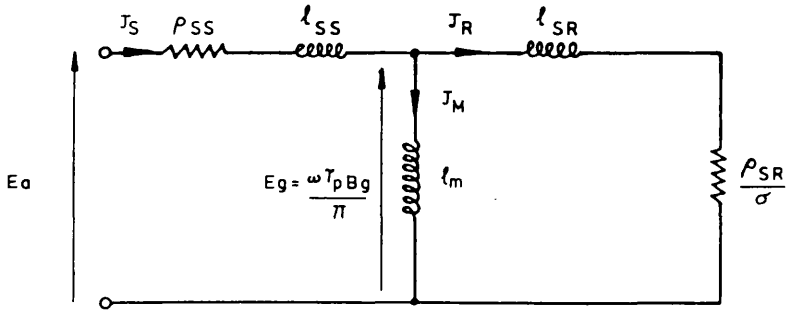

Fig 2.3 Induction Machine Surface Equivalent Circuit

where A is complex, then

$$-j\frac{g\pi}{\mu_o \tau_p} B_g = J_S - J_R \qquad (2.3)$$

The voltage induced in the machine windings is proportional to the electric field strength at the conductor surface.

The relationship between the electric field strength and the air gap flux density may be obtained by applying Faraday's Law around a path in the plane of the air gap i.e.

$$\frac{\partial e}{\partial y} = -\frac{\partial b_g}{\partial t}$$

or in complex RMS terms

$$\frac{\pi E_g}{\tau_p} = \omega B_g \qquad (2.4)$$

Combining equations (2.3) and (2.4) gives

$$J_S - J_R = -\frac{E_g}{j\omega \ell_m} \qquad (2.5)$$

where ℓ_m is the surface magnetising inductance of the air gap, and is given by

$$\ell_m = \frac{\mu_o \tau_p^2}{g\pi^2} \qquad (2.6)$$

The surface equivalent circuit representing equation (2.5) is shown in Fig. 2.2.

On the stator winding conductor sheet the resultant electric field strength is made up of two separate components, a component due to the air gap, and a component that results from the stator current sheet impedance drop, thus the electric field strength at the stator terminals is

$$E_a = J_S (\rho_{SS} + j\omega \ell_{SS}) + E_g \qquad (2.7)$$

where ρ_{SS} and ℓ_{SS} represent the surface resistance and leakage inductance, respectively, of the stator winding. On the rotor winding the surface current is circulated by the air-gap electric field. The air-gap electric field is generated by the air gap flux-wave, whose speed with respect to the rotor is given by

$$\omega - \omega_R = \sigma\omega \qquad \text{rads/sec}$$

Thus on the rotor the electric field strength is given by

$$\frac{\pi E_g'}{\tau_p} = \sigma\omega B_g \qquad (2.8)$$

Comparing equations (2.4) and (2.8) gives $E' = \sigma E$, so the rotor equation corresponding to equation (2.7) for the stator is:

$$E_g' = \sigma E_g = (\rho_{SR} + j\sigma\omega \ell_{SR}) J_R$$

$$\text{or} \quad E_g = \left[\frac{\rho_{SR}}{\sigma} + j\omega \ell_{SR}\right] J_R \qquad (2.9)$$

where ρ_{SR} and ℓ_{SR} represent the surface resistance and leakage inductance respectively of the rotor winding. Combining equations (2.5), (2.7) and (2.9) leads to the induction machine "surface equivalent circuit" of Fig. 2.3.

2.2.2 The synchronous machine

The round rotor synchronous machine model is similar to that of the induction machine given in Fig. 2.3, but in this case operation is at synchronous speed. In the synchronous machine the rotor currents are not driven by the air gap electric field, E_g, but are defined by a DC coil system. In the model of Fig. 2.1, the direction of rotor currents are assumed to be reversed and leads to the equivalent circuit of Fig. 2.4. As the resultant air gap flux is due to two independent components, it is more convenient to display the relationships between current density and flux density on a space and time phasor diagram, Fig. 2.5.

The electric field strength due to the stator surface current density, J_S, is given by

$$E_S = \frac{\omega \tau_p B_S}{\pi} = \frac{\mu_o \omega \tau_p^2}{\pi^2 g} J_S = \omega \ell_m J_S \qquad (2.10a)$$

and the electric field strength due to the rotor surface current density, J_R, is

$$E_R = \frac{\omega \tau_p B_R}{\pi} = \frac{\mu_o \omega \tau_p^2}{\pi^2 g} J_R = \omega \ell_m J_R \qquad (2.10b)$$

The machine output power is

$$P_{out} = E_R J_S A \sin \delta_T \qquad (2.11)$$

where δ_T is the torque angle and A the air gap surface area.

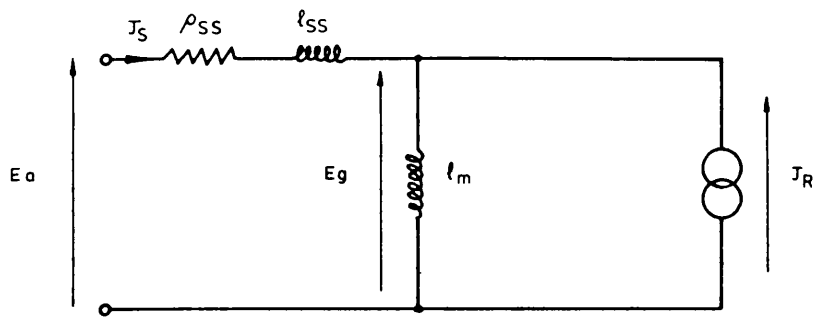

Fig 2.4 Round Rotor Synchronous Machine Surface Equivalent Circuit

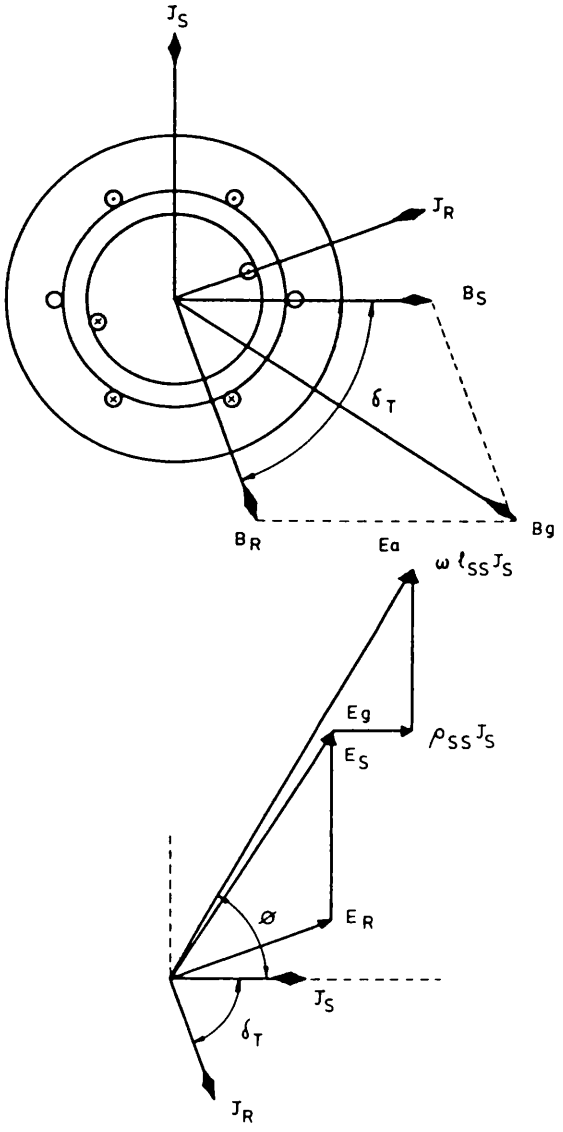

Fig 2.5 Round Rotor Synchronous Machine Phasor Diagram

In synchronous machines of the salient pole type the resultant flux distribution does not coincide with that of the resultant mmf of the windings. The air gap flux produced by a distributed mmf depends upon the orientation of the mmf axis with respect to the saliency and the gap reluctance presented to it.

The effect of a non uniform air gap length is represented by giving the stator flux separate components along each of the two axes of symmetry of the field structure. These components are related to the flux produced in a uniform air gap machine by the factors C_d and C_q, and are described in Appendix 2.7.3. The phasor diagram representation of the salient pole synchronous machine, in surface terms, is shown in Fig. 2.6.

The d and q axis components of the stator surface current density, from Fig. 2.6, are

$$J_d = J_s \cos \delta_T$$

and

$$J_q = J_s \sin \delta_T$$

The stator flux and electric field strength may be similarly resolved into two components along the two axes of symmetry. For the stator flux, B_s

$$B_d = \frac{C_d \mu_o \tau_p J_d}{\pi g} \qquad (2.12a)$$

and

$$B_q = \frac{C_q \mu_o \tau_p J_q}{\pi g} \qquad (2.12b)$$

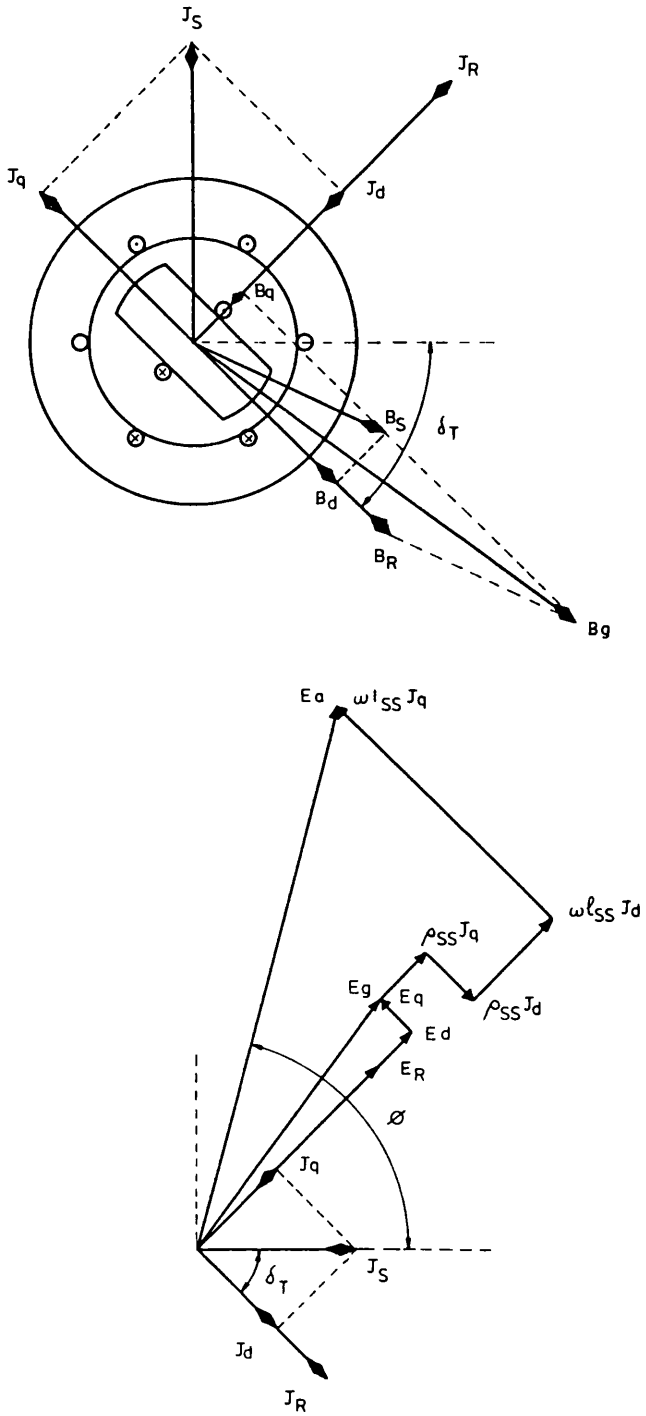

Fig 2.6 Salient Pole Synchronous Machine Phasor Diagram

and for the electric field strength, E_S

$$E_d = \frac{\omega \tau_p B_d}{\pi} = \frac{C_d \omega \mu_o \tau_p^2 J_d}{\pi^2 g} = \omega \ell_{md} J_d \qquad (2.13a)$$

and

$$E_q = \frac{\omega \tau_p B_q}{\pi} = \frac{C_q \omega \mu_o \tau_p^2 J_q}{\pi^2 g} = \omega \ell_{mq} J_q \qquad (2.13b)$$

For the rotor, which is aligned with the d axis, the electric field strength E_R due to the surface current density J_R, is

$$E_R = \frac{\omega \tau_p B_R}{\pi} = \frac{C_d \omega \mu_o \tau_p^2 J_R}{\pi^2 g} = \omega \ell_{md} J_R \qquad (2.14)$$

The output power, in surface terms, is then

$$P_{out} = \left[E_R J_S \sin \delta_T + \frac{\omega J_S^2}{2} (\ell_{md} - \ell_{mq}) \sin 2\delta_T \right] A \qquad (2.15)$$

The first term in equation (2.15) represents the excitation torque, and the second term the reluctance torque due to the saliency of the rotor.

2.3 A consideration of the geometric and magnetic circuit aspects of the design method

2.3.1 Stator

The design of any AC machine is initially concerned with the choice of a suitable stator. The most critical part of the stator magnetic circuit, Fig. 2.7, is likely to be the teeth. The tooth flux density is related to the gap density by the ratio of the minimum tooth width to the slot pitch. Hence, for any limiting value of flux density in the teeth, there is a corresponding maximum permissible density in the air-gap, which is determined by the ratio of slot width to tooth width[32]. The maximum allowable gap density, B_g, in terms of the ratio of slot width to slot pitch, β, assuming rectangular slots and a maximum core flux density of $\hat{B}$, is given by

$$B_g = \frac{\hat{B}}{\sqrt{2}} (1 - \beta) \qquad (2.16)$$

where B_g is in RMS terms and $\beta = \frac{w_s}{\tau_s}$.

The total pole flux divides into two equal components in the core to pass into the adjacent poles. In order to accommodate this flux at a density of $\hat{B}$, Tesla the backing core depth must be given by the following expression

$$\hat{B} d_c = \frac{2}{\pi} \sqrt{2}\, B_g \frac{\tau_p}{2} \qquad (2.17)$$

Combining equations (2.16) and (2.17) gives an expression for the core depth required, in terms of the pole pitch and the ratio β.

$$d_c = \frac{\tau_p}{\pi} (1 - \beta) \qquad (2.18)$$

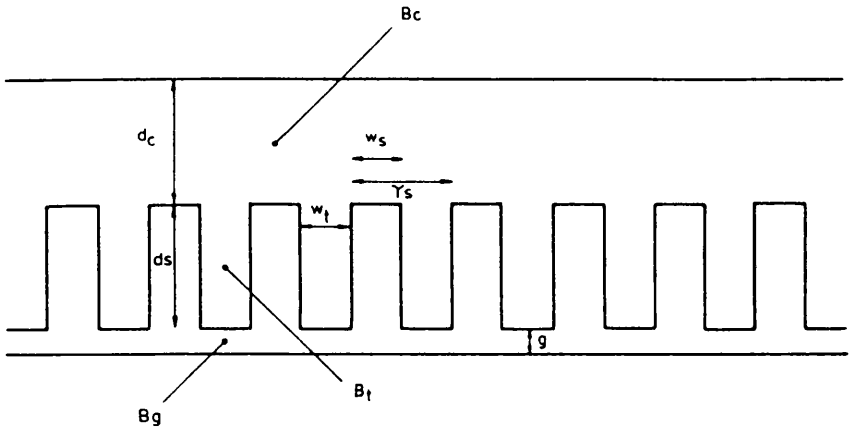

Bc - core density Bt - tooth density Bg - gap density

Fig 2.7 Flux Densities in the Stator

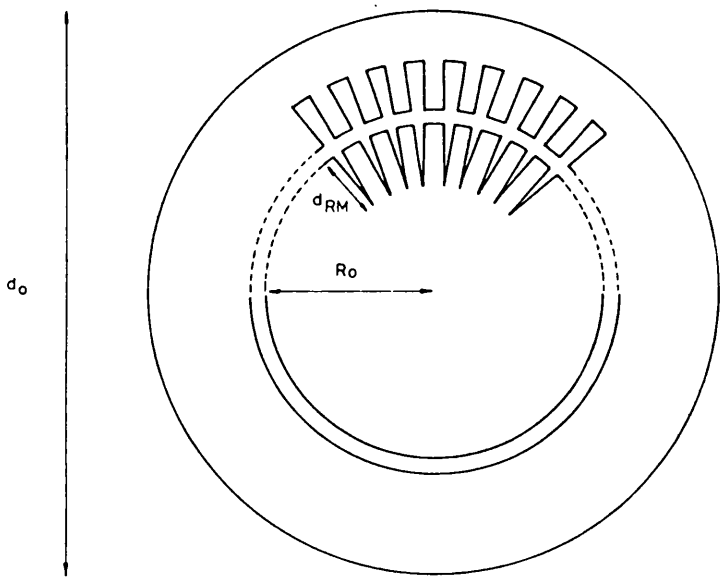

Fig 2.8 Machine Cross Section (squirrel cage or round rotor)

With the depth of backing core required given by equation (2.18), the pole pitch, for a specified slot depth, d_s, and core diameter, d_o, may be obtained from

$$\frac{d_o}{2} - d_c - d_s = \frac{2p\tau_p}{2\pi}$$

On combining this expression with equation (2.18) the pole pitch is given by

$$\tau_p = \frac{\pi(d_o - 2d_s)}{2[p + (1 - \beta)]} \qquad (2.19)$$

The stator iron cross section, Fig. 2.8, is then uniquely defined for a machine having p pole pairs, by only three variables, the outside diameter, d_o, and slot depth, d_s, and the ratio of slot width to slot pitch, β.

The total stator iron mass may now be determined for any core length, w_c, by use of the following expression

$$m_{is} = (w_c - n_v w_v)k_{is}\delta_i \left\{\pi\left[\left[\frac{d_o}{2}\right]^2 - \left[\frac{d_o}{2} - d_c - d_s\right]^2\right] - 6pq_s w_s d_s\right\}$$

This equation may be simplified by assuming that there are no cooling vents, to give

$$m_{is} = w_c k_{is}\delta_i\left\{\pi\left[\left[\frac{d_o}{2}\right]^2 - \left[\frac{d_o}{2} - d_c - d_s\right]^2\right] - 2p\beta\tau_p d_s\right\} \qquad (2.20)$$

where k_{is} is the stator iron packing factor.

At this stage it is appropriate to introduce an expression for the core loss, as this loss is proportional to the mass of the stator iron when the flux

density and frequency are known. The expression used is

$$P_C = K_C f^x B^z m_{is} \quad \text{Watts} \qquad (2.21)$$

For a typical electrical steel in 0.5 mm laminations the constants in equation (2.21) have the following values:

$K_C = 0.02$

$x = 1.136$

$z = 1.76$

These values are assumed throughout this work.

2.3.2 Salient pole rotor

Two types of laminated rotors are considered, the round rotor type and the salient pole type. The DC field winding in each case is fed by slip rings. The geometry of the salient pole structure is potentially the more difficult to describe accurately. To simplify the structure somewhat, a simple cross-shaped one piece lamination has been adopted, Fig. 2.10, which does not include the provision for damper windings. Any discrepancy between the simple iron circuit proposed and a production stamping may be accommodated by the use of an iron packing factor, k_{IR}, for the calculation of rotor mass. Similarly any discrepancy in the slot area available for the field winding may be taken care of by use of the slot packing factor, k_{PFR}.

The geometry of one-half of a salient pole rotor is shown in Fig. 2.9. If the rotor poles are assumed to be rectangular then the maximum interpolar depth is:

$$d_{RM} = R_O - \frac{w_p}{2 \sin \theta_p} \qquad (2.22)$$

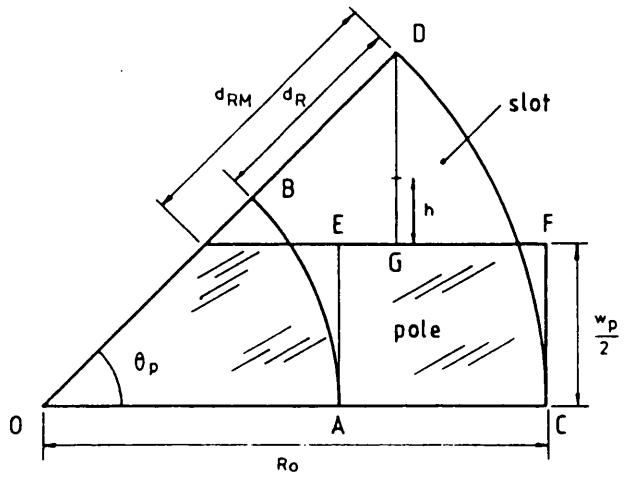

Fig 2.9 Rotor Slot Dimensions

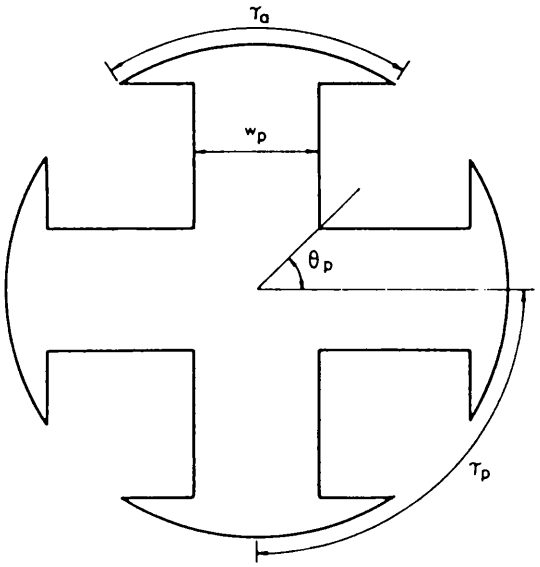

Fig 2.10 Salient Pole Rotor

where $\theta_p = \frac{\pi}{2p}$ and R_o is the rotor radius, and is given by

$$R_o = \frac{d_o}{2} - d_c - d_s - g \qquad (2.22a)$$

In order to accommodate the stator flux at the same flux density, the pole width, w_p, must be equal to twice the depth of the stator backing core.

An approximate value for the area of the conductor filled part of the slot, if the slot is filled to a depth d_R, Fig. 2.9, with conductors, can be obtained from

one half the slot area = (area of sector OCD)
- (area of sector OAB)
- (area of rectangle ACFE)

i.e. $$\frac{1}{2} A_{SR} = \frac{\theta_p}{2} R_o^2 - \frac{\theta_p}{2} (R_o - d_R)^2 - \frac{d_R w_p}{2}$$

or $$A_{SR} = \theta_p d_R (2R_o - d_R) - w_p d_R \qquad (2.23)$$

The maximum available slot area for the accommodation of the rotor winding, is therefore

$$A_{SRM} = \theta_p d_{RM} (2R_o - d_{RM}) - w_p d_{RM} \qquad (2.24)$$

and the corresponding pole area is

$$A_p = \theta_p R_o^2 - A_{SRM} \qquad (2.25)$$

The rotor iron mass for any core length, w_c, is then

$$m_{iR} = (w_c - n_v w_v)\, 2p\, k_{iR}\, \delta_i\, A_p$$

If the rotor is assumed to have no vents this equation may be simplified to

$$m_{iR} = w_c \, 2p \, k_{iR} \, \delta_i \, A_p \qquad (2.26)$$

2.3.3 Round rotor

Formulae for the slot dimensions of the round rotor are developed from those given in the previous section for the salient pole case. If the same diagram is used for the round rotor, Fig. 2.9, as for the salient pole rotor, for each slot pitch then

$$\sin \theta_p = \frac{w_t + w_R}{2R_o}$$

where w_R is the width of the slot opening, and w_t is the tooth width. Thus the maximum slot depth is given by

$$d_{RM} = R_o - \frac{w_t R_o}{w_t + w_R} \qquad (2.27)$$

If the rotor slot and tooth width are assumed to be equal to that of the stator, then equation (2.27) may be simplified to

$$d_{RM} = R_o \beta \qquad (2.28)$$

As the slot opening is usually small, when compared to the rotor circumference, the slot cross section is considered to be triangular, Fig. 2.8. This gives a maximum available slot area

$$A_{SRM} = \frac{d_{RM} w_R}{2}$$

If the slot is filled to a depth d_R with conductors, then the rotor slot area will be,

$$A_{SR} = w_R d_R \left[1 - \frac{d_R}{2d_{RM}}\right] \qquad (2.29)$$

This equation may be abbreviated by defining an effective slot depth.

$$d_{R'} = d_R \left[1 - \frac{d_R}{2d_{RM}}\right] \qquad (2.30)$$

Having defined the slot area, the rotor iron cross section and hence the iron mass may be calculated

$$m_{iR} = \delta_i k_{iR} (\pi R_o^2 - q_R p d_{RM} w_R)(w_C - n_v w_v) \qquad (2.31)$$

A simplified form of equation (2.31) may be obtained by making the following assumptions:

i) the rotor has no vents

ii) the stator and rotor have an equal number of slots per pole i.e. $q_R = 3q_S$

iii) the stator and rotor slot openings are equal i.e. $w_R = w_S$

This gives an iron mass of:

$$m_{iR} = w_C k_{iR} \delta_i R_o (\pi R_o - p\tau_p \beta^2) \qquad (2.32)$$

2.3.4 Squirrel cage rotor

The rotor of the induction machine is of a conventional squirrel cage construction. It was felt that a choice of rotor bar shapes would unduly complicate the method. Therefore a simple V shaped slot was adopted, similar to that used for the round rotor synchronous machine, Figs. 2.8 and 2.9.

If it is again assumed that the rotor slot width and pitch are equal to those of the stator, the maximum slot depth available for parallel teeth is

$$d_{RM} = R_o\beta \qquad (2.33)$$

The rotor core radius, R_o, is expressed in terms of the stator dimensions for a specified air gap length.

The rotor iron cross section is calculated in the same way as that leading to equation (2.31), but with three times as many slots, i.e.

$$m_{iR} = \delta_i k_{iR} (\pi R_o^2 - 3q_R p d_{RM} w_R)(w_c - n_v w_v) \qquad (2.34)$$

A simplified form of this equation may be obtained by assuming that

i) the rotor has no vents

ii) $q_R = q_S$

iii) $w_R = w_S$

This gives

$$m_{iR} = \delta_i k_{iR} R_o(\pi R_o - p\tau_p\beta^2)w_c \qquad (2.35)$$

2.4 Relationship between the surface equivalent models and actual machine quantities

2.4.1 Three phase winding current and voltage

The relationship between the actual winding phase current and a surface current distribution may be obtained from a consideration of mmf. Application of Ampere's law to a uniform air gap (section 2.2) shows that the mmf can be considered to be due to a sinusoidal distribution of surface current, i.e.

$$\hat{J}_S = \frac{\pi}{\tau_p} \hat{M}_S \qquad (2.36)$$

Considering only one phase of a balanced winding, the peak value of the fundamental component of mmf, in terms of the phase current, is given by:

$$\hat{M}_S = \frac{4}{\pi} \frac{z_S q_S k_{WS}}{2} \hat{I}_S \qquad (2.37)$$

Equations (2.36) and (2.37) may be combined to give an expression for the surface current density in terms of the actual phase current.

$$J_S = \frac{3 z_S q_S k_{WS}}{\tau_p} I_S \qquad (2.38)$$

where J_S and I_S are RMS quantities, and a factor of 3/2 has been introduced to account for the other two phases.

The surface current of equations (2.36) and (2.37) may be thought of as being due to a current flowing in a thin sheet of sinusoidally distributed conductors.

For one phase

$$\hat{J}_s = N_s \hat{I}_s$$

where $N_s = \dfrac{2z_s q_s k_{ws}}{\tau_p}$ conductors/metre

Having defined a conductor distribution, the induced phase voltage may be obtained by integrating the air-gap electric field strength distribution over the conductors.

If the field strength at the winding surface is:

$$e_a = \hat{E}_a \cos\left[\omega t - \frac{\pi y}{\tau_p}\right]$$

then the voltage induced in p pole-pairs is

$$v_a = w_c \int_0^{2p\tau_p} \hat{E}_a \cos\left[\omega t - \frac{\pi y}{\tau_p}\right] N_s \cos\frac{\pi y}{\tau_p}\, dy$$

The RMS induced voltage per phase is then

$$V_s = 2p\, w_c z_s q_s k_{ws} E_a \qquad (2.39)$$

A relationship between the conductor current density and the surface current density is obtained from the winding current. If one stator slot is considered, the conductor current density is, using RMS quantities

$$K_s = \frac{Z_s I_s}{k_{PFS}\, A_{SS}} \qquad (2.40)$$

where k_{PFS} is the slot packing factor. This factor takes account of the reduction in slot area caused by the need for conductor insulation and a slot wedge.

The surface current density, from equations (2.38) and (2.40) is

$$J_S = \frac{K_S \; 3q_S \; k_{WS} \; k_{PFS} \; A_{SS}}{\tau_p}$$

This expression may be simplified by assuming:

i) a rectangular stator slot whose area, $A_{SS} = w_S d_S$

ii) that each pole has $3q_S$ slots of pitch τ_S

i.e. $3q_S \tau_S = \tau_p$

iii) a distribution factor of 1

This gives

$$J_S = K_S \; k_{PFS} \; k_{PS} \; \beta \; d_S \qquad (2.41)$$

In the design process a limiting value is assigned to the stator conductor current density. This value determines the maximum permissible current loading when the stator geometry is known.

2.4.2 Stator winding impedance

The normal induction and synchronous machine equivalent circuit parameters, including expressions for conductor mass, are derived in Appendix (2.7.2). Most of the formulae presented there are based upon those given in references 33 and 34. Following each derivation a simplified form is given, and it is this reduced from that is used in the following determination of the surface equivalent impedances.

The relationship between the actual winding impedances and their equivalent surface quantities is obtained by equating VA. For a uniform air gap machine with no rotor conductors:

$$3I_S^2 \left[R_S + j\omega \left(L_S + L_m\right)\right] = 2p\tau_p w_c J_S^2 \left[\rho_{SS} + j\omega\left(\ell_{SS} + \ell_m\right)\right] \qquad (2.42)$$

Substituting the winding current, I_S, from equation (2.38) into the above expression and equating terms gives the following:

stator surface resistance $\rho_{SS} = R_S K_{SSURF}$

stator surface leakage inductance $\ell_{SS} = L_S K_{SSURF}$

surface magnetising inductance $\ell_m = L_m K_{SSURF}$

where the stator surface constant $K_{SSURF} = \dfrac{\tau_p}{6(z_S q_S k_{WS})^2 p w_c}$

The surface equivalent impedances in terms of the machine dimensions and constants, using the simplified version of the machine parameters from Appendix (2.7.2), are as follows:

$$\rho_{ss} = \frac{\rho_{cs}\ kend_{RS}}{k_{ps}^2\ k_{PFS}\ d_s \beta} \qquad (2.43)$$

$$\ell_{ss} = \frac{\mu_o\ k_{xco}\ d_s\ kend_{LS}}{3\beta\ k_{ps}^2} \qquad (2.44)$$

$$\ell_m = \frac{\mu_o\ \tau_p^2}{\pi^2 g} \qquad (2.45)$$

where the factor $kend_{RS}$ and $kend_{LS}$ are terms associated with the end connections of the winding, and are described in Appendix (2.7.2).

2.4.3 Squirrel cage winding currents and impedance

The squirrel cage rotor winding is equivalent to a balanced three phase winding with one conductor per slot. The conductor currents are sinusoidally distributed, as they are driven by a sinusoidal air gap field. A sinusoidal distribution of winding currents implies a winding factor of unity. Thus the rotor surface current density from equation (2.38) is,

$$J_R = \frac{3q_R\ I_R}{\tau_p} \qquad (2.46)$$

or in terms of the conductor current density

$$J_R = \frac{K_R\ 3q_R\ k_{PFR}\ A_{SR}}{\tau_p}$$

With the rotor slot defined as in section 2.3.4 this may be simplified to give

$$J_R = K_R\ k_{PFR}\ \beta\ d_R. \qquad (2.47)$$

As all the available slot area is used, for all induction machine designs presented in this work, the effective slot depth $d_{R'}$ from equation (2.30) is $d_{RM}/2$. A direct relationship now exists between the stator and rotor surface current loadings of the model and their respective conductor current densities (equations (2.41) and (2.47)). It is this relationship, via the machine dimensions and constants, for a given maximum core flux density, that sets the performance limits for a particular induction machine design.

The rotor equivalent surface impedances may again be found by equating VA i.e.:

$$3I_R^2 (R_R + j\omega L_R) = 2p\tau_p w_c J_R^2 (\rho_{SR} + j\omega \ell_{SR}) \qquad (2.48)$$

Substituting for the winding curent, I_R, from equation (2.46) gives the following

rotor surface resistance $\rho_{SR} = K_{RSURF}\, R_R$

rotor surface leakage inductance $\ell_{SR} = K_{RSURF}\, L_R$

where the rotor surface constant $K_{RSURF} = \dfrac{\tau_p}{6q_R^2\, pw_c}$

Using the expressions for the rotor resistance and inductance from Appendix (2.7.2), the rotor surface quantities may be obtained in terms of the machine dimensions, i.e.

$$\rho_{SR} = \frac{\rho_{CR}\, kend_{RR}}{k_{PFR}\, d_{R'}\, \beta} \qquad (2.49)$$

$$\ell_{SR} = \frac{\mu_o\, d_R\, kend_{LR}}{3\beta} \qquad (2.50)$$

2.4.4 Synchronous machine rotor windings

a) Round rotor

The rotor winding of a round rotor synchronous machine is equivalent to one phase of a three phase winding, and therefore an expression for the surface current density in terms of the actual winding current can be obtained from equation (2.38).

$$J_R = \frac{\sqrt{2}\, z_R q_R k_{wR} I_R}{\tau_p} \qquad (2.51)$$

or in terms of the rotor conductor current density, K_R.

$$J_R = \frac{\sqrt{2}\, q_R k_{wR} k_{PFR} A_{SR} K_R}{\tau_p}$$

A simplified form of the above expression can be obtained by making the following assumptions:

i) the coil sides of the winding are spread over one pole pitch. This gives a winding factor of $k_{wR} = \frac{2}{\pi}$

ii) the stator and rotor have an equal number of slots

i.e. $3q_S\tau_S = q_R\tau_R = \tau_p$

iii) the rotor slot width and pitch are equal to those of the stator

iv) the rotor slot geometry is as defined in section (2.3.3), with an effective depth, $d_{R'}$.

The rotor surface current density now becomes

$$J_R = \frac{2\sqrt{2}\, k_{PFR}\, \beta\, d_{R'}\, K_R}{\pi} \qquad (2.52)$$

The equivalent surface resistance of the rotor winding is obtained by equating the actual field loss to that incurred in the surface model

$$I_R^2 R_R = 2p\tau_p w_c J_R^2 \rho_{SR} \qquad (2.53)$$

If the actual field winding current from equation (2.51) is substituted into the expression for field loss, the surface equivalent field winding resistance in terms of the actual value is,

$$\rho_{SR} = R_R \frac{\tau_p}{4(z_R q_R k_{WR})^2 p w_c}$$

Using the expression for the winding resistance from Appendix (2.7.2), and making the same assumptions as above, the rotor surface resistance is given by

$$\rho_{SR} = \frac{\pi^2 \rho_{CR}\ kend_{RR}}{8\beta\ k_{PFR}\ d_R} \qquad (2.54)$$

where the surface resistance end factor, $kend_{RR}$, is assumed to be equal to that of the stator.

The DC field winding voltage, from equation (2.39) is

$$V_R = 2p\ w_c\ z_R q_R\ k_{wR}\ \sqrt{2}\ E_R \qquad (2.55)$$

where the rotor electric field strength, E_R, is as defined in section 2.2.2.

b) Salient pole

The salient pole rotor winding has one slot per pole and a winding factor that is approximately unity. The rotor surface current density in this case is,

$$J_R = \frac{\sqrt{2}\ z_R\ I_R}{\tau_p}$$

or in terms of the rotor conductor current density.

$$J_R = \frac{\sqrt{2}\, k_{PFR}\, A_{SR}\, K_R}{\tau_p} \qquad (2.56)$$

As the geometry is more complicated for the salient rotor construction, the expression for the area of slot occupied by rotor conductors, (equation 2.23) is not easily simplified, and therefore the above equation for the rotor surface current density is in its final form.

The equivalent surface resistance of the salient pole rotor winding is obtained as before by equating the actual and surface field loss. This gives,

$$\rho_{SR} = R_R \frac{\tau_p}{4 z_R^2\, p w_c}$$

The expression for the winding resistance, from Appendix (2.7.2), is given in terms of the mean turn length, as

$$R_R = \frac{\rho_{CR}\, \ell_{mtR}\, z_R^2\, p}{k_{PFR}\, A_{SR}}$$

The calculation of the mean turn length, ℓ_{mtR}, is based upon dimension "h" of Fig. 2.9. As the slot area is approximately triangular it was felt that a reasonable estimate of h would be given by one-third of the line GD. Thus,

$$h = \frac{1}{3} d_{RM} \sin \theta_p$$

and the mean turn length is therefore,

$$\ell_{mtR} = 2(w_c + w_p + \frac{4}{3} d_{RM} \sin \theta_p)$$

This gives a surface resistance of

$$\rho_{SR} = \frac{\rho_{CR}\ \tau_p\ kend_{RR}}{2\ k_{PFR}\ A_{SR}} \qquad (2.57)$$

where $kend_{RR} = 1 + \frac{w_p}{w_c} + \frac{4d_{RM}}{3\ w_c} \sin \theta_p \qquad (2.58)$

The DC field voltage, for the salient rotor, from equation (2.55) is

$$V_R = 2p\ w_c\ z_R\ \sqrt{2}\ E_R \qquad (2.59)$$

2.5 Induction machine design method

A simplified flow chart illustrating the induction machine design procedure is shown in Fig. 2.11.

Initially values have to be assigned to the independent variables, material and core loss constants and packing factors. The maximum values of conductor current density and core flux density are chosen empirically, according to permissible losses and heating[35]. An air gap length is also specified with regard to the expected shock loadings to be imposed on the shaft, and the environment in which the machine will operate. The design method proceeds initially by obtaining a suitable stator core geometry. This geometry is defined for a specified number of poles in terms of the core outside diameter d_o, slot depth d_s, and the ratio of slot width to slot pitch, β, (section 2.3.1).

For a known air gap length and a V shaped rotor slot as defined in section 2.3.4, the machine cross-section is described completely, and hence the total mass and length may be determined for any given core length.

A consideration is then made of the maximum surface current density and air gap flux density attainable by that geometry, for the specified maximum permissible values of core flux and conductor current densities.

The machine performance at the design point for a specified shaft speed is then determined by evaluating the surface equivalent circuit, Fig. 2.12, for increasing increments of slip. To illustrate the design method, the output data for a four pole induction machine is reproduced in Fig. 2.13. This design is rated at traction levels for a power output of 580 kW at 1500 rpm, and meets the requirements of an induction motor that is suitable for use in

a high speed diesel-electric locomotive application.

The choice of flux and conductor current densities, together with the geometrical constraints imposed on the design by the specification will be described in more detail in the following chapter.

The results show that although the efficiency decreases with increasing rotor frequency, the output power and power factor increase. The optimum performance occurs at the highest value of rotor frequency. This point is defined by the maximum stator current loading.

The design techniques discussed in this section enable the performance of a machine to be predicted for a given set of design variables at a set speed. In order to investigate the motoring and braking characteristics of a design over a range of operating frequencies, and with any suitable control algorithm, a further program has been developed, Fig. 2.14. This routine is structured around the surface equivalent representation of the induction machine, and contains the option of including a braking resistor, for use in the analysis of the traction motor braking performance described in Chapter 3.

Operating values of flux and conductor current density are not specified as an input to the performance program. This allows detail changes of machine geometry to be made to enable the design to be "trimmed".

Fig. 2.11 Induction Machine Design

A simplified flow chart (the relevant design equations are shown in brackets)

SET DESIGN PARAMETERS

$\hat{K}_S$	max RMS stator conductor current density	A/mm^2
$\hat{K}_R$	max RMS rotor conductor current density	A/mm^2
$\hat{B}$	max core flux density	T
RPM	synchronous speed	rpm
p	pole pairs	
w_c	core length	m
d_o	stator core outside diameter	m
d_s	stator slot depth	m
g	air gap length	m
β	slot width/slot pitch	
γ	coil pitch/pole pitch	
k_{PFS}	stator slot packing factor	
k_{PFR}	rotor slot packing factor	
k_{iS}	stator iron packing factor	
k_{iR}	rotor iron packing factor	
k_c, x, z	core loss constants	
ρ_{cS}	stator conductor resistivity	ohm-m
ρ_{cR}	rotor conductor resistivity	ohm-m
δ_S	stator conductor density	kg/m^3
δ_R	rotor conductor density	kg/m^3
δ_i	iron density	kg/m^3

PRINT DESIGN PARAMETERS

CALCULATE

τ_p	pole pitch (2.19)
d_c	stator backing core depth (2.18)
d_{RM}	maximum rotor slot depth (2.33)
k_{xco}, k_{sc}, k_{ps}	stator slot permeance correction,end ring
	permeance correction,and pitch factors (A2.7),(A2.18),(A2.1)
m_S, m_R	conductor mass (A2.5),(A2.17)
m_{iS}, m_{iR}	iron mass (2.20),(2.34)
m_{TOT}	total machine mass $m_S + m_R + m_{iS} + m_{iR}$
w_{TOT}	total machine length (core + end windings) $w_c + 2\ell_{oh}$ (A2.3)
P_c	core loss (2.21)
f	supply frequency p*RPM/60
B_g	RMS air gap flux density (2.16)
$\hat{J}_S$	maximum RMS stator surface current density (2.41)
$\hat{J}_R$	maximum RMS rotor surface current density (2.47)
$kend_{RS}, kend_{LS}$	stator and rotor surface resistance (A2.6),(A2.9)
$kend_{RR}, kend_{LR}$	and inductance end factors (A2.15),(A2.20)

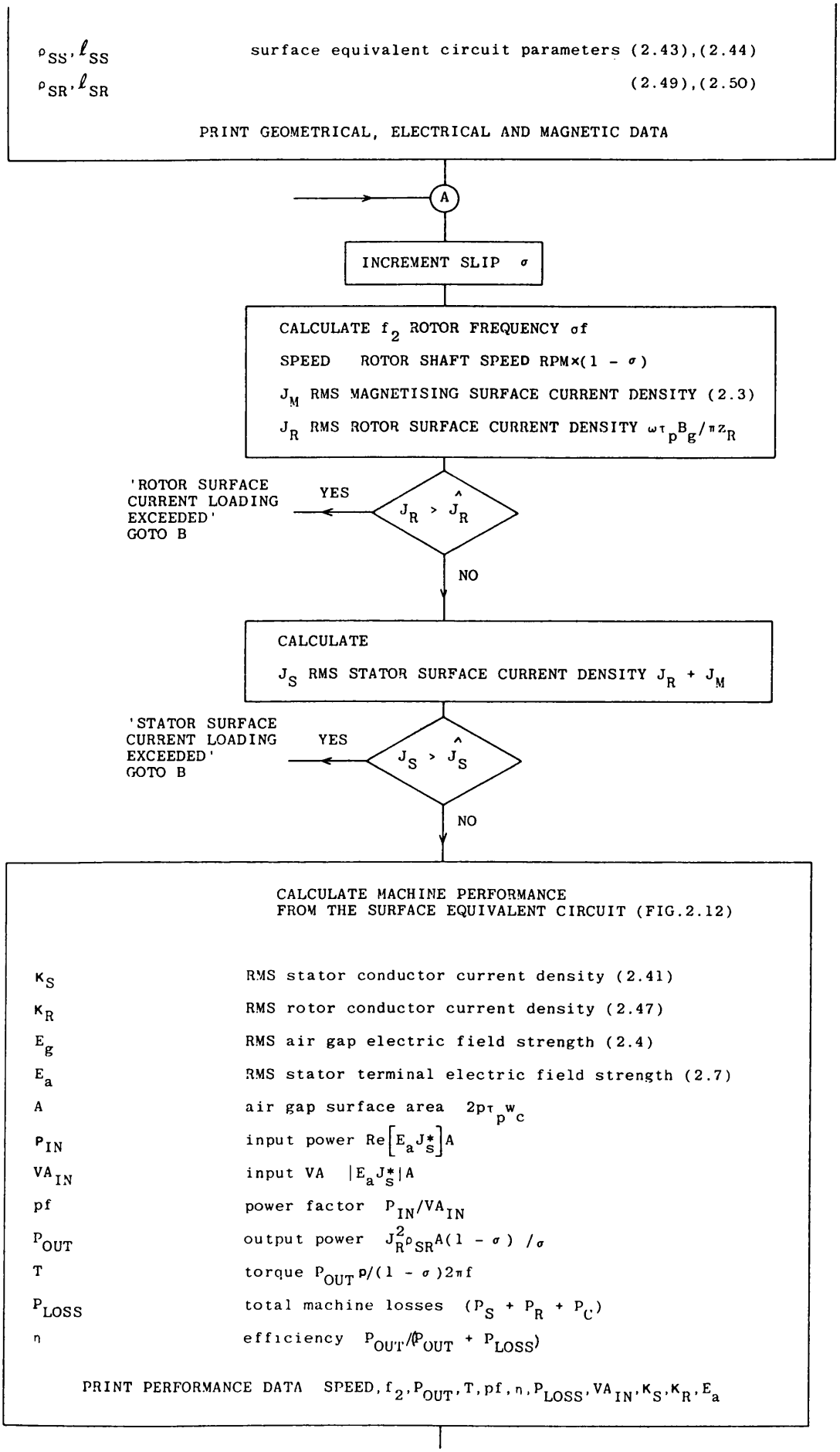
ρ_{SS}, ℓ_{SS} surface equivalent circuit parameters (2.43),(2.44)
ρ_{SR}, ℓ_{SR} (2.49),(2.50)
PRINT GEOMETRICAL, ELECTRICAL AND MAGNETIC DATA
A
INCREMENT SLIP σ
CALCULATE f_2 ROTOR FREQUENCY σf
SPEED ROTOR SHAFT SPEED RPM×(1 - σ)
J_M RMS MAGNETISING SURFACE CURRENT DENSITY (2.3)
J_R RMS ROTOR SURFACE CURRENT DENSITY $\omega\tau_p B_g/\pi z_R$
'ROTOR SURFACE CURRENT LOADING EXCEEDED' GOTO B
YES
$J_R > \hat{J}_R$
NO
CALCULATE
J_S RMS STATOR SURFACE CURRENT DENSITY $J_R + J_M$
'STATOR SURFACE CURRENT LOADING EXCEEDED' GOTO B
YES
$J_S > \hat{J}_S$
NO
CALCULATE MACHINE PERFORMANCE
FROM THE SURFACE EQUIVALENT CIRCUIT (FIG.2.12)
K_S RMS stator conductor current density (2.41)
K_R RMS rotor conductor current density (2.47)
E_g RMS air gap electric field strength (2.4)
E_a RMS stator terminal electric field strength (2.7)
A air gap surface area $2p\tau_p w_c$
P_{IN} input power $Re\left[E_a J_s^*\right]A$
VA_{IN} input VA $|E_a J_s^*|A$
pf power factor P_{IN}/VA_{IN}
P_{OUT} output power $J_R^2 \rho_{SR} A(1 - \sigma)/\sigma$
T torque $P_{OUT} p/(1 - \sigma)2\pi f$
P_{LOSS} total machine losses $(P_S + P_R + P_C)$
η efficiency $P_{OUT}/(P_{OUT} + P_{LOSS})$
PRINT PERFORMANCE DATA SPEED, $f_2, P_{OUT}, T, pf, \eta, P_{LOSS}, VA_{IN}, K_S, K_R, E_a$

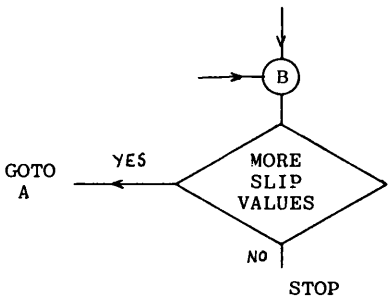
B
MORE
SLIP
VALUES
YES
GOTO
A
NO
STOP

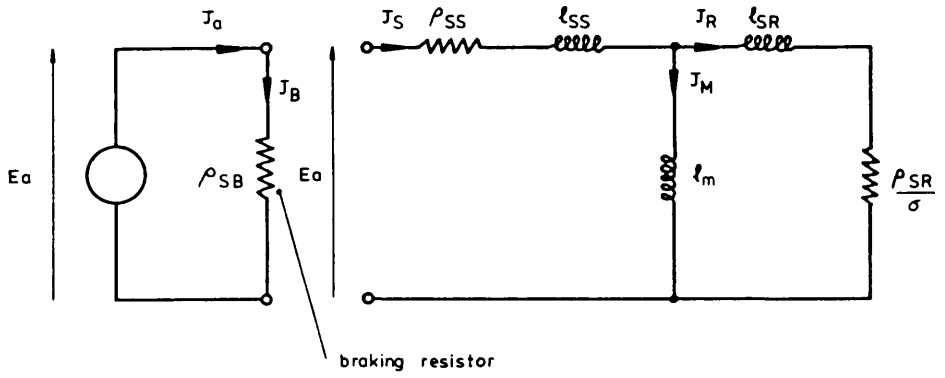

Fig 2.12 Induction Motor Surface Equivalent Circuit (motoring and braking)

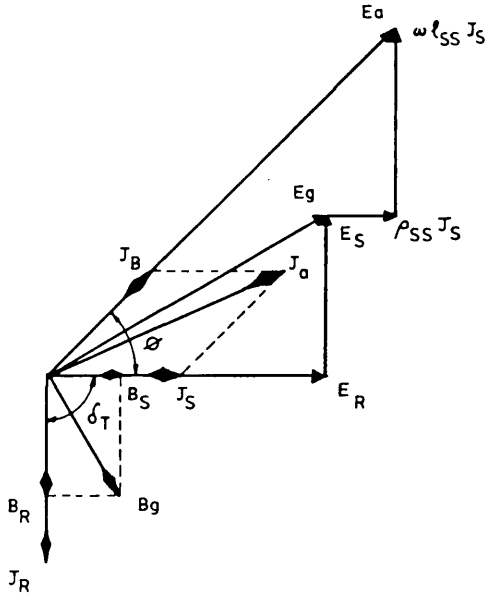

Fig 2.16 Synchronous Motor Phasor Diagram ($\delta_T = 90°$)

Fig.2.13 Induction Machine Design, Output Data

INDUCTION MOTOR

maximum stator conductor current density	0.8440E+01 A/mm2
maximum rotor conductor current density	0.8440E+01 A/mm2
maximum core flux-density	0.1400E+01 T
synchronous speed	0.1500E+04 RPM
number of poles	4
core length	0.3020E+00 M
stator core outside diameter	0.6000E+00 M
stator slot depth	0.5000E-01 M
air gap length	0.3000E-02 M
slot width / slot pitch	0.5000E+00
coil pitch / pole pitch	0.1000E+01
stator slot packing factor	0.5000E+00
rotor slot packing factor	0.1000E+01
stator iron packing factor	0.1000E+01
rotor iron packing factor	0.1000E+01

core loss constants

kc = 0.2000E-01 x = 0.1136E+01 z = 0.1760E+01

stator conductor resistivity	0.2000E-07 OHM-M
rotor conductor resistivity	0.2000E-07 OHM-M
stator conductor density	0.8930E+04 KG/M**3
rotor conductor density	0.8930E+04 KG/M**3
iron density	0.7871E+04 KG/M**3
pole pitch	0.3142E+00 M
depth of backing core	0.5000E-01 M
depth of rotor slot	0.9850E-01 M

slot , end ring and pitch factors

kxco= 0.1000E+01 ksc= 0.1800E+00 kps= 0.1000E+01

stator conductor mass	0.9325E+02 KG
rotor conductor mass	0.1387E+03 KG
stator iron mass	0.2987E+03 KG
rotor iron mass	0.2163E+03 KG
total motor mass	0.7469E+03 KG
total machine length	0.4834E+00 M
core loss	0.9194E+03 WATTS
supply frequency	0.5000E+02 HZ
RMS air-gap flux-density	0.4950E+00 T
maximum stator surface current density	0.1055E+06 A/M

maximum rotor surface current density	0.2078E+06	A/M
stator surface resistance end factor	0.2201E+01	
stator surface inductance end factor	0.1566E+01	
rotor surface resistance end factor	0.1662E+01	
rotor surface inductance end factor	0.1299E+01	
stator surface resistance	0.3522E-05	OHM
stator surface leakage inductance	0.6560E-07	H
rotor surface resistance	0.1350E-05	OHM
rotor surface leakage inductance	0.1072E-06	H

speed	slip-freq	Pout	T	pf	effy	Ploss	VAin	Ks	K_R	Ea
0.1500E+04	0.1250E-01	0.1699E+05	0.1082E+03	0.2353E+00	0.9381E+00	0.1122E+04	0.7305E+05	0.9744E+00	0.1169E+00	0.1580E+02
0.1499E+04	0.2500E-01	0.3396E+05	0.2163E+03	0.4315E+00	0.9667E+00	0.1170E+04	0.7928E+05	0.1057E+01	0.2339E+00	0.1582E+02
0.1499E+04	0.3750E-01	0.5092E+05	0.3244E+03	0.5778E+00	0.9761E+00	0.1249E+04	0.8870E+05	0.1181E+01	0.3507E+00	0.1583E+02
0.1499E+04	0.5000E-01	0.6786E+05	0.4325E+03	0.6802E+00	0.9804E+00	0.1360E+04	0.1004E+06	0.1336E+01	0.4676E+00	0.1584E+02
0.1498E+04	0.6250E-01	0.8478E+05	0.5404E+03	0.7505E+00	0.9826E+00	0.1503E+04	0.1137E+06	0.1512E+01	0.5844E+00	0.1586E+02
0.1498E+04	0.7500E-01	0.1017E+06	0.6482E+03	0.7990E+00	0.9838E+00	0.1678E+04	0.1282E+06	0.1703E+01	0.7011E+00	0.1587E+02
0.1497E+04	0.8750E-01	0.1185E+06	0.7558E+03	0.8331E+00	0.9844E+00	0.1884E+04	0.1434E+06	0.1903E+01	0.8178E+00	0.1589E+02
0.1497E+04	0.1000E+00	0.1353E+06	0.8633E+03	0.8574E+00	0.9846E+00	0.2121E+04	0.1592E+06	0.2111E+01	0.9343E+00	0.1590E+02
0.1497E+04	0.1125E+00	0.1521E+06	0.9706E+03	0.8752E+00	0.9845E+00	0.2390E+04	0.1755E+06	0.2323E+01	0.1051E+01	0.1592E+02
0.1496E+04	0.1250E+00	0.1688E+06	0.1078E+04	0.8884E+00	0.9843E+00	0.2690E+04	0.1921E+06	0.2540E+01	0.1167E+01	0.1594E+02
0.1496E+04	0.1375E+00	0.1855E+06	0.1184E+04	0.8983E+00	0.9840E+00	0.3021E+04	0.2089E+06	0.2759E+01	0.1283E+01	0.1596E+02
0.1496E+04	0.1500E+00	0.2022E+06	0.1291E+04	0.9057E+00	0.9835E+00	0.3383E+04	0.2259E+06	0.2980E+01	0.1399E+01	0.1598E+02
0.1495E+04	0.1625E+00	0.2188E+06	0.1397E+04	0.9114E+00	0.9830E+00	0.3775E+04	0.2432E+06	0.3203E+01	0.1515E+01	0.1600E+02
0.1495E+04	0.1750E+00	0.2353E+06	0.1503E+04	0.9157E+00	0.9825E+00	0.4198E+04	0.2605E+06	0.3427E+01	0.1631E+01	0.1603E+02
0.1494E+04	0.1875E+00	0.2517E+06	0.1609E+04	0.9189E+00	0.9819E+00	0.4652E+04	0.2780E+06	0.3652E+01	0.1746E+01	0.1605E+02
0.1494E+04	0.2000E+00	0.2681E+06	0.1714E+04	0.9213E+00	0.9812E+00	0.5136E+04	0.2956E+06	0.3877E+01	0.1862E+01	0.1607E+02
0.1494E+04	0.2125E+00	0.2845E+06	0.1819E+04	0.9230E+00	0.9805E+00	0.5649E+04	0.3133E+06	0.4103E+01	0.1977E+01	0.1610E+02
0.1493E+04	0.2250E+00	0.3007E+06	0.1923E+04	0.9241E+00	0.9798E+00	0.6193E+04	0.3311E+06	0.4329E+01	0.2092E+01	0.1612E+02
0.1493E+04	0.2375E+00	0.3169E+06	0.2027E+04	0.9248E+00	0.9791E+00	0.6766E+04	0.3490E+06	0.4555E+01	0.2206E+01	0.1615E+02
0.1493E+04	0.2500E+00	0.3330E+06	0.2131E+04	0.9250E+00	0.9784E+00	0.7368E+04	0.3669E+06	0.4782E+01	0.2321E+01	0.1618E+02
0.1492E+04	0.2625E+00	0.3490E+06	0.2234E+04	0.9250E+00	0.9776E+00	0.7999E+04	0.3850E+06	0.5008E+01	0.2435E+01	0.1620E+02
0.1492E+04	0.2750E+00	0.3649E+06	0.2336E+04	0.9246E+00	0.9768E+00	0.8658E+04	0.4031E+06	0.5234E+01	0.2549E+01	0.1623E+02
0.1491E+04	0.2875E+00	0.3808E+06	0.2438E+04	0.9240E+00	0.9760E+00	0.9347E+04	0.4212E+06	0.5460E+01	0.2662E+01	0.1626E+02
0.1491E+04	0.3000E+00	0.3965E+06	0.2540E+04	0.9232E+00	0.9753E+00	0.1006E+05	0.4394E+06	0.5685E+01	0.2776E+01	0.1629E+02
0.1491E+04	0.3125E+00	0.4122E+06	0.2640E+04	0.9221E+00	0.9745E+00	0.1081E+05	0.4577E+06	0.5910E+01	0.2889E+01	0.1632E+02
0.1490E+04	0.3250E+00	0.4277E+06	0.2741E+04	0.9209E+00	0.9736E+00	0.1158E+05	0.4760E+06	0.6135E+01	0.3001E+01	0.1636E+02
0.1490E+04	0.3375E+00	0.4432E+06	0.2840E+04	0.9196E+00	0.9728E+00	0.1238E+05	0.4944E+06	0.6359E+01	0.3113E+01	0.1639E+02
0.1490E+04	0.3500E+00	0.4585E+06	0.2940E+04	0.9181E+00	0.9720E+00	0.1320E+05	0.5128E+06	0.6583E+01	0.3225E+01	0.1642E+02

0.1489E+04	0.3625E+00	0.4737E+06	0.3038E+04	0.9164E+00	0.9712E+00	0.1405E+05	0.5313E+06	0.6806E+01	0.3337E+01	0.1646E+02
0.1489E+04	0.3750E+00	0.4889E+06	0.3136E+04	0.9147E+00	0.9704E+00	0.1493E+05	0.5498E+06	0.7029E+01	0.3448E+01	0.1649E+02
0.1488E+04	0.3875E+00	0.5039E+06	0.3233E+04	0.9128E+00	0.9695E+00	0.1583E+05	0.5684E+06	0.7251E+01	0.3559E+01	0.1652E+02
0.1488E+04	0.4000E+00	0.5188E+06	0.3329E+04	0.9108E+00	0.9687E+00	0.1676E+05	0.5870E+06	0.7472E+01	0.3670E+01	0.1656E+02
0.1488E+04	0.4125E+00	0.5336E+06	0.3425E+04	0.9088E+00	0.9679E+00	0.1772E+05	0.6056E+06	0.7692E+01	0.3780E+01	0.1660E+02
0.1487E+04	0.4250E+00	0.5482E+06	0.3520E+04	0.9066E+00	0.9670E+00	0.1869E+05	0.6243E+06	0.7912E+01	0.3889E+01	0.1663E+02
0.1487E+04	0.4375E+00	0.5628E+06	0.3614E+04	0.9044E+00	0.9662E+00	0.1970E+05	0.6430E+06	0.8132E+01	0.3999E+01	0.1667E+02
0.1487E+04	0.4500E+00	0.5772E+06	0.3708E+04	0.9021E+00	0.9653E+00	0.2072E+05	0.6618E+06	0.8350E+01	0.4108E+01	0.1671E+02
0.1486E+04	0.4625E+00	stator surface current loading exceeded								
0.1486E+04	0.4750E+00	stator surface current loading exceeded								
0.1485E+04	0.4875E+00	stator surface current loading exceeded								
0.1485E+04	0.5000E+00	stator surface current loading exceeded								
0.1485E+04	0.5125E+00	stator surface current loading exceeded								
0.1484E+04	0.5250E+00	stator surface current loading exceeded								
0.1484E+04	0.5375E+00	stator surface current loading exceeded								
0.1484E+04	0.5500E+00	stator surface current loading exceeded								
0.1483E+04	0.5625E+00	stator surface current loading exceeded								
0.1483E+04	0.5750E+00	stator surface current loading exceeded								
0.1482E+04	0.5875E+00	stator surface current loading exceeded								
0.1482E+04	0.6000E+00	stator surface current loading exceeded								
0.1482E+04	0.6125E+00	stator surface current loading exceeded								
0.1481E+04	0.6250E+00	stator surface current loading exceeded								
0.1481E+04	0.6375E+00	stator surface current loading exceeded								
0.1481E+04	0.6500E+00	stator surface current loading exceeded								
0.1480E+04	0.6625E+00	stator surface current loading exceeded								
0.1480E+04	0.6750E+00	stator surface current loading exceeded								
0.1479E+04	0.6875E+00	stator surface current loading exceeded								
0.1479E+04	0.7000E+00	stator surface current loading exceeded								
0.1479E+04	0.7125E+00	stator surface current loading exceeded								
0.1478E+04	0.7250E+00	stator surface current loading exceeded								
0.1478E+04	0.7375E+00	stator surface current loading exceeded								
0.1478E+04	0.7500E+00	stator surface current loading exceeded								

Fig. 2.14 Induction Machine Performance,
A simplified flow chart

SET MACHINE PARAMETERS

p	pole pairs	
d_o	stator core outside diameter	m
d_s	stator slot depth	m
w_c	core length	m
g	air gap length	m
β	slot width/slot pitch	
γ	coil pitch/pole pitch	
k_{PFS}	stator slot packing factor	
k_{PFR}	rotor slot packing factor	
k_{iS}	stator iron packing factor	
k_{iR}	rotor iron packing factor	
k_c, x, z	core loss constants	
ρ_{cS}	stator conductor resistivity	ohm-m
ρ_{cR}	rotor conductor resistivity	ohm-m
δ_S	stator conductor density	kg/m^3
δ_R	rotor conductor density	kg/m^3
δ_i	iron density	kg/m^3

PRINT MACHINE PARAMETERS

CALCULATE

τ_p	pole pitch (2.19)	
d_c	stator backing core depth (2.18)	
d_{RM}	maximum rotor slot depth (2.33)	
k_{xco}, k_{sc}, k_{ps}	stator slot permeance correction, end ring permeance correction and pitch factors (A2.7),(A2.18) (A2.1)	
m_S, m_R, m_{iS}, m_{iR}	conductor and iron mass (A2.5),(A2.17),(2.20),(2.34)	
m_{TOT}	total machine mass $m_S + m_R + m_{iS} + m_{iR}$	
w_{TOT}	total machine length (core + end windings) $w_c + 2\ell_{oh}$ (A2.3)	
P_c	core loss (2.21)	
$kend_{RS}, kend_{LS}$	stator and rotor surface resistance (A2.6),(A2.9)	
$kend_{RR}, kend_{LR}$	and inductance end factors (A2.15),(A2.20)	
ρ_{SS}, ℓ_{SS}	surface equivalent circuit parameters (2.43),(2.44)	
ρ_{SR}, ℓ_{SR}	surface equivalent circuit parameters (2.49),(2.50)	
ℓ_m	surface equivalent circuit parameters (2.6)	

PRINT $\tau_p, d_c, d_{RM}, m_S, m_R, m_{iS}, m_{iR}, m_{TOT}, w_{TOT}$

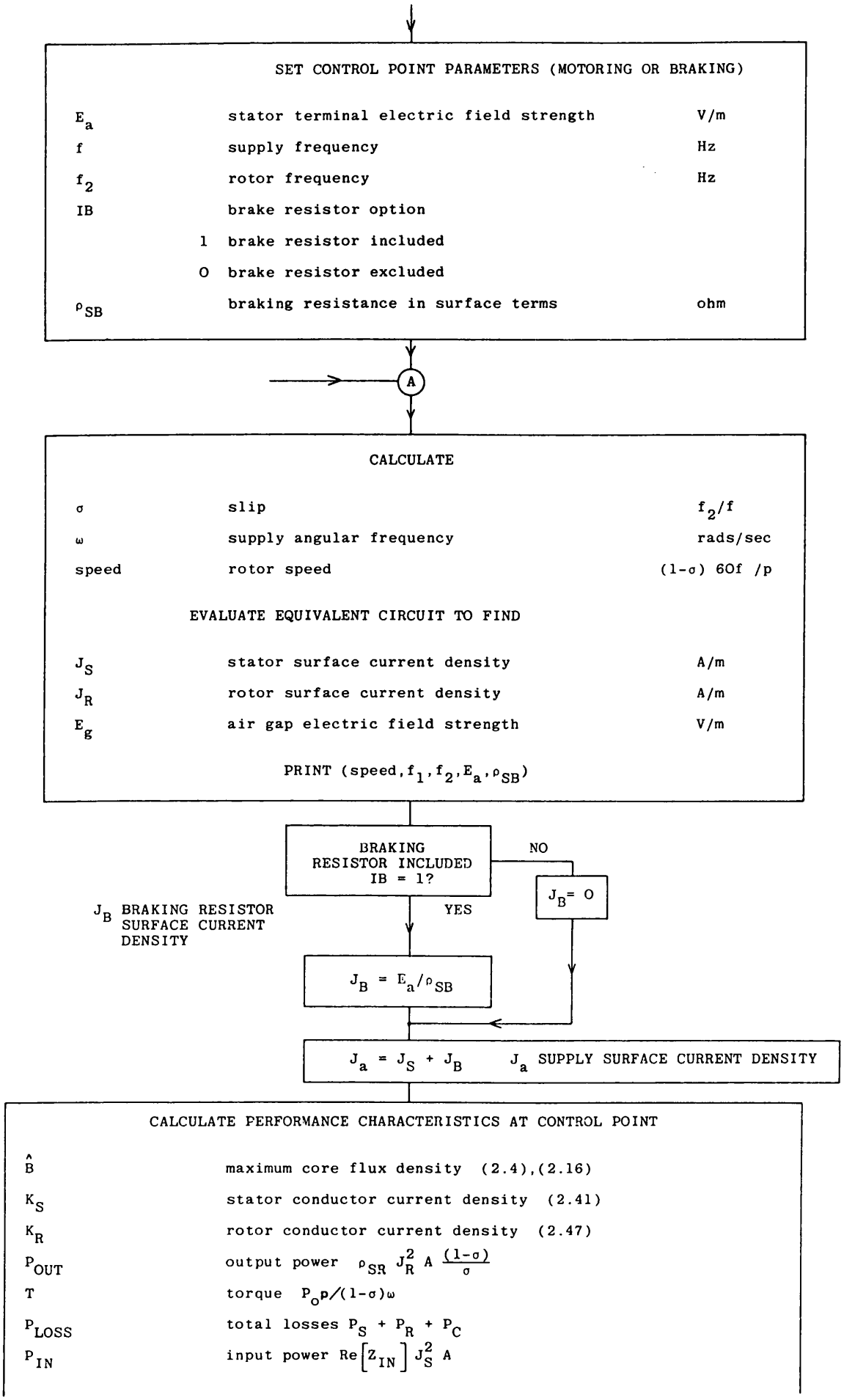
SET CONTROL POINT PARAMETERS (MOTORING OR BRAKING)
E_a stator terminal electric field strength V/m
f supply frequency Hz
f_2 rotor frequency Hz
IB brake resistor option
1 brake resistor included
0 brake resistor excluded
ρ_{SB} braking resistance in surface terms ohm
A
CALCULATE
σ slip f_2/f
ω supply angular frequency rads/sec
speed rotor speed (1-σ) 60f /p
EVALUATE EQUIVALENT CIRCUIT TO FIND
J_S stator surface current density A/m
J_R rotor surface current density A/m
E_g air gap electric field strength V/m
PRINT (speed, f_1, f_2, E_a, ρ_{SB})
BRAKING RESISTOR INCLUDED IB = 1?
NO
YES
J_B= 0
J_B BRAKING RESISTOR SURFACE CURRENT DENSITY
$J_B = E_a/\rho_{SB}$
$J_a = J_S + J_B$ J_a SUPPLY SURFACE CURRENT DENSITY
CALCULATE PERFORMANCE CHARACTERISTICS AT CONTROL POINT
$\hat{B}$ maximum core flux density (2.4),(2.16)
K_S stator conductor current density (2.41)
K_R rotor conductor current density (2.47)
P_{OUT} output power $\rho_{SR} J_R^2 A \frac{(1-\sigma)}{\sigma}$
T torque $P_o p/(1-\sigma)\omega$
P_{LOSS} total losses $P_S + P_R + P_C$
P_{IN} input power $Re[Z_{IN}] J_S^2 A$

$SUPP_{VA}$	supply VA $\lvert E_a J_a^* \rvert$ A
P_B	braking resistor loss $\rho_{SB} J_B^2$ A
pf	angle between E_a and J_S
η	efficiency $P_{OUT}/(P_{OUT} + P_{LOSS})$

PRINT $P_{IN}, P_{OUT}, P_{LOSS}, P_B, T, pf, \eta, SUPP_{VA}, \hat{B}, K_S, K_R$

PERFORMANCE DATA

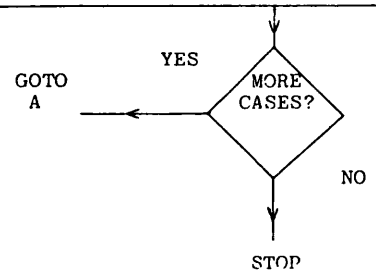

2.6 Synchronous machine design method

The synchronous machine design method illustrated by the flow chart of Fig. 2.15, proceeds initially in a similar manner to the induction machine. The method requires the same input variables to be specified, with the addition of one extra variable for the salient pole rotor construction. This is the ratio of pole arc to pole pitch, α, and is required for the calculation of the d and q axis magnetising inductance factors C_d and C_q.

Throughout the design process the synchronous machines of both the round rotor and salient pole type are assumed to be controlled at a torque angle, δ_T, of 90 degrees. This will produce the maximum excitation torque per unit current, Fig. 2.16.

The stator geometry is determined as before, and again sets the maximum permissable values of air gap flux density, B_g, and stator surface current density, J_s, for a specified core flux and conductor current density. To find a starting point in the iterative design process, the air gap length is increased in steps until the stator component of air gap flux, B_s, is equal to or less than the maximum permitted air gap flux density, B_g.

From equation (2.10) for the round rotor machine,

$$B_s = \frac{\mu_o \tau_p J_s}{\pi g}$$

and for the salient pole machine, using equation (2.12)

$$B_s = \frac{\mu_o \tau_p C_q J_s}{\pi g}$$

As the torque angle is held constant at 90 degrees, the stator and rotor components of air-gap flux are at right angles and therefore the rotor component of the air gap flux can be found from,

$$B_R = \sqrt{B_g^2 - B_s^2}$$

Having determined an air gap length that satisfies the above condition, it is possible to define the rotor cross-section (sections 2.3.2 and 2.3.4) and hence calculate the available slot area. The value of rotor surface current density, J_R, required to set up the rotor component of air-gap flux, B_R, is then determined using equations (2.10b) and (2.14) for the round and salient pole rotor structures respectively. Thus, for the round rotor machine

$$J_R = \frac{\pi g \, B_R}{\mu_o \, \tau_p}$$

and for the salient pole machine,

$$J_R = \frac{\pi g \, B_R}{\mu_o \, \tau_p \, C_d}$$

The rotor slot area available must be large enough to accommodate a total conductor cross-section, that is able to support the required level of rotor surface current loading, J_R, at the specified conductor current density, K_R. If sufficient slot area is available, the depth to which it need be filled with conductors, for operation at the given rotor conductor current density is found (d_R). If both the air-gap and rotor slot area criteria are met, the machine performance for that particular air-gap length is evaluated.

The air-gap length is then increased in increments of 1 mm. for each subsequent pass around the design loop. For each increase in the air-gap length, the stator component of flux loading, B_S, will be reduced and the rotor flux loading, B_R, will increase for a fixed value of air gap flux density, B_g.

For a fixed stator cross-section and core length, and a maximum value of stator surface current loading, the output power will increase as the rotor surface current and flux loadings increase with progressive increases in air-gap length. The output power will continue to rise until a gap length is reached for which there is insufficient rotor slot space available to support the required value of rotor surface current loading, for a fixed rotor conductor current density. The power factor also increases with increasing gap length. This is due to a consequent decrease in the surface magnetising inductance. The best design was therefore taken at the maximum allowable gap.

To illustrate the design method, the output data for both a round rotor and salient pole design is reproduced in Fig. 2.17. These designs again represent a machine that is suitable for the traction application described in the following chapter.

As for the induction machine, there is a need to predict the performance of the synchronous machine for any control algorithm, under both motoring and braking conditions. The flow chart of Fig. 2.18 illustrates a method which enables this to be done. The method is based on surface equivalent quantities, and provision has been made for the inclusion of a resistor for analysis of the braking duty. All input variables regarding the machine geometry and material constants are unchanged from those used in the

design process, with the exception of the air-gap length which is now defined initially. The rotor slot depth may also be defined, or the maximum slot depth used, depending upon the setting of the flag IS. No stipulation is made regarding the choice of stator conductor current density or maximum core flux density. These quantities are evaluated as a consequence of the control point parameters. This approach again enables the effect of small geometrical changes to be evaluated so that the design can be "trimmed".

Fig. 2.15 Synchronous Machine Design

A simplified flow chart

* round rotor

** salient pole

SET DESIGN PARAMETERS

$\hat{K}_S$	max RMS stator conductor current density	A/mm^2
$\hat{K}_R$	max RMS rotor conductor current density	A/mm^2
$\hat{B}$	max core flux density	T
RPM	synchronous speed	rpm
p	pole pairs	
w_c	core length	m
d_o	stator core outside diameter	m
d_s	stator slot depth	m
β	slot width/slot pitch	
γ	coil pitch/pole pitch	
α	pole arc/pole pitch	
k_{PFS}	stator slot packing factor	
k_{PFR}	rotor slot packing factor	
k_{iS}	stator iron packing factor	
k_{iR}	rotor iron packing factor	
$k_{c,x,z}$	core loss constants	
ρ_{CS}	stator conductor resistivity	ohm-m
ρ_{CR}	rotor conductor resistivity	ohm-m
δ_S	stator conductor density	kg/m^3
δ_R	rotor conductor density	kg/m^3
δ_i	iron density	kg/m^3

PRINT DESIGN PARAMETERS

CALCULATE

τ_p	pole pitch (2.19)
d_c	stator backing core depth (2.18)
w_p	pole body width $2d_c$**
k_{xco}, k_{ps}	slot permeance correction and pitch factors (A2.7),(A2.1)
C_d, C_q	magnetising inductance d and q axis factors (A2.30),(A2.31)**
m_S, m_{iS}	stator conductor and iron mass (A2.5),(2.20)
w_{TOT}	total machine length (core + end windings) $w_c + 2\ell_{oh}$ (A2.3)
P_c	core loss (2.21)

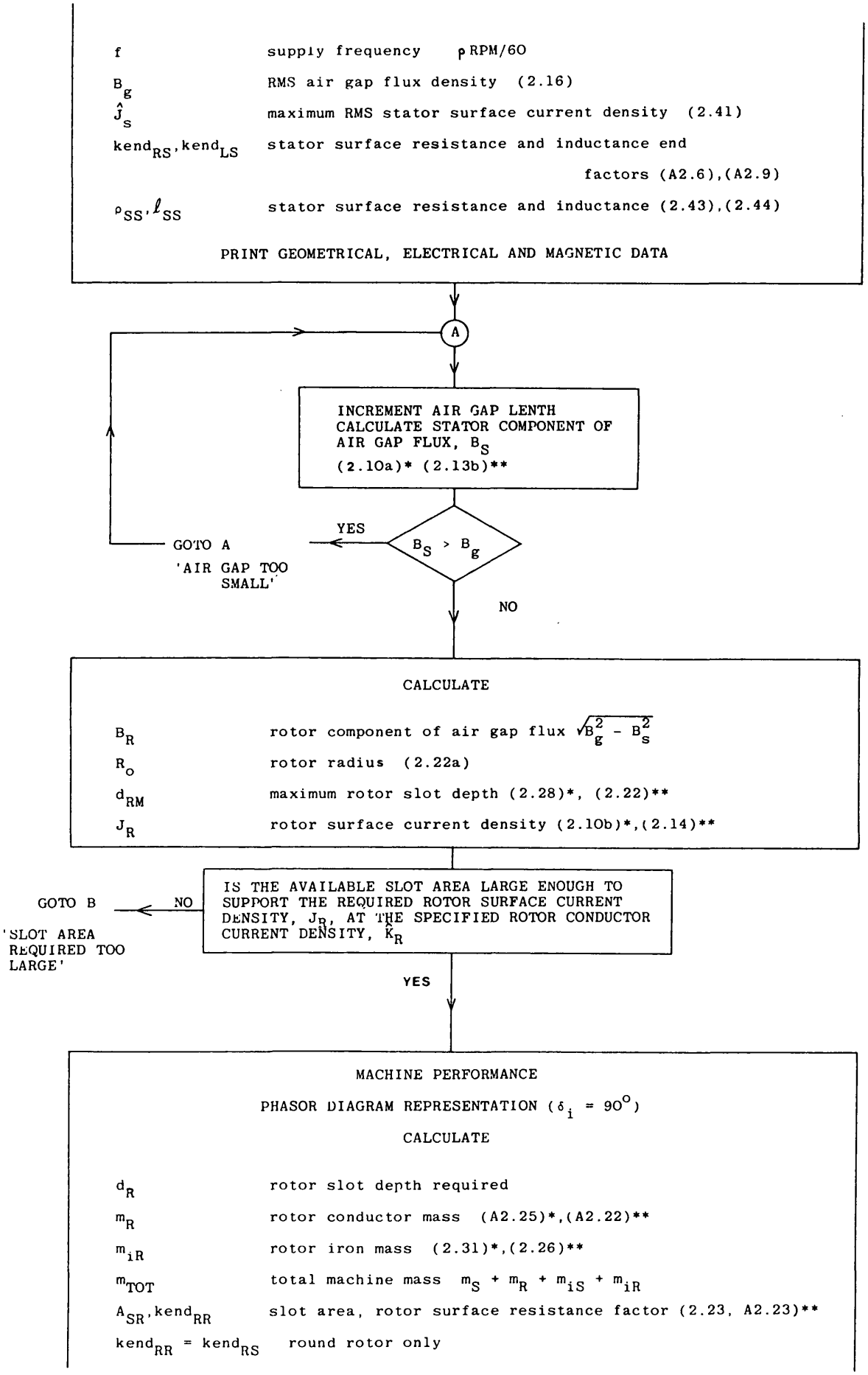
f supply frequency ρ RPM/60
B_g RMS air gap flux density (2.16)
$\hat{J}_s$ maximum RMS stator surface current density (2.41)
$kend_{RS}, kend_{LS}$ stator surface resistance and inductance end factors (A2.6),(A2.9)
ρ_{SS}, ℓ_{SS} stator surface resistance and inductance (2.43),(2.44)
PRINT GEOMETRICAL, ELECTRICAL AND MAGNETIC DATA
A
INCREMENT AIR GAP LENTH
CALCULATE STATOR COMPONENT OF AIR GAP FLUX, B_S
(2.10a)* (2.13b)**
YES
$B_S > B_g$
GOTO A
'AIR GAP TOO SMALL'
NO
CALCULATE
B_R rotor component of air gap flux $\sqrt{B_g^2 - B_s^2}$
R_o rotor radius (2.22a)
d_{RM} maximum rotor slot depth (2.28)*, (2.22)**
J_R rotor surface current density (2.10b)*,(2.14)**
IS THE AVAILABLE SLOT AREA LARGE ENOUGH TO SUPPORT THE REQUIRED ROTOR SURFACE CURRENT DENSITY, J_R, AT THE SPECIFIED ROTOR CONDUCTOR CURRENT DENSITY, $\hat{K}_R$
NO
GOTO B
'SLOT AREA REQUIRED TOO LARGE'
YES
MACHINE PERFORMANCE
PHASOR DIAGRAM REPRESENTATION ($\delta_i = 90^o$)
CALCULATE
d_R rotor slot depth required
m_R rotor conductor mass (A2.25)*,(A2.22)**
m_{iR} rotor iron mass (2.31)*,(2.26)**
m_{TOT} total machine mass $m_S + m_R + m_{iS} + m_{iR}$
$A_{SR}, kend_{RR}$ slot area, rotor surface resistance factor (2.23, A2.23)**
$kend_{RR} = kend_{RS}$ round rotor only

A	air gap surface area
$E_P = \rho_{SS}\hat{J}_S + 2\tau_p f B_R$	$E_Q = 2\tau_p f B_S + \hat{J}_S \omega \ell_{SS}$
E_a	stator terminal electric field strength $\sqrt{E_P^2 + E_Q^2}$
ρ_{SR}	rotor surface resistance (2.54)*,(2.57)**
E_R	rotor terminal electric field strength $\rho_{SR}J_R$
P_S, P_R	stator and rotor conductor losses
P_{LOSS}	total machine loss $P_S + P_R + P_C$
P_{OUT}	output power (2.11)*,(2.15)**
T	torque $P_o p/2\pi f$
η	efficiency $P_o/(P_o + P_{LOSS})$
pf	power factor E_p/E_a

PRINT PERFORMANCE DATA g, d_{RM}, d_R, pf, $P_{LOSS}, T, P_{OUT}, \eta, M_{TOT}, E_a, E_R$

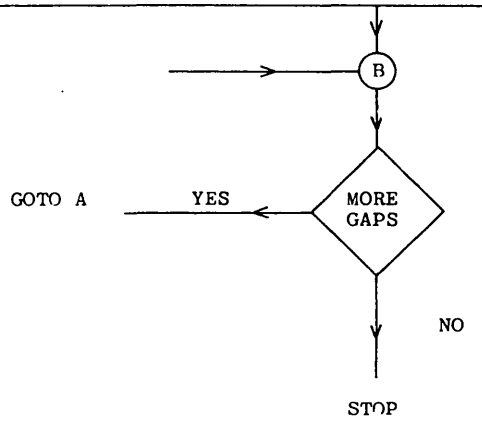

Fig.2.17a Synchronous Machine Design, Output Data

(Round Rotor)

SYNCHRONOUS MOTOR ROUND ROTOR

maximum stator conductor current density	0.8440E+01	A/mm2
maximum rotor conductor current density	0.8440E+01	A/mm2
maximum core flux density	0.1400E+01	T
synchronous speed	0.1500E+04	RPM
number of poles	4	
core length	0.4820E+00	M
stator core outside diameter	0.6000E+00	M
stator slot depth	0.5000E-01	M
slot width / slot pitch	0.5000E+00	
coil pitch / pole pitch	0.1000E+01	
stator slot packing factor	0.5000E+00	
rotor slot packing factor	0.5000E+00	
stator iron packing factor	0.1000E+01	
rotor iron packing factor	0.1000E+01	

core loss constants

kc = 0.2000E-01 x = 0.1136E+01 z = 0.1760E+01

stator conductor resistivity	0.2000E-07	OHM-M
rotor conductor resistivity	0.2000E-07	OHM-M
stator conductor density	0.8930E+04	KG/M**3
rotor conductor density	0.8930E+04	KG/M**3
iron density	0.7871E+04	KG/M**3
pole pitch	0.3142E+00	M
depth of backing core	0.5000E-01	M

slot and pitch factors

kxco = 0.1000E+01 kps = 0.1000E+01

stator conductor mass	0.1185E+03	KG
stator iron mass	0.4767E+03	KG
total machine length	0.6634E+00	M
core loss	0.1467E+04	WATTS
supply frequency	0.5000E+02	HZ
resultant air-gap flux-density	0.4950E+00	T
maximum stator surface current density	0.1055E+06	A/M
stator surface resistance end factor	0.1753E+01	
stator surface inductance end factor	0.1355E+01	
stator surface resistance	0.2804E-05	OHM
stator surface leakage inductance	0.5674E-07	H

g	drm	dr	pf	Ploss	T	Pout	effy	Mtot	Ea	ER
0.1000E-01	****	air gap too small								
0.1100E-01	****	air gap too small								
0.1200E-01	****	air gap too small								
0.1300E-01	****	air gap too small								
0.1400E-01	****	air gap too small								
0.1500E-01	****	air gap too small								
0.1600E-01	****	air gap too small								
0.1700E-01	****	air gap too small								
0.1800E-01	****	air gap too small								
0.1900E-01	****	air gap too small								
0.2000E-01	****	air gap too small								
0.2100E-01	****	air gap too small								
0.2200E-01	****	air gap too small								
0.2300E-01	****	air gap too small								
0.2400E-01	****	air gap too small								
0.2500E-01	****	air gap too small								
0.2600E-01	****	air gap too small								
0.2700E-01	0.8650E-01	0.7378E-02	0.1294E+00	0.2304E+05	0.7981E+03	0.1254E+06	0.8447E+00	0.8656E+03	0.1745E+02	0.3286E+00
0.2800E-01	0.8600E-01	0.1903E-01	0.2769E+00	0.2677E+05	0.1844E+04	0.2896E+06	0.9154E+00	0.8854E+03	0.1744E+02	0.3286E+00
0.2900E-01	0.8550E-01	0.2746E-01	0.3595E+00	0.2909E+05	0.2425E+04	0.3809E+06	0.9291E+00	0.8965E+03	0.1741E+02	0.3286E+00
0.3000E-01	0.8500E-01	0.3538E-01	0.4202E+00	0.3097E+05	0.2849E+04	0.4476E+06	0.9353E+00	0.9048E+03	0.1737E+02	0.3286E+00
0.3100E-01	0.8450E-01	0.4362E-01	0.4686E+00	0.3261E+05	0.3185E+04	0.5003E+06	0.9388E+00	0.9116E+03	0.1734E+02	0.3286E+00
0.3200E-01	0.8400E-01	0.5307E-01	0.5088E+00	0.3410E+05	0.3461F+04	0.5437E+06	0.9410E+00	0.9176E+03	0.1730E+02	0.3286E+00
0.3300E-01	0.8350E-01	0.6626E-01	0.5431E+00	0.3548E+05	0.3695E+04	0.5805E+06	0.9424E+00	0.9228E+03	0.1727E+02	0.3286E+00
0.3400E-01	****	rotor slot area required too large								
0.3500E-01	****	rotor slot area required too large								
0.3600E-01	****	rotor slot area required too large								
0.3700E-01	****	rotor slot area required too large								
0.3800E-01	****	rotor slot area required too large								
0.3900E-01	****	rotor slot area required too large								
0.4000E-01	****	rotor slot area required too large								
0.4100E-01	****	rotor slot area required too large								
0.4200E-01	****	rotor slot area required too large								
0.4300E-01	****	rotor slot area required too large								
0.4400E-01	****	rotor slot area required too large								
0.4500E-01	****	rotor slot area required too large								
0.4600E-01	****	rotor slot area required too large								
0.4700E-01	****	rotor slot area required too large								
0.4800E-01	****	rotor slot area required too large								
0.4900E-01	****	rotor slot area required too large								
0.5000E-01	****	rotor slot area required too large								
0.5100E-01	****	rotor slot area required too large								
0.5200E-01	****	rotor slot area required too large								
0.5300E-01	****	rotor slot area required too large								
0.5400E-01	****	rotor slot area required too large								
0.5500E-01	****	rotor slot area required too large								
0.5600E-01	****	rotor slot area required too large								
0.5700E-01	****	rotor slot area required too large								

Fig.2.17b Synchronous Machine Design, Output Data

(Salient Pole)

SYNCHRONOUS MOTOR SALIENT POLE

maximum stator conductor current density	0.8440E+01	A/mm2
maximum rotor conductor current density	0.8440E+01	A/mm2
maximum core flux density	0.1400E+01	T
synchronous speed	0.1500E+04	RPM
number of poles	4	
core length	0.2970E+00	M
stator core outside diameter	0.6000E+00	M
stator slot depth	0.5000E-01	M
slot width / slot pitch	0.5000E+00	
coil pitch / pole pitch	0.1000E+01	
pole arc / pole pitch	0.7000E+00	
stator slot packing factor	0.5000E+00	
rotor slot packing factor	0.5000E+00	
stator iron packing factor	0.1000E+01	
rotor iron packing factor	0.1000E+01	

core loss constants

kc = 0.2000E-01 x = 0.1136E+01 z = 0.1760E+01

stator conductor resistivity	0.2000E-07	OHM-M
rotor conductor resistivity	0.2000E-07	OHM-M
stator conductor density	0.8930E+04	KG/M**3
rotor conductor density	0.8930E+04	KG/M**3
iron density	0.7871E+04	KG/M**3
pole pitch	0.3142E+00	M
depth of backing core	0.5000E-01	M
rotor pole width	0.1000E+00	M

slot and pitch factors

kxco = 0.1000E+01 kps = 0.1000E+01

magnetising inductance d and q axis factors

cd = 0.9575E+00 cq = 0.4425E+00

stator conductor mass	0.9255E+02	KG
stator iron mass	0.2938E+03	KG
total machine length	0.4784E+00	M
core loss	0.9042E+03	WATTS
supply frequency	0.5000E+02	HZ
resultant air-gap flux-density	0.4950E+00	T
maximum stator surface current density	0.1055E+06	A/M
stator surface resistance end factor	0.2221E+01	
stator surface inductance end factor	0.1576E+01	

stator surface resistance 0.3554E-05 OHM

stator surface leakage inductance 0.6600E-07 H

g	drm	dr	pf	Ploss	T	Pout	effy	Mtot	Ea	E_R
0.1000E-02	****	air gap too small								
0.2000E-02	****	air gap too small								
0.3000E-02	****	air gap too small								
0.4000E-02	****	air gap too small								
0.5000E-02	****	air gap too small								
0.6000E-02	****	air gap too small								
0.7000E-02	****	air gap too small								
0.8000E-02	****	air gap too small								
0.9000E-02	****	air gap too small								
0.1000E-01	****	air gap too small								
0.1100E-01	****	air gap too small								
0.1200E-01	0.1173E+00	0.2104E-02	0.1583E+00	0.1626E+05	0.6113E+03	0.9602E+05	0.8552E+00	0.5364E+03	0.1777E+02	0.2040E+00
0.1300E-01	0.1163E+00	0.6123E-02	0.3821E+00	0.1734E+05	0.1602E+04	0.2516E+06	0.9355E+00	0.5422E+03	0.1771E+02	0.2036E+00
0.1400E-01	0.1153E+00	0.8708E-02	0.4910E+00	0.1799E+05	0.2075E+04	0.3259E+06	0.9477E+00	0.5454E+03	0.1762E+02	0.2032E+00
0.1500E-01	0.1143E+00	0.1094E-01	0.5648E+00	0.1853E+05	0.2389E+04	0.3753E+06	0.9529E+00	0.5478E+03	0.1754E+02	0.2029E+00
0.1600E-01	0.1133E+00	0.1302E-01	0.6197E+00	0.1901E+05	0.2619E+04	0.4113E+06	0.9558E+00	0.5499E+03	0.1746E+02	0.2025E+00
0.1700E-01	0.1123E+00	0.1502E-01	0.6625E+00	0.1945E+05	0.2795E+04	0.4390E+06	0.9576E+00	0.5517E+03	0.1739E+02	0.2021E+00
0.1800E-01	0.1113E+00	0.1700E-01	0.6970E+00	0.1986E+05	0.2934E+04	0.4608E+06	0.9587E+00	0.5534E+03	0.1733E+02	0.2017E+00
0.1900E-01	0.1103E+00	0.1898E-01	0.7255E+00	0.2026E+05	0.3047E+04	0.4786E+06	0.9594E+00	0.5549E+03	0.1727E+02	0.2013E+00
0.2000E-01	0.1093E+00	0.2098E-01	0.7493E+00	0.2064E+05	0.3140E+04	0.4932E+06	0.9598E+00	0.5564E+03	0.1722E+02	0.2010E+00
0.2100E-01	0.1083E+00	0.2302E-01	0.7696E+00	0.2101E+05	0.3218E+04	0.5055E+06	0.9601E+00	0.5578E+03	0.1717E+02	0.2006E+00
0.2200E-01	0.1073E+00	0.2510E-01	0.7870E+00	0.2137E+05	0.3284E+04	0.5158E+06	0.9602E+00	0.5591E+03	0.1712E+02	0.2002E+00
0.2300E-01	0.1063E+00	0.2725E-01	0.8021E+00	0.2172E+05	0.3341E+04	0.5247E+06	0.9603E+00	0.5603E+03	0.1708E+02	0.1998E+00
0.2400E-01	0.1053E+00	0.2948E-01	0.8154E+00	0.2206E+05	0.3389E+04	0.5324E+06	0.9602E+00	0.5615E+03	0.1704E+02	0.1994E+00
0.2500E-01	0.1043E+00	0.3180E-01	0.8271E+00	0.2240E+05	0.3432E+04	0.5391E+06	0.9601E+00	0.5627E+03	0.1701E+02	0.1991E+00
0.2600E-01	0.1033E+00	0.3422E-01	0.8375E+00	0.2273E+05	0.3469E+04	0.5450E+06	0.9600E+00	0.5639E+03	0.1697E+02	0.1987E+00
0.2700E-01	0.1023E+00	0.3677E-01	0.8468E+00	0.2305E+05	0.3502E+04	0.5501E+06	0.9598E+00	0.5650E+03	0.1694E+02	0.1983E+00
0.2800E-01	0.1013E+00	0.3947E-01	0.8551E+00	0.2338E+05	0.3532E+04	0.5547E+06	0.9596E+00	0.5661E+03	0.1691E+02	0.1979E+00
0.2900E-01	0.1003E+00	0.4235E-01	0.8626E+00	0.2370E+05	0.3558E+04	0.5588E+06	0.9593E+00	0.5671E+03	0.1689E+02	0.1975E+00
0.3000E-01	0.9929E-01	0.4544E-01	0.8694E+00	0.2401E+05	0.3581E+04	0.5625E+06	0.9591E+00	0.5682E+03	0.1686E+02	0.1972E+00
0.3100E-01	0.9829E-01	0.4878E-01	0.8756E+00	0.2432E+05	0.3602E+04	0.5658E+06	0.9588E+00	0.5692E+03	0.1684E+02	0.1968E+00
0.3200E-01	0.9729E-01	0.5246E-01	0.8813E+00	0.2463E+05	0.3621E+04	0.5687E+06	0.9585E+00	0.5702E+03	0.1682E+02	0.1964E+00
0.3300E-01	0.9629E-01	0.5657E-01	0.8865E+00	0.2494E+05	0.3638E+04	0.5714E+06	0.9582E+00	0.5712E+03	0.1679E+02	0.1960E+00
0.3400E-01	0.9529E-01	0.6127E-01	0.8912E+00	0.2524E+05	0.3653E+04	0.5739E+06	0.9579E+00	0.5721E+03	0.1677E+02	0.1957E+00
0.3500E-01	0.9429E-01	0.6685E-01	0.8956E+00	0.2554E+05	0.3668E+04	0.5761E+06	0.9575E+00	0.5731E+03	0.1676E+02	0.1953E+00
0.3600E-01	0.9329E-01	0.7397E-01	0.8997E+00	0.2584E+05	0.3681E+04	0.5782E+06	0.9572E+00	0.5740E+03	0.1674E+02	0.1949E+00
0.3700E-01	0.9229E-01	0.8505E-01	0.9034E+00	0.2614E+05	0.3693E+04	0.5800E+06	0.9569E+00	0.5749E+03	0.1672E+02	0.1945E+00
0.3800E-01	****	rotor conductor area required too large								
0.3900E-01	****	rotor conductor area required too large								
0.4000E-01	****	rotor conductor area required too large								
0.4100E-01	****	rotor conductor area required too large								
0.4200E-01	****	rotor conductor area required too large								
0.4300E-01	****	rotor conductor area required too large								
0.4400E-01	****	rotor conductor area required too large								
0.4500E-01	****	rotor conductor area required too large								
0.4600E-01	****	rotor conductor area required too large								
0.4700E-01	****	rotor conductor area required too large								
0.4800E-01	****	rotor conductor area required too large								
0.4900E-01	****	rotor conductor area required too large								
0.5000E-01	****	rotor conductor area required too large								

Fig. 2.18 Synchronous Machine Performance

A simplified flow chart

SEt MACHINE PARAMETERS

p	pole pairs	
d_o	stator core outside diameter	m
d_s	stator slot depth	m
w_c	core length	m
g	air gap length	m
β	slot width/slot pitch	
γ	coil pitch/pole pitch	
α	pole arc/pole pitch	
k_{PFS}	stator slot packing factor	
k_{PFR}	rotor slot packing factor	
k_{iS}	stator iron packing factor	
k_{iR}	rotor iron packing factor	
$K_{c',x,z}$	core loss constants	
ρ_{CS}	stator conductor resistivity	ohm-m
ρ_{CR}	rotor conductor resistivity	ohm-m
δ_S	stator conductor density	kg/m^3
δ_R	rotor conductor density	kg/m^3
δ_i	iron density	kg/m^3
I_S	1 - for given rotor slot depth	
	0 - to use maximum slot depth	

PRINT MACHINE PARAMETERS

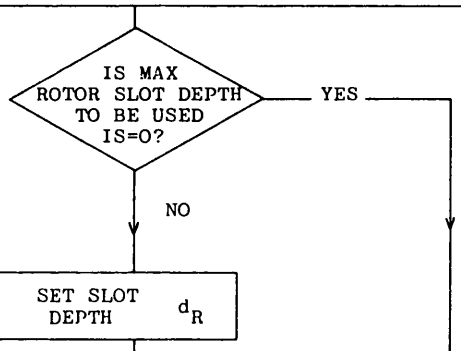

CALCULATE

τ_p	pole pitch (2.19)
d_c	stator backing core depth (2.18)
w_p	pole body width $2d_c$**
k_{xco}, k_{ps}	slot permeance correction and pitch factors (A2.7),(A2.1)
C_d, C_q	magnetic inductance d and q axis factors (A2.30),(A2.31)**
R_o	rotor radius (2.22a)
d_{RM}	max slot depth (2.28)*,(2.22)**
w_{TOT}	total machine length (core + end windings) (A2.3)

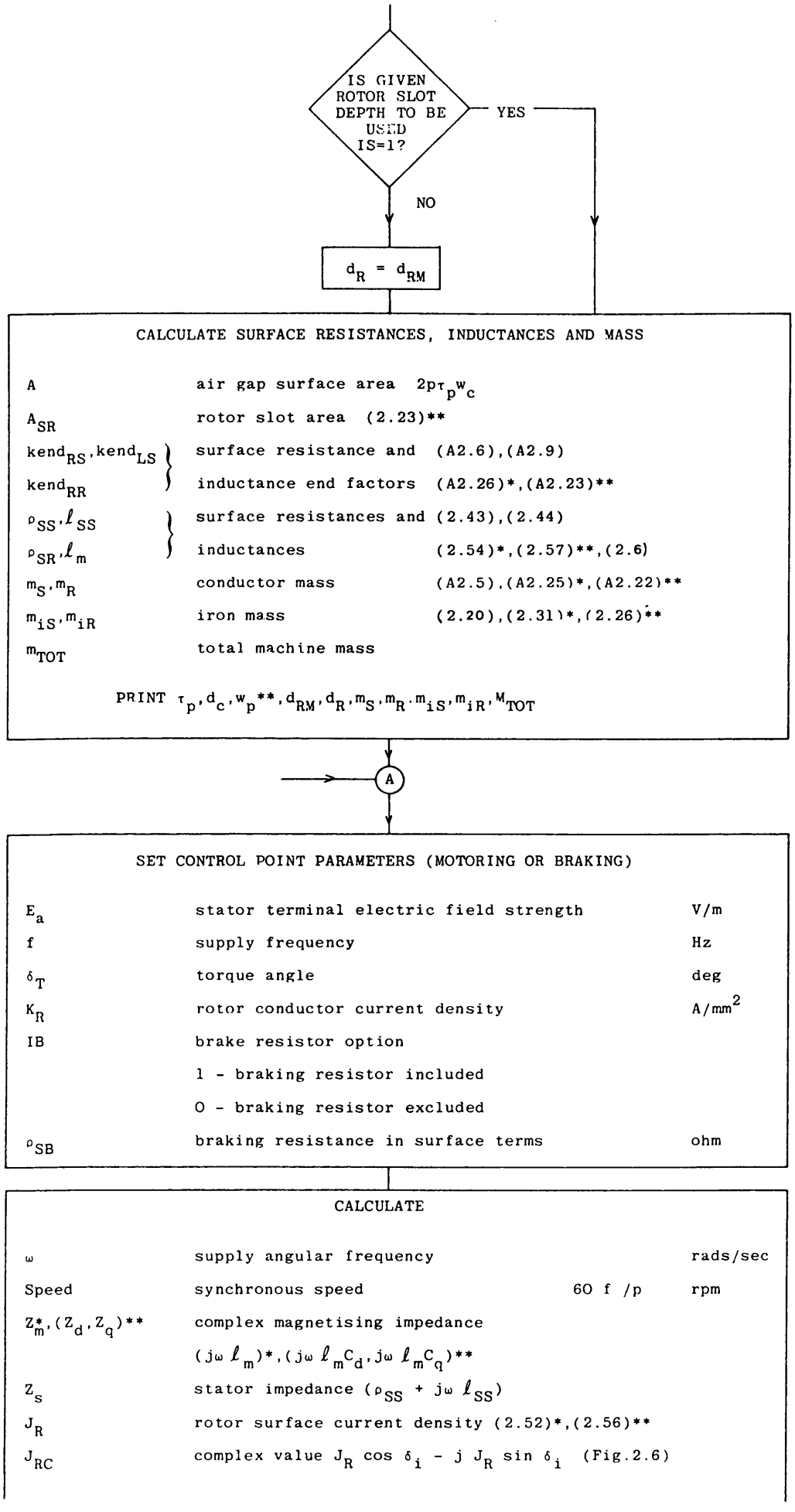
IS GIVEN ROTOR SLOT DEPTH TO BE USED IS=1?
YES
NO
$d_R = d_{RM}$
CALCULATE SURFACE RESISTANCES, INDUCTANCES AND MASS
A air gap surface area $2p\tau_p w_c$
A_{SR} rotor slot area (2.23)**
$kend_{RS}, kend_{LS}$ surface resistance and (A2.6),(A2.9)
$kend_{RR}$ inductance end factors (A2.26)*,(A2.23)**
ρ_{SS}, ℓ_{SS} surface resistances and (2.43),(2.44)
ρ_{SR}, ℓ_m inductances (2.54)*,(2.57)**,(2.6)
m_S, m_R conductor mass (A2.5),(A2.25)*,(A2.22)**
m_{iS}, m_{iR} iron mass (2.20),(2.31)*,(2.26)**
m_{TOT} total machine mass
PRINT τ_p, d_c, w_p**, $d_{RM}, d_R, m_S, m_R, m_{iS}, m_{iR}, M_{TOT}$
A
SET CONTROL POINT PARAMETERS (MOTORING OR BRAKING)
E_a stator terminal electric field strength V/m
f supply frequency Hz
δ_T torque angle deg
K_R rotor conductor current density A/mm^2
IB brake resistor option
1 - braking resistor included
0 - braking resistor excluded
ρ_{SB} braking resistance in surface terms ohm
CALCULATE
ω supply angular frequency rads/sec
Speed synchronous speed 60 f /p rpm
$Z_m^*, (Z_d, Z_q)$** complex magnetising impedance
$(j\omega \ell_m)^*, (j\omega \ell_m C_d, j\omega \ell_m C_q)$**
Z_s stator impedance $(\rho_{SS} + j\omega \ell_{SS})$
J_R rotor surface current density (2.52)*,(2.56)**
J_{RC} complex value $J_R \cos \delta_i - j J_R \sin \delta_i$ (Fig.2.6)

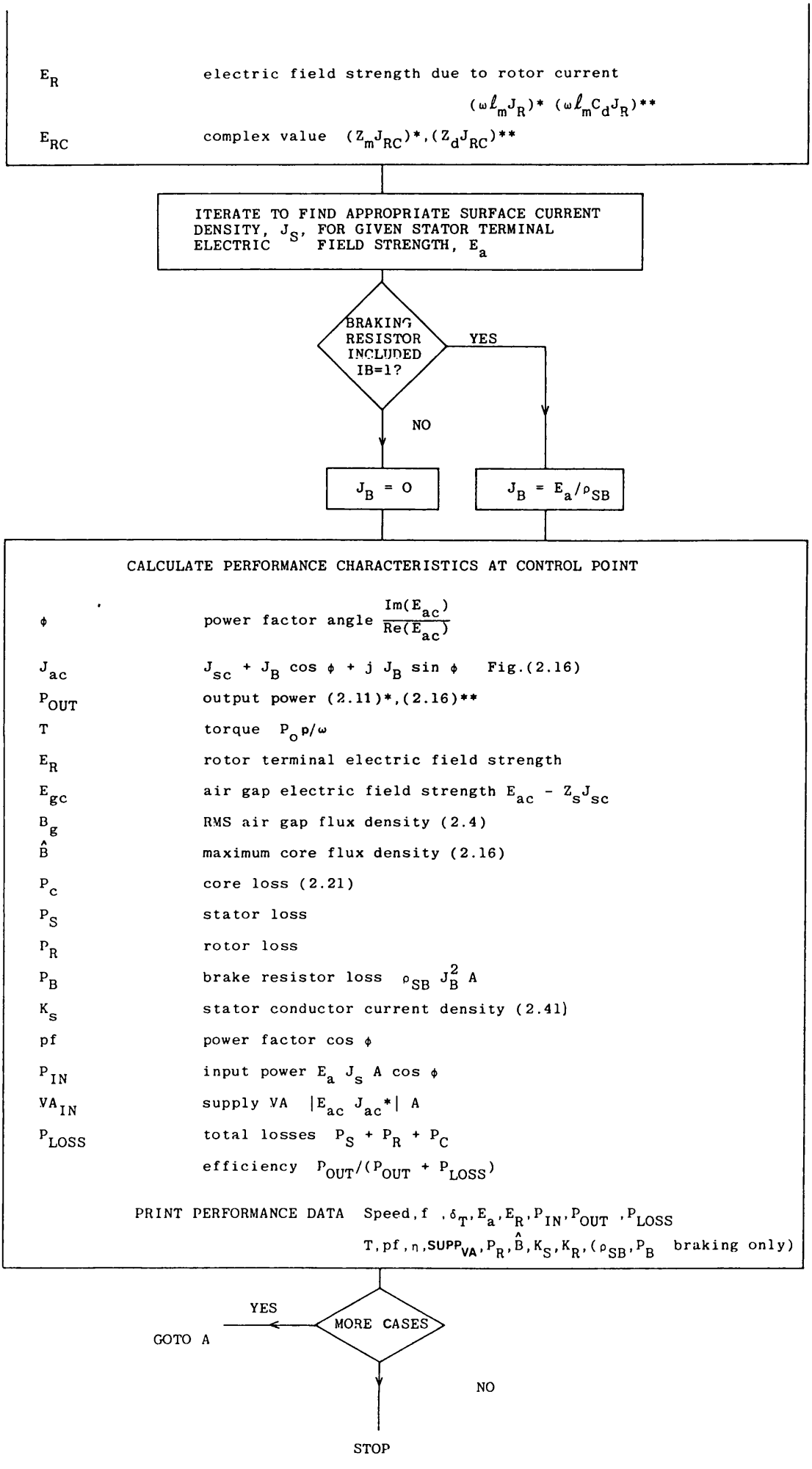
E_R electric field strength due to rotor current $(\omega \ell_m J_R)^*$ $(\omega \ell_m C_d J_R)^{**}$
E_{RC} complex value $(Z_m J_{RC})^*, (Z_d J_{RC})^{**}$
ITERATE TO FIND APPROPRIATE SURFACE CURRENT DENSITY, J_S, FOR GIVEN STATOR TERMINAL ELECTRIC FIELD STRENGTH, E_a
BRAKING RESISTOR INCLUDED IB=1?
YES
NO
$J_B = 0$
$J_B = E_a/\rho_{SB}$
CALCULATE PERFORMANCE CHARACTERISTICS AT CONTROL POINT
ϕ power factor angle $\frac{Im(E_{ac})}{Re(E_{ac})}$
J_{ac} $J_{sc} + J_B \cos\phi + j J_B \sin\phi$ Fig.(2.16)
P_{OUT} output power (2.11)*,(2.16)**
T torque $P_o p/\omega$
E_R rotor terminal electric field strength
E_{gc} air gap electric field strength $E_{ac} - Z_s J_{sc}$
B_g RMS air gap flux density (2.4)
$\hat{B}$ maximum core flux density (2.16)
P_c core loss (2.21)
P_S stator loss
P_R rotor loss
P_B brake resistor loss $\rho_{SB} J_B^2 A$
K_s stator conductor current density (2.41)
pf power factor cos ϕ
P_{IN} input power $E_a J_s A \cos\phi$
VA_{IN} supply VA $|E_{ac} J_{ac}^*| A$
P_{LOSS} total losses $P_S + P_R + P_C$
efficiency $P_{OUT}/(P_{OUT} + P_{LOSS})$
PRINT PERFORMANCE DATA Speed, f, δ_T, E_a, E_R, P_{IN}, P_{OUT}, P_{LOSS}
T, pf, η, $SUPP_{VA}$, P_R, $\hat{B}$, K_S, K_R, (ρ_{SB}, P_B braking only)
YES
MORE CASES
GOTO A
NO
STOP

2.7 APPENDICES

2.7.1 List of symbols used in the machine design process

Final subscript S or R denotes stator or rotor quantity.

CONSTANTS and FACTORS

p	number of pole pairs
k_w	winding factor
k_p	coil pitch factor
k_{xt}, k_{xco}	slot permeance correction factors
k_{sc}	squirrel-cage end ring permeance correction factor
k_{endR}	surface resistance end factor
k_{endL}	surface inductance end factor
k_{pF}	slot packing factor
k_i	iron packing factor
k_g	tooth flux fringing factor
k_v	vent flux fringing factor
k_{VL}	vent flux fringing factor for slot leakage
n_v	number of vents
K_c, x, z	constants for core loss calculation
δ	conductor density
δ_i	iron density
δ_{er}	squirrel cage end ring density
k_d	distribution factor
μ_o	magnetic constant $4\pi \times 10^{-7}$ H/m

DIMENSIONS

τ	slot pitch
τ_p	pole pitch
τ_c	coil pitch
τ_a	pole arc
g	air gap length
d	slot depth
w	slot width
w_t	tooth width
w_l	slot opening (semi-closed slots)
w_p	pole width (salient rotor)
ℓ_{oh}	slot conductor overhang
A_s	slot area
w_v	cooling vent width
τ_v	vent pitch
d_c	stator core depth
d_o	stator core outside diameter
θ	angle between core and end winding conductor for diamond-ended coils
D_{er}	mean diameter of squirrel cage end ring
A_{er}	cross-sectional area of end ring
t_{er}	thickness of end ring
w_{er}	width of end ring
ℓ_{mt}	mean length of coil turn
w_c	core length
θ_p	half pole angle (salient rotor)
m	conductor mass
m_i	iron mass
A	air gap surface area

ELECTRICAL AND MAGNETIC

$\hat{B}$	maximum core flux density	T
B_g	RMS air-gap flux density	T
ρ_C	conductor resistivity	ΩM
ρ_S	conductor surface resistance	Ω
ℓ_S	surface leakage inductance	H
ℓ_m	surface magnetising inductance	H
R	phase resistance	Ω
L	phase leakage inductance	H
L_m	phase magnetising inductance	H
β	slot width/slot pitch	
γ	coil pitch/pole pitch	
α	pole arc/pole pitch	
z	series conductors per slot	
q	slots per pole phase	
λ	specific permeance	
K	conductor current density	A/mm^2
J	surface current density	A/M
V	terminal voltage	V
E	electric field strength	V/M
P	conductor loss	W
P_C	core loss	W
P_{OUT}	output power	W
T	torque	Nm
δ_T	torque angle	degree
ω	supply angular frequency	rad/sec
ω_R	angular frequency of rotor currents	rad/sec
σ	slip	pu
Re	indicates the complex real part	

*	indicates the complex conjugate	
e	instantaneous electric field strength	V/m
b	instantaneous magnetic flux density	T
j	instantaneous surface current density	A/m
M	magneto-motive force	AT
I	RMS phase current	A
Q	total number of slots	
f	supply frequency	Hz
f_2	rotor frequency	Hz

2.7.2 Machine parameters

Formulae for machine winding resistances, inductances and masses are derived in this section. Most of the expressions are based on those given in references 33,34. Following the derivation of each formula, a simplified form is given which is more suitable for initial design use.

1) Magnetising inductance

The magnetising inductance seen by one phase of a balanced three-phase winding driving flux across a uniform gap, Fig(A2.1a), is:

$$L_m = \frac{\mu_o 6(z_s q_s k_{ws})^2 \tau_p w_c p}{\pi^2 k_v k_g g}$$

Fringing of the tooth flux is accounted for by a factor k_g. For one slotted member:

$$k_g = \frac{\tau_s(5g + w_s)}{\tau_s(5g + w_s) - w_s^2} \qquad \text{(Open slots)}$$

$$k_g = \frac{\tau_s(4.4g + 0.75w_1)}{\tau_s(4.4g + 0.75w_1) - w_1^2} \qquad \text{(Semi-closed slots)}$$

If both the stator and rotor core are slotted then k_g is evaluated for both, and their resultant is given by

$$k_g = k_{gS} \times k_{gR}$$

A factor k_v takes account of flux fringing at radial vents, Fig. A2.1b. For a vented member

$$k_v = \frac{\tau_v(5g + w_v)}{\tau_v(5g + w_v) - w_v^2}$$

where the vent pitch is:

$$\tau_v = \frac{w_c + w_v}{n_v + 1}$$

If both the stator and rotor contain cooling vents, then k_v is evaluated for both and the resultant is given by:

$$k_v = k_{vS} \times k_{vR}$$

A simplified form of the expression for L_m can be obtained by assuming that $k_v = k_g = 1$. Also, since the distribution factor will be close to unity, the winding factor can be replaced by the pitch factor:

$$k_{ps} = \sin \frac{\gamma \pi}{2} \qquad \text{(A2.1)}$$

where γ is the ratio of coil pitch to pole pitch

The final form is then,

$$L_m = \frac{6(z_s q_s k_{ps})^2 w_{cp}}{\tau_p} \frac{\mu_o \tau_p^2}{g\pi^2} \qquad \text{(A2.2)}$$

2) Stator winding resistance and mass

The phase resistance and total mass of the three phase stator winding is given by the expressions:

$$R_s = \frac{\rho_{cs} \ell_{mts} z_s^2 q_s p}{k_{pFS} A_{SS}}$$

$$m_s = 3 \ell_{mts} \delta_s q_s p k_{pFS} A_{SS}$$

Each stator turn has a mean length, the dimensions of which are defined in Fig. A2.2a. of

$$\ell_{mts} = 2(w_c + 2\ell_{ohs} + \frac{2\ell_{oh}}{\sin\theta} + 1.6\,\pi d_s)$$

These formulae can be usefully simplified by ignoring the detail of the nose and slot conductor overhang. If a minimum end-turn configuration is assumed, Fig. A2.2b, then

$$\sin\theta = \beta = \frac{w_s}{\tau_s}$$

and $$\ell_{oh} = \frac{\beta\tau_c}{2}\,\frac{1}{\sqrt{1-\beta^2}} \qquad \text{(A2.3)}$$

If the slot is assumed to be rectangular, then the slot area $A_{SS} = w_s d_s$, and the final expression for the phase resistance is,

$$R_s = \frac{6\rho_{cs} z_s^2 q_s^2 p w_c k_{endRS}}{k_{pFS} d_s \beta\tau_p} \qquad \text{(A2.4)}$$

and the conductor mass,

$$m_s = 2\delta_s p k_{pFS} \beta\tau_p d_s w_c k_{endRS} \qquad \text{(A2.5)}$$

where $$k_{endRS} = 1 + \frac{2\ell_{oh}}{\beta w_c} \qquad \text{(A2.6)}$$

3) Stator winding leakage inductance

Stator winding phase leakage is given by

$$L_s = \mu_o z_s^2 2pq_s \frac{w_c}{k_{VL}} (\lambda_s + \lambda_e)$$

The factor k_{VL} accounts for the fringing of leakage flux due to the presence of radial vents and is given by:

$$k_{VL} = \frac{\tau_v(5w_1 + 2w_v)}{\tau_v(5w_1 + 2w_v) - 2w_v^2}$$

$$\tau_v = \frac{w_c + w_v}{n_v + 1}$$

End-winding specific permeance can be estimated from (Fig. A2.2a)

$$\lambda_e = \frac{1.2\, q_s k_{VL} k_{ws}^2 (\ell_{ohs} + \frac{1}{2}\ell_{oh})}{w_c}$$

The slot specific permeance is given by

$$\lambda_s = k_{xt}\lambda_{st} + k_{xco}\lambda_{sco}$$

where

λ_{st} = specific permeance of the slot above the conductor

λ_{sco} = specific permeance of the slot containing conductor

} Fig.A2.3

For an open slot $\lambda_{st} = \frac{d_3}{w_s}$ and $\lambda_{sco} = \frac{d_1}{3w_s}$

and for a semi-closed slot $\lambda_{st} = \frac{d_3}{w_s} + \frac{2d_4}{w_1 + w_s} + \frac{d_5}{w_1}$

and $\lambda_{sco} = \frac{d_1}{3w_s}$

The factors k_{xt} and k_{xco} correct for short-pitching of the coils and are defined by:

for $\frac{2}{3} < \frac{\tau_c}{\tau_p} < 1$ and for $\frac{1}{2} < \frac{\tau_c}{\tau_p} < \frac{2}{3}$

$$k_{xt} = \frac{1}{4}\left[\frac{3\tau_c}{\tau_p} + 1\right] \qquad k_{xt} = \frac{1}{4}\left[\frac{6\tau_c}{\tau_p} + 1\right] \qquad \text{(A2.7)}$$

$$k_{xco} = \frac{1}{16}\left[\frac{9\tau_c}{\tau_p} + 7\right] \qquad k_{xco} = \frac{1}{16}\left[\frac{18\tau_c}{\tau_p} + 7\right]$$

The following assumptions are made to obtain a simplified expression for the phase leakage inductance

i) $k_{VL} = 1$

ii) the slot conductor overhang (ℓ_{ohs}) is ignored

iii) the winding has a minimum end turn configuration so that

$$\ell_{oh} = \frac{\beta\tau_c}{2}\,\frac{1}{\sqrt{1-\beta^2}} \quad \text{where} \quad \beta = \frac{w_s}{\tau_s}$$

iv) the slot is rectangular and completely filled

$$\text{i.e.} \quad \lambda_s = \frac{d_s}{3w_s}\,k_{xco}$$

v) the distribution factor is close to unity

This gives (using $3q_s\tau_s = \tau_p$)

$$L_s = \frac{6(Z_s q_s)^2 w_c p}{\tau_p}\,\frac{\mu_o k_{xco} d_s}{3\beta}\,k_{endLS} \qquad \text{(A2.8)}$$

$$\text{where} \quad k_{endLS} = 1 + \frac{0.6k_{ps}^2 l_{oh}\tau_p\beta}{w_c k_{xco} d_s} \qquad \text{(A2.9)}$$

4) Squirrel cage phase resistance and mass

Fig. A2.4 shows the relationship between squirrel cage end-ring and bar currents. From the geometry of the diagram

$$I_e = \frac{I_R}{2 \sin \frac{\theta_{se}}{2}} \qquad (A2.10)$$

where θ_{se} is the slot angle in electrical degrees, i.e.

$$\theta_{se} = \frac{2\pi}{6q_R}$$

The resistance of an individual rotor bar is:

$$r_b = \frac{\rho_{cR}(w_c + 2\, l_{ohR})}{k_{pFR}\, A_{SR}} \qquad (A2.11)$$

For that part of the end ring between adjacent slots (Fig. A2.5)

$$r_e = \frac{\rho_{er}\pi D_{er}}{A_{er} 6 P_{qR}} \qquad (A2.12)$$

The resistance of the winding can now be found by equating losses i.e.

$$I_R^2 R_R = 2pq_R(I_R^2 r_b + 2I_e^2 r_e)$$

Using equations (A2.10), (A2.11) and (A2.12) and assuming that θ_{se} is small gives the result:

$$R_R = 2pq_R \left[\frac{\rho_{cR}(w_c + 2l_{ohR})}{k_{pFR}\, A_{SR}} + \frac{\rho_{er} D_{er} 3q_R}{\pi A_{er} p}\right] \qquad (A2.13)$$

The winding has a total of 6 $q_R p$ rotor bars and 12 $q_R p$ end-ring bars. The total conductor mass in the rotor is therefore:

$$m_R = 6pq_R k_{pFR} A_{SR}(w_c + 2\ell_{ohR})\delta_R + 2\pi D_{er} A_{er} \delta_{er} \qquad (A2.14)$$

Simpler forms of equations (A2.13) and (A2.14) can be obtained by making the following assumptions:

i) ℓ_{ohR} is negligible

ii) bars and end rings are made of the same material

iii) the peak current density in the end-rings is equal to that in the bars, i.e.

$$A_{er} = \frac{k_{PFR}A_{SR}3q_R}{\pi}$$

iv) the number of rotor slots is equal to the number of stator slots

v) the length of an end-ring segment is equal to the slot pitch, i.e.

$$\tau_s = \frac{D_{er}\pi}{6q_sp}$$

With these simplifications, equations (A2.13) and (A2.14) become

$$R_R = \frac{6q_s^2w_cp}{\tau_p} \frac{\rho_{cR}\tau_s}{k_{PFR}A_{SR}} k_{endRR}$$

$$m_R = 2\delta_R p k_{PFR} \frac{\tau_p}{\tau_s} A_{SR}w_c k_{endRR}$$

where $k_{endRR} = 1 + \frac{2\tau_p}{\pi w_c}$ (A2.15)

Consideration of the rotor slot geometry (2.3.4) shows that, for a tapered slot with parallel teeth, the slot area

$$A_{SR} = w_s d_R \left[1 - \frac{d_R}{2d_{RM}}\right]$$

With an effective slot depth d_R, (equation 2.30), defined as

$$d'_R = d_R \left[1 - \frac{d_R}{2d_{RM}}\right]$$

then the above equation becomes

$$R_R = \frac{6q_s w_{cP}}{\tau_p} \frac{\rho_{cR}}{k_{PFR} d'_R \beta} k_{endRR} \qquad (A2.16)$$

$$m_R = 2\delta_R p k_{PFR} \beta \tau_p d'_R w_c k_{endRR} \qquad (A2.17)$$

5) Squirrel cage phase leakage inductance

By considering the bar and end ring currents, as in section 4, and also by equating VAr, the phase leakage inductance is found to be

$$L_R = 2p q_R \mu_o \frac{w_c}{k_{VL}} (\lambda_s + \lambda_e)$$

In this expression k_{VL} can be found by the methods discussed in section 3. Formulae for slot specific permeance (λ_s) are also given in section 3 but in this case the correction factors k_{xco} and k_{xt} are set to unity.

The end-ring specific permeance is given by:

$$\lambda_e = \frac{k_{VL} q_R}{w_c} \left[1.32\ l_{ohR} + \frac{k_{sc} D_{er} \pi}{2p}\right]$$

$$\left.\begin{array}{l} \text{where } k_{sc} = 0.36 \text{ for } p = 1 \\ \text{and } k_{sc} = 0.18 \text{ for } p > 1 \end{array}\right\} \qquad (A2.18)$$

A simplified expression for the slot leakage inductance can be obtained with the following assumptions:

i) $k_{VL} = 1$

ii) $q_R = q_S$

iii) ignoring the slot conductor overhang (ℓ_{ohR})

iv) the length of each end-ring segment is equal to the slot pitch, i.e.

$$\tau_s = \frac{D_{er}\pi}{6q_{sp}}$$

It is also assumed that for the purposes of slot leakage, the tapered slot used can be considered to be rectangular[33], i.e.

$$\lambda_s = \frac{d_R}{3w_s}$$

With these simplifications, the slot leakage inductance is given by the expression

$$L_R = \frac{6q_s^2 w_{cp}}{\tau_p} \frac{\mu_o d_R}{3\beta} k_{endLR} \qquad \text{(A2.19)}$$

where $k_{endLR} = 1 + \frac{k_{sc}\beta\tau_p^2}{d_R w_c}$ (A2.20)

6) Salient pole field winding resistance and mass

The resistance of a salient pole winding is

$$R_R = \frac{\rho_{cR} l_{mtR} z_{Rp}^2}{k_{PFR} A_{SR}}$$

and its mass is

$$m_R = \ell_{mtR}\delta_{Rp}k_{PFR}A_{SR}$$

Because of the complex slot geometry it is not possible to express A_{SR} in terms of effective widths and depths. The only simplification that can be made in this case is to use the formula for turn length (2.58) from (section 2.4.4). In this case

$$R_R = \frac{2z_{Rp}^2 w_c}{\tau_p} \frac{\rho_{cR}\tau_p}{k_{pfR}A_{SR}} k_{endRR} \qquad \text{(A2.21)}$$

$$m_R = 2\delta_R p k_{pfR} A_{SR} w_c k_{endRR} \qquad \text{(A2.22)}$$

where $k_{endRR} = 1 + \frac{w_p}{w_c} + \frac{4d_{RM}}{3w_c} \sin\theta_p$ (A2.23)

and $d_{RM} = R_o - \frac{w_p}{2 \sin\theta_p}$ where $\theta_p = \frac{\pi}{2p}$

7) Round-rotor field winding resistance and mass

The formulae for the round rotor case can be obtained from those of the salient case by considering z_R slot conductors to be distributed into q_R slots. This gives.

$$R_R = \frac{\rho_{cR} l_{mtR} q_R z_{Rp}^2}{k_{pfR} A_{SR}}$$

$$m_R = l_{mtR}\delta_R q_R p k_{pfR} A_{SR}$$

Simplified forms are obtained, by making the following assumptions

i) coils have diamond ends so that equation A2.3 is appropriate. The noses and conductor overhangs are ignored and a minimum end-turn configuration is assumed.

ii) q_R slots span one pole.

iii) $\tau_R = \tau_S$.

iv) slot area $A_{SR} = w_S d_R'$

This gives:

$$R_R = \frac{2(3q_S z_R)^2 P w_C}{\tau_p} \frac{\rho_{CR}}{k_{PFR} d_R' \beta} k_{endRR} \qquad \text{(A2.24)}$$

$$m_R = 2\delta_R p k_{PFR} \beta \tau_p d_R' w_C k_{endRR} \qquad \text{(A2.25)}$$

where $k_{endRR} = 1 + \frac{2\ell_{oh}}{\beta \omega_C}$ (A2.26)

8) Referred quantities

For the inverter fed machine performance predictions of Chapter 4, the referred values of the rotor quantities are required.

For the squirrel cage induction machine, the turns ratio is given by

$$n = \frac{z_S q_S k_{ws}}{q_R} \qquad \text{(A2.27)}$$

For the round rotor synchronous machine:

$$n = \frac{\sqrt{3}\ z_S\ q_S\ k_{ws}}{\sqrt{2}\ z_R\ q_R\ k_{wR}} \qquad \text{(A2.28)}$$

and for the salient pole case:

$$n = \frac{\sqrt{3}\ z_S\ q_S\ k_{ws}}{\sqrt{2}\ z_R} \qquad \text{(A2.29)}$$

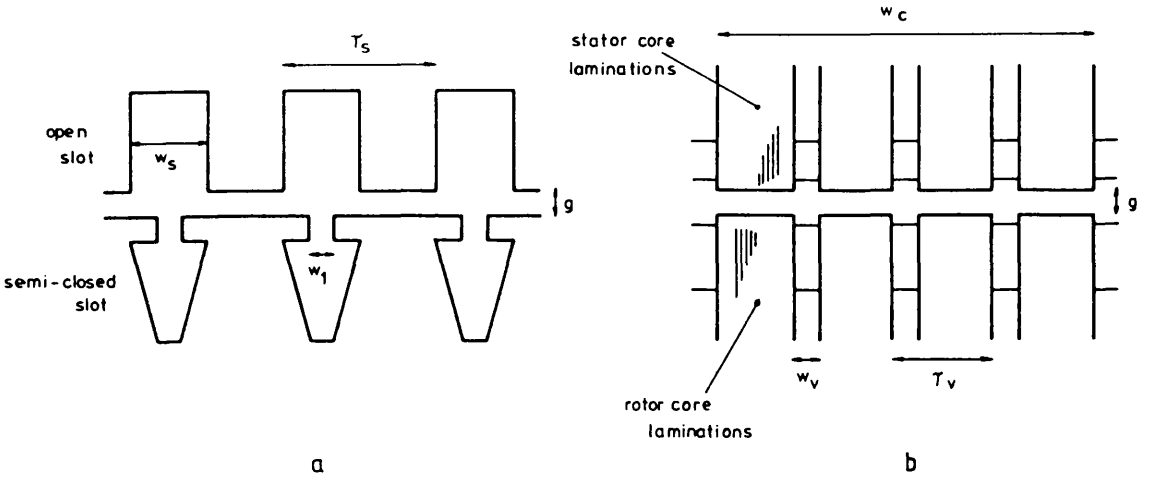

Fig A 2.1 Dimensions for slot and vent fringing factors

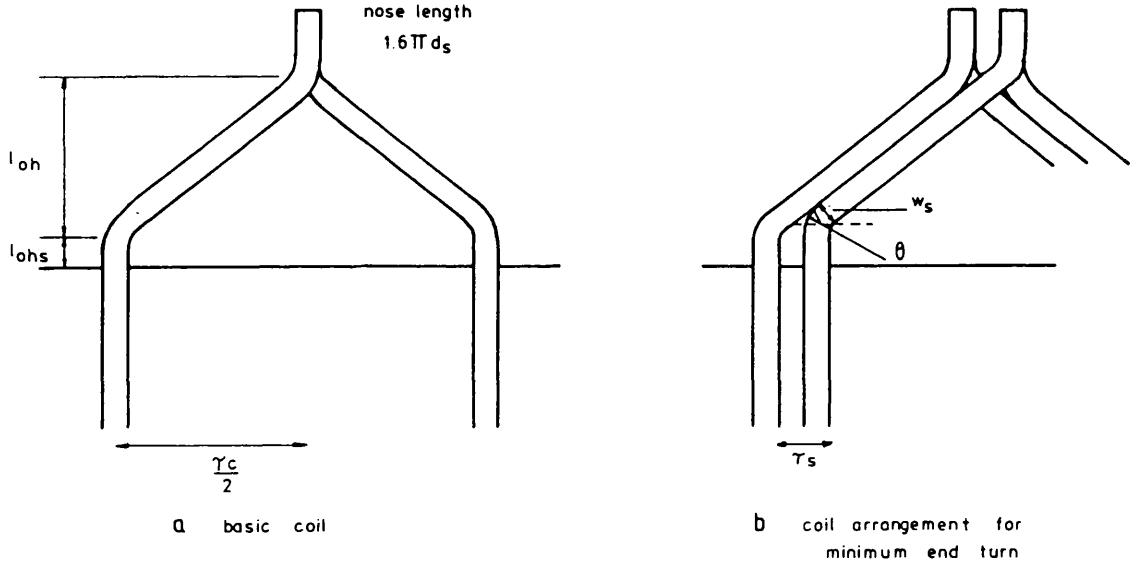

Fig A 2.2 Dimensions for the calculation of mean turn length

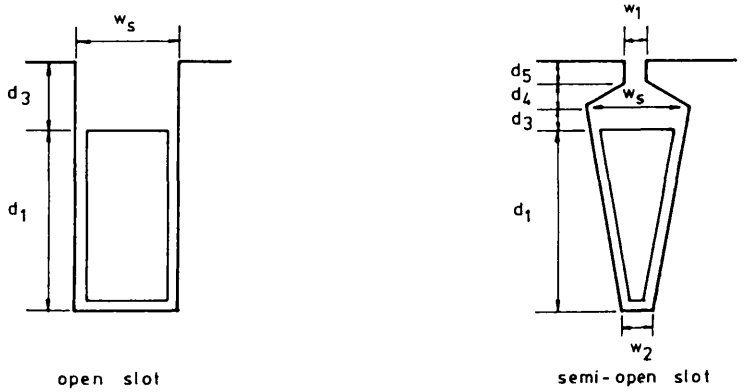

Fig A 2.3 Slot dimensions for the calculation of specific permeance

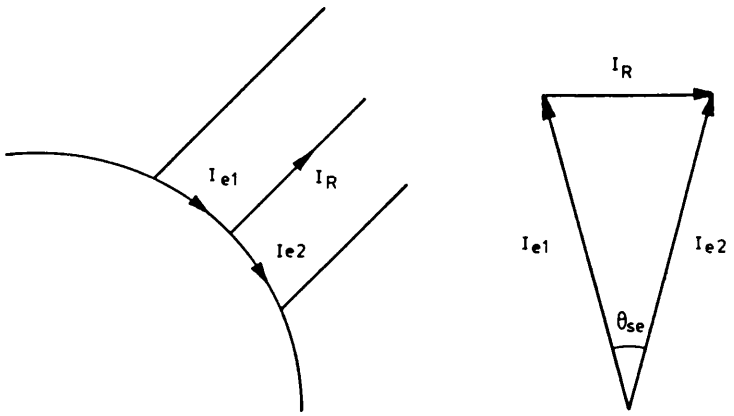

Fig A 2.4 Squirrel Cage rotor winding currents

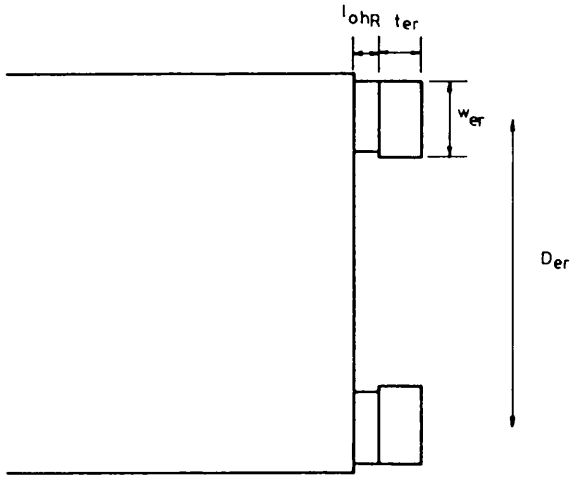

Fig A 2.5 Dimensions of Squirrel Cage end ring

2.7.3 Calculation of the salient pole factors C_d and C_q

The salient rotor gives rise to non sinusoidal air-gap flux components. However the sinusoidally distributed winding conductors will respond only to flux density components having the same pole pitch. This means that only the fundamental components need be considered and these are accounted for by the factors C_d and C_q.

The field winding produces a flux density distribution as shown in Fig. A2.6. The amplitude of the fundamental component is given by

$$B_R = \bar{B}_R \frac{1}{\pi} (\alpha\pi + \sin \alpha\pi)$$

where $\bar{B}_R$ is the amplitude produced in a uniform gap of length, g, and α is the ratio of pole arc to pole pitch. This expression can be written as

$$B_R = \bar{B}_R C_d$$

where $C_d = \frac{1}{\pi} (\alpha\pi + \sin \alpha\pi)$ (A2.30)

The resultant armature flux is considered to be due to two separate components along the two axes of symmetry of the rotor. The amplitude of the component which is centred on the poles, Fig. A2.6b, is

$$B_d = \bar{B}_s C_d$$

and at the centre of the interpolar space, Fig. A2.6c , the corresponding component is

$$B_q = \bar{B}_s C_q$$

where $C_q = \frac{1}{\pi} (\alpha\pi - \sin \alpha\pi)$ (A2.31)

and $\bar{B}_s$ is the amplitude of the air-gap flux density that would be produced by the stator winding in a uniform gap of length, g.

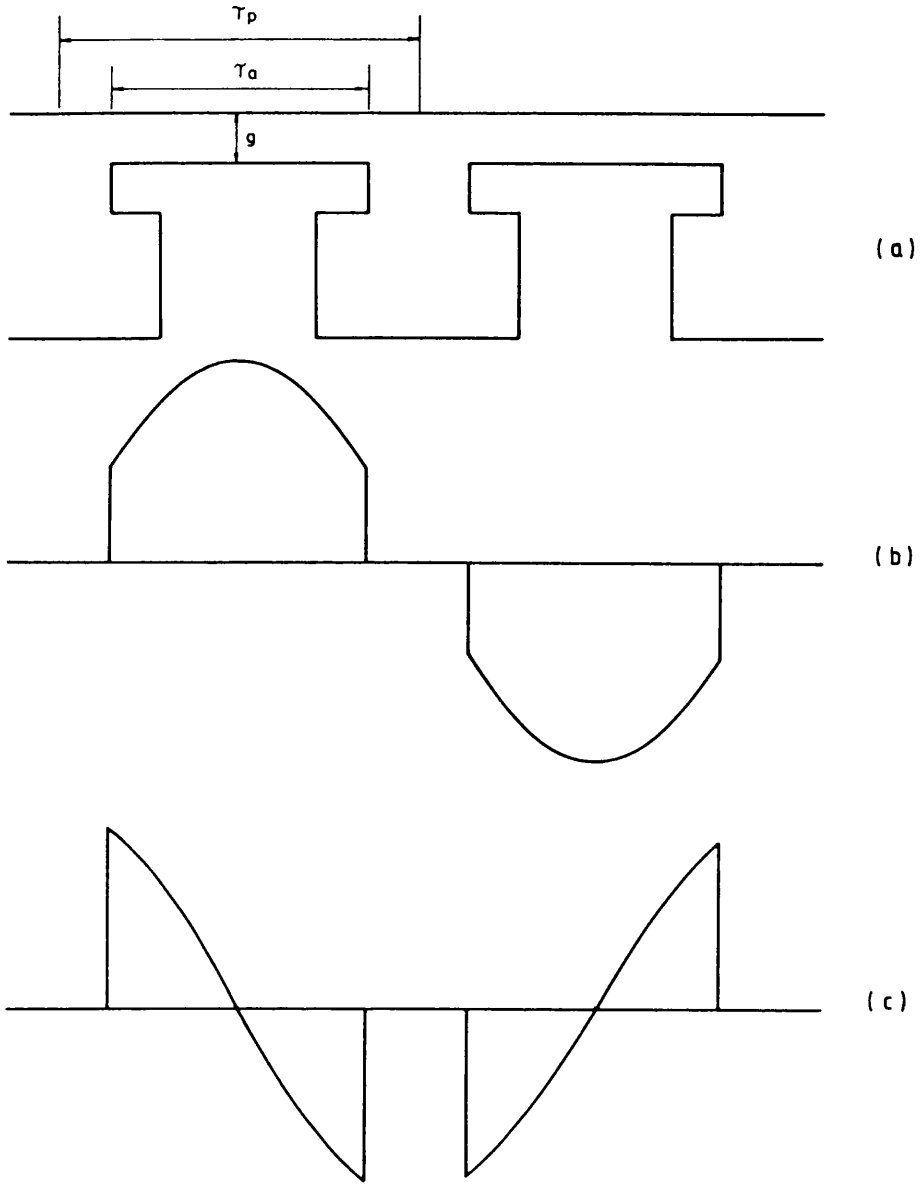

(a) pole geometry

(b) d - axis flux distribution

(c) q - axis flux distribution

Fig A2.6 Pole geometry for the calculation of the factors Cd and Cq

CHAPTER 3

AC TRACTION MOTOR DESIGN AND PERFORMANCE PREDICTIONS FOR A HIGH SPEED DIESEL LOCOMOTIVE

3.1 Introduction

Traction motors used by British Rail range in output from less than 100KW on some multiple units, up to almost 1MW on main line locomotives. Without exception they are DC machines, seperately excited, series or compound wound. These motors are operated at a constant torque from standstill up to a knee-point speed, thereafter the torque falls rapidly with increasing speed as the air gap flux density decreases.

The smaller DC motors are usually axle hung via single reduction gearing. Larger and heavier motors cannot be axle hung as the unsprung mass would be excessive. The larger motors are therefore bogie mounted and drive the axle through gearing and a flexible coupling. For high speed applications such as the Advanced Passenger Train [44], the drive to each powered axle is through a mechanical transmission from the traction motors, which are mounted in the power car body, Fig 3.1. Power is transmitted via a body mounted transfer gearbox, cardan shaft, final drive gearbox, which is fully suspended on the bogie frame, and a flexible quill to the axle.

Replacement of the DC motor with an AC induction or synchronous machine has many advantages.

Reduced weight - The removal of the commutator saves weight directly and also allows the motor to run at higher speeds to give a smaller machine for a given power output.

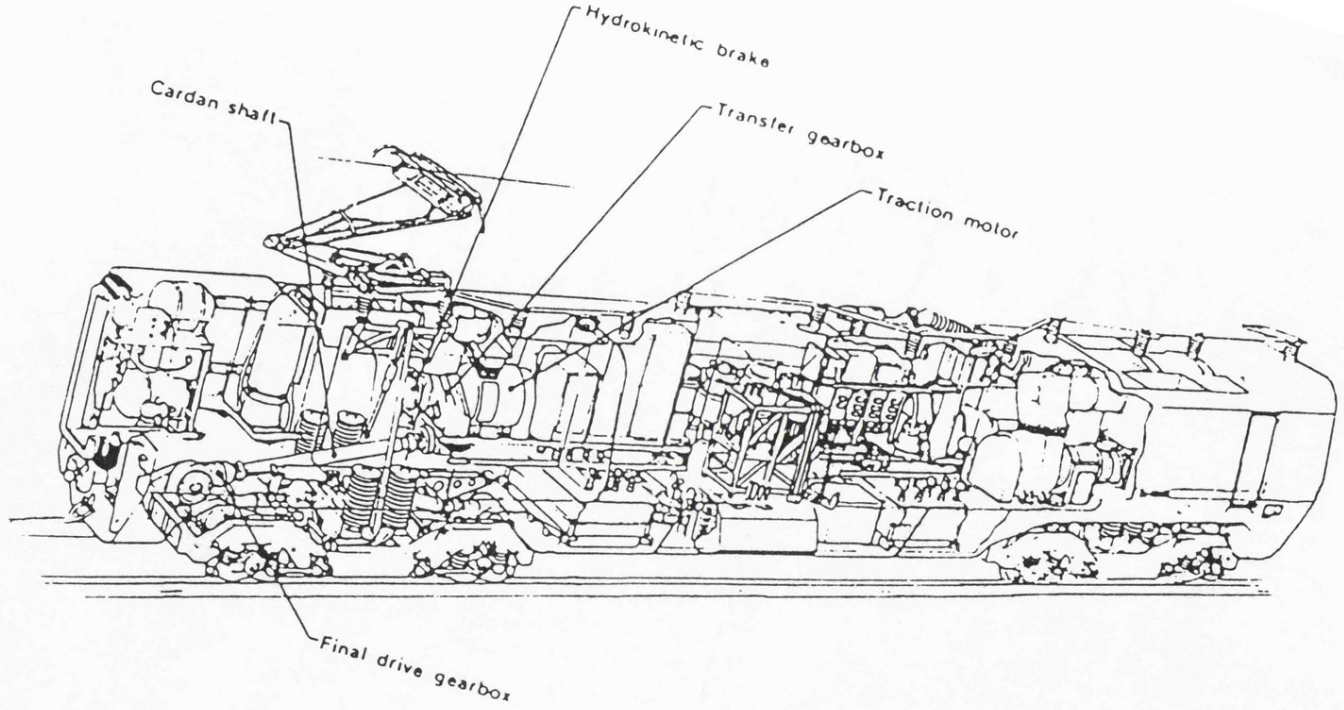

Fig 3.1 Electric Power Car (ref. 44)

Less maintainance - As an AC machine has no commutator or brushes to inspect, the resulting design is generally simpler and more rugged. This leads to greater reliability, less maintainance and a lower first cost. A synchronous machine will of course require brushes to feed the rotor slip rings, but this is a much simpler arrangement.

Increased power at high speeds - Commutator motors are frequently unable to supply rated power up to maximum speed because the reactance voltages become too large.

Unfortunately, the basic torque - speed characteristic for a single cage induction motor driven from a constant voltage, constant frequency supply, is clearly unsuitable for traction applications. Useful torque is only available over a very restricted speed range near synchronous speed, and the starting torque and efficiency are poor. By variation of the supply voltage and frequency however, a family of torque curves can be produced to give a composite curve of the required form, Fig 3.2.

The principle drawback of AC traction systems is the need for a variable voltage, variable frequency supply. Over the last decade or so, advances in power semiconductor technology have made inverters with suitable power ratings a practical reality. Various basic inverter circuit configurations are employed, each offering particular advantages. This aspect of the traction system will be looked at in greater depth in the following chapter.

The Brush Hawk [17,18] was the first attempt in Britain to evaluate an AC traction system under practical conditions using thyristor inverters, and the failure of this project can be attributed to the lack of suitable

semiconductor devices being available at that time. As better devices have appeared research into the prospects of three phase traction systems has increased. This research has produced many experimental railway vehicles for evaluation [19], some of which have now reached production status [20].

It has been proposed that the mechanical transmission system and DC traction motor be replaced by a bogie mounted AC machine, to produce a variable speed drive for a high speed diesel-electric locomotive. A highly rated AC machine would seem well suited to this particular application where the available space is restricted and where the weight must be kept to a minimum.

In this chapter designs are presented for squirrel cage induction and slip ring synchronous machines that will meet the motoring and braking requirements of this application.

The relative sizes of the machine and power supply are dependant upon the manner in which the system is controlled. It was therefore decided to consider the designs resulting from two commonly used control schemes, in order to illustrate the resulting motor weights and power supply capacities.

The techniques described in the previous chapter are used to demonstrate the influence of the pole number on the main requirement for a minimum size and weight design. From this comparison, which includes an assessment of the power factor and losses, six competing designs (one for each machine type and control method), are chosen for further study at what is considered to be the optimum pole number.

In section 3.3 performance predictions are shown for these six designs over the motoring and braking regions of the traction characteristic, and an appraisal is made of their suitability for this traction application.

The machines presented in this chapter have been designed assuming sinusoidal supply conditions. As in practice the traction motors would be supplied by an inverter of an appropriate type, the most suitable induction and synchronous designs are carried forward into Chapter 4 , where their performance is predicted when they are fed with a voltage or current source inverter.

3.2 The traction motor characteristic and control strategy

The traction motor specification for a high speed diesel-electric locomotive is as follows:

1 The train configuration is to consist of one power and seven trailing cars giving a total mass of 320 tonne.
2 The duty cycle for a typical journey from London, Euston to Glasgow Central is to be as shown in Appendix 3.5.1.
3 Power car to have four traction motors.
4 A constant force of 36 KN required from standstill to 55 Km/hr.
5 A constant power of 2.2 MW required from 55 to 225 Km/hr.
6 A constant braking force of 22.5 KN required from 225 Km/hr to a speed of less than 55 Km/hr.
7 Maximum motor dimensions to be 900 mm in length and 600 mm in diameter.
8 Motor weight to be less than 1.6 tonne.
9 Maximum motor speed to be about 6000 rpm.
10 Maximum AC line voltages to be about 1 KV.
11 Maximum DC field voltages to be about 110V.
12 Current densities to be suitable for class H insulation.
13 Wheel diameters are 853 mm (new), and 823 mm (worn).

It is desirable to use as high a motor speed as is possible. This implies the use of an axle mounted gearbox. On the axle, the pinion diameter is limited by the wheelsize, and thus the highest speed ratio available is determined by the minimum practical diameter of the motor pinion. The main considerations for determining the minimum pinion diameter are the material strength, and the number of teeth meshing with the axle pinion.

A ratio of approximately 4:1 is considered to be the practical limit[36].
In order to give a round figure of 1500 rpm at 55 Km/hr with a new wheel, a gear ratio of 4.39:1 was adopted. The motor shaft speeds for the upper and lower limits on wheelsize are given in table 3.1.

Train speed (Km/hr)	Wheel diameter (mm)	Motor speed (rpm)
225	853 823	6143 6367
55	853 823	1500 1556

Table 3.1 Motor shaft speed with a 4.39:1 gearbox

It can be seen that the maximum motor speed is 6367 rpm at a train speed of 225 Km/hr. This value is felt to be close enough to the specified maximum motor speed of about 6000 rpm.

The traction motor characteristics for one motor are shown in Fig 3.2. In the motoring mode a constant torque of 3.7 KNm is required to produce the desired constant acceleration period up to the knee point of the characteristic. A period of constant power acceleration is then required above the corner speed of 55 Km/hr. This gives an output torque that is inversely proportional to speed. The motor output power throughout this period has to be 580 KW. In order to meet the braking requirements, the braking torque at the motor shaft has to be 2.28 KNm from maximum speed to standstill. A gearbox efficiency of 0.95 is assumed throughout.

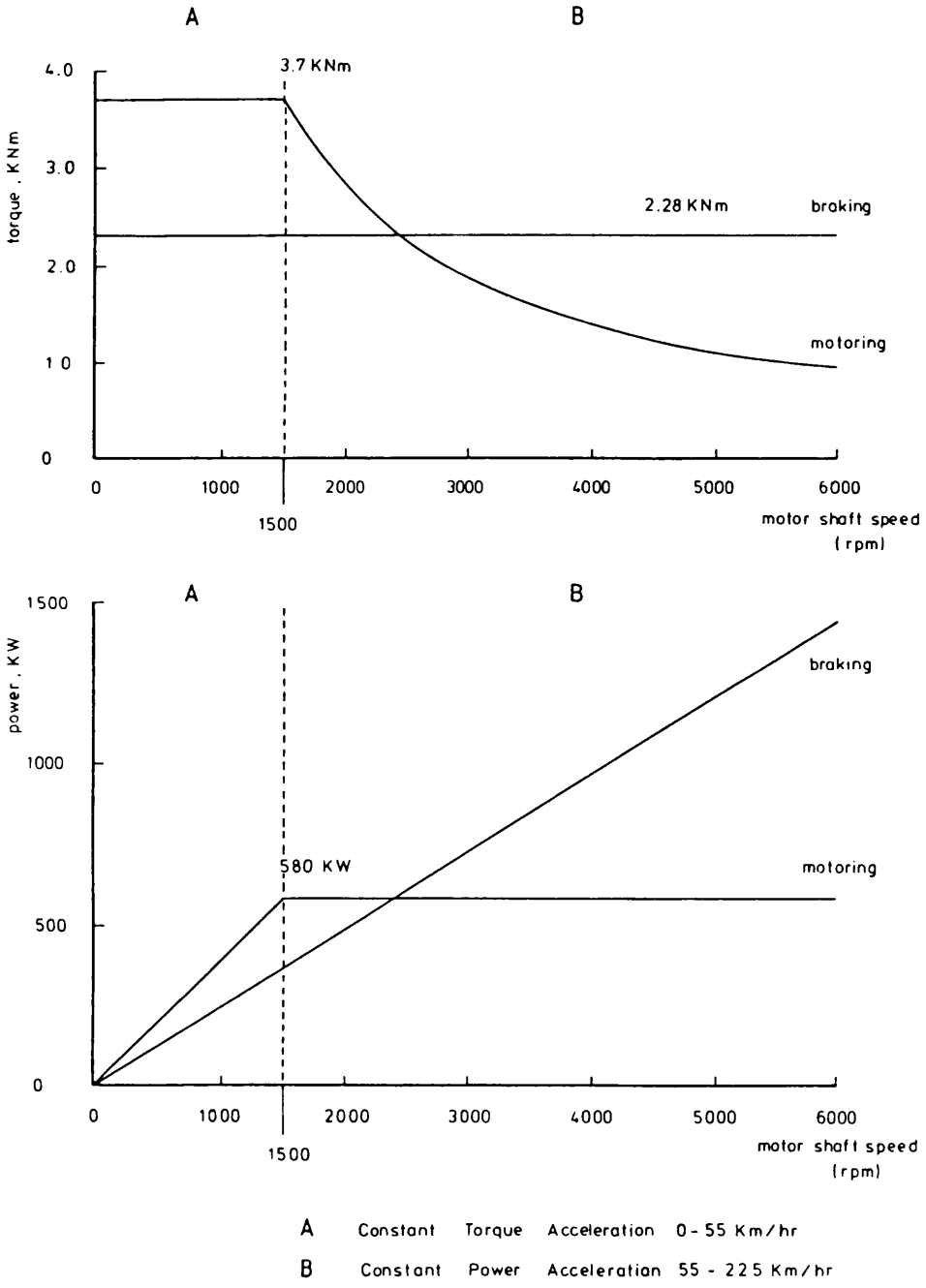

A Constant Torque Acceleration 0 - 55 Km/hr

B Constant Power Acceleration 55 - 225 Km/hr

Fig 3.2 Traction Motor Characteristics

The relative size and power supply requirements of a particular machine design are dependant upon the way in which it is controlled. Two methods of control in common use are considered. These are:

1 A 'rising voltage' control scheme

2 A 'constant voltage' control scheme

A constant output torque is required for acceleration and braking. This type of characteristic is achieved under both control methods by maintaining a constant voltage-frequency ratio. The rotor frequency of the induction machine is held constant during these periods, as is the field current of the synchronous machine. At all times the synchronous machine is operated at a torque angle of 90 degrees.

The two control schemes differ in the method by which a constant power acceleration period is produced. The 'rising voltage' control scheme utilises a supply voltage that is varied in proportion to the square root of the speed. This gives a stator current that decreases for increasing speed, for all machine types. For an induction machine operating in this mode the rotor frequency is again held constant. Equivalent performance is obtained from a synchronous machine, by varying the field current in direct proportion to the armature current. The 'constant voltage' control scheme uses a supply voltage that is held nominally constant for a constant power output. This gives a stator current that remains constant for increasing speed. The induction machine is operated at a constant per unit slip value, and the synchronous machine with a field current that is varied in inverse proportion to the speed.

3.3 Design and performance predictions

As the current and flux densities are highest at the end of the constant torque region, this point is chosen as the design point. For machine designs of the type being considered, for use with class H insulation, a current density of 5 A/mm^2 was chosen. Higher current density values of up to 8 A/mm^2 have been used in the design of traction motors [36], but it is felt that machines could not be designed with confidence at this rating, without performing a detailed study of the heat transfer process.

For traction machines, the use of the RMS current density over the duty cycle is considered to be equivalent to a continuous rating. From an analysis of the duty cycle, Appendix 3.5.1, and having set a continuous current density rating, an estimate of the current densities required for each part of the traction motor characteristic may be obtained. The resulting current densities for motor operation under the two control schemes considered is shown in Fig 3.3. Most electrical steels are able to support a flux density of 1.4 Tesla without undue saturation or loss, and therefore this value is taken to be the maximum allowable in each of the following designs.

The main geometrical constraint on the design of the stator is imposed by the choice of outside diameter, which must be no greater than 600 mm to meet the specification. This dimension is therefore fixed for all designs. A simple open rectangular stator slot is used, 50 mm in depth and with a slot width to slot pitch ratio of 0.5. All stator coils are assumed to be full pitched. All stator and rotor slots are assumed to have a packing factor of 0.5, with the exception of the squirrel cage rotor, where in view of the close contact possible between the conductor and slot

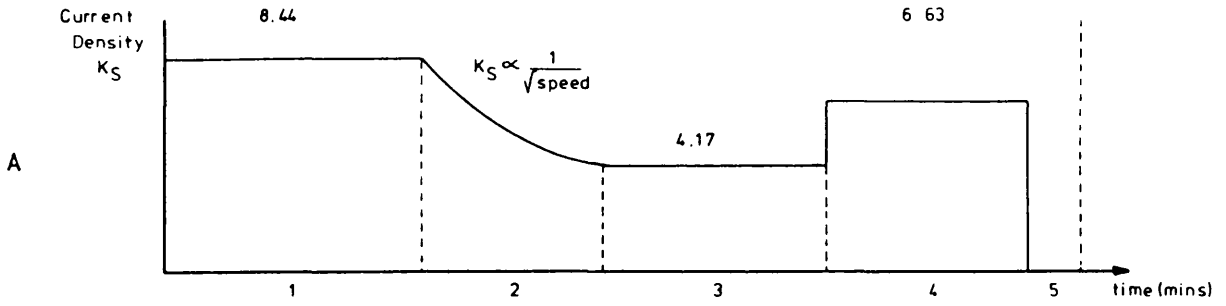

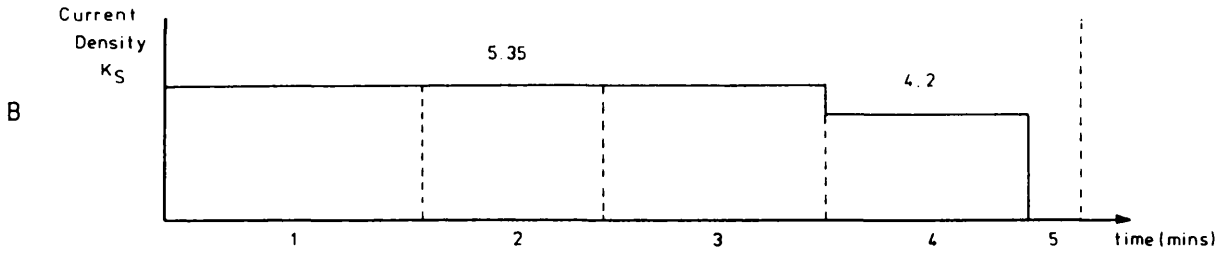

STATOR

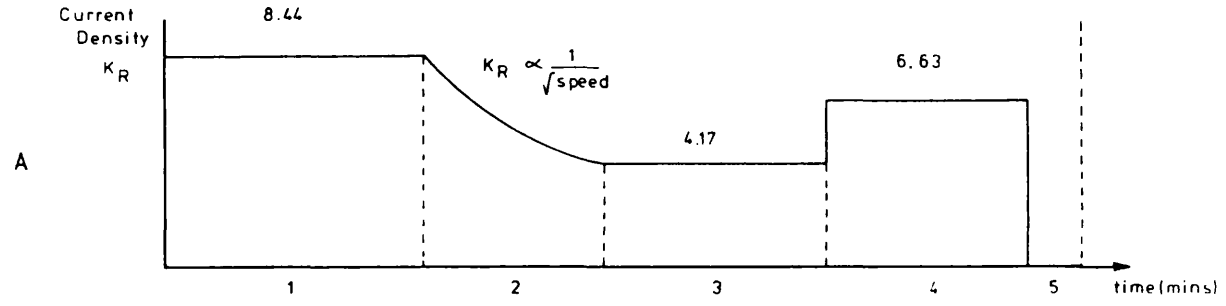

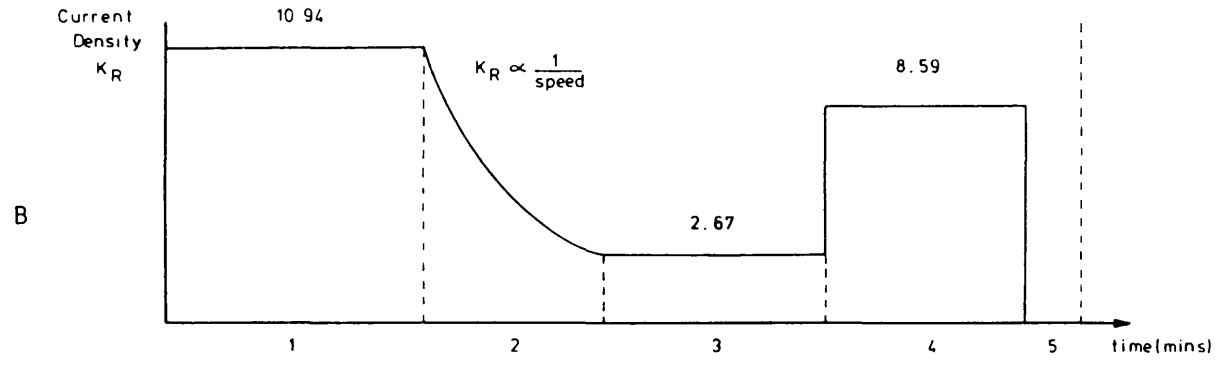

ROTOR

A Rising Voltage Control B Constant Voltage Control

1 Constant Torque (0.566 min)
2 Constant Power (4.454 min)
3 Balancing
4 Constant Torque Braking (3.7 mins)
5 Stationary

Fig 3.3 Winding Current Densities

a packing factor of unity is assumed. The only remaining variable to be specified for the induction machine is the air gap length. In view of the expected shock loadings to be imposed on the shaft, the gap length is set to 3 mm.

A complete summary of the input variables to the design process is shown in Table 3.2. Machines labelled '1' are for a 'rising voltage' operation and machines labelled '2' are for operation under a 'constant voltage' control scheme.

The variation of the total machine weight and length, (including core and end windings, but excluding case details), for 2,4,6 and 8 pole designs is shown in Figs. 3.4 and 3.5. The 4 pole design points for a rising voltage control scheme, are those whose computer data is reproduced at the end of the previous chapter to illustrate the design method.

As the stator core outside diameter is fixed, the output power available, from a geometrical point of view, is a function of the core length. In each design case shown , the core length has been adjusted to give the required output power at the design point of 580 KW.

The 'rising voltage' control scheme allows the use of a higher starting current density for a given duty cycle RMS value. This enables a shorter and therefore lighter design to be produced. Machine operation under a 'constant voltage' control scheme gives a starting current density that is close to the duty cycle RMS value. This leads to the requirement for a longer core and consequently a heavier machine.

As the pole number is increased the length of the stator and rotor end windings is reduced. This inactive part of the machine, although essential

	INDUCTION 1	INDUCTION 2	ROUND ROTOR SYNCHRONOUS 1	ROUND ROTOR SYNCHRONOUS 2	SALIENT POLE SYNCHRONOUS 1	SALIENT POLE SYNCHRONOUS 2
max. stator conductor current density K_S A/mm^2	8·44	5·53	8·44	5·53	8·44	5·35
max. rotor conductor current density K_R A/mm^2	8·44	5·53	8·44	10·94	8·44	10·94
max. core flux density T $\hat{B}$	1·4	1·4	1·4	1·4	1·4	1·4
synchronous speed rpm	1500	1500	1500	1500	1500	1500
stator core outside dia. mm d_0	600	600	600	600	600	600
stator slot depth mm d_s	50	50	50	50	50	50
air gap length mm g	3	3	-	-	-	-
slot width / slot pitch β	0·5	0·5	0·5	0·5	0·5	0·5
coil pitch / pole pitch γ	1·0	1·0	1·0	1·0	1·0	1·0
pole arc / pole pitch α	-	-	-	-	0·7	0·7
stator packing factor k_{PFS}	0·5	0·5	0·5	0·5	0·5	0·5
rotor packing factor k_{PFR}	1·0	1·0	0·5	0·5	0·5	0·5
stator and rotor iron packing factor k_{is} , k_{iR}	1·0	1·0	1·0	1·0	1·0	1·0
stator and rotor conductor resistivity $\times 10^{-8}$ ohm M ρ_c	2·0	2·0	2·0	2·0	2·0	2·0
stator and rotor conductor density $\times 10^4$ Kg/M^3 δ_s δ_R	0·8930	0·8930	0·8930	0·8930	0·8930	0·8930
iron density $\times 10^4$ Kg/M^3 δ_i	0·7871	0·7871	0·7871	0·7871	0·7871	0·7871

Table 3.2 Input variables to the design process

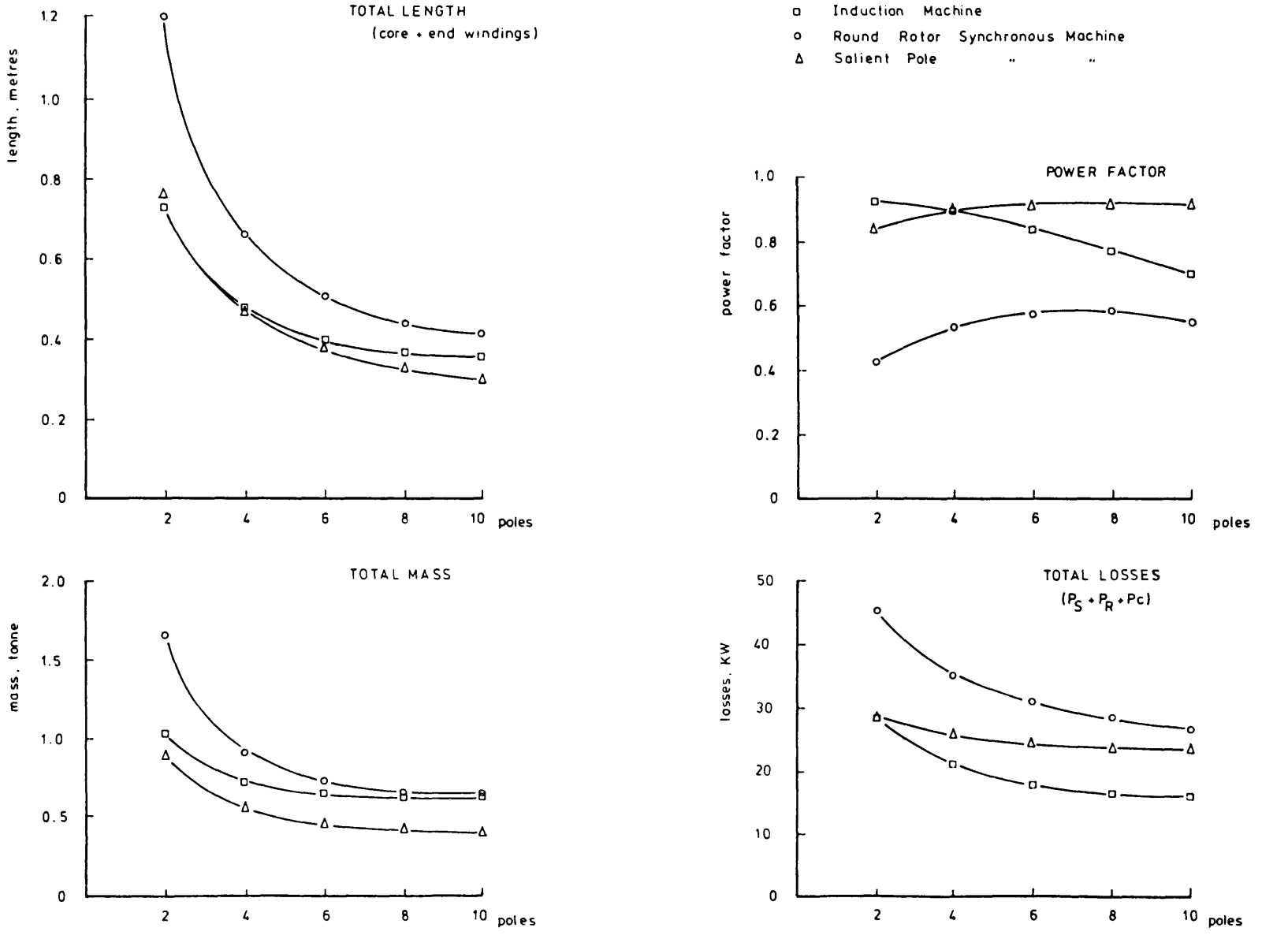

Fig 3.4 Design point performance predictions of a 580 KW machine for a variable pole number (Rising Voltage Control)

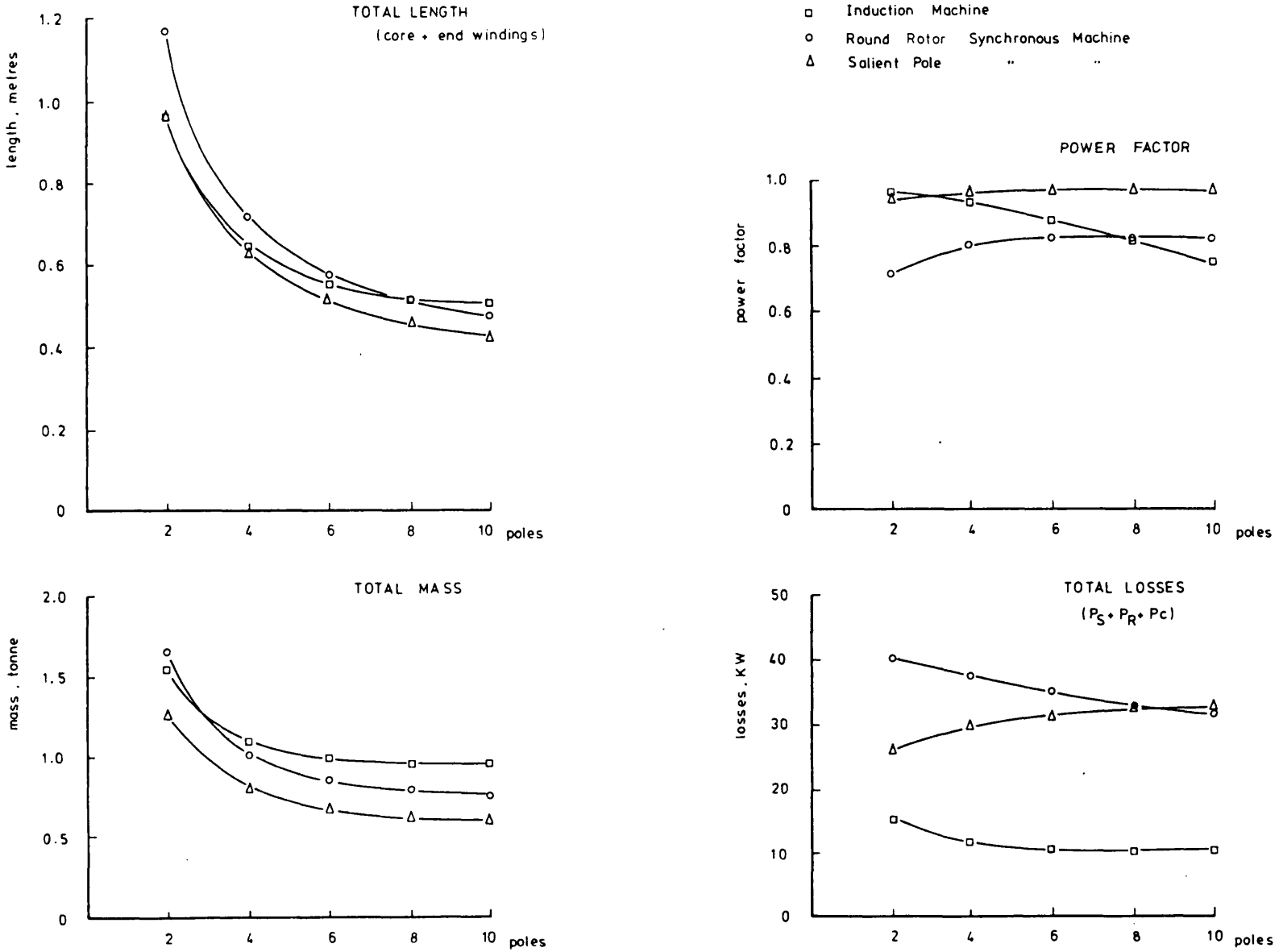

Fig 3.5 Design point performance predictions of a 580 KW machine for a variable pole number (Constant Voltage Control)

to its operation, contributes nothing to the output. For an increasing pole number the influence of the inactive end windings diminishes, and comparable machine weights and lengths are produced for a particular machine type. For machines operating under both types of control a considerable reduction in weight is possible by increasing the pole number from 2 to 4. Further reductions are available by raising the pole number further, but this is at the expense of higher supply frequencies and shorter slot pitches. The effect of the pole number upon the power factor is similar in character for machine operation under both control schemes. The round rotor synchronous machine has markedly the poorest power factor, whilst designs of the salient pole type give a power factor that is essentially constant above 4 poles. The power factor of the induction machine is reduced for an increasing pole number, due to an increased leakage reactance associated with the corresponding requirement for a higher supply frequency.

A comparison of the total machine losses, comprising of the total conductor loss and an estimation of the core loss, (section 2.3.1), is also shown in Figs 3.4 and 3.5. As would be expected, the induction machine incurs significantly less losses than either type of synchronous machine, due to its greater utilization of slot area.

In view of the above results and the desirability of keeping the supply frequency as low as possible, the 4 pole designs seem best suited to this particular application. Table 3.3 gives the main dimensions of the 4 pole designs, and Fig 3.6 shows the motoring and braking characteristics of each of these machines.

The supply VA capacity is determined by the product of the voltage required at the highest operating speed, and the starting current. The

	INDUCTION 1	INDUCTION 2	ROUND ROTOR SYNCHRONOUS 1	ROUND ROTOR SYNCHRONOUS 2	SALIENT POLE SYNCHRONOUS 1	SALIENT POLE SYNCHRONOUS 2
core length w_c	302	470	482	531	297	451
air gap g	3	3	33	31	37	42
slot pitch τ_s	34·9	34·9	34·9	34·9	34·9	34·9
pole pitch τ_p	314·2	314·2	314·2	314·2	314·2	314·2
depth stator backing core d_c	50	50	50	50	50	50
stator slots / pole phase q_s	3	3	3	3	3	3
rotor slots/ pole phase q_R	3	3	9	9	1	1
stator conductors per slot z_S	4	4	4	4	4	4
rotor conductors per slot z_R	1	1	20	15	300	200
rotor winding factor k_{WR}	1	1	$2/\pi$	$2/\pi$	≈1	≈1
pole body width w_p	-	-	-	-	100	100
nos. of vents n_v	0	0	0	0	0	0
nos. of parallels for braking	2	2	2	2	2	2

all dimensions in mm

Table 3.3 Machine dimensions Diesel-electric traction specification

much larger VA produced in braking is accomodated by the use of parallel connections and braking resistors, (section 2.5).

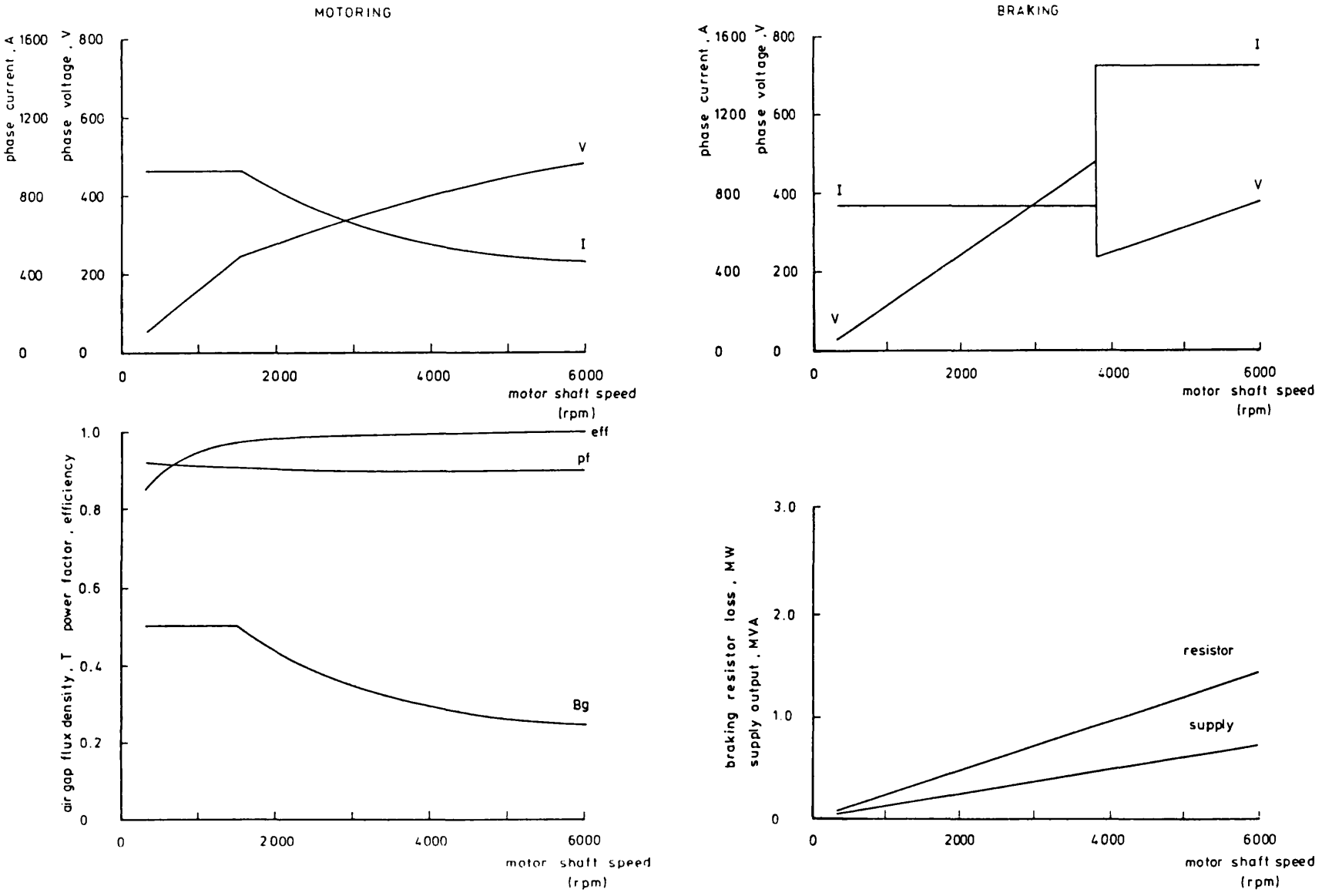

Fig 3.6a Induction Motor , Rising Voltage Control

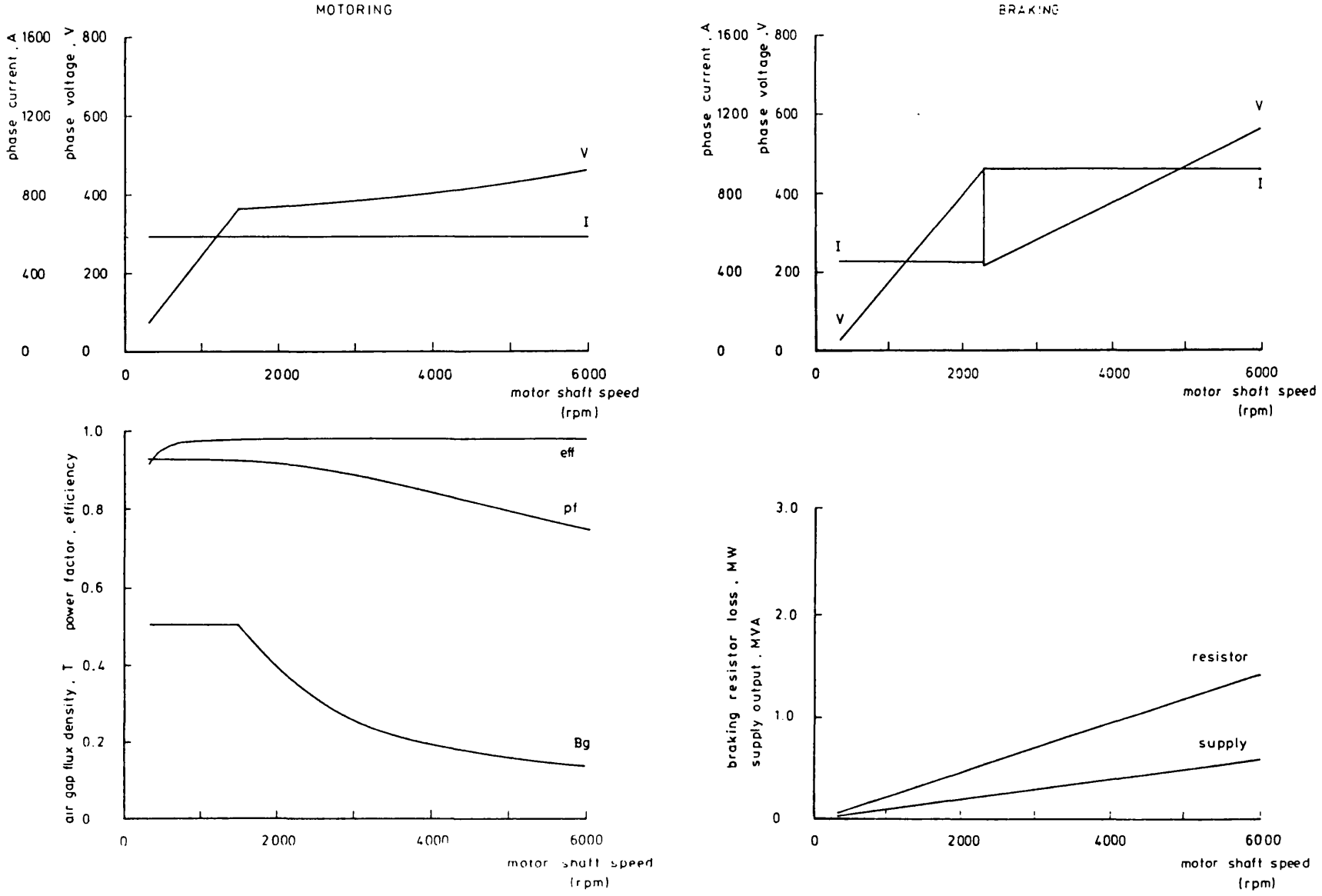

Fig 3.6b Induction Motor , Constant Voltage Control

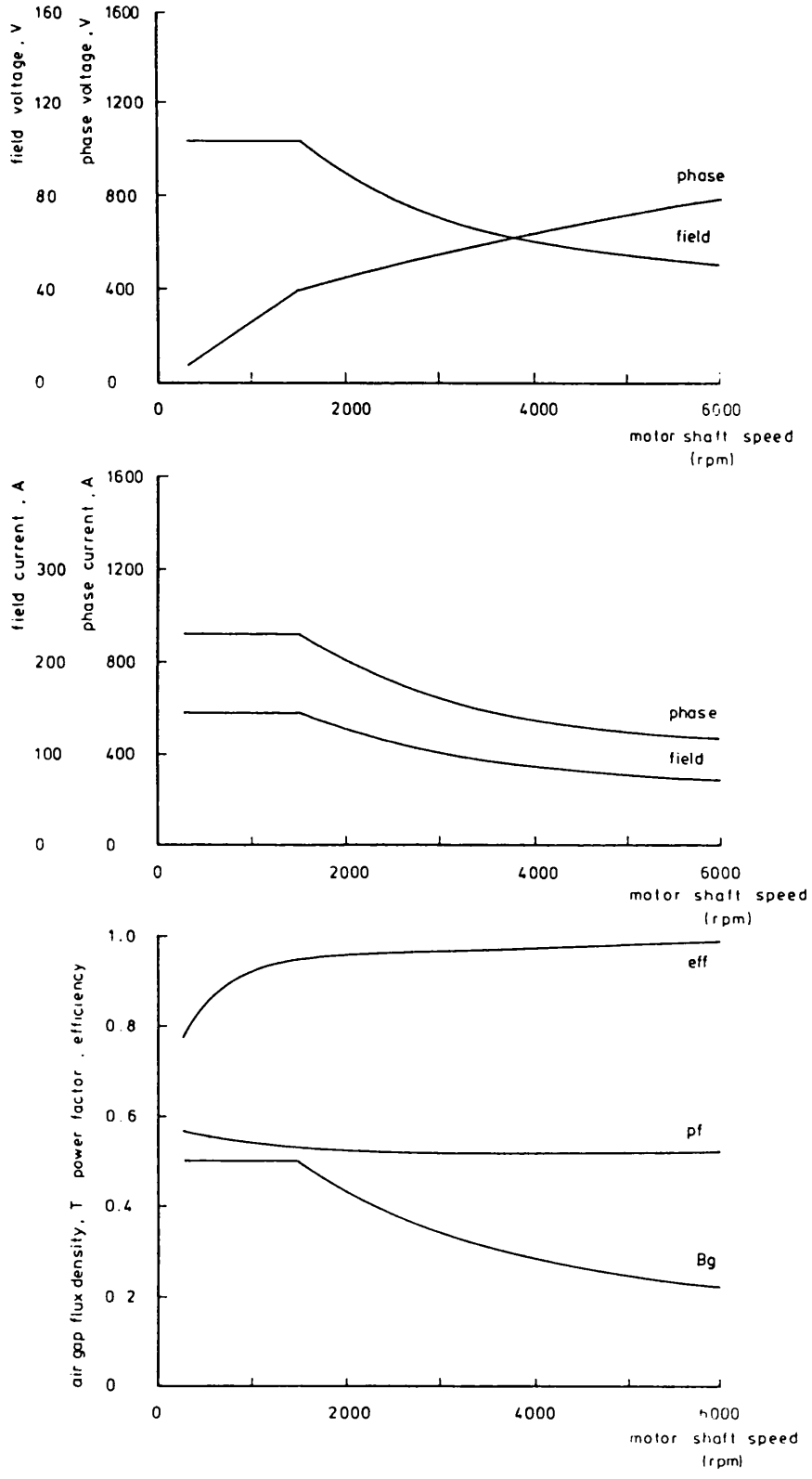

Fig 3.6c Synchronous Motor (Round Rotor) , Rising Voltage Control - Motoring

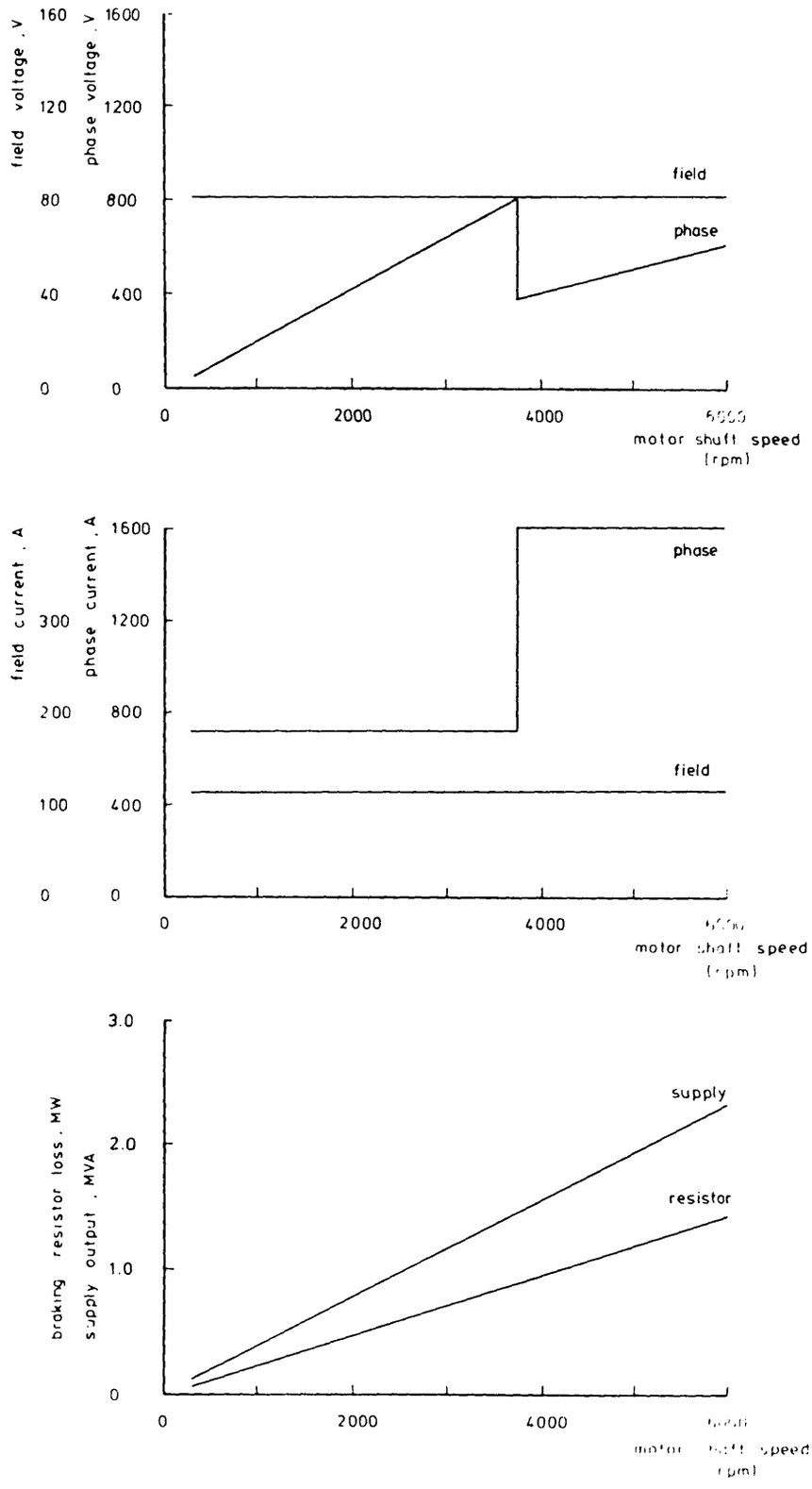

Fig 3.6d Synchronous Motor (Round Rotor), Rising Voltage Control - Braking

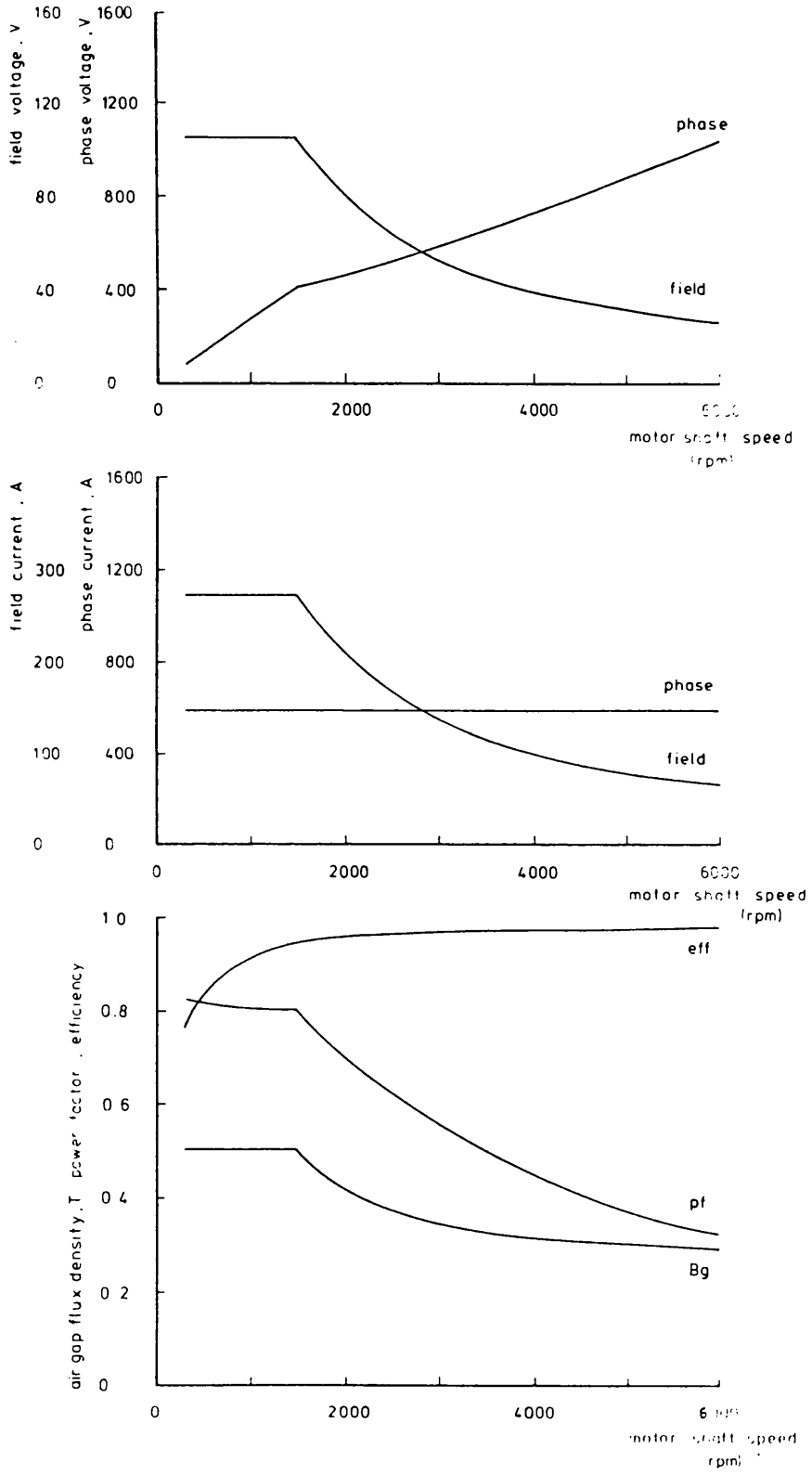

Fig 3.6e Synchronous Motor (Round Rotor), Constant Voltage Control - Motoring

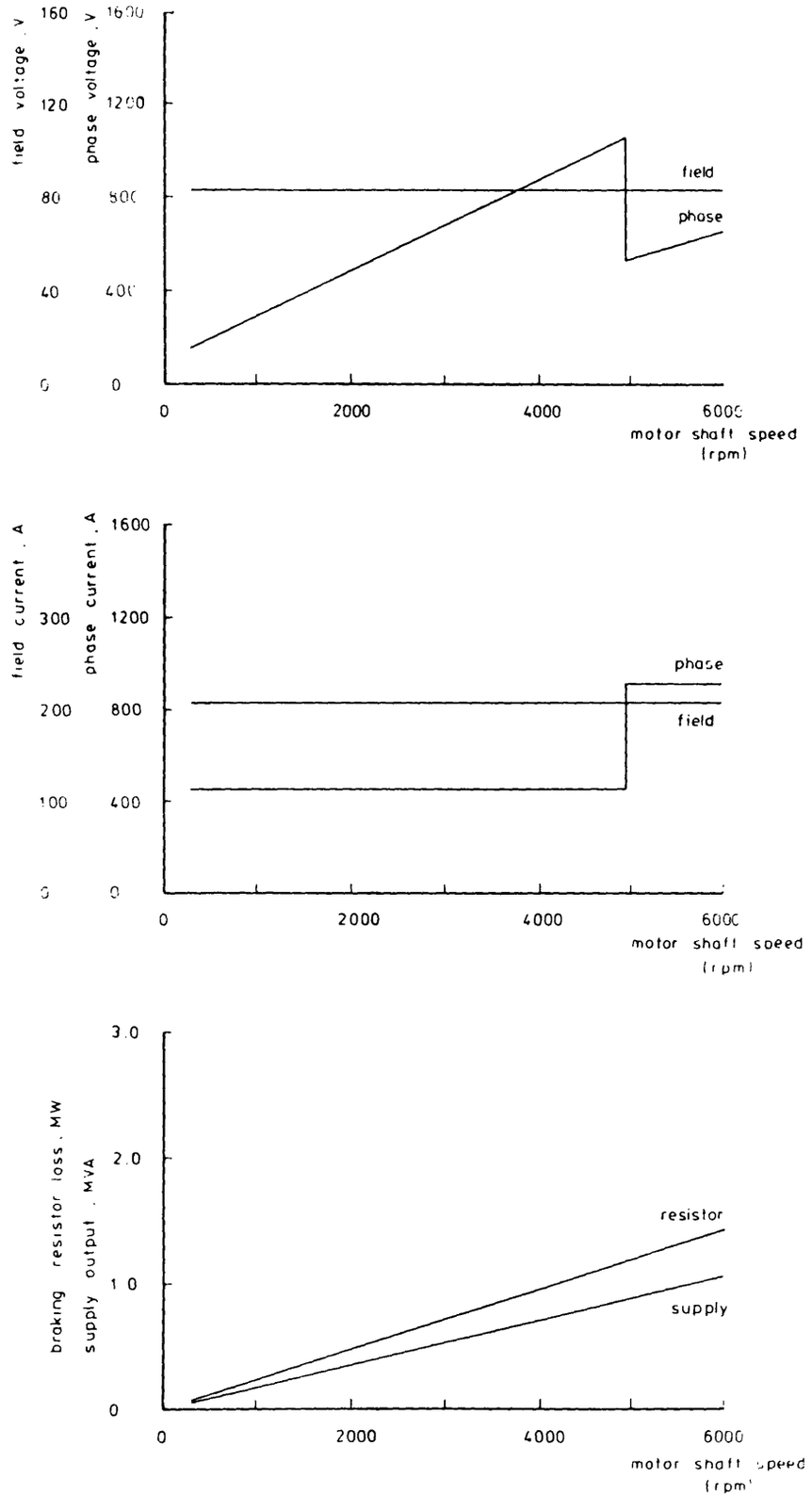

Fig 3.6f Synchronous Motor (Round Rotor), Constant Voltage Control - Braking

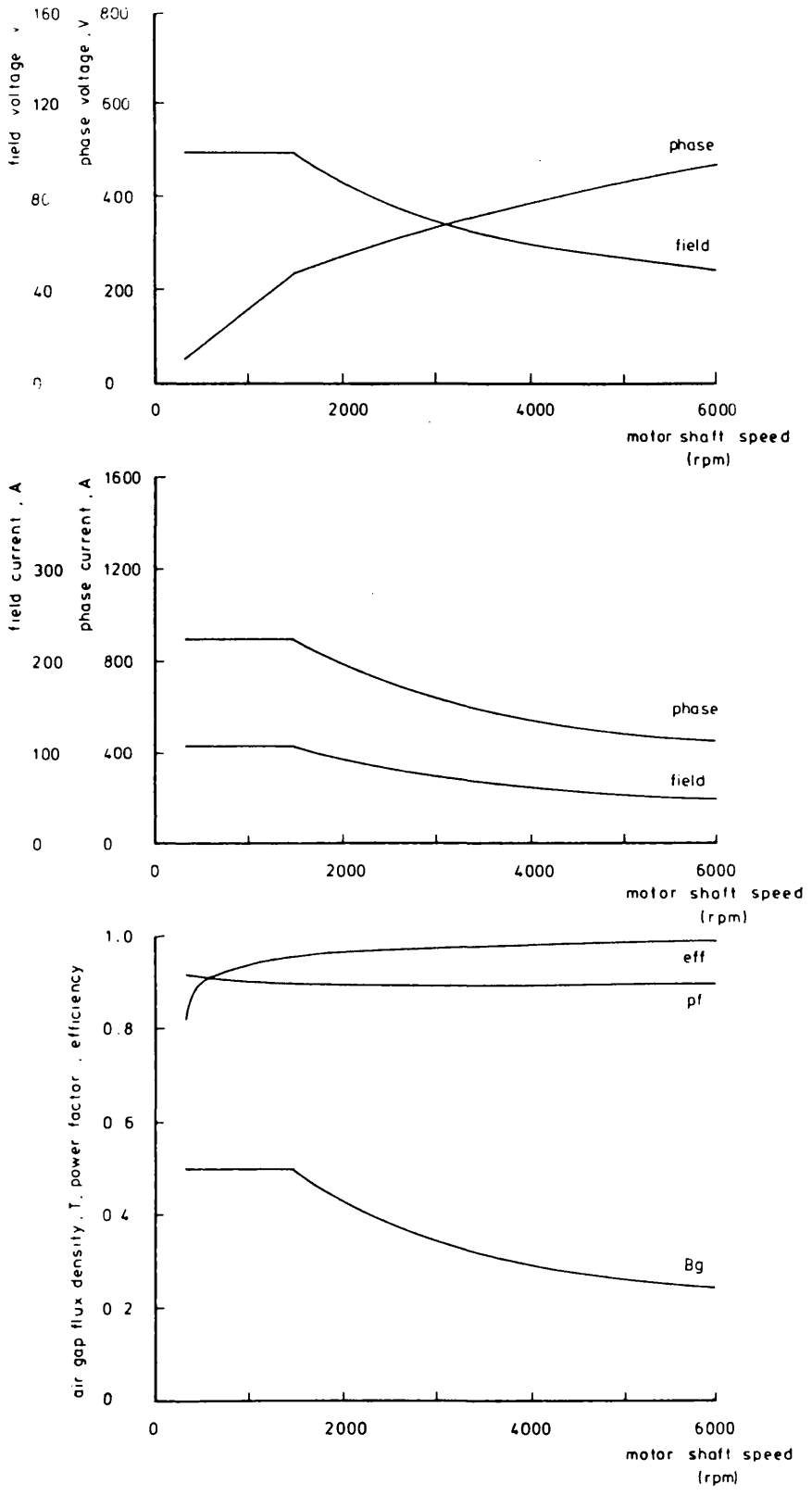

Fig 3.6g Synchronous Motor (Salient Pole), Rising Voltage Control - Motoring

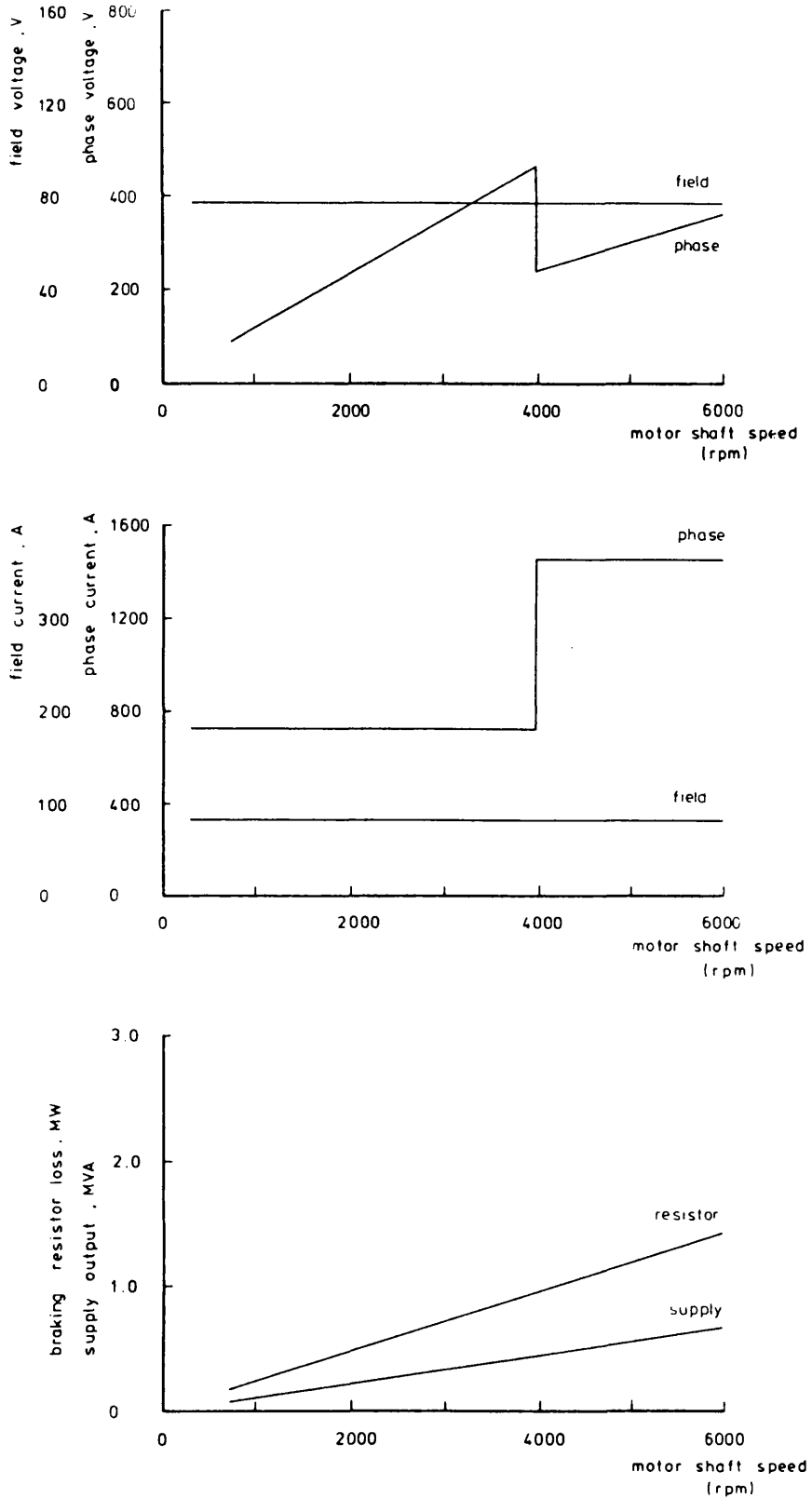

Fig 3.6h Synchronous Motor (Salient Pole), Rising Voltage Control - Braking

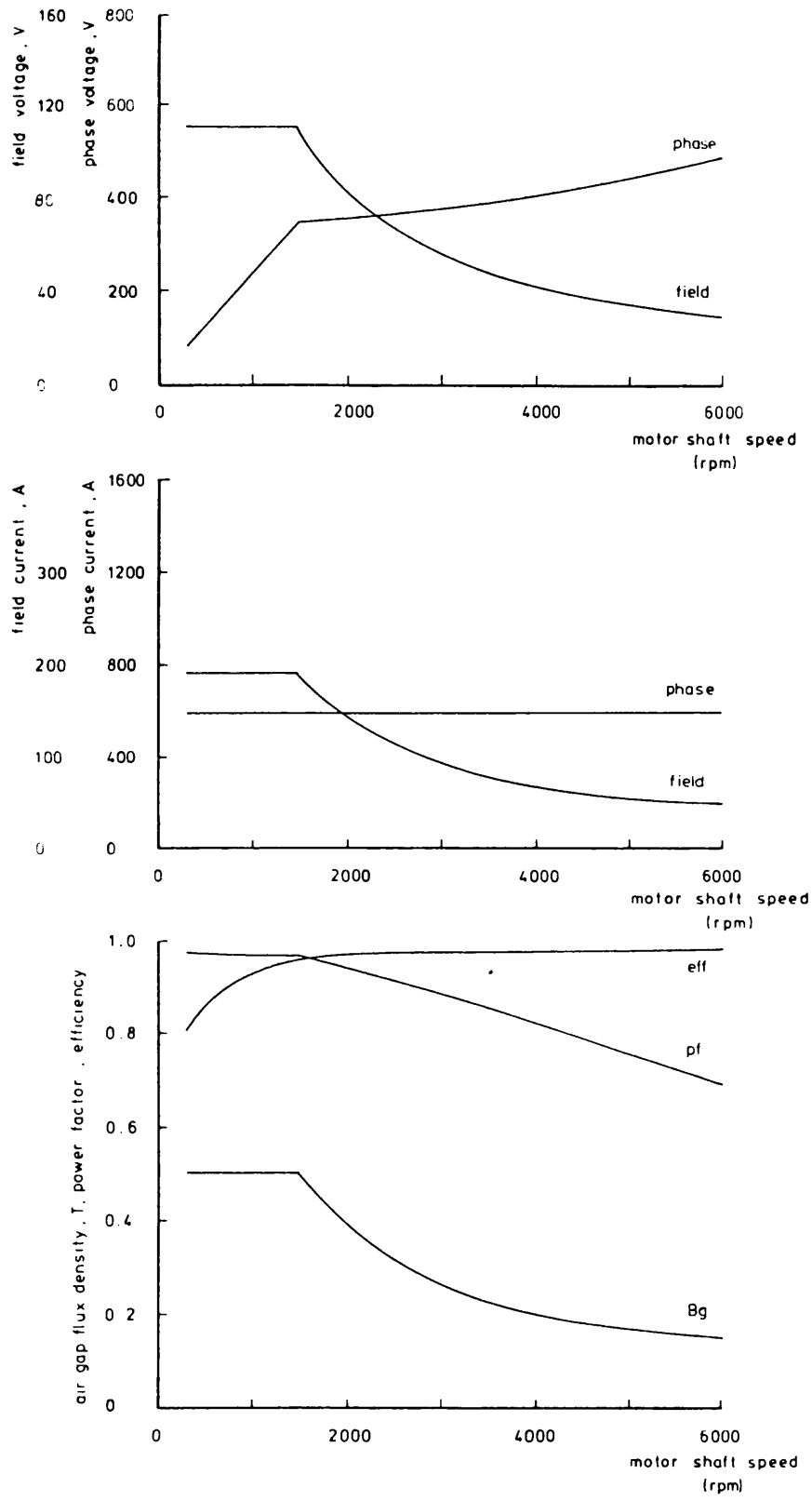

Fig 3.6j Synchronous Motor (Salient Pole), Constant Voltage Control - Motoring

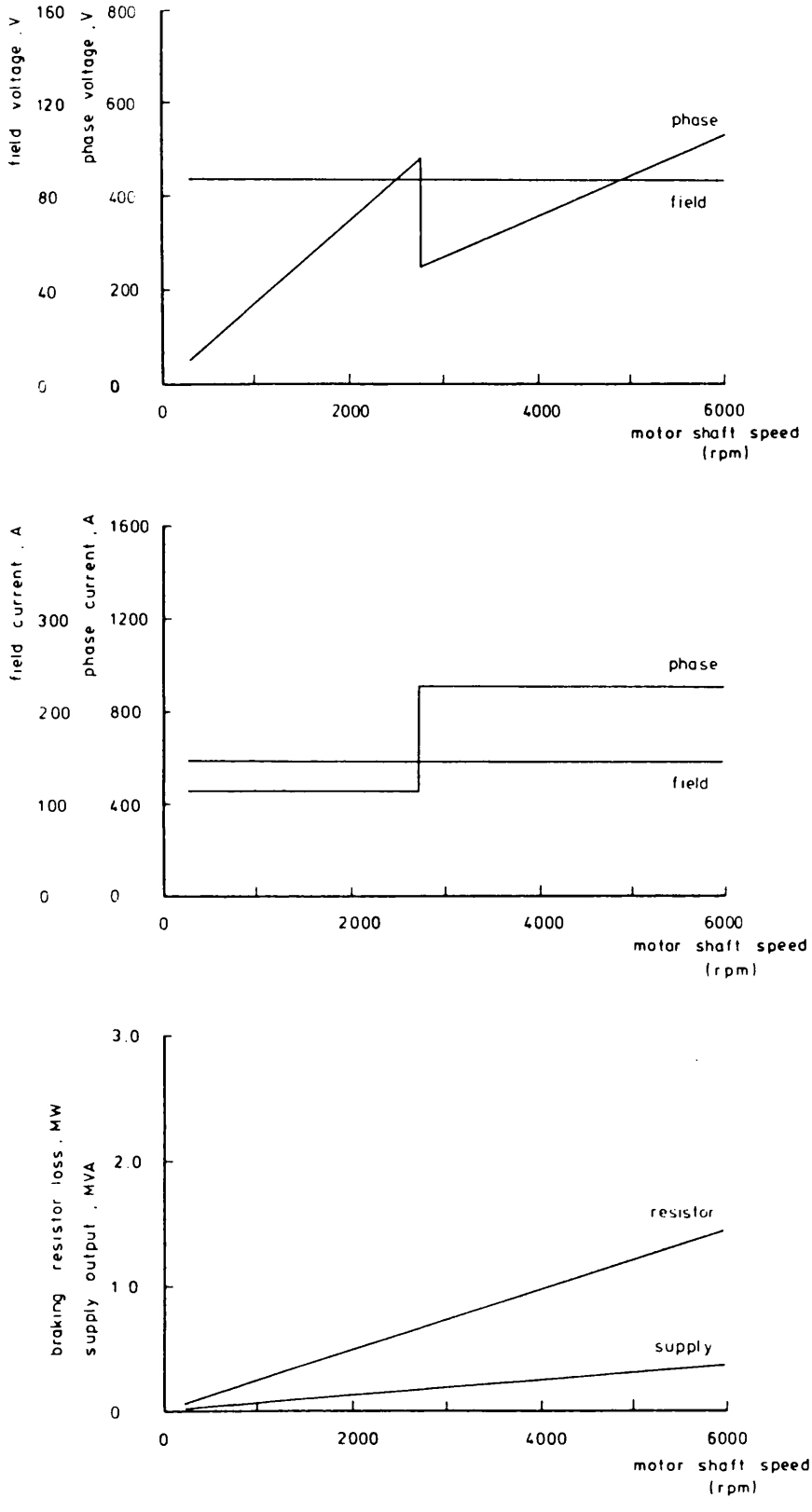

Fig 3.6k Synchronous Motor (Salient Pole), Constant Voltage Control - Braking

3.4 Conclusions

Table 3.4 shows that even with the modest values of RMS current density used of 5 A/mm^2, it is possible to design an AC machine well within the weight specification of 1600 KG. Even lighter designs may be possible, as ultimately it is the temperature at which the winding can be safely operated that will determine the maximum value of conductor current density. In order to determine these limits a heat transfer study would have to be undertaken.

The 'rising voltage' control scheme produces lighter designs but incurs the penalty of requiring a higher supply capacity. Operation under a 'constant voltage' control has the benefit of requiring a smaller supply capacity but leads to a heavier design. This form of control is also associated with a falling machine power factor throughout the constant power region.

Of the three types of machine considered the round rotor synchronous appears the least attractive. This is because of the large supply capacity required due to its inherently low power factor.

The induction and salient pole machines are similar in both physical size and performance, and require supplies of a similar capacity. However because of the large air gap, both types of salient pole machine are approximately 25% lighter than the corresponding induction machine. This appears to make the salient pole synchronous machine the most suitable for this particular application, but the following points must be weighed against it.

	machine length core+end wdgs. mm	iron weight KG	copper weight KG	total weight KG	armature supply MVA	field supply KVA
INDUCTION 1	483	515	232	747	1·33	-
INDUCTION 2	651	801	302	1103	0·81	-
SYNCHRONOUS 1 R.R.	663	710	213	923	2·2	15·1
SYNCHRONOUS 2 R.R.	712	789	229	1018	1·8	27·9
SYNCHRONOUS 1 S.P.	478	417	158	575	1·3	10·5
SYNCHRONOUS 2 S.P.	632	625	192	817	0·84	20·9

Table 3.4 Comparison of machine weight , length and power supply capacities

1 The control system required to keep the torque angle constant is relatively complex.

2 The cost of a separate field supply.

3 The use of slip rings.

4 A less rugged and more costly rotor construction.

In the following chapter, the performance of the lightest designs of induction and synchronous machine is investigated, when being fed by non-sinusoidal supplies with discontinuous phase currents. Two inverters are considered, one of the constant voltage, and one of the constant current type.

In order to furnish the equivalent circuit parameters necessary for this investigation, a further computer program has been written to enable these parameters to be calculated from the physical machine dimensions. The parameter calculations are based upon the material presented in Appendix 2.7.2, prior to any simplifying assumptions being made for their use in the design process. The resulting parameters for the two machines are as follows:

Induction machine Fig 3.7

Stator resistance	7.015	mΩ
Stator leakage inductance	0.1873	mH
Referred rotor resistance	2.404	mΩ
Referred rotor leakage inductance	0.1991	mH
Magnetising inductance	5.879	mH
Motor weight	787	KG

Synchronous machine Fig 3.8

Stator resistance	6.977	mΩ
Stator leakage inductance	0.1851	mH
Referred field winding resistance	1.998	mΩ
Direct axis magnetising inductance	0.4874	mH
Quadrature axis magnetising inductance	0.2252	mH
Motor weight	624 KG	

Arising out of the machine design work presented in this chapter are a number of areas in which further study would be beneficial. Firstly the computer methods presented should be checked against practical results from suitable highly rated machines.

Secondly in order to establish whether higher values of RMS current density could be used, a study of the heat transfer characteristics of AC machines should be undertaken. If the use of higher values of current density is feasible further reductions in machine weight would be possible.

Finally as the simplified design formulae used to compare the different machine types use the minimum number of variables, a sensitivity analysis could easily be incorporated into the design method. This would lead naturally to the use of optimisation techniques in completing a design.

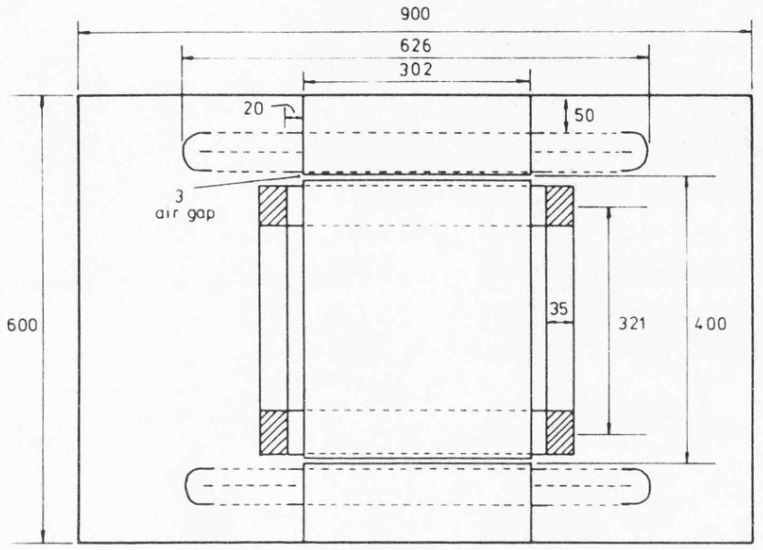

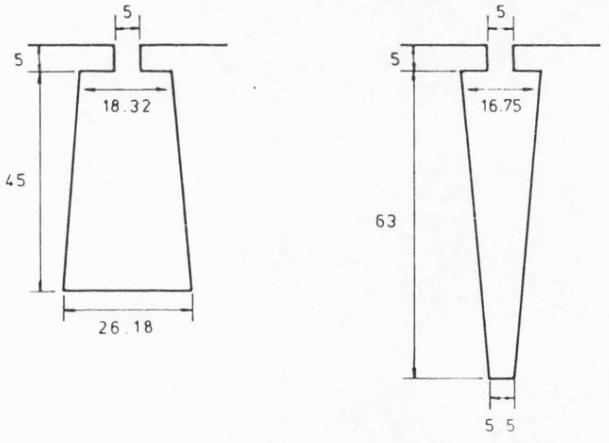

Fig 3.7 Induction Motor Traction Specification

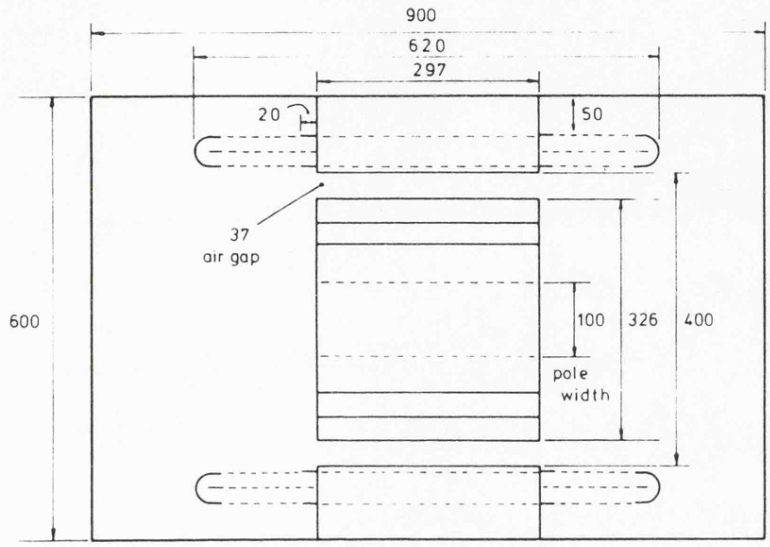

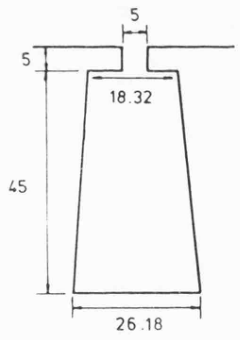

STATOR SLOT

Fig 3.8 Synchronous Motor (Salient Pole) Traction Specification

3.5 APPENDIX

3.5.1 The traction motor duty cycle

DISTANCE (KM)		STATION	TIME (minutes)		
FROM ORIGIN	INCREMENT		INCREMENT	STATION DWELL	ACCUM. TOTAL
0.0		LONDON, EUSTON		-	0.0
	28.1		13.7		
28.1		WATFORD		1.0	14.7
	104.7		34.4		
132.8		RUGBY		1.0	50.0
	23.5		10.0		
156.3		NUNEATON		1.0	61.0
	58.7		20.6		
214.9		STAFFORD		1.0	82.6
	39.4		15.9		
254.3		CREWE		2.0	99.4
	38.8		15.8		
293.1		WARRINGTON		1.0	117.2
	18.9		8.9		
312.1		WIGAN		1.0	127.1
	24.3		10.7		
336.4		PRESTON		2.0	139.8
	33.8		13.4		
370.2		LANCASTER		1.0	154.2
	111.3		42.3		
481.6		CARLISLE		2.0	198.5
	118.6		42.4		
600.1		CARSTAIRS		1.0	241.9
	25.5		11.5		
625.6		MOTHERWELL		1.0	254.4
	20.6		11.6		
646.3		GLASGOW CENTRAL		-	266.0

13 acceleration periods under motoring characteristic Fig 3.2
13 deceleration periods under braking characteristic Fig 3.2
15 mins when motor currents are zero
Train operates at 225 Km/hr at all other times so no account is taken of banking or other forms of reduced speed operation.

CHAPTER 4

THE PERFORMANCE OF INVERTER FED AC MACHINES WHOSE PHASE CURRENT IS DISCONTINUOUS

4.1 Introduction

In this chapter a computer method is presented that enables the steady state performance of induction and slip ring synchronous machines to be evaluated when the phase current becomes discontinuous.

The operation and analysis of two types of inverter is considered and computer predictions are presented to demonstrate the performance of the induction and salient pole synchronous motor designs, of Chapter 3.
The two types of inverter considered are:

1 Voltage Source Inverter (VSI)
2 Current Source Inverter (CSI)

Both inverter types are operated in the 120 degree conduction mode.

For a voltage source inverter operating in the 120 degree conduction mode, only two output thyristors are gated on at any one instant, and each thyristor will conduct for 120 degrees of the output period. Logic circuitry and gate pulse information, can in this case, be simplified as a thyristor is not gated into conduction until 60 degrees after its complimentary thyristor has been turned off. However for high power factor loads, which is the case for the two motor designs under consideration, the phase current is unable to reverse direction in the 60 degree period following thyristor turn off. During this zero current interval the machine back emf appears at the inverter output terminals. Thus for inverter operation in the 120 degree mode, the inverter output voltage is a function of the machine parameters and the loading condition.

When modelling a current source inverter, it is frequently assumed that the DC link current is constant. This requires an infinite value of link inductance, which in practice is unrealistic. Additional approximations have also been made,[31] by neglecting the stator resistance and assuming the machine back emf to be constant during the commutation period.

An exact model of the Current Source Inverter is presented here, in which the effect of the DC link inductance is taken into account, by considering the inverter to be supplied from an ideal voltage source. The foregoing approximations regarding stator resistance and machine back emf are not made in this study, and the machine models employed use all the normal equivalent circuit parameters.

Because of the thyristor switching symmetry inherent in both the VSI and CSI, it is necessary to consider only one sixth of a cycle of inverter operation. A steady state solution may then be determined for any operating point, by the integration of the system equations over this 60 degree period, and equating the initial and final values. A complete solution for one cycle of inverter operation may then be constructed by symmetry, from the 60 degree solution.

An induction machine model is presented in this chapter, in which rotor variables are transformed to the stator, thus removing the dependancy of the elements of the machine matrix on the rotor position. This transformation has advantages over a d-q representation of the induction machine, in this application, because as the actual three phase currents are available, the changes of state within the inverter are readily detectable, without the need to transform a two axis system of currents back into a three phase system.

Machine voltage and current waveforms are shown for the VSI and CSI fed induction and synchronous traction motor designs, and a comparison is made of the harmonic content present in the output torque waveforms. These machines are operated under a rising voltage control scheme, described in the previous chapter, to give an output characteristic that meets the requirements of a high speed diesel-electric traction motor.

4.2 Machine Models

4.2.1 Induction machine

The normal direct three-phase representation of the induction machine gives an inductance matrix, in which the elements are a function of the rotor position. The performance equations are therefore differential equations with variable coefficients.[37,38] An induction machine model has been developed, that is based upon a coordinate system that is fixed in the stator. This model is described fully in Appendix 4.8.2. As the transformed rotor currents are at the same frequency as the stator, the time taken to evaluate a steady state solution is reduced. Also, as the three phase voltages and currents are used, the inverter-machine equations are able to be set up with relative ease. The induction machine differential equations, Fig 4.1, are presented in the following form, in matrix notation

$$v = (R + \omega_R G + Lp) i \qquad (4.1)$$

where the vectors v and i represent the phase and referred voltages and currents respectively. For ease of presentation the inductance matrix L, impedance matrix G and diagonal resistance matrix R have been combined. Note that the components of impedance matrix G do not vary with the rotor position.

The performance equations of Fig 4.1 contain coefficients that are dependant only upon the normal equivalent circuit values and the steady rotor angular velocity, ω_R.

$$
\begin{bmatrix} v_{aS} \\ v_{bS} \\ v_{cS} \\ v_{aR'} \\ v_{bR'} \\ v_{cR'} \end{bmatrix} =
\begin{bmatrix}
R_S + p(l_S + \frac{2Lm}{3}) & -p\frac{Lm}{3} & -p\frac{Lm}{3} & p2\frac{Lm}{3} & -p\frac{Lm}{3} & -p\frac{Lm}{3} \\
-p\frac{Lm}{3} & R_S + p(l_S + \frac{2Lm}{3}) & -p\frac{Lm}{3} & -p\frac{Lm}{3} & p2\frac{Lm}{3} & -p\frac{Lm}{3} \\
-p\frac{Lm}{3} & -p\frac{Lm}{3} & R_S + p(l_S + \frac{2Lm}{3}) & -p\frac{Lm}{3} & -p\frac{Lm}{3} & p2\frac{Lm}{3} \\
p2\frac{Lm}{3} & -p\frac{Lm}{3} + w_R\sqrt{3}\frac{Lm}{3} & -p\frac{Lm}{3} - w_R\sqrt{3}\frac{Lm}{3} & R_{R'} + p(l_{R'} + \frac{2Lm}{3}) & -p\frac{Lm}{3} + w_R\sqrt{3}(l_{R'} + Lm) & -p\frac{Lm}{3} - w_R\sqrt{3}(l_{R'} + Lm) \\
-p\frac{Lm}{3} - w_R\sqrt{3}\frac{Lm}{3} & p2\frac{Lm}{3} & -p\frac{Lm}{3} + w_R\sqrt{3}\frac{Lm}{3} & -p\frac{Lm}{3} - w_R\sqrt{3}(l_{R'} + Lm) & R_{R'} + p(l_{R'} + \frac{2Lm}{3}) & -p\frac{Lm}{3} + w_R\sqrt{3}(l_{R'} + Lm) \\
-p\frac{Lm}{3} + w_R\sqrt{3}\frac{Lm}{3} & -p\frac{Lm}{3} - w_R\sqrt{3}\frac{Lm}{3} & p2\frac{Lm}{3} & -p\frac{Lm}{3} + w_R\sqrt{3}(l_{R'} + Lm) & -p\frac{Lm}{3} - w_R\sqrt{3}(l_{R'} + Lm) & R_{R'} + p(l_{R'} + \frac{2Lm}{3})
\end{bmatrix}
\begin{bmatrix} i_{aS} \\ i_{bS} \\ i_{cS} \\ i_{aR'} \\ i_{bR'} \\ i_{cR'} \end{bmatrix}
$$

Fig 4.1 Induction Machine Performance Equations

Inverters of the type to be considered produce an output current waveform that has a high harmonic content. This leads to the production of harmonic torques that tend to induce speed oscillations of the rotor.[39] It is assumed for the purposes of this study that the rotor has sufficient inertia to minimise this effect, and thus revolves at a constant speed.

In the following analysis, core losses, MMF space harmonics and magnetic saturation effects have been neglected, and all machine parameters are assumed constant and independant of frequency. Both the induction and synchronous machines are star connected.

The electromagnetic torque developed by an induction motor having p pole pairs is given by

$$T_e = \frac{p}{2} i^T \frac{dL}{d\theta} i \qquad (4.2)$$

where i^T is the transpose of i. This equation becomes, from appendix 4.7.2

$$T_e = -p\frac{\sqrt{3}}{3} Lm \left[i_{aS} (i_{bR'} - i_{cR'}) + i_{bS} (-i_{aR'} + i_{cR'}) + i_{cS} (i_{aR'} - i_{bR'}) \right] \qquad (4.3)$$

The phase and referred currents of equation (4.3) are the instantaneous values.

4.2.2 Synchronous Machine

The synchronous machine model is shown in Fig 4.2. and is based upon material presented in reference 40. The stator is assumed to be wound with a balanced set of three phase coils, and the rotor has a single field coil. There are no d and q axis damper windings. All space harmonics of MMF and flux density above the fundamental are considered to be negligible. Coil 'F' represents the field winding and is fed via slip rings from a DC supply.

For the coil system of Fig 4.2. the instantaneous voltages of the machine in terms of flux and current are given by the matrix equation

$$v = Ri + p\Phi \qquad (4.4)$$

where $\Phi = Li$

This expression may be expanded to give

$$v = Ri + \omega_R Gi + Lpi \qquad (4.5)$$

where the matrix $G = \frac{dL}{d\theta}$ and the rotor speed $\omega_R = \frac{d\theta}{dt}$

The voltage vector v represents the stator phase and referred field voltages.

$$v = [\, v_{aS} \quad v_{bS} \quad v_{cS} \quad v_F' \,]^T$$

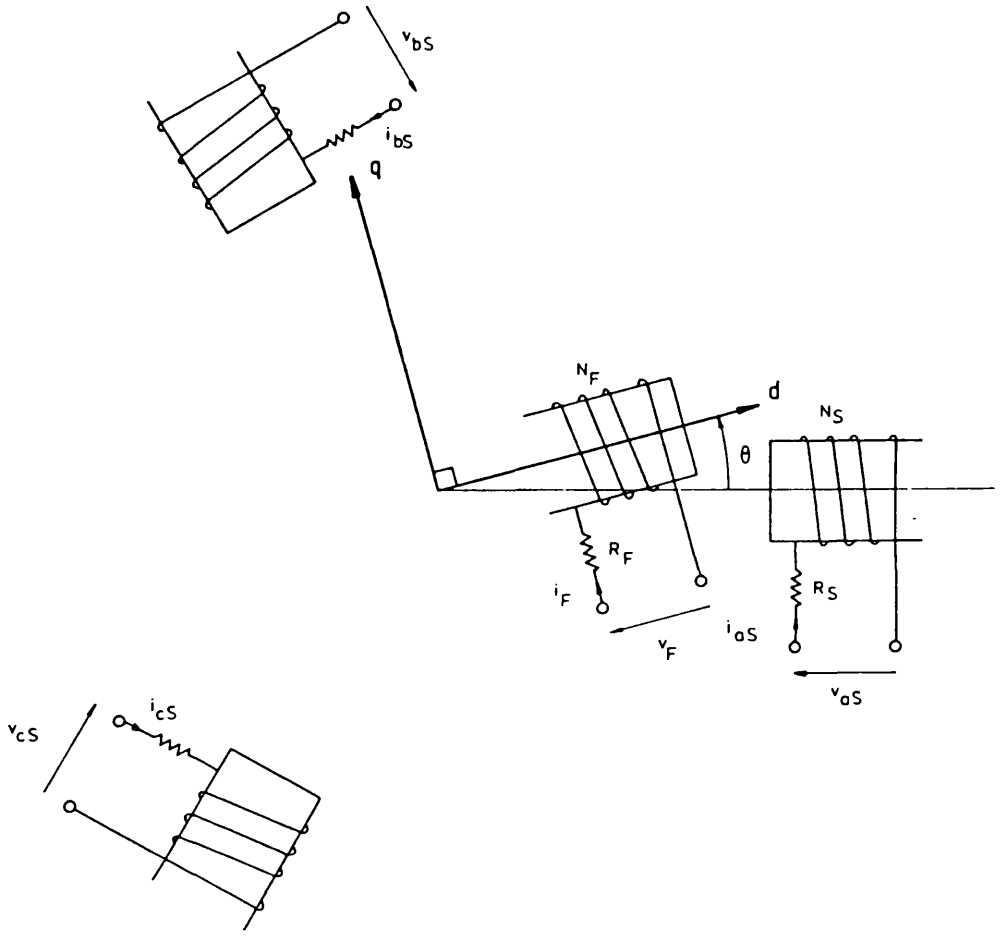

N_S - effective stator turns per phase

N_F - " turns of field winding

$$Lmd = \frac{3 Ns^2}{2 \mathcal{R}_d} \qquad Lmq = \frac{3 Ns^2}{2 \mathcal{R}_q}$$

Fig 4.2 Synchronous Machine Model

Vector i represents the phase and referred field currents.

$$i = [\, i_{aS} \quad i_{bS} \quad i_{cS} \quad i_F' \,]^T$$

and $R = \text{diagonal}\,[\, R_S \quad R_S \quad R_S \quad R_F' \,]$

The synchronous machine inductance matrix L is shown in Fig 4.3 and is applicable to both salient pole and round rotor machines. In the case of the round rotor machine Lmd = Lmq. The elements of the L matrix are dependant upon the instantaneous position of the rotor at any time, t. The angular position of the rotor with reference to the 'a' phase axis is given by,

$$\theta = \omega_R t + \gamma - \frac{\pi}{2} - \delta_T \qquad (4.6)$$

where δ_T is the torque angle. The angle γ corresponds to the electrical phase displacement of the fundamental component of the motor current, with respect to the commutation point t_o, Fig 4.5 and 4.10, at the start of the 60 degree period over which the machine equations are to be integrated.

The electromagnetic torque developed by a synchronous motor having p pole pairs is given by, in matrix notation

$$T_e = \frac{p}{2}\, i^T G\, i \qquad (4.7)$$

The instantaneous value of output torque is readily available by consideration of the intantaneous phase and referred rotor currents, and the matrix G.

$$La = (Lmd + Lmq) \qquad Lb = (Lmd - Lmq) \qquad \epsilon = \frac{2\pi}{3}$$

$l_S + \frac{La}{3} + \frac{Lb}{3}\cos 2\theta$	$-\frac{La}{6} + \frac{Lb}{3}\cos 2(\theta+\epsilon)$	$-\frac{La}{6} + \frac{Lb}{3}\cos 2(\theta+2\epsilon)$	$\sqrt{\frac{2}{3}}\, Lmd \cos\theta$
$-\frac{La}{6} + \frac{Lb}{3}\cos 2(\theta+\epsilon)$	$l_S + \frac{La}{3} + \frac{Lb}{3}\cos 2(\theta+2\epsilon)$	$-\frac{La}{6} + \frac{Lb}{3}\cos 2\theta$	$\sqrt{\frac{2}{3}}\, Lmd \cos(\theta+2\epsilon)$
$-\frac{La}{6} + \frac{Lb}{3}\cos 2(\theta+2\epsilon)$	$-\frac{La}{6} + \frac{Lb}{3}\cos 2\theta$	$l_S + \frac{La}{3} + \frac{Lb}{3}\cos 2(\theta+\epsilon)$	$\sqrt{\frac{2}{3}}\, Lmd \cos(\theta+\epsilon)$
$\sqrt{\frac{2}{3}}\, Lmd \cos\theta$	$\sqrt{\frac{2}{3}}\, Lmd \cos(\theta+2\epsilon)$	$\sqrt{\frac{2}{3}}\, Lmd \cos(\theta+\epsilon)$	$l_F' + Lmd$

Fig 4.3 Synchronous Machine Inductance Matrix L

4.3 Voltage Source Inverter: Operating states and formulation of system equations.

The voltage source inverter considered in the following analysis is shown in Fig 4.4. Thyristors T1 to T6 are gated sequentially according to the switching pattern of Fig 4.5, and remain in the conducting state for 120 degrees of the ouput period. Diodes D1 to D6 enable the reactive load energy to be circulated, and allow regeneration back into the DC link if required. The DC source voltage, Vs, is assumed to be ideal.

The time interval T, Fig 4.5, chosen for the analysis of the system performance is the 60 degree period initiated by the firing of thyristor T1, at time t_o. During the time interval T, two distinct circuit states exist.

State A - all three machine phases are connected to the inverter

State B - machine phase 'c' is disconnected from the inverter

(Fig 4.6)

Prior to time t_o, thyristors T5 and T6 have been conducting and machine phase 'a' has been disconnected from the inverter output terminals. At time t_o, thyristor T1 is gated on and thyristor T5 will be extinguished. Diode D2 is now connected across the machine terminals B and C, and is biased in such a way as to permit conduction. The equations describing this operating state are obtained by considering the two conduction loops of Fig 4.6, which is equivalent to. For State A

$$Vs = v_{aS} - v_{bS} \qquad (4.8)$$

$$Vs = v_{aS} - v_{cS}$$

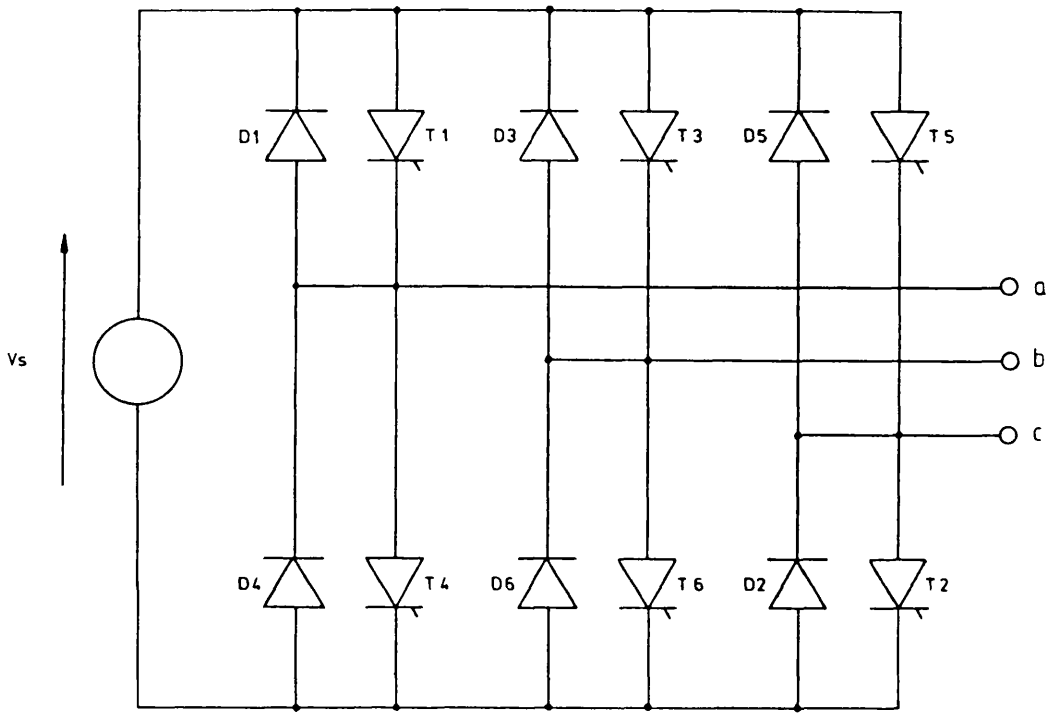

Fig 4.4 Voltage Source Inverter

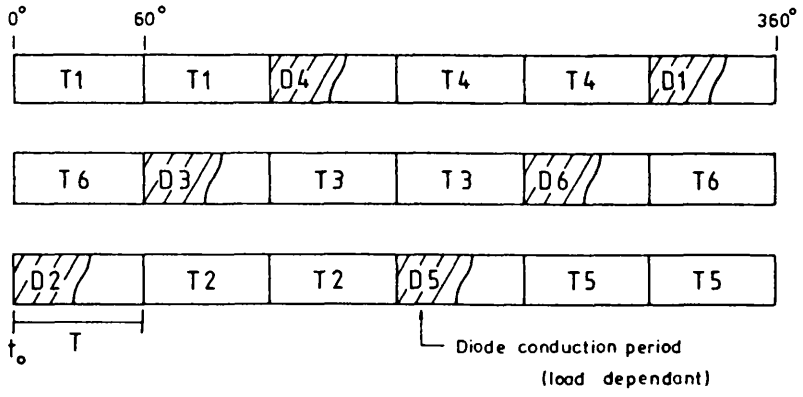

Fig 4.5 Thyristor Switching Sequence

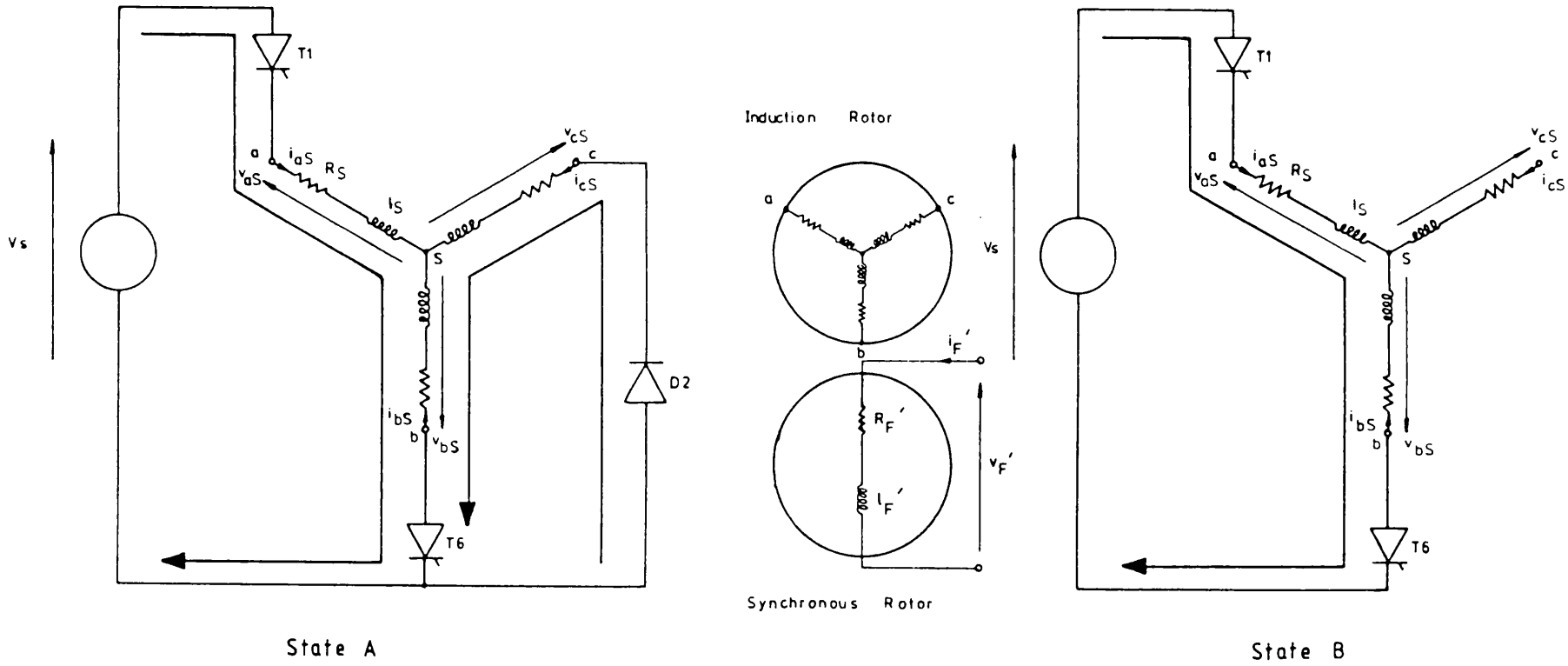

Fig 4.6 Operating States of the Voltage Source Inverter

noting that the machine phase 'a' current is given by

$$i_{aS} = -(i_{bS} + i_{cS}) \qquad (4.9)$$

The system will continue to operate in this mode until the diode current i_{D2} has fallen to zero. This conduction period is a function of the load parameters. When diode D2 ceases to conduct, machine phase 'c' will be disconnected from the inverter. The sytem is now in State B, and is described by the following equations.

$$Vs = v_{aS} - v_{bS} \qquad (4.10)$$

where the machine phase currents are given by

$$i_{bS} = - i_{aS} \qquad (4.11)$$

and $i_{cS} = 0$

State B continues for the remainder of the 60 degree period under observation and ends with the gating on of the next thyristor in sequence, which in this case is thyristor T2.

The inverter-machine system equations may now be determined, by the substitution of the appropriate model of the induction or synchronous machine into the above expressions for source voltage, (4.8, 4.10), taking into account the phase current relationships, (4.9, 4.11), that exist in the two circuit states. The differential equations representing State A and State B, Figs 4.7 and 4.8, are integrated over the period T by digital computer methods. The point at which the circuit experiences a change of state, is found by monitoring the magnitude and direction of the current in diode D2.

$$
\begin{bmatrix} V_s \\ V_s \\ 0 \\ 0 \\ 0 \end{bmatrix} =
\begin{bmatrix}
-2[R_S + p(l_S + Lm)] & -[R_S + p(l_S + Lm)] & pLm & -pLm & 0 \\
-[R_S + p(l_S + Lm)] & -2[R_S + p(l_S + Lm)] & pLm & 0 & -pLm \\
-pLm + w_R\sqrt{\frac{3Lm}{3}} & -pLm - w_R\sqrt{\frac{3Lm}{3}} & R_R' + p(l_R' + \frac{2Lm}{3}) & -p\frac{Lm}{3} + w_R\frac{\sqrt{3}}{3}(l_R' + Lm) & -p\frac{Lm}{3} - w_R\frac{\sqrt{3}}{3}(l_R' + Lm) \\
pLm + w_R\sqrt{\frac{3Lm}{3}} & 2w_R\sqrt{\frac{3Lm}{3}} & -p\frac{Lm}{3} - w_R\frac{\sqrt{3}}{3}(l_R' + Lm) & R_R' + p(l_R' + \frac{2Lm}{3}) & -p\frac{Lm}{3} + w_R\frac{\sqrt{3}}{3}(l_R' + Lm) \\
-2w_r\sqrt{\frac{3Lm}{3}} & pLm - w_R\sqrt{\frac{3Lm}{3}} & -p\frac{Lm}{3} + w_R\frac{\sqrt{3}}{3}(l_R' + Lm) & -p\frac{Lm}{3} - w_R\frac{\sqrt{3}}{3}(l_R' + Lm) & R_R' + p(l_R' + \frac{2Lm}{3})
\end{bmatrix}
\begin{bmatrix} i_{bS} \\ i_{cS} \\ i_{aR'} \\ i_{bR'} \\ i_{cR'} \end{bmatrix}
$$

Fig 4.7a Voltage Source Inverter fed Induction Motor State A

$$
\begin{bmatrix} V_s \\ 0 \\ 0 \\ 0 \end{bmatrix} = \begin{bmatrix} 2[R_S + p(l_S + Lm)] & pLm & -pLm & 0 \\ pLm - w_R\frac{\sqrt{3}Lm}{3} & R_R' + p(l_R' + \frac{2Lm}{3}) & -p\frac{Lm}{3} + w_R\frac{\sqrt{3}}{3}(l_R' + Lm) & -p\frac{Lm}{3} - w_R\frac{\sqrt{3}}{3}(l_R' + Lm) \\ -pLm - w_R\frac{\sqrt{3}Lm}{3} & -p\frac{Lm}{3} - w_R\frac{\sqrt{3}}{3}(l_R' + Lm) & R_R' + p(l_R' + \frac{2Lm}{3}) & -p\frac{Lm}{3} + w_R\frac{\sqrt{3}}{3}(l_R' + Lm) \\ 2w_R\frac{\sqrt{3}Lm}{3} & -p\frac{Lm}{3} + w_R\frac{\sqrt{3}}{3}(l_R' + Lm) & -p\frac{Lm}{3} - w_R\frac{\sqrt{3}}{3}(l_R' + Lm) & R_R' + p(l_R' + \frac{2Lm}{3}) \end{bmatrix} \begin{bmatrix} i_{aS} \\ i_{aR}' \\ i_{bR}' \\ i_{cR}' \end{bmatrix}
$$

Fig 4.7b Voltage Source Inverter Fed Induction Motor State B

$K1 = \theta \qquad K2 = (\theta + \epsilon) \qquad K3 = (\theta + 2\epsilon)$

$$
\begin{bmatrix} V_S \\ V_S \\ V_F' \end{bmatrix} = \begin{bmatrix} -2R_S + \frac{2}{3}w_R L_b[\sin 2K1 - 2\sin 2K2 + \sin 2K3] - p[2l_S + L_a + \frac{L_b}{3}(\cos 2K1 - 2\cos 2K2 + \cos 2K3)] & -R_S + \frac{2}{3}w_R L_b[2\sin 2K1 - \sin 2K2 - \sin 2K3] - p[l_S + \frac{L_a}{2} + \frac{L_b}{3}[2\cos 2K1 - \cos 2K2 - \cos 2K3)] & w_R\sqrt{\frac{2}{3}}L_{md}[\sin K3 - \sin K1] + p\sqrt{\frac{2}{3}}L_{md}[\cos K1 - \cos K3] \\ (1,2) & -2R_S + \frac{2}{3}w_R L_b[\sin 2K1 + \sin 2K2 - 2\sin 2K3 - p[2l_S + L_a + \frac{L_b}{3}(\cos 2K1 + \cos 2K2 - 2\cos 2K3)] & w_R\sqrt{\frac{2}{3}}L_{md}[\sin K2 - \sin K1] + p\sqrt{\frac{2}{3}}L_{md}[\cos K1 - \cos K2] \\ -(1,3) & -(2,3) & R_F' + p(l_F' + L_{md}) \end{bmatrix} \begin{bmatrix} i_{bS} \\ i_{cS} \\ i_F' \end{bmatrix}
$$

State A

$$
\begin{bmatrix} V_S \\ V_F' \end{bmatrix} = \begin{bmatrix} 2R_S - \frac{2}{3}w_R L_b[\sin 2K1 - 2\sin 2K2 + \sin 2K3] + p[2l_S + L_a + \frac{L_b}{3}[\cos 2K1 - 2\cos 2K2 + \cos 2K3] & -w_R\sqrt{\frac{2}{3}}L_{md}[\sin K1 - \sin K3] + p\sqrt{\frac{2}{3}}L_{md}[\cos K1 - \cos K3] \\ (1,2) & R_F' + p(l_F' + L_{md}) \end{bmatrix} \begin{bmatrix} i_{aS} \\ i_F' \end{bmatrix}
$$

State B

Fig 4.8 Voltage Source Inverter Fed Synchronous Motor

Whilst the computer model developed for the VSI has been primarily designed to solve for discontinuous phase currents, if the load is sufficiently inductive the currents will not become discontinuous. In this case the circuit will remain in State A and the integration procedure will be repeated as before. Thus a steady state solution for the 180 degree conduction mode may be found, producing the characteristic quasi-square terminal voltage waveform associated with this mode of operation.

4.4 Current Source Inverter: Operating states and formulation of system equations

The current source inverter is shown in Fig 4.9. The current source is modelled by an ideal voltage source in series with a link inductor, Ldc, which has to be rated at operating current levels.

Thyristors T1 to T6 switch the DC link current, Idc, at a rate necessary to establish the desired machine operating frequency. Capacitors C1 to C6 provide the energy storage requirements for satisfactory thyristor commutation, and the diodes D1 to D6 isolate the capacitors from the output terminals except during commutation.

During commutation, the capacitors become charged to peak voltages which are largely determined by the level of machine current being commutated. This enables the inverter to commutate satisfactorily over a wide range of output frequency and voltage.

The 60 degree period, T, for which the system is to be observed, commences at time t_o, Fig 4.10. During this period the DC link current is transferred from phase 'a' to phase 'b'. For each commutation period, T, the inverter circuit has three distinct operating modes, these are

State A - charging mode

State B - current transfer mode

State C - normal mode

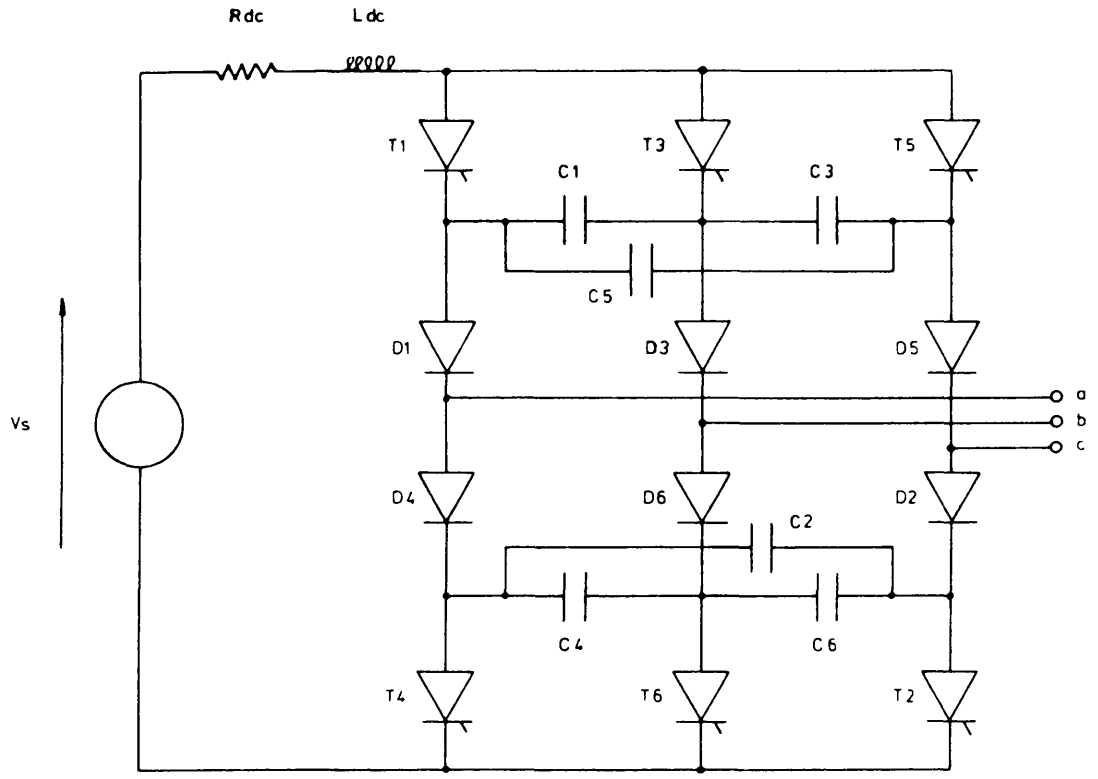

Fig 4.9 Current Source Inverter

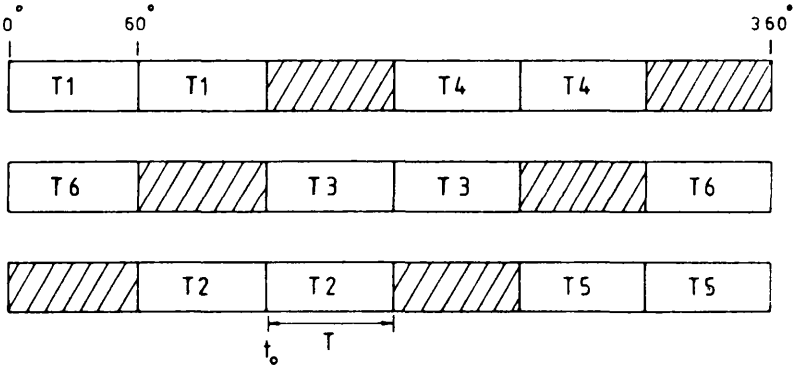

Fig 4.10 Thyristor Switching Sequence

It is assumed that no commutation overlap occurs, ie commutation of the phase currents is successfully completed within the 60 degree period.

Prior to the commencement of the charging mode, at time t_o, thyristors T1 and T2 have been conducting, Fig 4.11a. At time t_o, thyristor T3 is gated on and the charge stored across the commutation capacitor Ceq, is presented across thyristor T1, which is extinguished. As the time taken to successfully commutate thyristor T1 is very small compared to the total commutation period, the transfer of current from T1 to T3 is assumed to be instantaneous. During State A, Fig 4.11b, the delta connected capacitor bank C1, C3 and C5 (forming the equivalent capacitor Ceq), is charged linearly by the constant link current, Idc.

Initially the machine terminal voltage , v_{ba} , is more positive than the voltage, v_{ceq} , across the equivalent capacitance, so reverse biasing the series diode D3, which therefore does not conduct. The equations describing this mode of operation are obtained by considering the conduction loop of Fig 4.11b.

For State A

$$Vs = (Rdc + pLdc) i_{aS} + v_{ceq} + v_{aS} - v_{cS} \qquad (4.12)$$

and $$Ceq\ p\ v_{ceq} = i_{aS}$$

noting that the machine phase currents are

$$Idc = i_{aS} = - i_{cS} \qquad (4.13)$$

and $$i_{bS} = 0$$

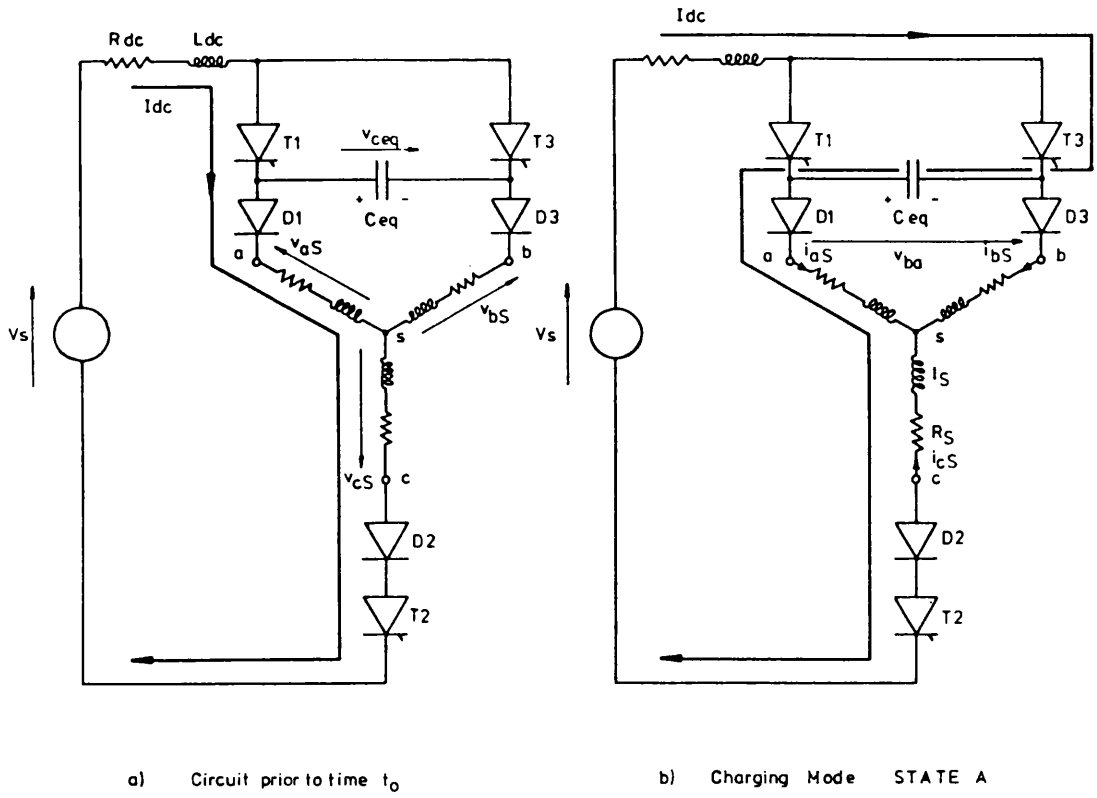

a) Circuit prior to time t_o

b) Charging Mode STATE A

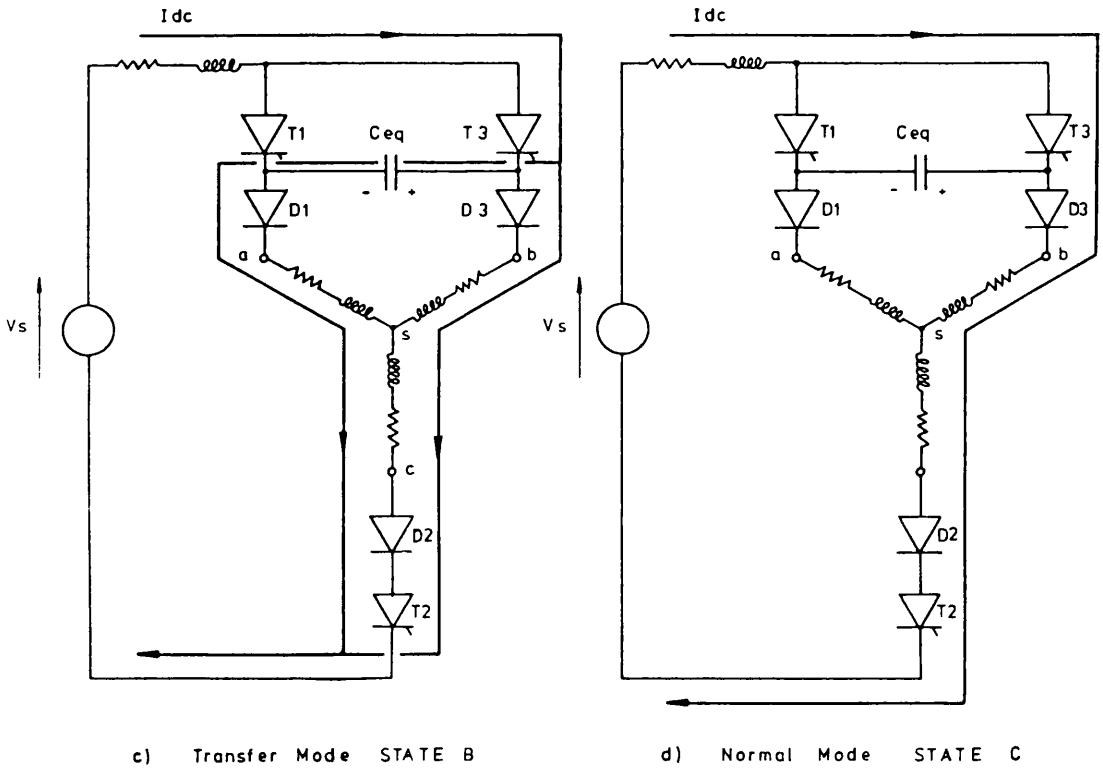

c) Transfer Mode STATE B

d) Normal Mode STATE C

Fig 4.11 Commutation Modes of the Current Source Inverter

The charge on the equivalent capacitor, Ceq, reverses until $v_{ceq} = v_{ba}$ and the series diode D3 becomes forward biased. As soon as diode D3 starts to conduct, the DC link is presented with a parallel path through the outgoing phase 'a' and the incoming phase 'c'.

The inverter circuit is now operating in the transfer mode, in which the link current rapidly transfers from phase 'a' to phase 'b', Fig 4.11c. During current transfer the machine phase resistance and leakage inductances form a part of the commutating circuit together with the equivalent commutation capacitance, and hence the variation of motor current will follow a damped sinusoid. At all times during this mode the sum of phase 'a' and 'b' currents will equal the DC link value. The equations describing this mode, for the two conduction loops of Fig 4.11c are, for State B

$$Vs = (Rdc + pLdc) (i_{aS} + i_{bS}) + v_{bS} - v_{cS} \qquad (4.14)$$

$$Vs = (Rdc + pLdc) (i_{aS} + i_{bS}) + v_{ceq} + v_{aS} - v_{cS} \qquad (4.15)$$

and $$Ceq\ p\ v_{ceq} = i_{aS} \qquad (4.16)$$

where the machine phase 'c' current is given by

$$i_{cS} = - (i_{aS} + i_{bS}) \qquad (4.17)$$

The main characteristic of the transfer mode is the production of voltage spikes across the machine output terminals. The voltage spikes are generated by the rapidly changing currents in the machine leakage inductances.

State B continues until the phase 'a' current reaches zero. When this occurs, the series diode D1 ensures that the current cannot reverse direction, and thus isolates machine phase 'a' from the inverter output terminals. Commutation capacitor C1 is now charged to the correct polarity for its next commutation duty.

Current transfer is now complete and the inverter enters the normal mode, State C, Fig 4.11d. During this mode the commutation capacitor voltages remain constant, and the DC link current flows through machine phases 'b' and 'c'.

For State C therefore,

$$V_s = (R_{dc} + pL_{dc}) i_{bS} + v_{bS} - v_{cS} \qquad (4.18)$$

and the machine phase currents are

$$-i_{cS} = i_{bS} \quad \text{and} \quad i_{aS} = 0 \qquad (4.19)$$

This state continues for what remains of the period T, after which a further commutation period is initiated by the gating on of thyristor T4.

The complete inverter-machine equations may now be set up in a similar manner to the voltage source inverter system, by the substitution of the appropriate machine model into the above expressions for the three circuit states. The resulting equations for the CSI fed induction and synchronous machines are shown in Figs 4.12 and 4.13, respectively.

These differential equations are evaluated for each mode of operation, over the period T. The two changes of state are found by observing the

$$
\begin{bmatrix} 0 \\ V_s \\ 0 \\ 0 \\ 0 \end{bmatrix} =
\begin{bmatrix}
pC_{eq} & -1 & 0 & 0 & 0 \\
1 & 2R_S + R_{dc} + p[2(l_S + L_m) + L_{dc}] & pL_m & 0 & -pL_m \\
0 & pL_m + w_R\sqrt{3}\frac{L_m}{3} & R_R' + p(l_R' + \frac{2L_m}{3}) & -p\frac{L_m}{3} + w_R\sqrt{3}\frac{(l_R' + L_m)}{3} & -p\frac{L_m}{3} - w_R\sqrt{3}\frac{(l_R' + L_m)}{3} \\
0 & -2w_R\sqrt{3}\frac{L_m}{3} & -p\frac{L_m}{3} - w_R\sqrt{3}\frac{(l_R' + L_m)}{3} & R_R' + p(l_R' + \frac{2L_m}{3}) & -p\frac{L_m}{3} + w_R\sqrt{3}\frac{(l_R' + L_m)}{3} \\
0 & -pL_m + w_R\sqrt{3}\frac{L_m}{3} & -p\frac{L_m}{3} + w_R\sqrt{3}\frac{(l_R' + L_m)}{3} & -p\frac{L_m}{3} - w_R\sqrt{3}\frac{(l_R' + L_m)}{3} & R_R' + p(l_R' + \frac{2L_m}{3})
\end{bmatrix}
\begin{bmatrix} V_{ceq} \\ i_{aS} \\ i_{aR}' \\ i_{bR}' \\ i_{cR}' \end{bmatrix}
$$

Fig 4.12a Current Source Inverter Fed Induction Motor State A

0	=	pCeq	0	-1	0	0	0	v_{ceq}
Vs		0	$2R_S + Rdc + p[2(l_S + Lm) + Ldc]$	$R_S + Rdc + p[l_S + Lm + Ldc]$	0	pLm	-pLm	i_{bS}
Vs		1	$R_S + Rdc + p[l_S + Lm + Ldc]$	$2R_S + Rdc + p[2(l_S + Lm) + Ldc]$	pLm	0	-pLm	i_{aS}
0		0	0	$2w_R\sqrt{\frac{3}{3}}Lm$	$pLm + w_R\sqrt{\frac{3}{3}}Lm$			i_{aR}'
0		0	0	$pLm - w_R\sqrt{\frac{3}{3}}Lm$	$-2w_R\sqrt{\frac{3}{3}}Lm$	equations as for State A		i_{bR}'
0		0	0	$-pLm - w_R\sqrt{\frac{3}{3}}Lm$	$-pLm + w_R\sqrt{\frac{3}{3}}Lm$			i_{cR}'

Fig 4.12b Current Source Inverter Fed Induction Motor State B

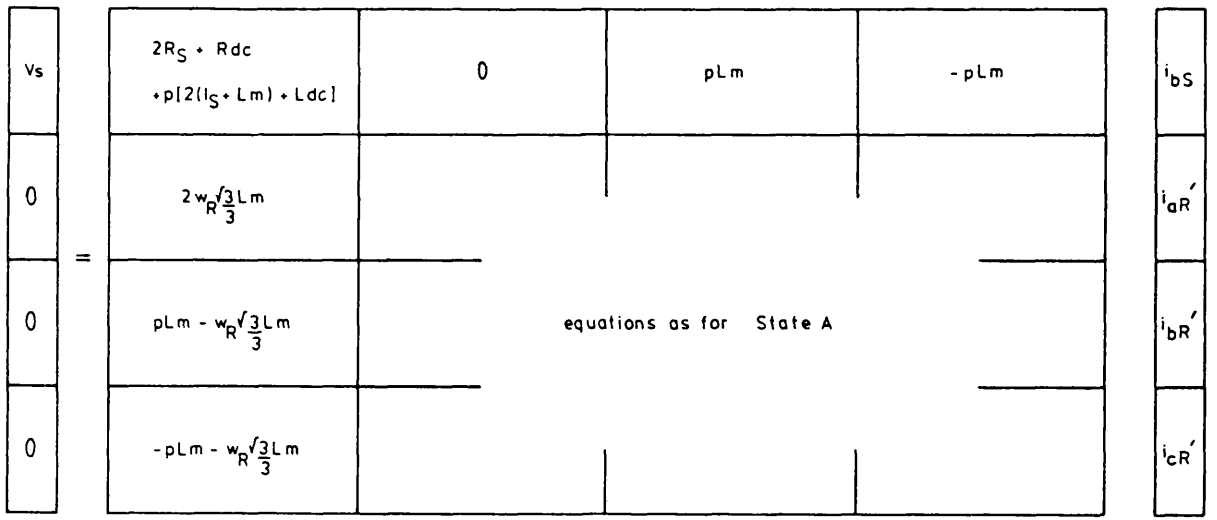

Fig 4.12c Current Source Inverter Fed Induction Motor State C

$K1 = \theta \qquad K2 = (\theta + \epsilon) \qquad K3 = (\theta + 2\epsilon)$

$$\begin{bmatrix} 0 \\ V_s \\ v_F' \end{bmatrix} = \begin{bmatrix} pCeq & -1 & 0 \\ 1 & \begin{matrix} 2R_S + Rdc + \frac{2}{3} w_R Lb \\ [-\sin 2K1 - \sin 2K2 + 2\sin 2K3] \\ + p[Ldc + 2l_S + La + \frac{Lb}{3} \\ (\cos 2K1 + \cos 2K2 - 2\cos 2K3] \end{matrix} & \begin{matrix} w_R \sqrt{\frac{2}{3}} Lmd[\sin K2 - \sin K1] \\ + p\sqrt{\frac{2}{3}} Lmd[\cos K1 - \cos K2] \end{matrix} \\ 0 & (2,3) & R_F' + p(l_F' + Lmd) \end{bmatrix} \begin{bmatrix} V_{ceq} \\ i_{aS} \\ i_F' \end{bmatrix}$$

Fig 4.13a Current Source Inverter Fed Synchronous Motor State A

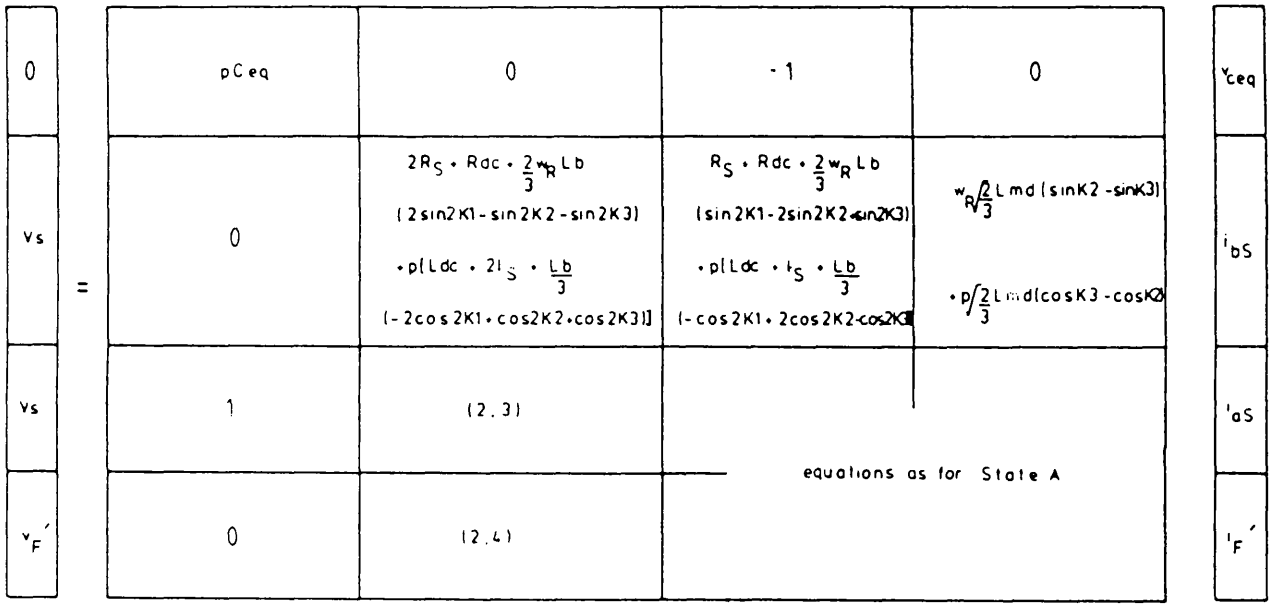

Fig 4.13b Current Source Inverter Fed Synchronous Motor State B

$$
\begin{bmatrix} V_s \\ v_F' \end{bmatrix} = \begin{bmatrix} 2R_S + \frac{2}{3}w_R L_b \,(2\sin 2K1 - \sin 2K2 - \sin 2K3) + p[L_{dc} + 2l_S + L_a + \frac{L_b}{3}\,(-2\cos 2K1 + \cos 2K2 + \cos 2K3)] & w_R\sqrt{\frac{2}{3}}L_{md}(\sin K2 - \sin K3) + p\sqrt{\frac{2}{3}}L_{md}(\cos K3 - \cos K2) \\ (1.2) & R_F' + p(l_F' + L_{md}) \end{bmatrix} \begin{bmatrix} i_{bS} \\ i_F' \end{bmatrix}
$$

Fig 4.13c Current Source Inverter Fed Synchronous Motor State C

point at which the voltage across D3 goes positive and the current through D1 has reduced to zero.

If instantaneous commutation is assumed the phase current waveforms are rectangular, in 120 degree blocks. In this case the DC link current is given by

$$Idc = \frac{\pi}{\sqrt{6}} Iph_{rms} \qquad (4.20)$$

This equation gives a good approximate value for the DC link current, and is used as the starting value in the iterative process to evaluate a steady state solution.

An initial value for the voltage across the commutation capacitor C1, for a star connected machine and neglecting the machine back emf, is given by [31]

$$v_{c1} = v_{ceq} = \frac{2Idc}{3C\omega_c} \qquad (4.21)$$

where $\omega_c = \frac{1}{\sqrt{3L_T C}}$

and L_T is the total machine leakage inductance and C, the inverter capacitance value. The appropriate value of source voltage, Vs, at any machine operating torque may be found by equating the DC link power and the total machine input power.

4.5 Computational Procedure

The differential equations that describe the inverter-machine performance, may be solved by any numerical integration procedure using a step by step method, providing the step length is small enough. In general two methods are available

1 multistep methods - in which the knowledge of a previous solution is used at each integration step for the calculation of future points.
2 single step methods - in which all evaluations of the algorithm are confined to a single integration step and previous solutions are not required.

Predictor-Corrector methods belong to the first group, whereas Runge-Kutta methods belong to the second. Although a choice between these methods tends to be difficult to make, the general considerations when selecting an algorithm, apart from the nature of the problem to be solved are, numerical stability, simplicity of the algorithm in terms of its implementation on the computer, and the time and memory requirements.
A Runge-Kutta-Merson integration method,[40] is employed throughout this investigation, for the following reasons.

1 no special starting procedure is required, which has advantages during transients and where the number of equations to be solved is changing.
2 the step length is easily changed.
3 a straightforward computational procedure is repeated throughout the integration process and gives accurate results.

An estimate of the accuracy of the method is given by the computation of an error function, from the weighted sum of the individual estimates at each integration step.[41] A suitable step length was chosen to keep this error within reasonable limits.

The system equations are evaluated for one sixth of a cycle only. The integration procedure is then repeated for successive 60 degree periods until a steady state solution is reached. At the end of each period, T, the system variables, eg. the phase and referred rotor currents, and commutation capacitor voltage (in the case of the current source inverter), are redesignated and used as the new starting conditions for the next integration period. When the initial and final values for one sixth of a cycle have settled to within a given tolerance the system is assumed to have reached the steady state. The 60 degree solution is then used to construct the machine performance waveforms for one complete cycle of inverter operation.

Iterative loops are provided within the computer program to accurately determine the point at which a change of state occurs. The step size is progressively reduced until the variable under observation has reached the desired value to within a given tolerence.

All computer programs were written using the FORTRAN language and all calculations were performed on a Honeywell 68DPS computer at the University of Bath.

4.6 Performance predictions for induction and salient pole synchronous motors.

Steady state performance predictions for the induction and salient pole synchronous designs of Chapter 3, are shown in Figs 4.16 and 4.17, for the voltage and current source inverters respectively. Three sample frequency points are shown, 10, 50 to 200Hz, to demonstrate the machine responses over the required speed range.

Both inverters are operated under a rising voltage control. In each case the inverter source voltage, Vs, has been set to give the output torque required by the traction motor characteristic of Fig 3.2.

A harmonic analysis of the output torque waveform has been performed to determine the magnitudes of the 6th and 12th harmonic torques present. These two harmonics dominate, due to the nature of the switching sequence in the inverter. The results of this analysis can be seen in Table 4.1. The percentage figures quoted represent the ratio of peak harmonic torque to average torque levels.

It can be seen from Fig 4.16 that the machine phase voltages, for a VSI fed machine, are dependant upon the motor back emf during the periods for which one of the motor phases is disconnected from the inverter. At all other times the terminal voltage is well defined. Table 4.1 shows that the magnitude of the harmonic torques present in the output of VSI fed machines, are considerably reduced for the synchronous machine. This would suggest that a VSI fed synchronous machine would be preferable in this application, but the same restrictions regarding the complexity of the rotor position control system, and the cost of a separate field supply must again be weighed against its reduced torque ripple capabilities.

	INDUCTION		SALIENT POLE SYNCHRONOUS		
frequency	VSI	CSI	VSI	CSI	% harmonic
10	10.6	7.4	2·9	12·3	6
	3·5	2·4	1·2	4·8	12
50	10·4	6·9	2·6	11·6	6
	3·5	1·9	1·1	4·7	12
200	11·4	4·4	2·7	10·9	6
	4·0	0·8	1·4	4·3	12

Table 4.1 Harmonic torques present in output

The DC link inductance of the CSI, Ldc, has been set to ten times the total leakage inductance of the induction motor. Ldc = 4 mH. For comparison purposes this value was unaltered for determining the performance of the salient pole synchronous motor. The link resistance, Rdc, was set to zero. A commutation capacitor of 10μF was used as this value successfully commutates the link current at the upper frequency limit of the system, with no commutation overlap.

The resulting phase voltage waveform of the CSI fed machines is sinusoidal, with superimposed commutation spikes due to the rapidly changing currents in the machine leakage inductances. The magnitude of the phase voltage is dependant upon the fundamental current component, and the operating point of the machine. One advantage of the CSI, is that this voltage is useful for control purposes with a minimal amount of filtering.

The commutation voltage is also a function of the motor current, so that as the motor current increases due to a change in the operating point, the ability of the inverter to commutate that current is increased accordingly. This means that the largest commutation spikes occur during the high current requirements of the constant acceleration period, up to a train speed of 55 Km/hr. This fact is illustrated in Fig 4.17. As a result of the increased voltage stress at low operating frequencies a careful choice of insulating materials will be required to prevent long term deterioration of the winding insulation.

Comparing the magnitude of the harmonic torques present in the output of the CSI fed machines, suggests that the induction motor design would be more suitable, as the percentage torque ripple present in the output is considerably lower than for the synchronous design.

Throughout this analysis the equivalent circuit parameters have been assumed to be independant of frequency. This is only approximately so, as skin effects will lead to an increase in rotor resistance and a decrease in leakage reactance as the frequency increases. However this factor will have minimal effects upon the model, which it is felt produces a sufficiently accurate indication of the motor terminal characteristics, to allow for the realistic rating of the inverter components.

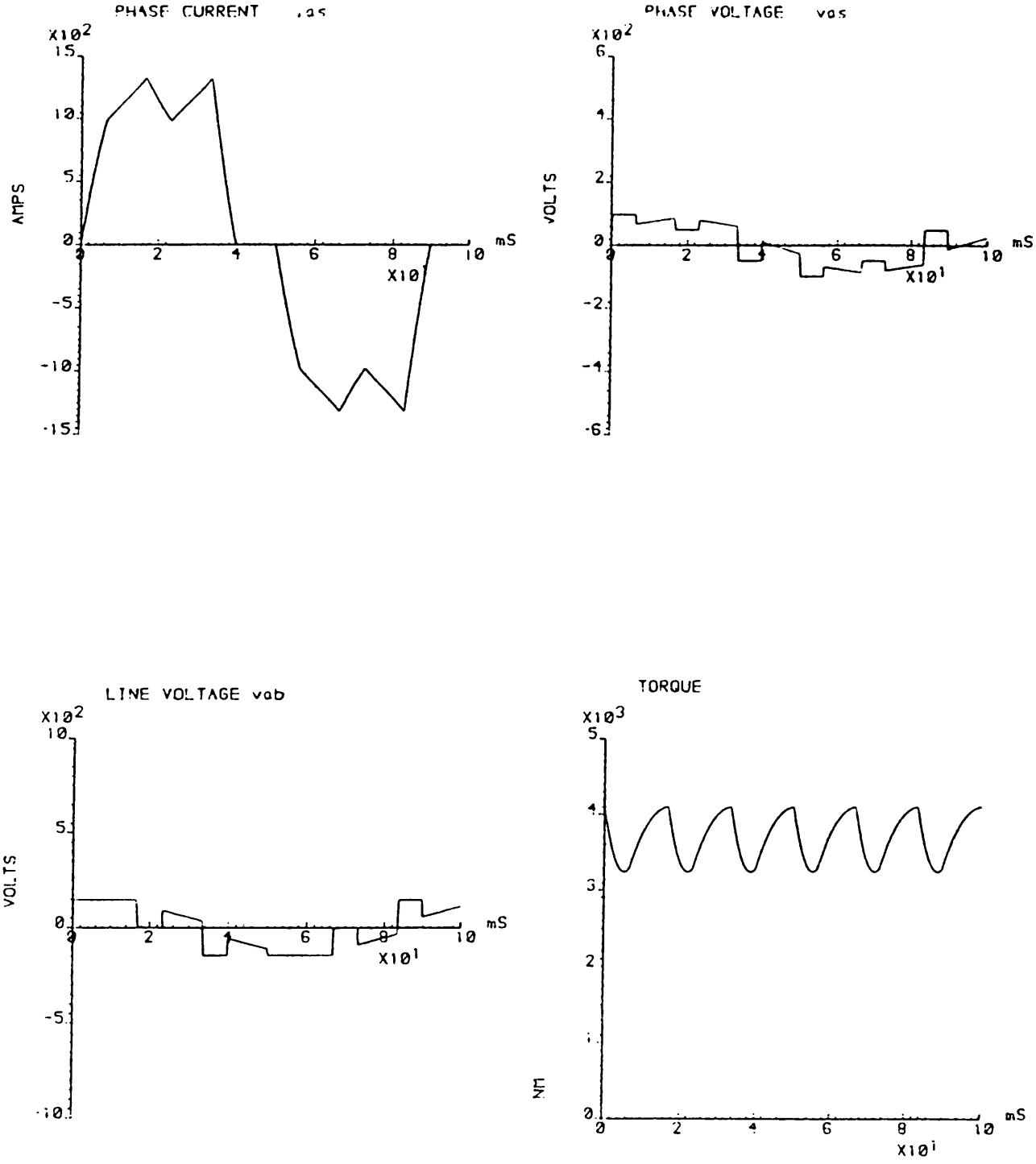

Fig 4.16a VSI Induction Motor 10 Hz

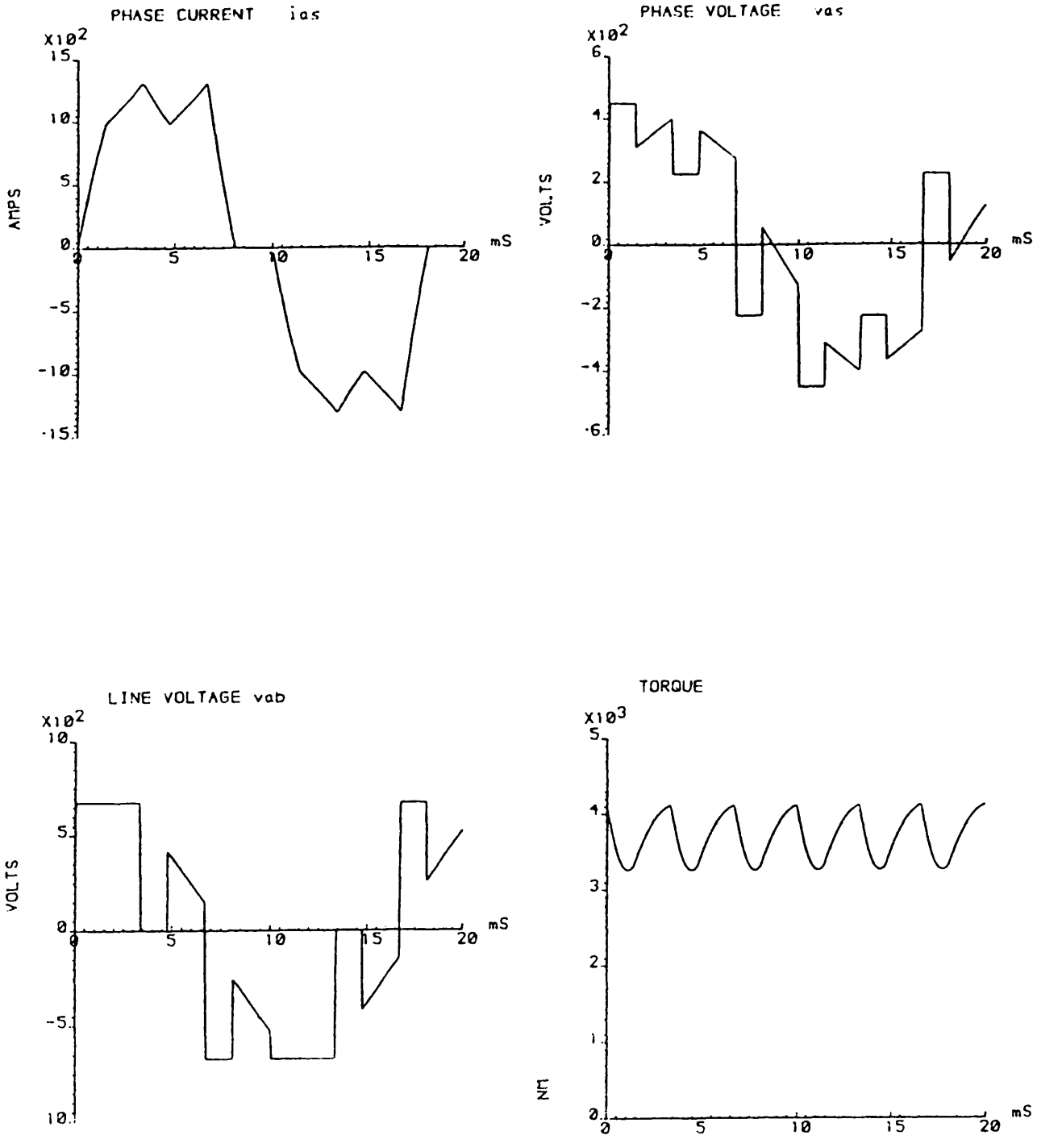

Fig 4.16b VSI Induction Motor 50 Hz

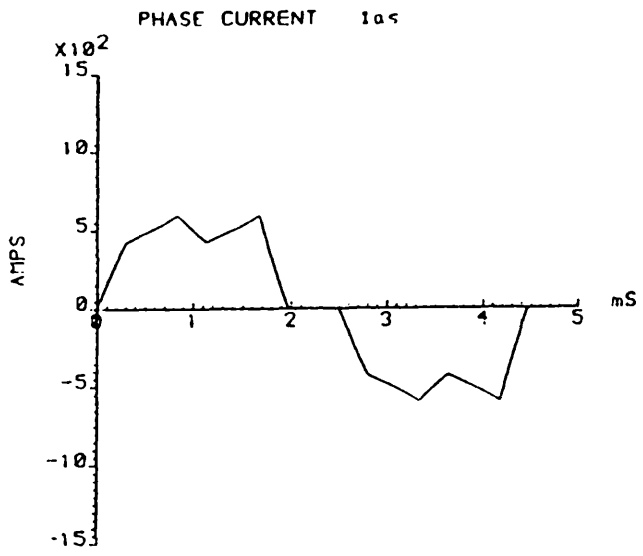

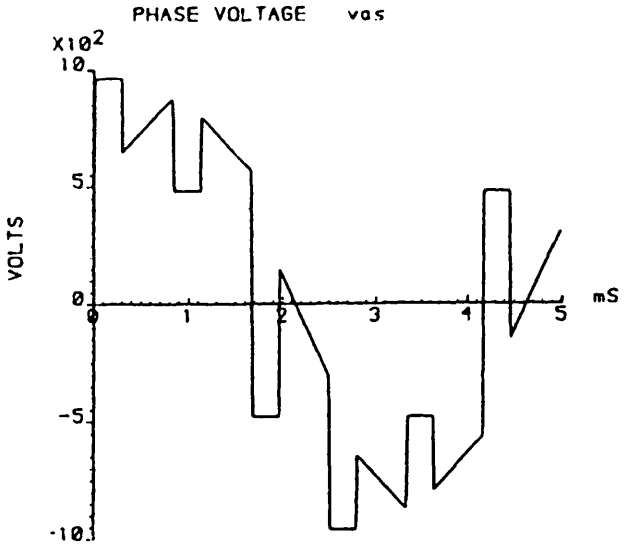

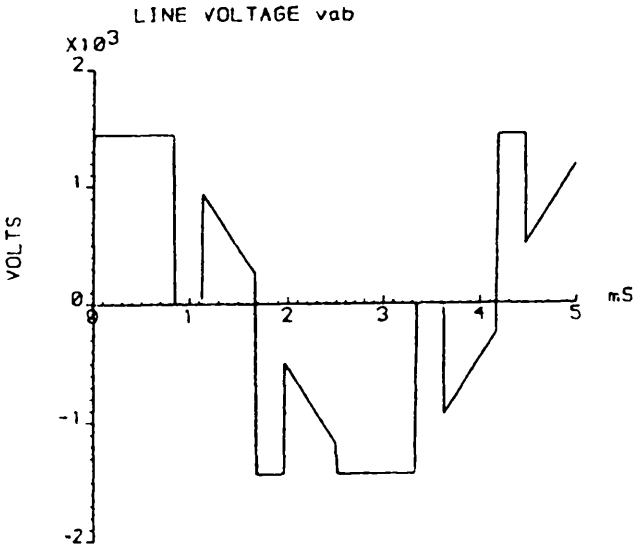

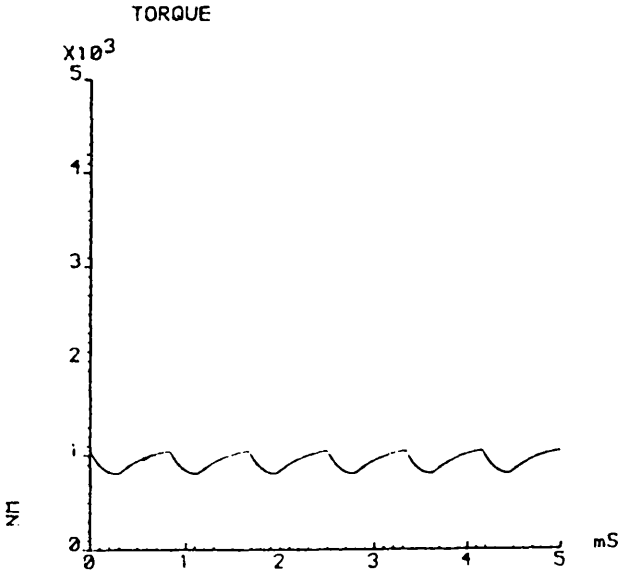

Fig 4.16c VSI Induction Motor 200 Hz

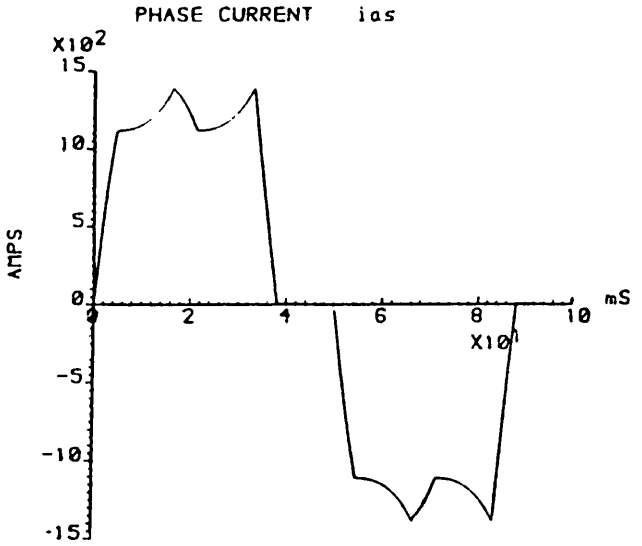

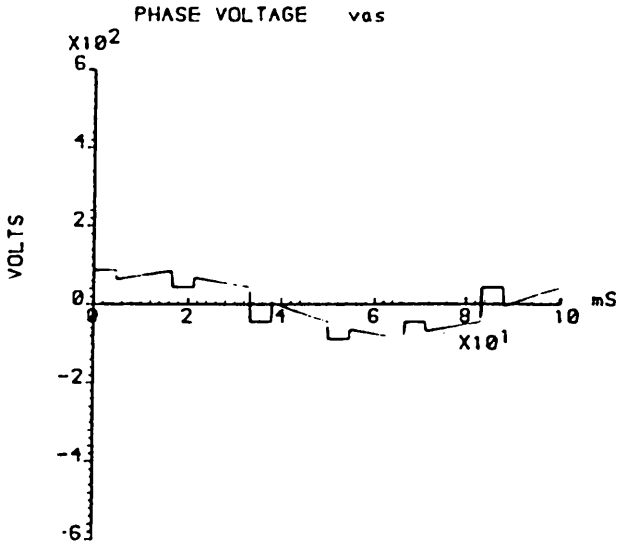

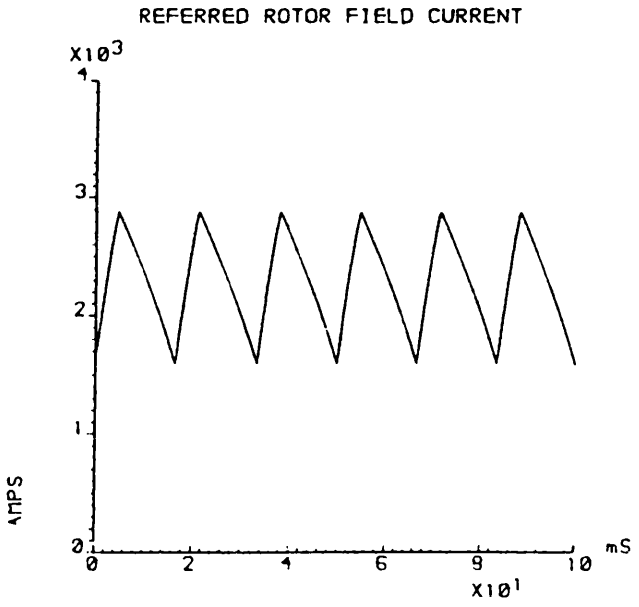

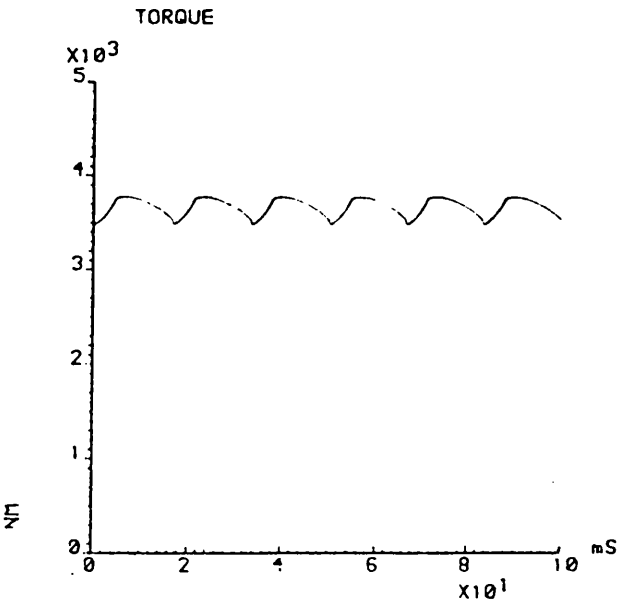

Fig 4.16d VSI Synchronous Motor 10 Hz

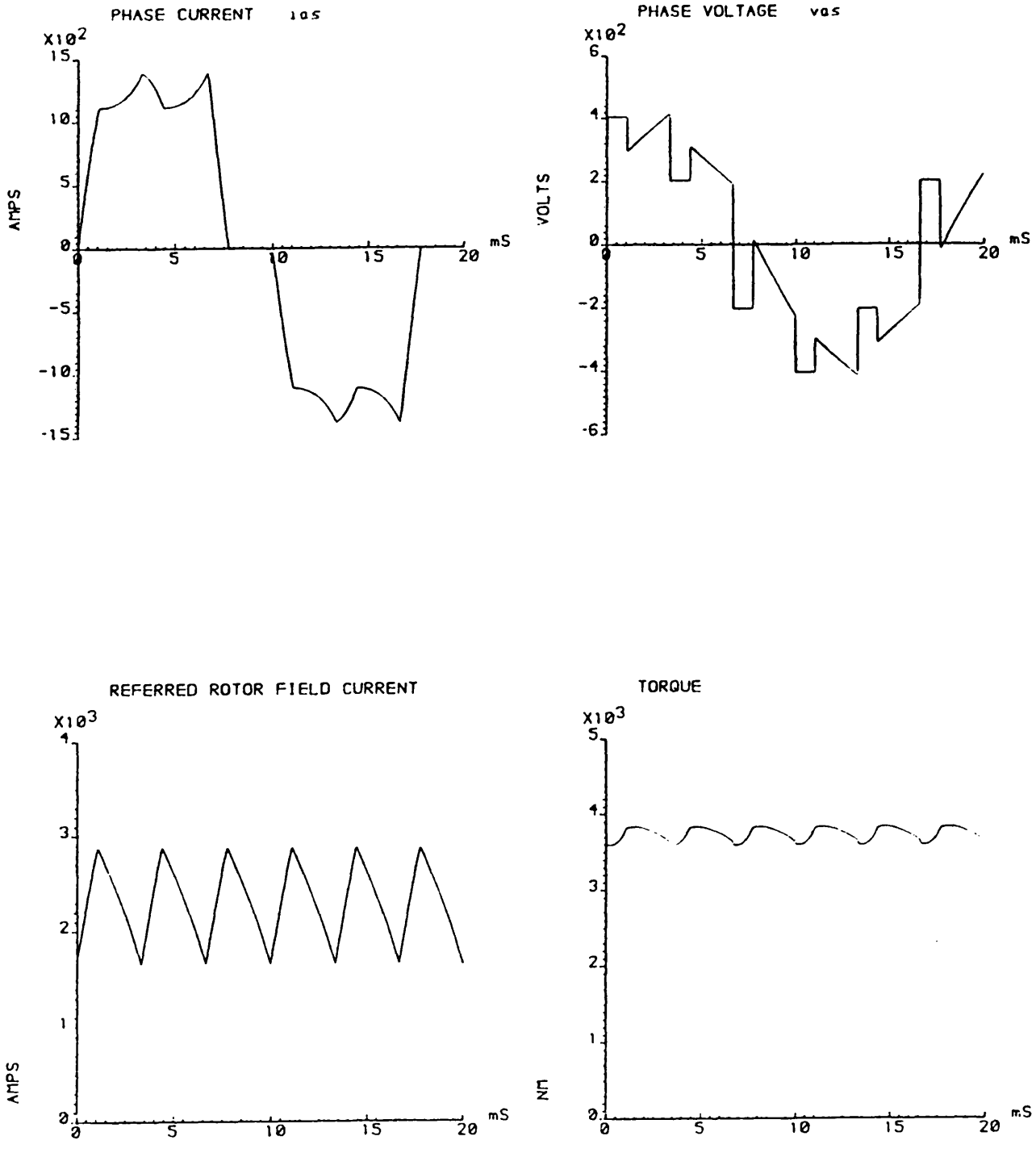

Fig 4.16e VSI Synchronous Motor 50 Hz

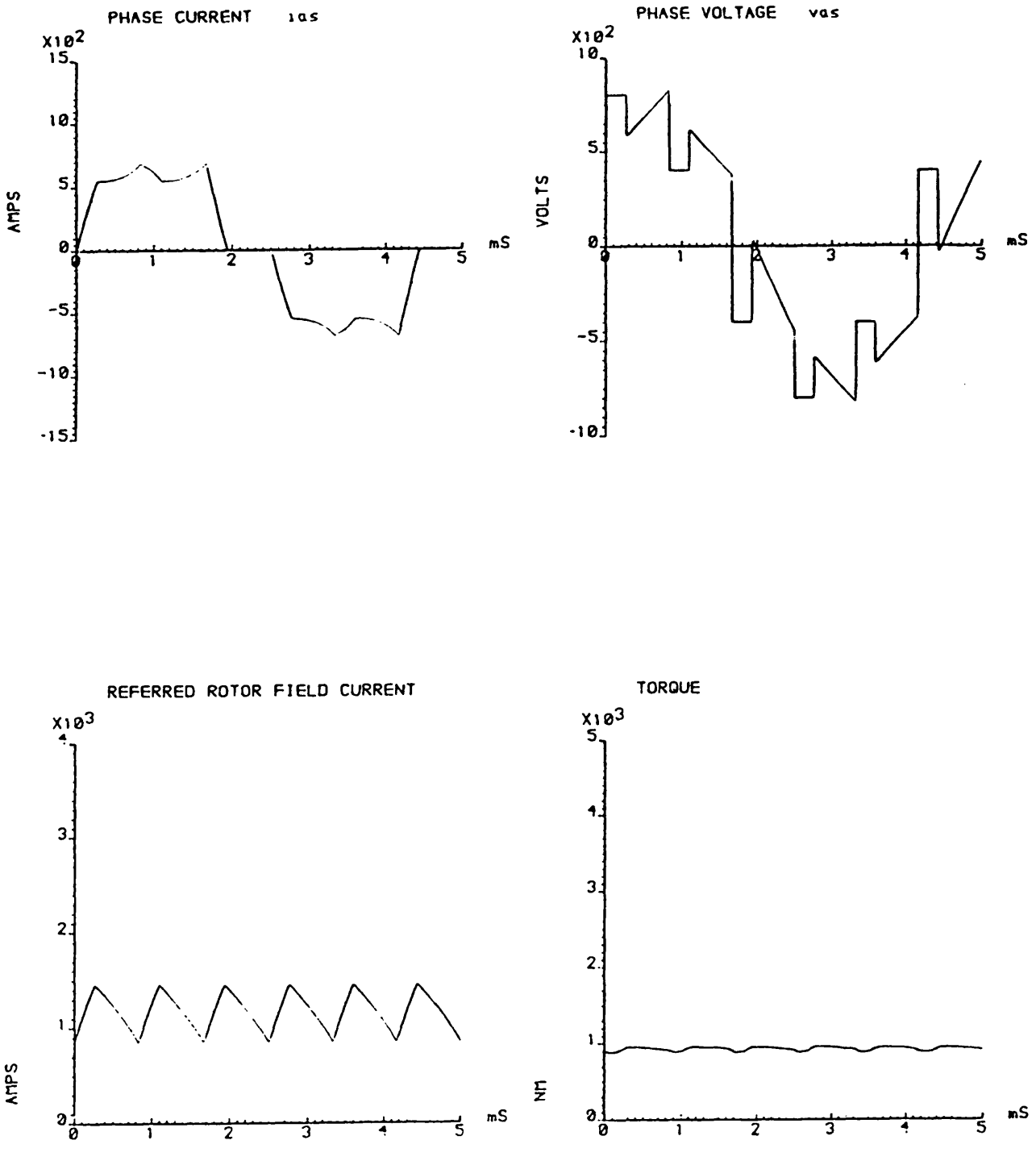

Fig 4.16f VSI Synchronous Motor 200 Hz

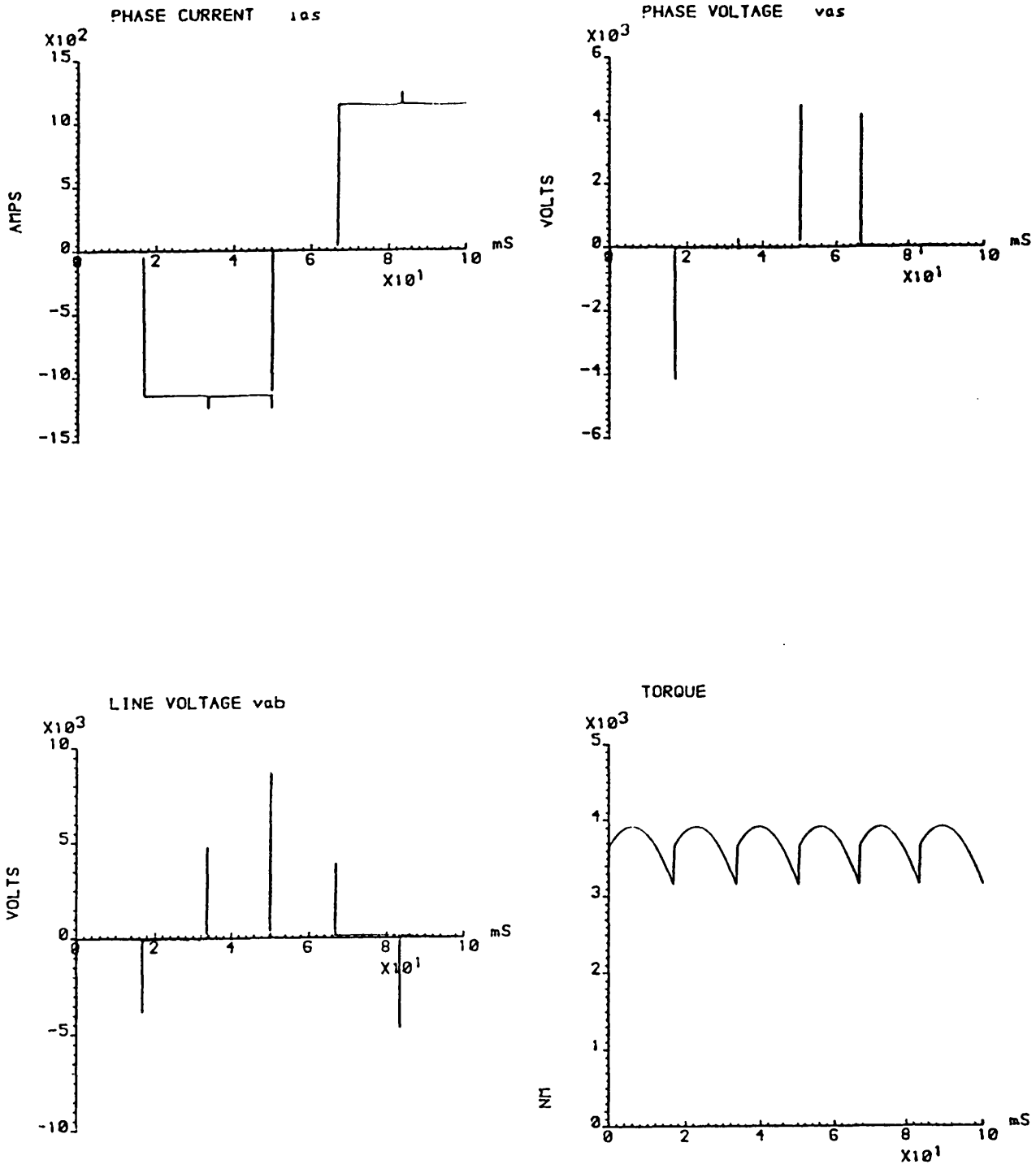

Fig 4.17a CSI Induction Motor 10 Hz

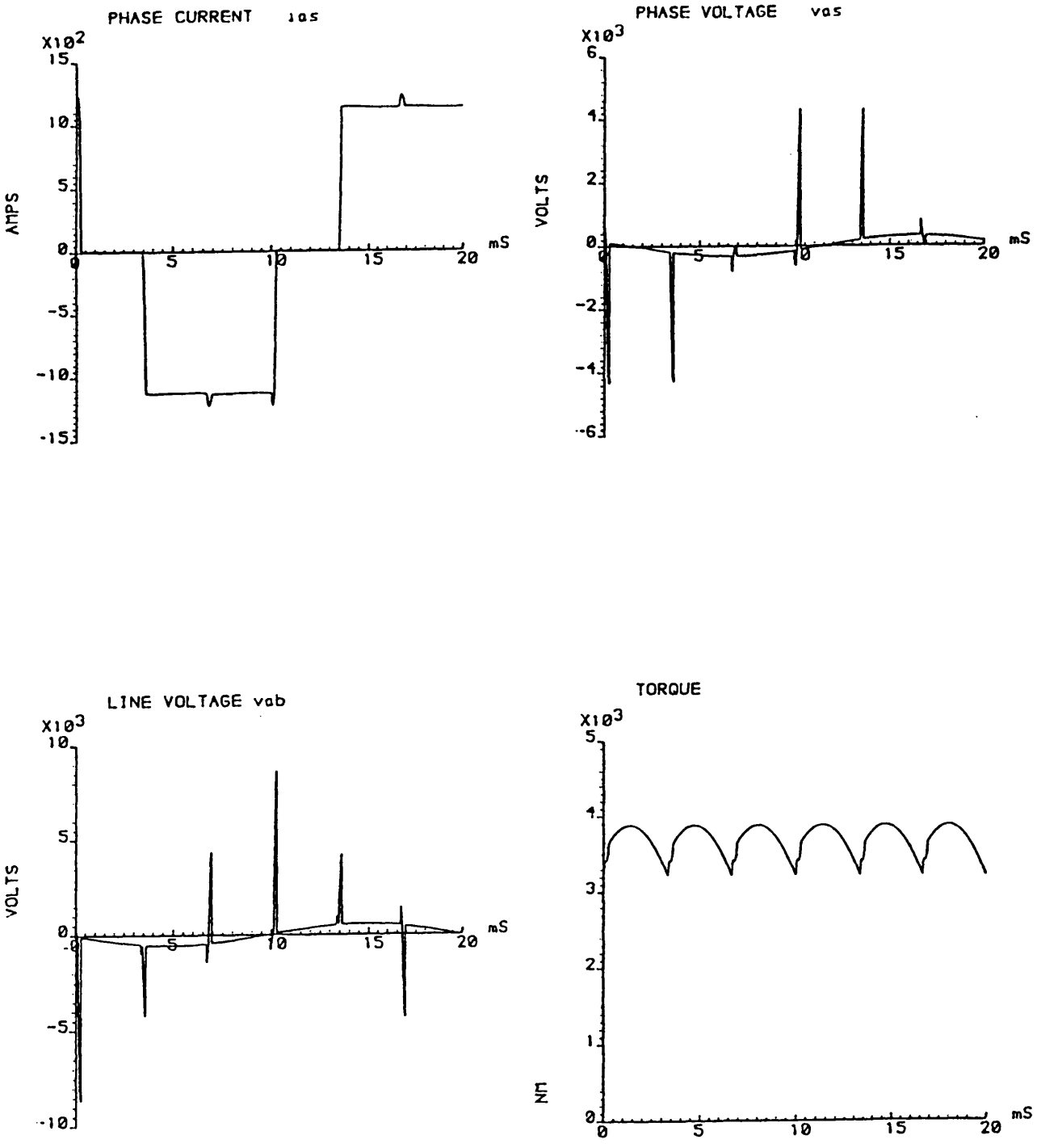

Fig 4.17b CSI Induction Motor 50 Hz

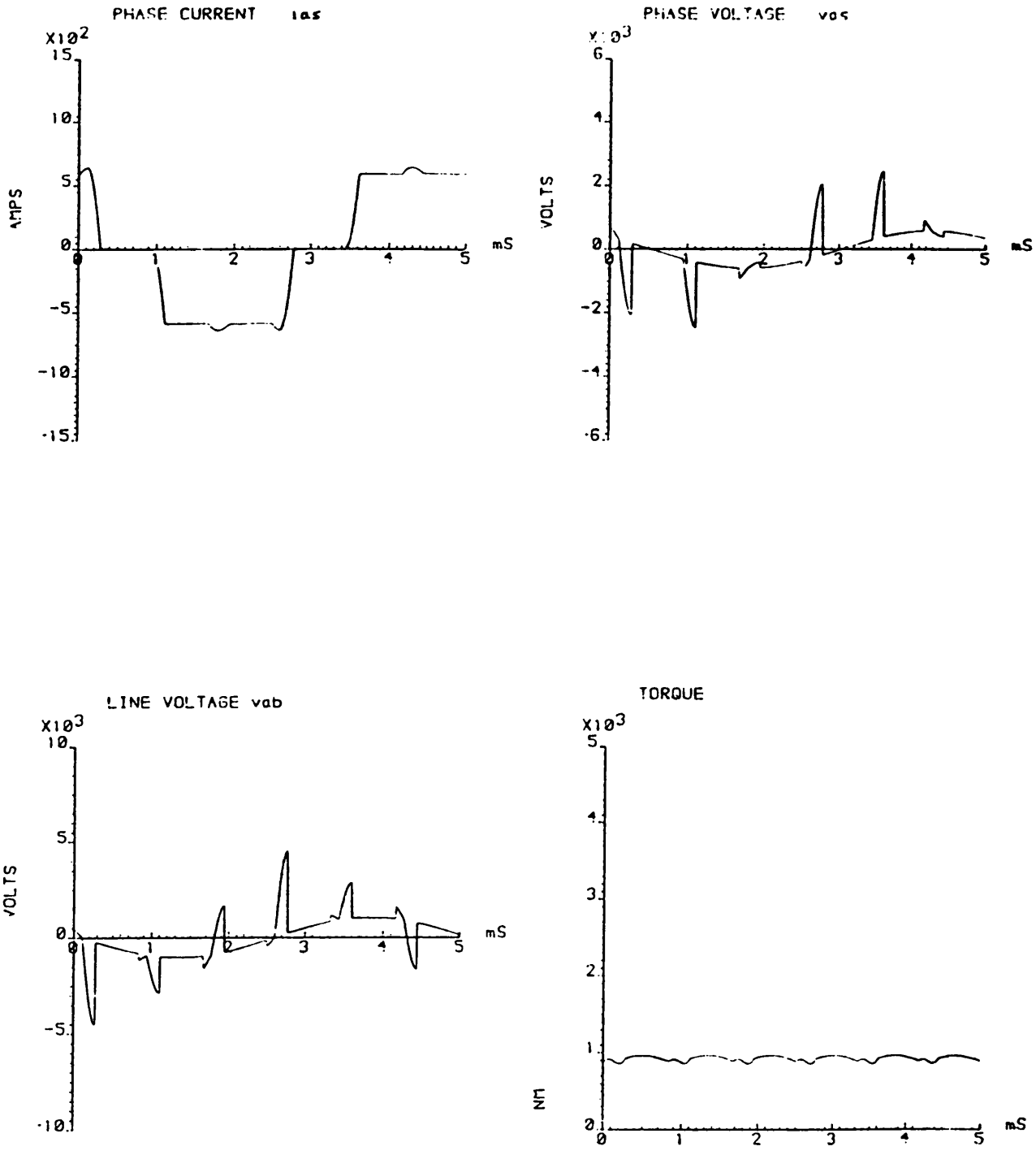

Fig 4.17c CSI Induction Motor 200 Hz

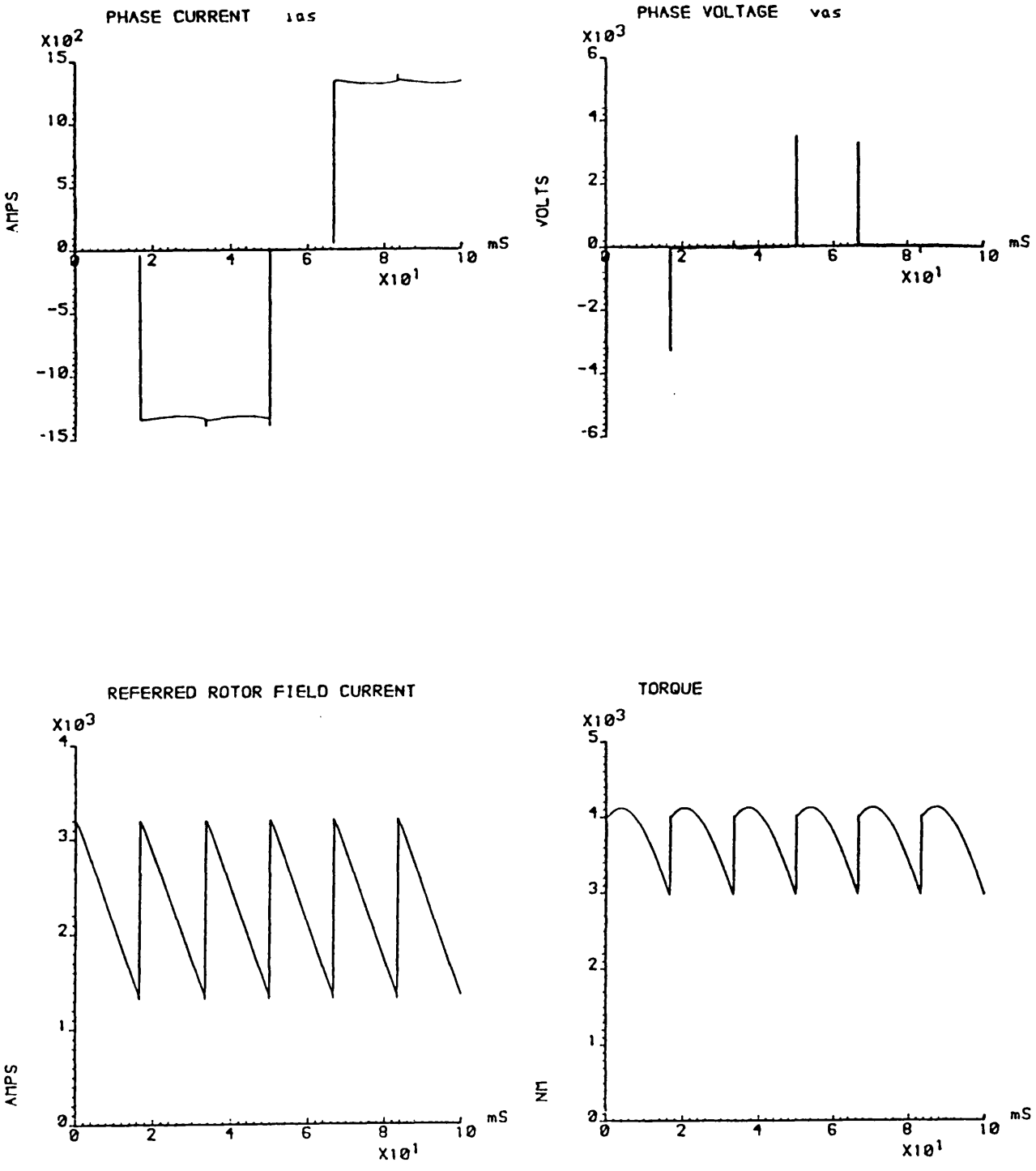

Fig 4.17d CSI Synchronous Motor 10 Hz

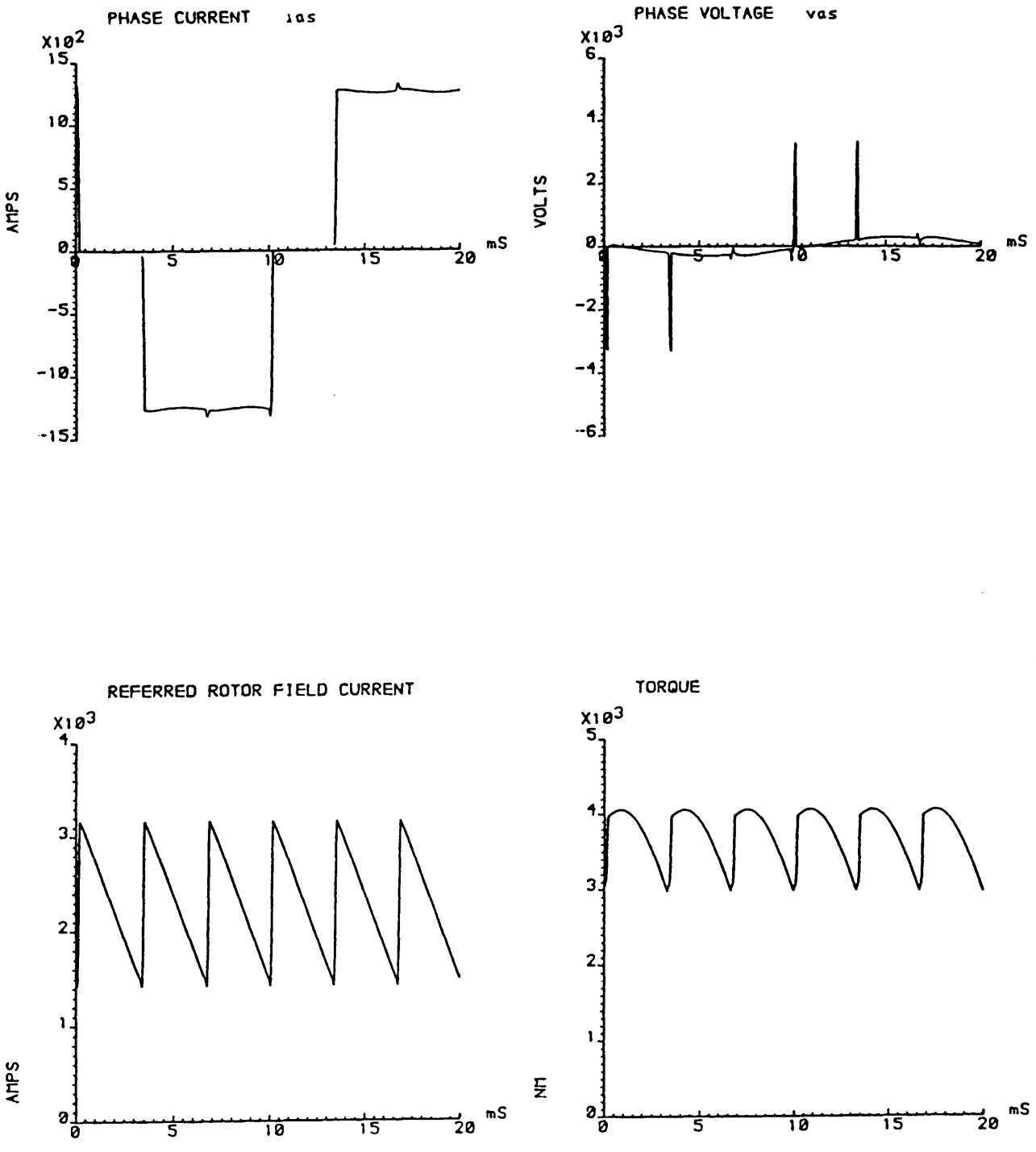

Fig 4.17e CSI Synchronous Motor 50 Hz

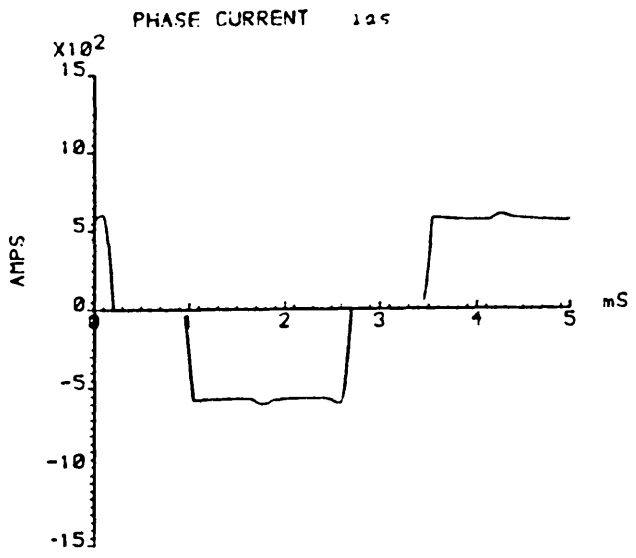

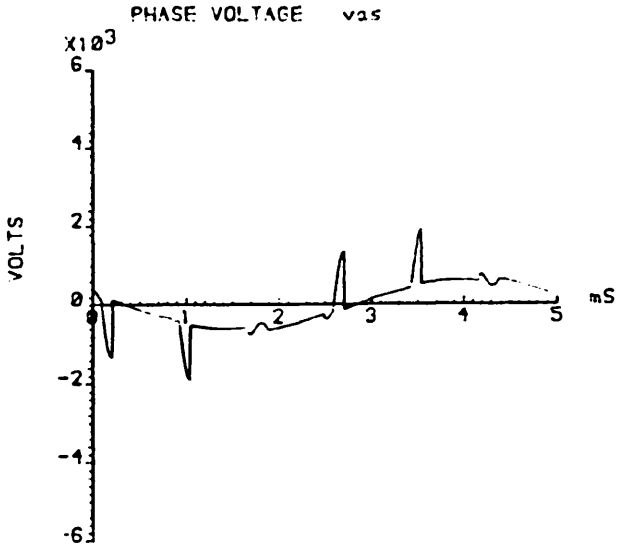

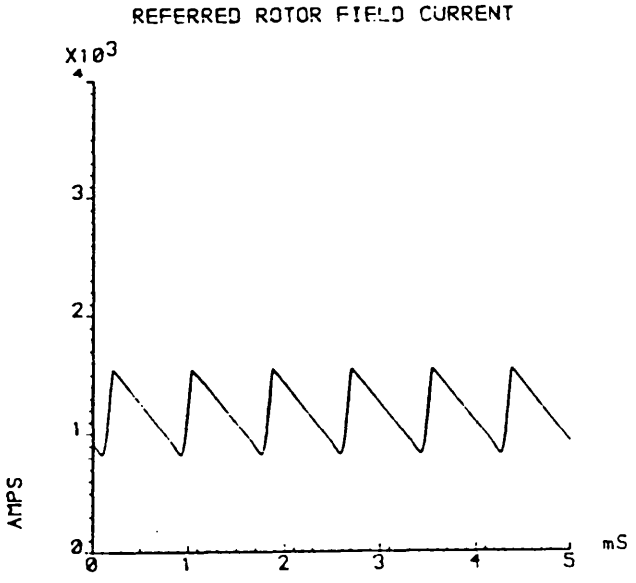

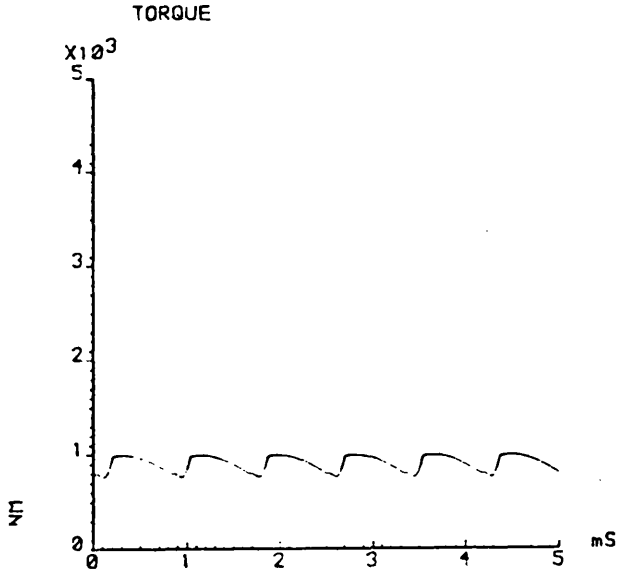

Fig 4.17f CSI Synchronous Motor 200 Hz

4.7 Conclusions

The use of a voltage or current source inverter gives rise to conflicting requirements for the machine design. For a VSI fed machine, a high value of leakage inductance is desirable to minimise the harmonic currents. Whereas, ideally the leakage inductance of a CSI fed motor should be as low as possible to limit the magnitude of the commutation voltages. This in turn would reduce the machine insulation stress and enable inverter components of a lower rating to be used.

An initial step towards the reduction of leakage reactance in the induction motor design considered in this work, can be made by ensuring that the slot depth is as small as possible. The effect of a change in slot depth is readily demonstrated using the induction motor design program of Chapter 2. The results of this excercise are shown in Fig 4.18.

As the rotor conductor current density for the induction motor design is below its permitted maximum value, Fig 2.13, the rotor slot area may be substantially reduced. If the slot depth is reduced to the point where the stator and rotor conductor densities are equal, ($8.44\ A/mm^2$), the rotor surface leakage inductance can be reduced, theoretically by 50%, Fig 4.18. In practice this figure would be reduced to approximately 20% due to the inclusion of the slot opening in the leakage calculations. It can also be seen that the decrease in rotor leakage is accompanied by a fall in the total motor weight, due to the fact that the core length can be reduced slightly. There is also a slight increase in the overall power factor. Fig 4.18 also demonstrates the effect of varying the stator slot depth , for equal stator and rotor conductor current densities. The core length has been adjusted in each case to give the required power output of 580 KW, and all other input variables to the design program remain

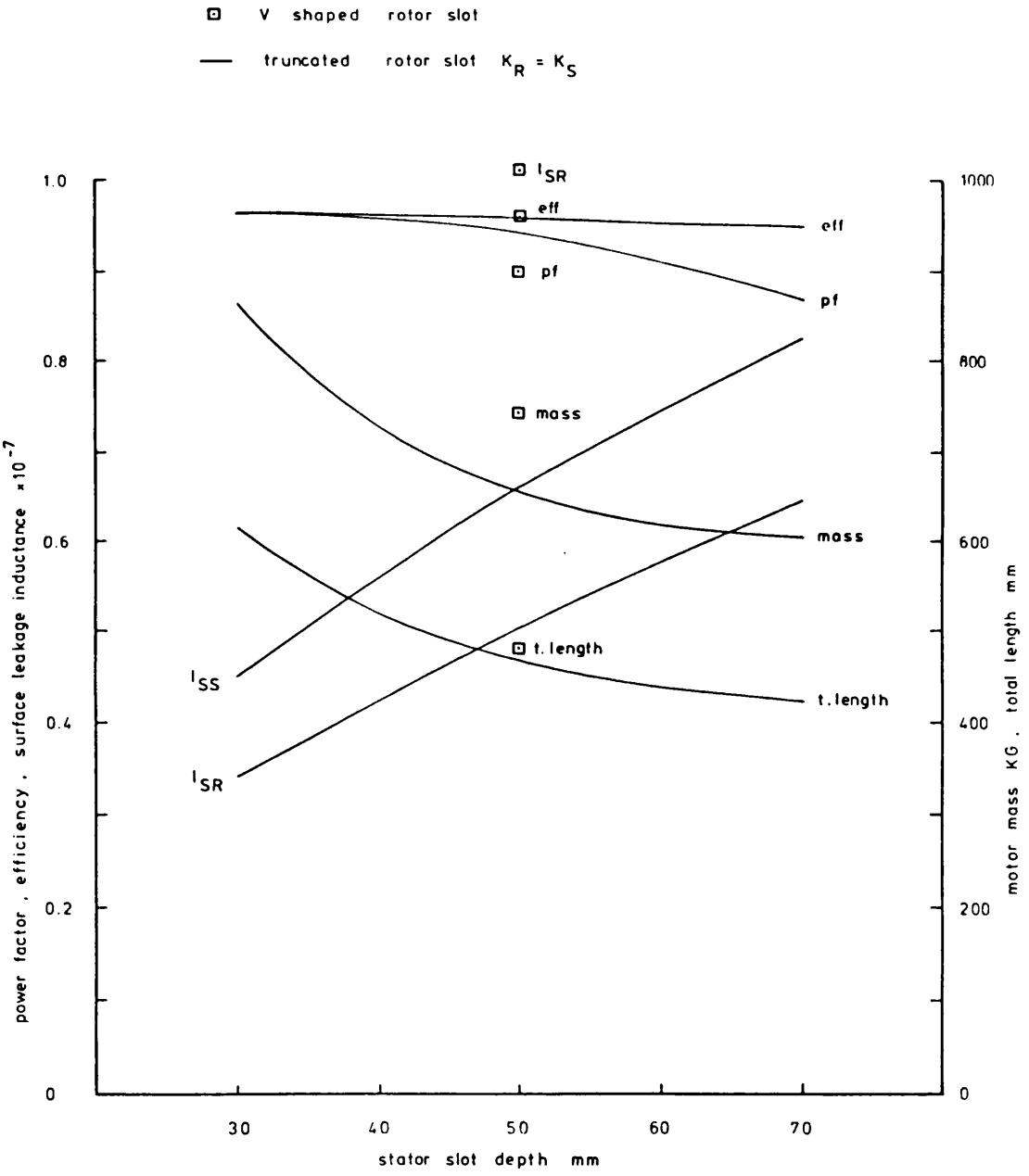

Fig 4.18 Effect of stator slot depth variation

unchanged from those shown in Table 3.2.

Variation of the stator slot depth produces changes in pole pitch, core length and rotor slot depth. For an increase in slot depth above 50 mm, the net effect of these changes is a reduction of the end winding leakage factors k_{endLS} and k_{endLR}. However this reduction is offset by an increase in the stator and rotor slot leakage component, which is due directly to the increase in slot depth. As the stator slot depth is reduced, the maximum available rotor slot area is correspondingly reduced, because of the restrictions on the core diameter. This means that, the depth to which the rotor slot needs to be filled with conductor, d_R, has to be increased accordingly. Thus for a deeper stator slot a shorter motor results with a corresponding reduction in weight, however as this is also accompanied by a falling power factor, the choice of a 50 mm slot for the traction designs considered is felt to be justified.

In this chapter computer models have been presented that predict the performance of induction and synchronous machines whilst being fed from a thyristor inverter of the constant voltage or constant current type. The resulting system equations may be solved by readily available iterative techniques.

The model proposed for the current source inverter includes the effect of the DC link filter by considering a regulated voltage, rather than a regulated current supply. From the output waveform predictions, the size of the inverter components may be accurately determined, and any area of voltage stress identified.

One area that requires to be looked at in more detail, is the mechanical coupling to the locomotive axle, because of the high harmonic torque content at the machine output shaft, particularly at low speeds. If the

torque harmonics coincide with the mechanical resonances of the power transmission system, which inevitably some will, a method of current modulation may be required to avoid problems. Some methods available to do this have been suggested in references 42 and 43.

4.8 APPENDICES

4.8.1 List of principal symbols used in the analysis of the voltage and current source inverter

Induction machine

R_S	stator phase resistance	Ω
l_S	stator phase leakage inductance	H
$R_{R'}$	referred rotor phase resistance	Ω
$l_{R'}$	referred rotor phase leakage inductance	H
L_m	magnetising inductance	H

Synchronous machine

R_S	stator phase resistance	Ω
l_S	stator phase leakage inductance	H
$R_{F'}$	referred field winding resistance	Ω
$l_{F'}$	referred field winding leakage inductance	H
L_{md}	direct axis magnetising inductance	H
L_{mq}	quadrature axis magnetising inductance	H
v_{aS}, v_{bS}, v_{cS}	machine phase voltages	V
i_{aS}, i_{bS}, i_{cS}	machine phase currents	A
$i_{aR'}, i_{bR'}, i_{cR'}$	referred rotor currents (induction machine)	A
$i_{F'}$	referred field winding currents (synchronous machine)	A
p	pole pairs	
ω_R	steady rotor angular velocity	rad/sec
θ	angular position of rotor	degree
T_e	electro-magnetic torque	Nm
δ_T	torque angle	degree

γ	phase displacement between the fundamental component of the machine phase current and the commutation point t_o	degree
V_s	DC source voltage	V
I_{dc}	DC link current	A
R_{dc}, L_{dc}	DC link resistance and inductance	Ω,H
C	inverter capacitance value	F
C_{eq}	equivalent capacitance value used in inverter model	F

4.8.2 The induction machine expressed in stator coordinates

The basic machine model is shown in Fig. A4.1. The rotor is represented by coils on the d and q axis, and is assumed to be travelling at a constant arbitrary speed ω_a.

Also

$$\omega_a = \frac{d\theta_a}{dt} = \frac{d\alpha}{dt}$$

1) Voltage induced in a stator coil

The voltage induced in a stator coil may be expressed as follows. For stator coil A,

$$v_{aS} = R_S i_{aS} + p\ell_S i_{aS} + pN_S\Phi_{aS} \qquad (A4.1)$$

Resolving the flux Φ_{aS} into its d and q axis components gives

$$\Phi_{aS} = \Phi_d \cos\alpha - \Phi_q \sin\alpha \qquad (A4.2)$$

Substituting equation (A4.2) into equation (A4.1) and differentiating gives

$$v_{aS} = R_S i_{aS} + p\ell_S i_{aS} + pN_S (\Phi_d \cos\alpha - \Phi_q \sin\alpha) - \omega_a N_S (\Phi_d \sin\alpha + \Phi_q \cos\alpha) \qquad (A4.3)$$

The d axis flux is given by,

$$\Phi_d = \frac{1}{R} [N_S i_{aS} \cos\theta_a + N_S i_{bS} \cos(\theta_a + 2\epsilon) + N_S i_{cS} \cos(\theta_a + \epsilon) + N_R i_{aR} \cos\beta + N_R i_{bR} (\beta + 2\epsilon) + N_R i_{cR} \cos(\beta + \epsilon)] \qquad (A4.4a)$$

and the q axis by,

$$\Phi_q = \frac{1}{R}[-N_S\, i_{aS} \sin\theta_a - N_S\, i_{bS} \sin(\theta_a + 2\epsilon) - N_S\, i_{cS} \sin(\theta_a + \epsilon)$$

$$- N_R\, i_{aR} \sin\beta - N_R\, i_{bR} \sin(\beta + 2\epsilon) - N_R\, i_{cR} \sin(\beta + \epsilon)] \qquad (A4.4b)$$

where N_S and N_R are the effective number of stator and rotor turns respectively and $\epsilon = \frac{2\pi}{3}$.

By the application of the voltage and current transforms of Fig. A4.2. to the rotor currents of equations (A4.4) the expression for the d and q axis flux become.

$$\Phi_d = \frac{1}{R}[N_S\, i_{aS} \cos\theta_a + N_S\, i_{bS} \cos(\theta_a + 2\epsilon) + N_S\, i_{cS} \cos(\theta_a + \epsilon)$$

$$+ N_R \sqrt{\frac{3}{2}}\, i_{dR}] \qquad (A4.5a)$$

and

$$\Phi_q = \frac{1}{R}[-N_S\, i_{aS} \sin\theta_a - N_S\, i_{bS} \sin(\theta_a + 2\epsilon) - N_S\, i_{cS} \sin(\theta_a + \epsilon)$$

$$+ N_R \sqrt{\frac{3}{2}}\, i_{qR}] \qquad (A4.5b)$$

It follows that

$$N_S(\Phi_d \cos\alpha - \Phi_q \sin\alpha) = L_S\, i_{aS} \cos(\alpha - \theta_a)$$

$$+ L_S\, i_{bS} \cos(\alpha - \theta_a - 2\epsilon)$$

$$+ L_S\, i_{cS} \cos(\alpha - \theta_a - \epsilon) + \sqrt{\frac{3}{2}}\, M\, i_{dR} \cos\alpha - \sqrt{\frac{3}{2}}\, M\, i_{qR} \sin\alpha \qquad (A4.6a)$$

and

$$N_S(\Phi_d \sin\alpha + \Phi_q \cos\alpha) = L_S\, i_{aS} \sin(\alpha - \theta_a)$$

$$+ L_S\, i_{bS} \sin(\alpha - \theta_a - 2\epsilon)$$

$$+ L_S\, i_{cS} \sin(\alpha - \theta_a - \epsilon) + \sqrt{\frac{3}{2}}\, M\, i_{dR} \sin\alpha - \sqrt{\frac{3}{2}}\, M\, i_{qR} \cos\alpha \qquad (A4.6b)$$

Where L_S and M are the self and mutual inductance terms.

$$L_S = \frac{N_S^2}{R} \qquad \text{and} \qquad M = \frac{N_S N_R}{R}$$

If phase 'a' is aligned with the reference axis then

for phase a $\alpha = \theta_a$

for phase b $\alpha = \theta_a + 2\epsilon$

for phase c $\alpha = \theta_a + \epsilon$

On substitution of equation (A4.6) into equation (A4.3) expressions for the stator voltages may be found. The resulting expressions are the first three rows of the set of equations shown in Fig. A4.3.

2) Voltage induced in a rotor coil

The voltage induced in a rotor coil may be expressed as follows, for phase 'a'

$$v_{aR} = R_R\, i_{aR} + p\ell_R + pN_R\Phi_{aR} \qquad \text{(A4.7)}$$

where $\Phi_{aR} = \Phi_d \cos\beta - \Phi_q \sin\beta$ (A4.8)

Combining equations (A4.7) and (A4.8,) expanding v_{aR} and i_{aR} using the transformation of Fig. (A4.2), and differentiating gives:

$$v_{dR}\cos\beta - v_{qR}\sin\beta + \frac{1}{\sqrt{2}} v_{oR} = R_R[i_{dR}\cos\beta - i_{qR}\sin\beta + \frac{1}{\sqrt{2}} i_{oR}]$$

$$+ p\ell_R[i_{dR}\cos\beta - i_{qR}\sin\beta + \frac{1}{\sqrt{2}} i_{oR}] - \dot{\beta}\ell_R[i_{dR}\sin\beta + i_{qR}\cos\beta]$$

$$+ p\sqrt{\frac{3}{2}} N_R[\Phi_d\cos\beta + \Phi_q\sin\beta] - \dot{\beta}\sqrt{\frac{3}{2}} N_R[\Phi_d\sin\beta - \Phi_q\cos\beta]$$

Collecting terms yields

$$\left.\begin{aligned} v_{dR} &= (R_R + p\ell_R)i_{dR} - \beta\ell_R i_{qR} + p\sqrt{\tfrac{3}{2}}\,N_R\,\Phi_d - \beta\sqrt{\tfrac{3}{2}}\,N_R\,\Phi_q \\ v_{qR} &= (R_R + p\ell_R)i_{qR} + \beta\ell_R i_{dR} + p\sqrt{\tfrac{3}{2}}\,N_R\,\Phi_q + \beta\sqrt{\tfrac{3}{2}}\,N_R\,\Phi_d \\ v_{oR} &= (R_R + p\ell_R)i_{oR} \end{aligned}\right\} \quad (A4.9)$$

Substitution of equation (A4.5) into equation (A4.9) gives expressions for the remaining axis voltages, v_{dR}, v_{qR} and v_{oR}, and completes the set of machine equations shown in Fig. A4.3.

3) Transformation into stator coordinates

The set of equations shown in Fig. A4.3 are valid for the following conditions, that

a) Stator phase 'a' coil is aligned with the fixed reference axis

b) The rotor is travelling at a speed ω_R

c) The transformed rotor is travelling at an arbitrary speed ω_a or at a speed $\dot{\beta}$ with respect to the rotor

In order to bring the rotor to rest in the stator reference frame θ_a is set to zero and hence $\omega_a = 0$.

As $\theta_a = \theta_R + \beta$, $\beta = -\theta_R$ and $\dot{\beta} = -\omega_R$.

The rotor which is now expressed in d_{qo} coordinates must be transformed back to three phase coordinates.

The machine equations of Fig. A4.3 may be expressed in the following general matrix form

$$\left.\begin{aligned} v_S &= z_{SS}\, i_S + z_{SR}\, i_{dqo} \\ vd_{qo} &= z_{RS}\, i_S + z_{dqo}\, i_{dqo} \end{aligned}\right\} \qquad \text{(A4.10)}$$

where z_{SS}. z_{SR}. z_{RS}. z_{dqo} are sub-matrices of the total impedance matrix z.

Using the transformations of Fig. A4.2 with $\beta = 0$ gives.

$$\begin{bmatrix} v_{aR'} \\ v_{bR'} \\ v_{cR'} \end{bmatrix} = \sqrt{\frac{2}{3}} \begin{bmatrix} 1 & 0 & \frac{1}{\sqrt{2}} \\ -\frac{1}{2} & \frac{\sqrt{3}}{2} & \frac{1}{\sqrt{2}} \\ -\frac{1}{2} & -\frac{\sqrt{3}}{2} & \frac{1}{\sqrt{2}} \end{bmatrix} \begin{bmatrix} v_{dR} \\ v_{qR} \\ v_{oR} \end{bmatrix}$$

$$v_{R'} = \sqrt{\frac{2}{3}}\; C^T\, v_{dqo}$$

$$\begin{bmatrix} i_{dR} \\ i_{qR} \\ i_{oR} \end{bmatrix} = \sqrt{\frac{2}{3}} \begin{bmatrix} 1 & -\frac{1}{2} & -\frac{1}{2} \\ 0 & \frac{\sqrt{3}}{2} & -\frac{\sqrt{3}}{2} \\ \frac{1}{\sqrt{2}} & \frac{1}{\sqrt{2}} & \frac{1}{\sqrt{2}} \end{bmatrix} \begin{bmatrix} i_{aR'} \\ i_{bR'} \\ i_{cR'} \end{bmatrix}$$

$$i_{dqo} = \sqrt{\frac{2}{3}}\; C\, i_{R'}$$

Using the above relationships equation (A4 10) becomes.

$$v_S = z_{SS}\, i_S + z_{SR} \sqrt{\frac{2}{3}}\, C\, i_{R'} \qquad \text{(A4.11)}$$

$$v_{R'} = \sqrt{\frac{2}{3}}\, C^T z_{RS}\, i_S + \frac{2}{3}\, C^T z_{dqo}\, C\, i_{R'} \qquad \text{(A4.12)}$$

From equations (A4.11) and (A4.12) and using the following self and mutual inductance relationships, the complete set of stator referred machine equations may be constructed.

$$M = L_S = L_R = \frac{2L_m}{3}$$

where L_m is the per phase machine magnetising inductance.

The completed set of transformed performance equations for the induction machine is shown in Fig. 4.1, Chapter 4.

4) Electromagnetic Torque

The electromagnetic torque developed by an induction motor having p pole pairs is given by,

$$T_e = \frac{p}{2}\, i^T \frac{dL}{d\theta}\, i$$

where L is the machine inductance matrix, Fig. A4.4. On differentation of the L matrix with respect to e the expression for torque becomes

$$\frac{p}{2} \begin{array}{|c|c|} \hline i_S^T & i_R^T \\ \hline \end{array} \begin{array}{|c|c|} \hline 0 & L \\ \hline L^T & 0 \\ \hline \end{array} \begin{array}{|c|} \hline i_S \\ \hline i_R \\ \hline \end{array}$$

$$\text{i.e. } T_e = \frac{p}{2}\left[i_S^T L i_R + i_R^T L i_S^T \right] = p\, i_S^T L i_R \qquad \text{(A4.13)}$$

where

$$Li_R = -M \begin{bmatrix} \sin\theta_R & \sin(\theta_R + \epsilon) & \sin(\theta_R + 2\epsilon) \\ \sin(\theta_R - \epsilon) & \sin\theta_R & \sin(\theta_R + \epsilon) \\ \sin(\theta_R - 2\epsilon) & \sin(\theta_R - \epsilon) & \sin\theta_R \end{bmatrix} \begin{bmatrix} i_{aR} \\ i_{bR} \\ i_{cR} \end{bmatrix}$$

Using the transformations of Fig. A4.2 to transform to an arbitrary dq axis, and bringing the frame to rest with respect to the rotor i.e. $\beta = -\theta_R$ then,

$$Li_R = -\frac{3}{2} M \sqrt{\frac{2}{3}} \begin{bmatrix} 0 & 1 & 0 \\ -\frac{\sqrt{3}}{2} & -\frac{1}{2} & 0 \\ -\frac{\sqrt{3}}{2} & -\frac{1}{2} & 0 \end{bmatrix} \begin{bmatrix} i_{dR} \\ i_{qR} \\ i_{oR} \end{bmatrix}$$

Again using the transformation of Fig. A4.2 with $\beta = 0$ to transform back into three phase quantities, and finally referring the inductance coefficients to the stator, the expression for the instantaneous torque is given as,

$$T_e = -p \frac{\sqrt{3}\, L_m}{3} \left[i_{aS}(i_{bR'} - i_{cR'}) + i_{bS}(-i_{aR'} + i_{cR'}) + i_{cS}(i_{aR'} - i_{bR'}) \right]$$

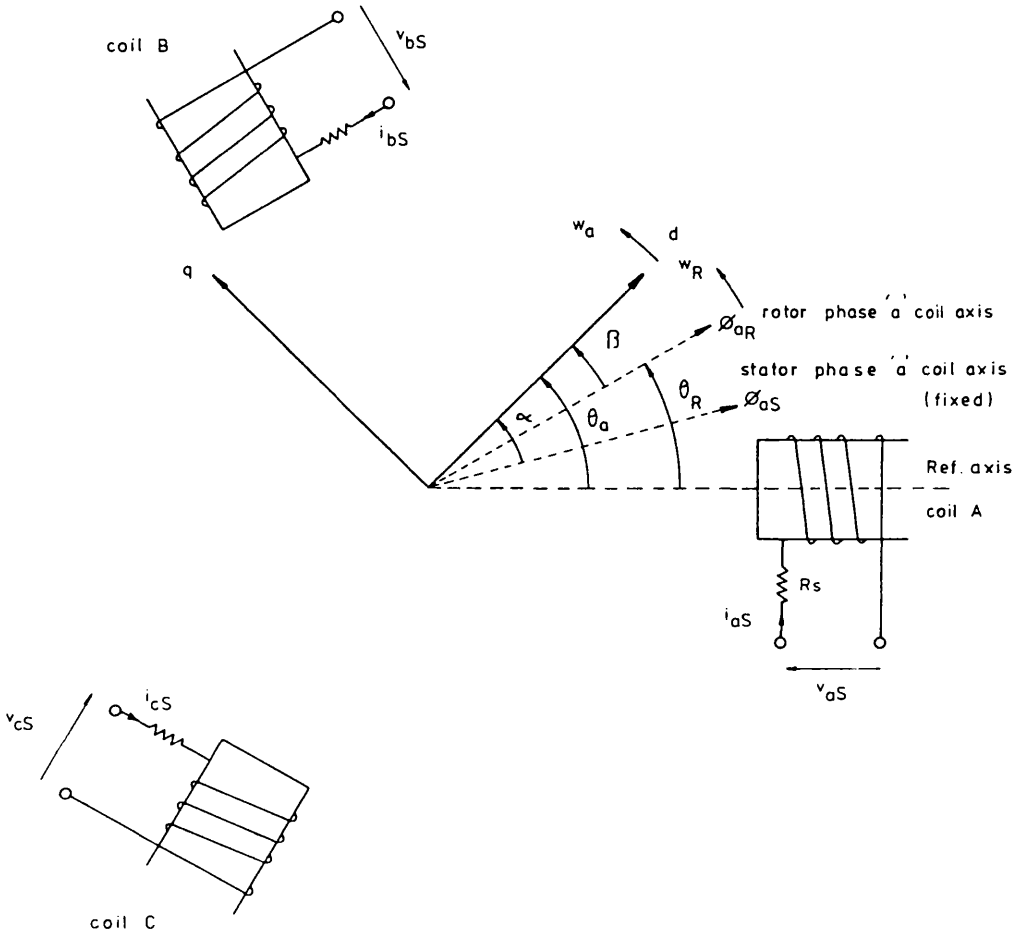

Fig A4.1 Induction Machine Model

$$\begin{bmatrix} v_{dR} \cdot i_{dR} \\ v_{qR} \cdot i_{qR} \\ v_{oR} \cdot i_{oR} \end{bmatrix} = \sqrt{\frac{2}{3}} \begin{bmatrix} \cos\beta & \cos(\beta+2\epsilon) & \cos(\beta+\epsilon) \\ -\sin\beta & -\sin(\beta+2\epsilon) & -\sin(\beta+\epsilon) \\ \frac{1}{\sqrt{2}} & \frac{1}{\sqrt{2}} & \frac{1}{\sqrt{2}} \end{bmatrix} \begin{bmatrix} v_{aR} \cdot i_{aR} \\ v_{bR} \cdot i_{bR} \\ v_{cR} \cdot i_{cR} \end{bmatrix}$$

$$\begin{bmatrix} v_{aR} \cdot i_{aR} \\ v_{bR} \cdot i_{bR} \\ v_{cR} \cdot i_{cR} \end{bmatrix} = \sqrt{\frac{2}{3}} \begin{bmatrix} \cos\beta & -\sin\beta & \frac{1}{\sqrt{2}} \\ \cos(\beta+2\epsilon) & -\sin(\beta+2\epsilon) & \frac{1}{\sqrt{2}} \\ \cos(\beta+\epsilon) & -\sin(\beta+\epsilon) & \frac{1}{\sqrt{2}} \end{bmatrix} \begin{bmatrix} v_{dR} \cdot i_{dR} \\ v_{qR} \cdot i_{qR} \\ v_{oR} \cdot i_{oR} \end{bmatrix}$$

Fig A 4.2 Transformations for voltage and current

$$\epsilon = \frac{2\pi}{3}$$

$$
\begin{bmatrix} v_{aS} \\ v_{bS} \\ v_{cS} \\ v_{dR} \\ v_{qR} \\ v_{oR} \end{bmatrix} =
\begin{bmatrix}
R_s + p(l_s + L_s) & -p\frac{L_s}{2} - w_a L_s\sqrt{\frac{3}{2}} & -p\frac{L_s}{2} + w_a L_s\sqrt{\frac{3}{2}} & \sqrt{\frac{3}{2}}M(p\cos\theta_a - w_a\sin\theta_a) & \sqrt{\frac{3}{2}}M(-p\sin\theta_a - w_a\cos\theta_a) & \\
-p\frac{L_s}{2} + w_a L_s\sqrt{\frac{3}{2}} & R_s + p(l_s + L_s) & -p\frac{L_s}{2} - w_a L_s\sqrt{\frac{3}{2}} & \sqrt{\frac{3}{2}}M[p\cos(\theta_a + 2\epsilon) - w_a\sin(\theta_a + 2\epsilon)] & \sqrt{\frac{3}{2}}M[-p\sin(\theta_a + 2\epsilon) - w_a\sin(\theta_a + 2\epsilon)] & \\
-p\frac{L_s}{2} - w_a L_s\sqrt{\frac{3}{2}} & -p\frac{L_s}{2} + w_a L_s\sqrt{\frac{3}{2}} & R_s + p(l_s + L_s) & \sqrt{\frac{3}{2}}M[p\cos(\theta_a + \epsilon) - w_a\sin(\theta_a + \epsilon)] & \sqrt{\frac{3}{2}}M[-p\sin(\theta_a + \epsilon) - w_a\sin(\theta_a + \epsilon)] & \\
\sqrt{\frac{3}{2}}M[p\cos\theta_a + \dot{\beta}\sin\theta_a] & \sqrt{\frac{3}{2}}M[p\cos(\theta_a + 2\epsilon) + \dot{\beta}\sin(\theta_a + 2\epsilon)] & \sqrt{\frac{3}{2}}M[p\cos(\theta_a + \epsilon) + \dot{\beta}\sin(\theta_a + \epsilon)] & R_R + p(l_R + \frac{3}{2}L_R) & -\dot{\beta}(l_R + \frac{3}{2}L_R) & \\
\sqrt{\frac{3}{2}}M[-p\sin\theta_a + \dot{\beta}\cos\theta_a] & \sqrt{\frac{3}{2}}M[-p\sin(\theta_a + 2\epsilon) + \dot{\beta}\cos(\theta_a + 2\epsilon)] & \sqrt{\frac{3}{2}}M[-p\sin(\theta_a + \epsilon) + \dot{\beta}\cos(\theta_a + \epsilon)] & \dot{\beta}(l_R + \frac{3}{2}L_R) & R_R + p(l_R + \frac{3}{2}L_R) & \\
 & & & & & R_R + pl_R
\end{bmatrix}
\begin{bmatrix} i_{aS} \\ i_{bS} \\ i_{cS} \\ i_{dR} \\ i_{qR} \\ i_{oR} \end{bmatrix}
$$

Fig A4.3 Induction machine expressed in an arbitrary reference frame

$l_s + L_s$	$-\frac{L_s}{2}$	$-\frac{L_s}{2}$	$M\cos\theta$	$M\cos(\theta+\epsilon)$	$M\cos(\theta+2\epsilon)$
$-\frac{L_s}{2}$	$l_s + L_s$	$-\frac{L_s}{2}$	$M\cos(\theta-\epsilon)$	$M\cos\theta$	$M\cos(\theta+\epsilon)$
$-\frac{L_s}{2}$	$-\frac{L_s}{2}$	$l_s + L_s$	$M\cos(\theta-2\epsilon)$	$M\cos(\theta-\epsilon)$	$M\cos\theta$
$M\cos\theta$	$M\cos(\theta-\epsilon)$	$M\cos(\theta-2\epsilon)$	$l_R + L_R$	$-\frac{L_R}{2}$	$-\frac{L_R}{2}$
$M\cos(\theta+\epsilon)$	$M\cos\theta$	$M\cos(\theta-\epsilon)$	$-\frac{L_R}{2}$	$l_R + L_R$	$-\frac{L_R}{2}$
$M\cos(\theta+2\epsilon)$	$M\cos(\theta+\epsilon)$	$M\cos\theta$	$-\frac{L_R}{2}$	$-\frac{L_R}{2}$	$l_R + L_R$

Fig A4.4 Induction machine L matrix

CHAPTER 5

EXPERIMENTAL VERIFICATION OF THE CURRENT SOURCE INVERTER MODEL

In this chapter experimental results are shown to verify the computer model of the current source inverter described in chapter 4.

5.1 The test machine and torque measuring system

Fig 5.1 shows a general view of the induction machine used, and the DC load machine. The stator frame of the induction machine was mounted on a force measuring table. The rotor was held between two bearing posts at each end of the shaft, Fig 5.2, which are rigidly bolted to a supporting frame. Also mounted on this frame was the DC load machine whose speed was controlled by a Ward Leonard system. This arrangement enables the forces generated between the stator and rotor members to be transmitted directly to the force table for measurement.

The induction machine was of a four pole design, with a squirrel cage rotor winding, and was rated at 200V, 25A. A full description of this machine including all the relevant dimensions is given in Appendix 5.4.1. To demonstrate the validity of the induction machine parameter calculations of Chapter 2, the equivalent circuit values of this machine have been calculated using the formulae given in Appendix 2.7.2. The calculated parameters are shown together with the measured values for comparison in Table 5.1. The measured values were obtained using the normal induction machine open circuit and locked rotor tests. It can be seen that there is good agreement between the two sets of parameters. Throughout this chapter the equivalent circuit values obtained by measurement are used in the computer model.

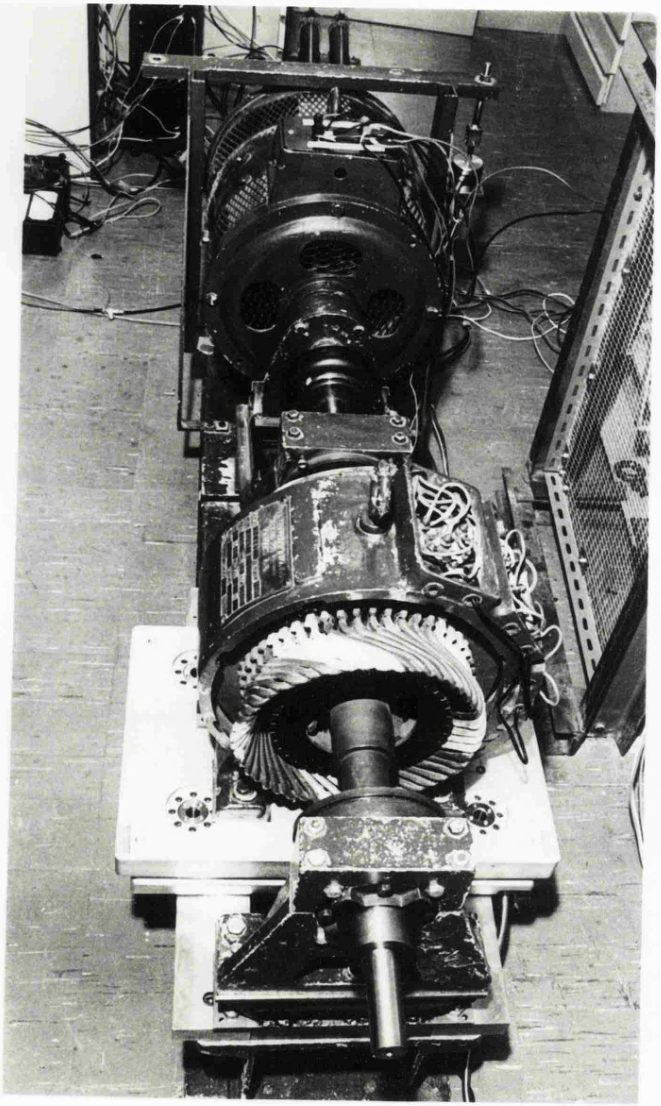

Fig 5.1 General view of machine layout

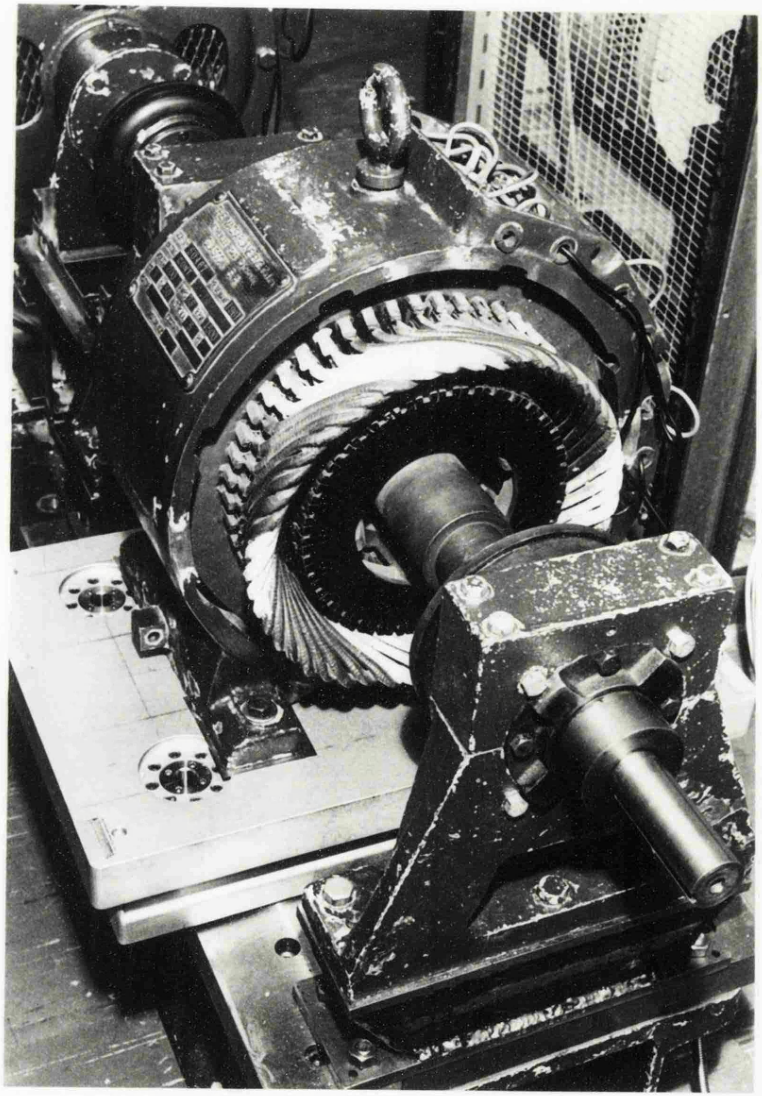

Fig 5.2 Test induction machine and force platform

	CALCULATED		MEASURED
stator resistance	0.537 Ω		0.53 Ω
referred rotor resistance	0.7235 Ω		0.8366 Ω
stator leakage inductance	3.035 mH	6.908 mH (l_S+l_R')	7.53 mH
referred rotor leakage inductance	3.873 mH		
magnetising inductance	0.1115 H		0.1237 H

Table 5.1 Induction machine equivalent circuit parameters

The measuring platform consists of a base frame bolted to the machine bed, and an aluminium top plate, with four 3-component force transducers fitted between them under a high prestress. Each transducer consists of three quartz discs, each sensitive to pressure in one of three preferred axis, x,y or z. The rotor is aligned with the x axis. Forces in this direction were not measured. The electrical charges yielded by the force transducers are converted via charge amplifiers to voltages suitable for direct measurement. The quartz transducers are able to be preloaded and still remain sensitive to small time varying components of force, provided of course the preload is not excessive. Thus by summing the appropriate forces from each transducer and scaling by the torque arm length in each case, the torque produced by the machine can be measured dynamically. When the forces in the y and z direction are transferred to the centre of the rotor, Fig 5.3, the resultant machine torque is,

$$T_m = (Fz_{(3+4)} - Fz_{(1+2)})d + Fy_{(1+2+3+4)} h$$

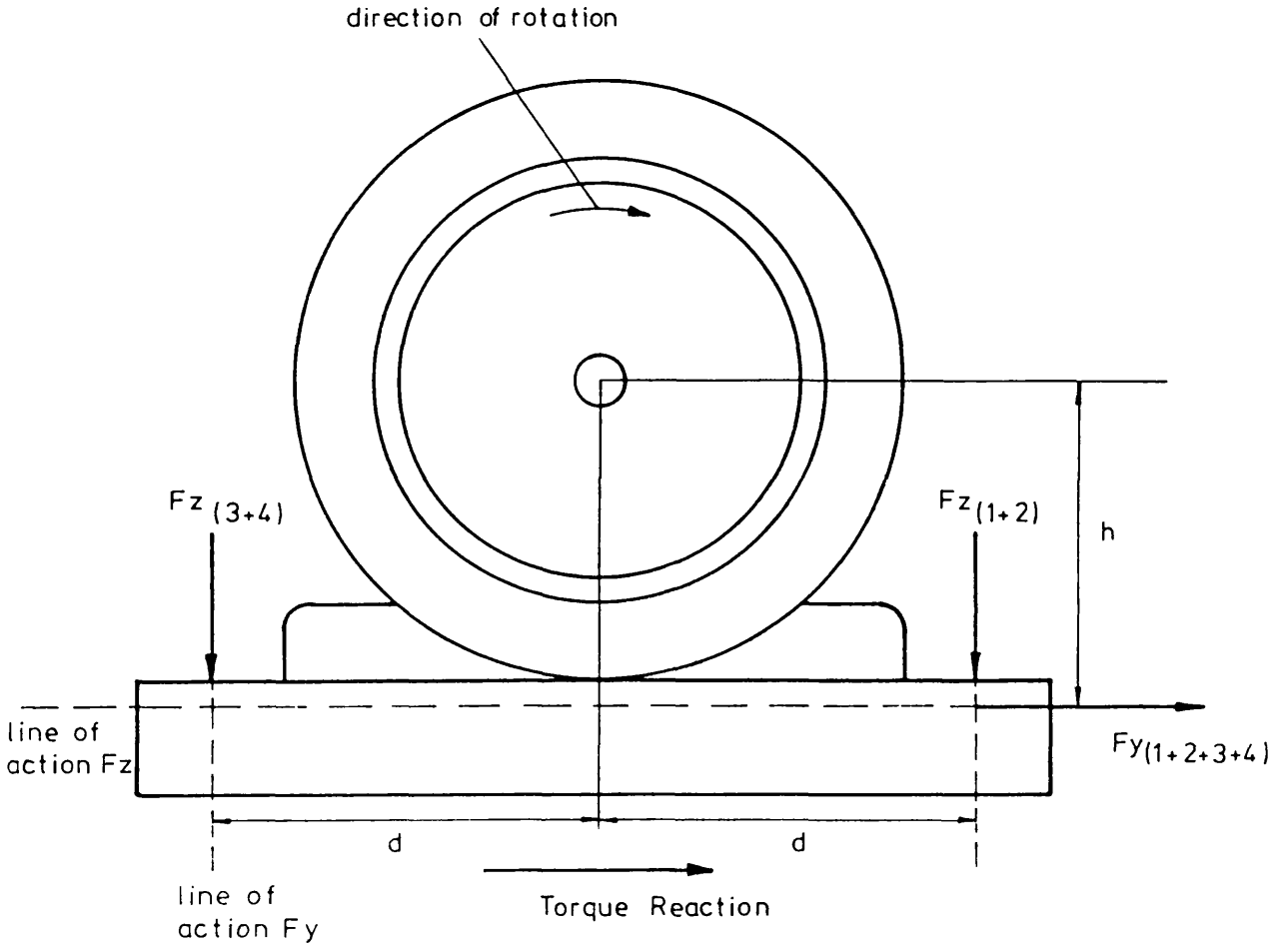

Fig 5.3 Two axis forces for torque measurement

where h is the distance from the centre of the rotor shaft to the line of action of the force transducer in the z direction, and d is the distance from the centre of the shaft to the line of action of the force transducer in the y direction. In practice the summing operation was performed by two operational amplifiers, the torque arm lengths being scaled by suitable resistor values.

5.2 Discussion of results

The DC link inductor was chosen to be approximately ten times the total machine leakage inductance, to allow a reasonably constant current within the motor. The inductor used has the following parameters:

Rdc = 0.26 ohms

Ldc = 80 mH

The commutation capacitors used were 100 uF, 400V devices. As the upper frequency limit is determined by the value of commutation capacitor, this restricts the highest test frequency to a theoretical maximum of approximately 40 Hz. An upper frequency limit of 15 Hz was therefore imposed to stay comfortably within the commutation capabilities of the inverter.

A comparison of the calculated and measured machine characteristics, for different loading conditions, is shown in Figs 5.4, 5.5 and 5.6, for operating frequencies of 5, 10 and 15 Hz.

Typically, a steady state solution was obtained after 5 minutes of CPU time. This required approximately 50 iterations over the 60 degree computing period, and gave a solution that had an average error of less than two decimal places for the five input variables, (capacitor voltage, phase and rotor currents).

There is good agreement between the computed and measured phase

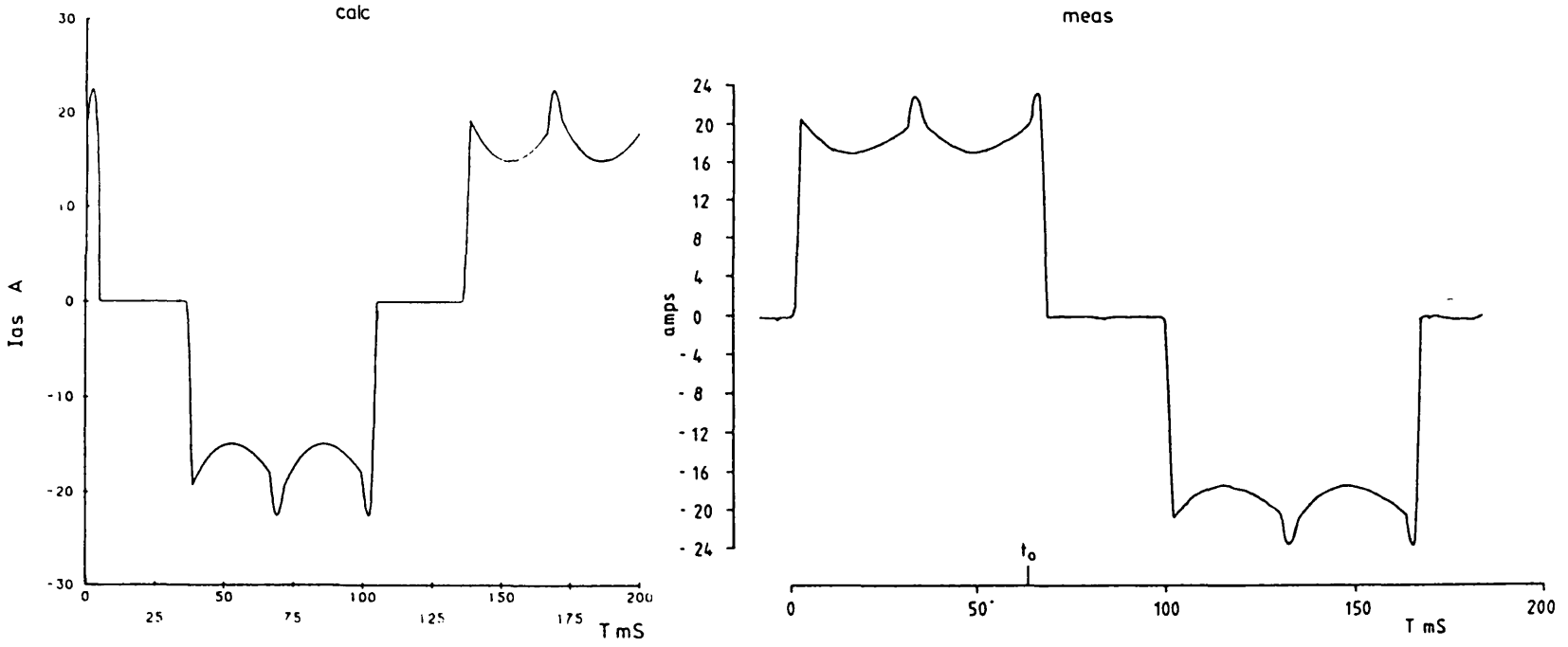

Fig 5.4 a) phase 'a' current, Ias freq = 5 Hz Vs = 56 volts σ = 0·06 (141 rpm)

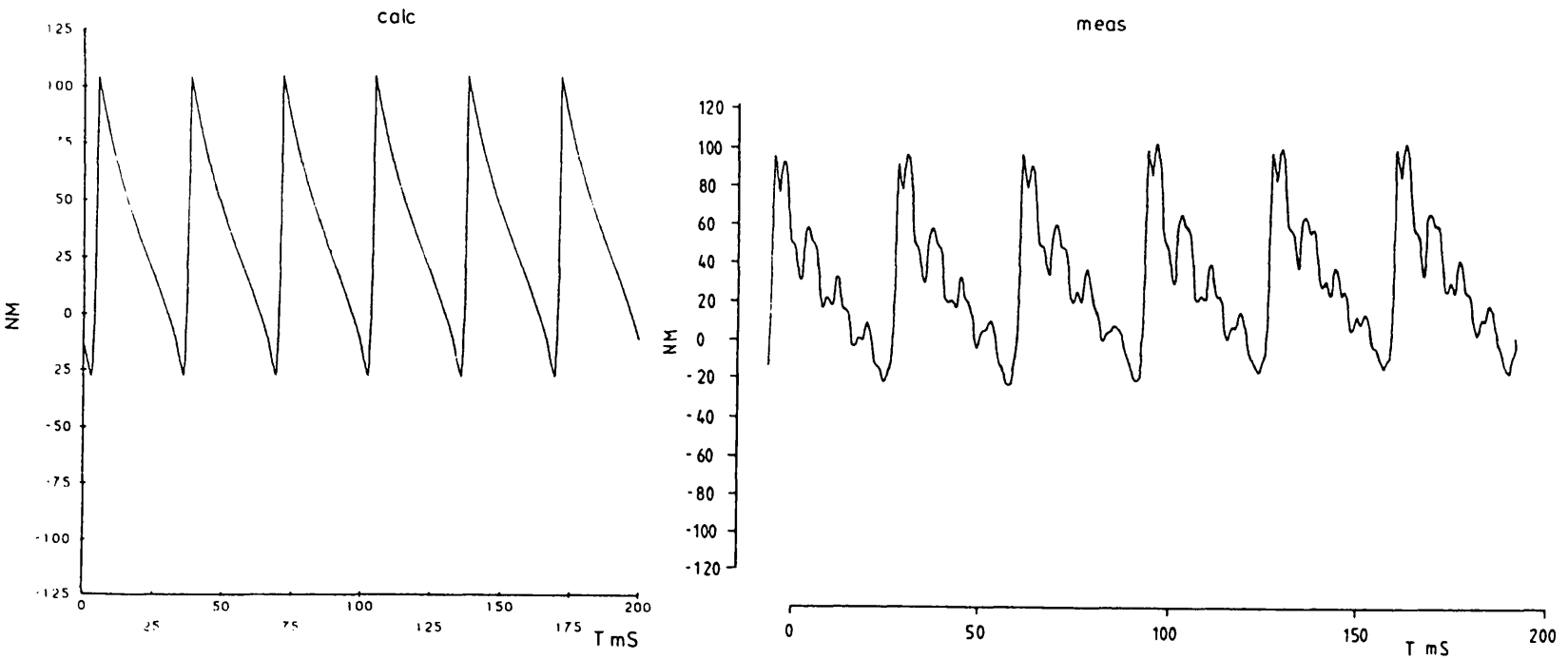
calc
meas
NM
T mS
125
100
50
25
0
-50
-75
-100
-125
120
80
60
40
20
-20
-40
-60
-80
-120
0
50
100
150
175
200

b) torque

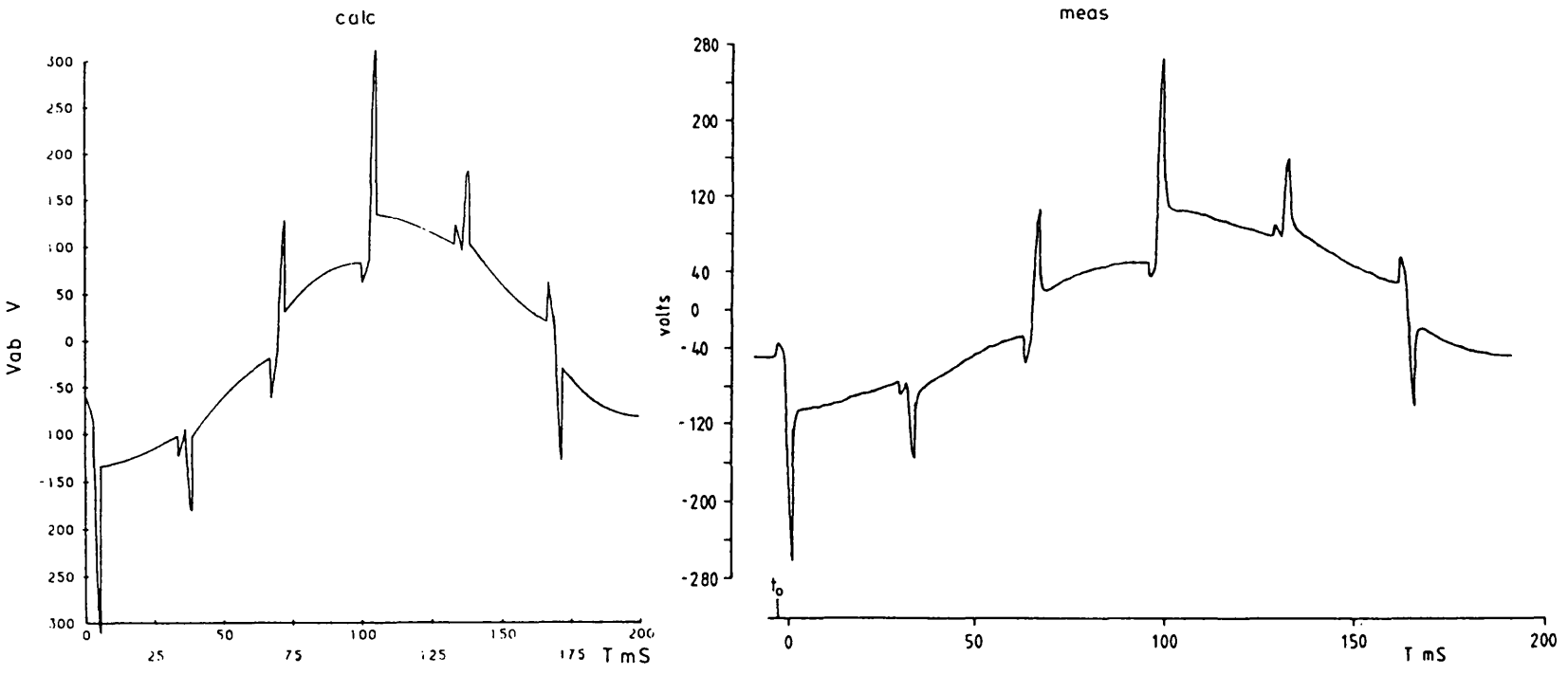

c) motor l-l voltage Vab

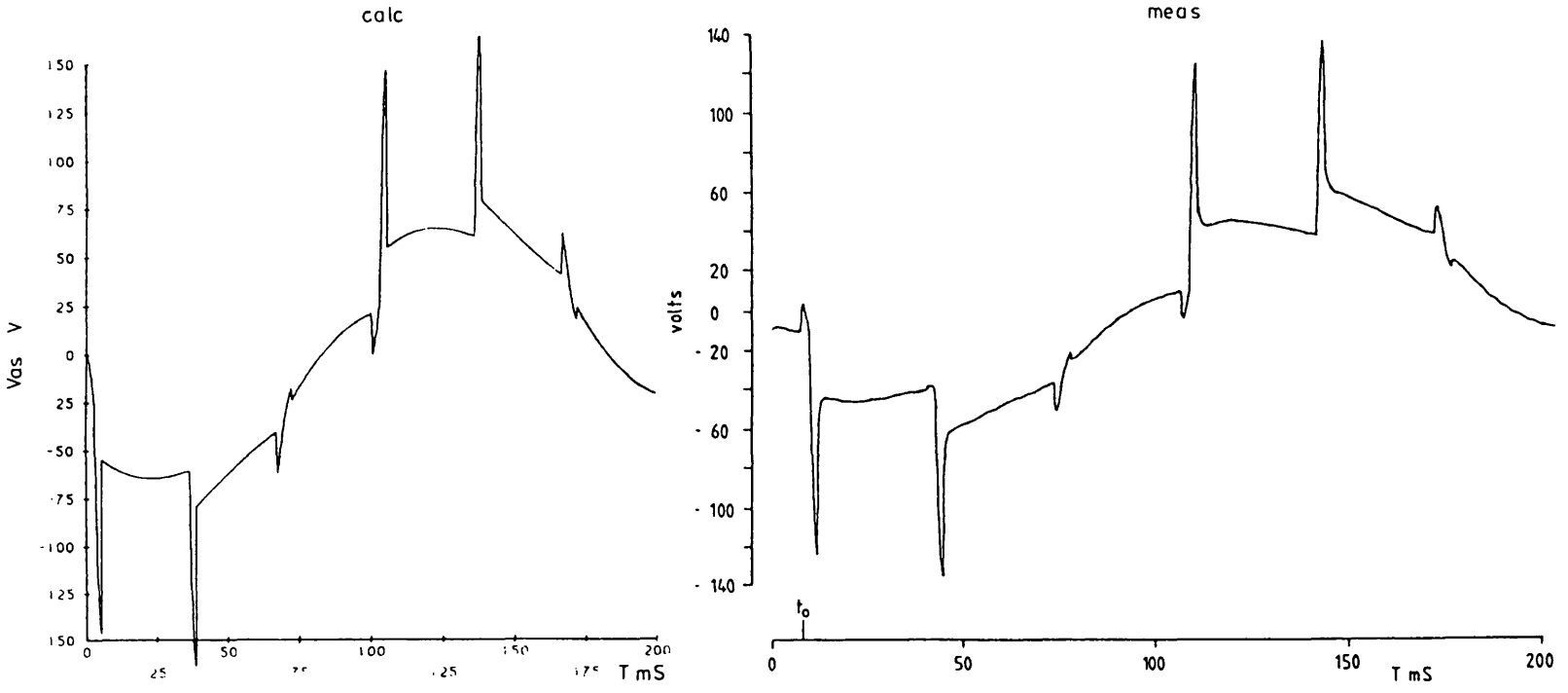

d) motor phase voltage Vas

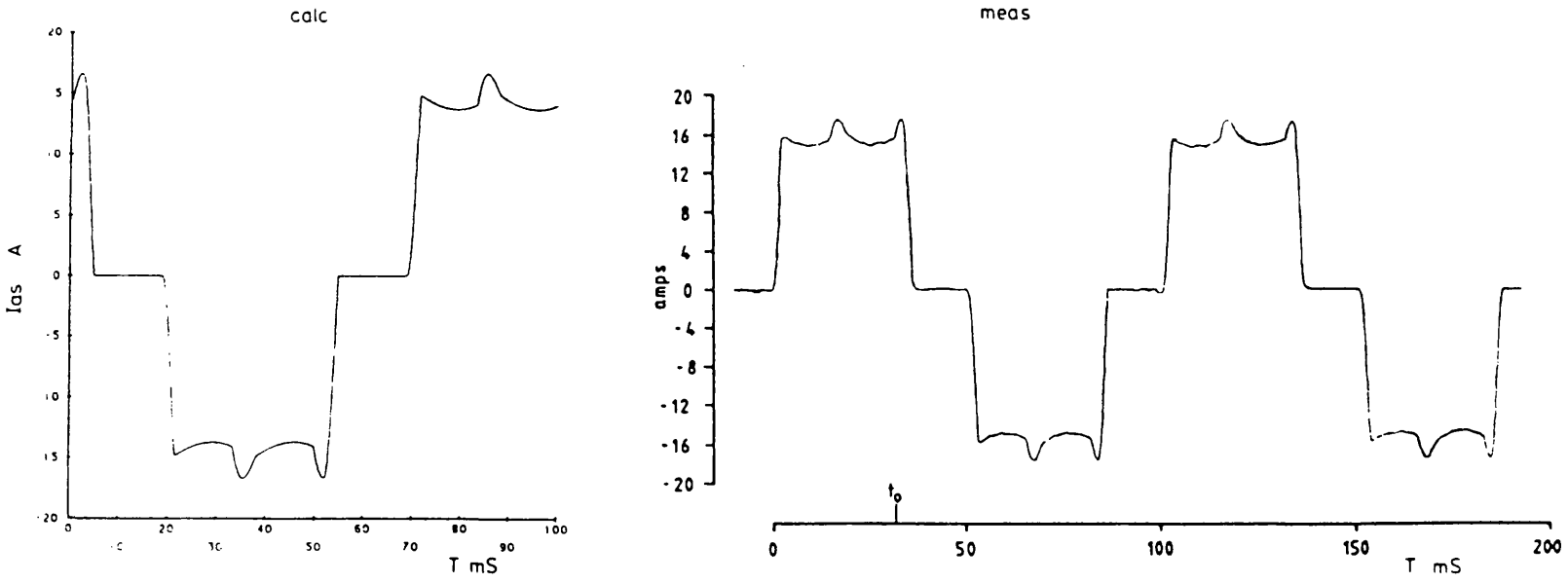

Fig 5.5 a) phase 'a' current, Ias freq = 10 Hz Vs = 112 volts σ = 0·16 (252 rpm)

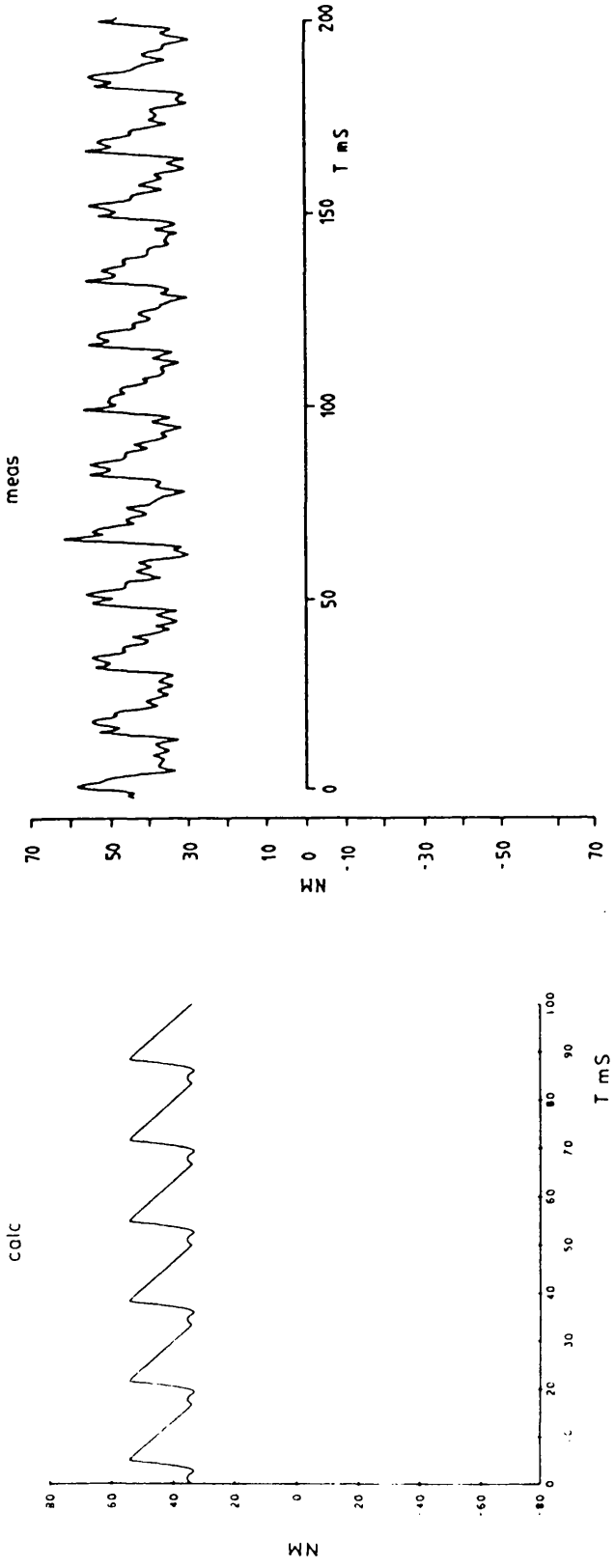
meas
NM
70
50
30
10
0
-10
-30
-50
0
50
100
150
200
T mS
calc
NM
80
60
40
20
0
20
40
60
80
0
10
20
30
40
50
60
70
80
90
100
T mS

b) torque

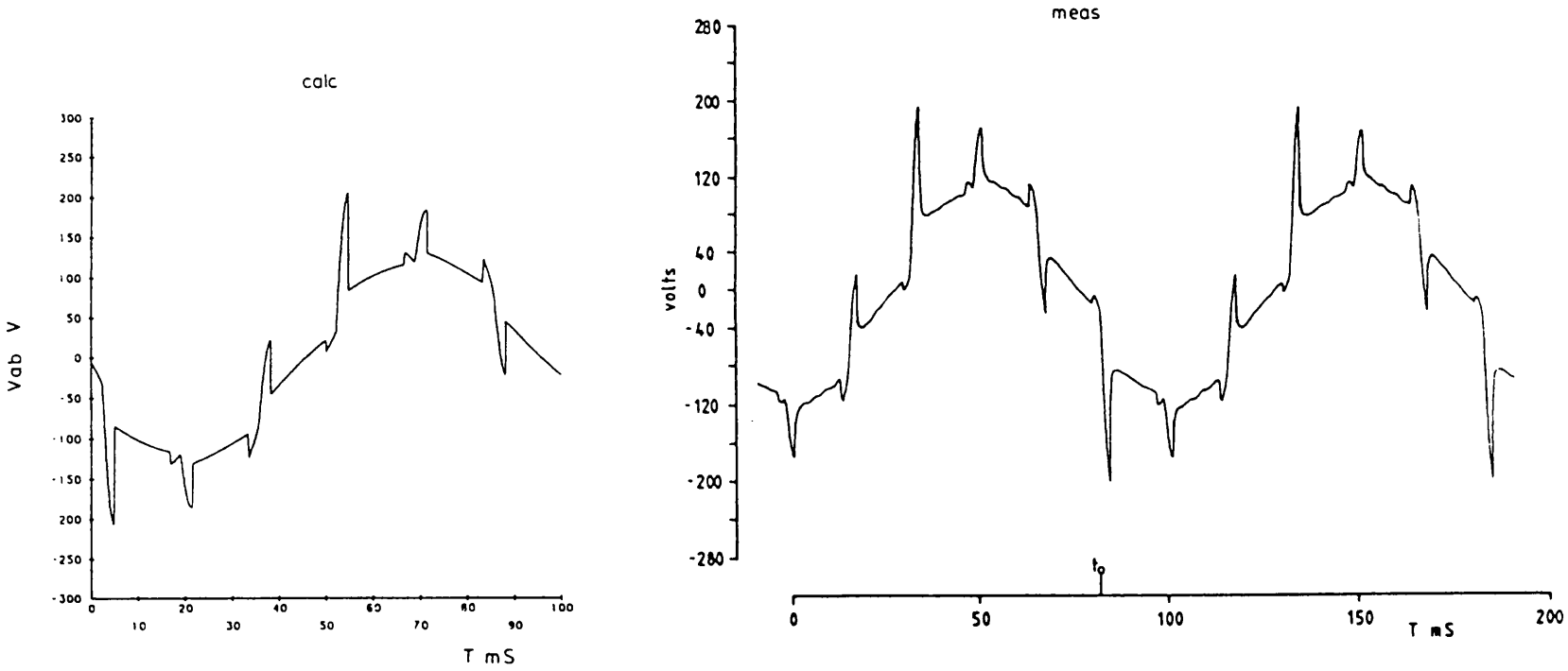

c) motor l-l voltage Vab

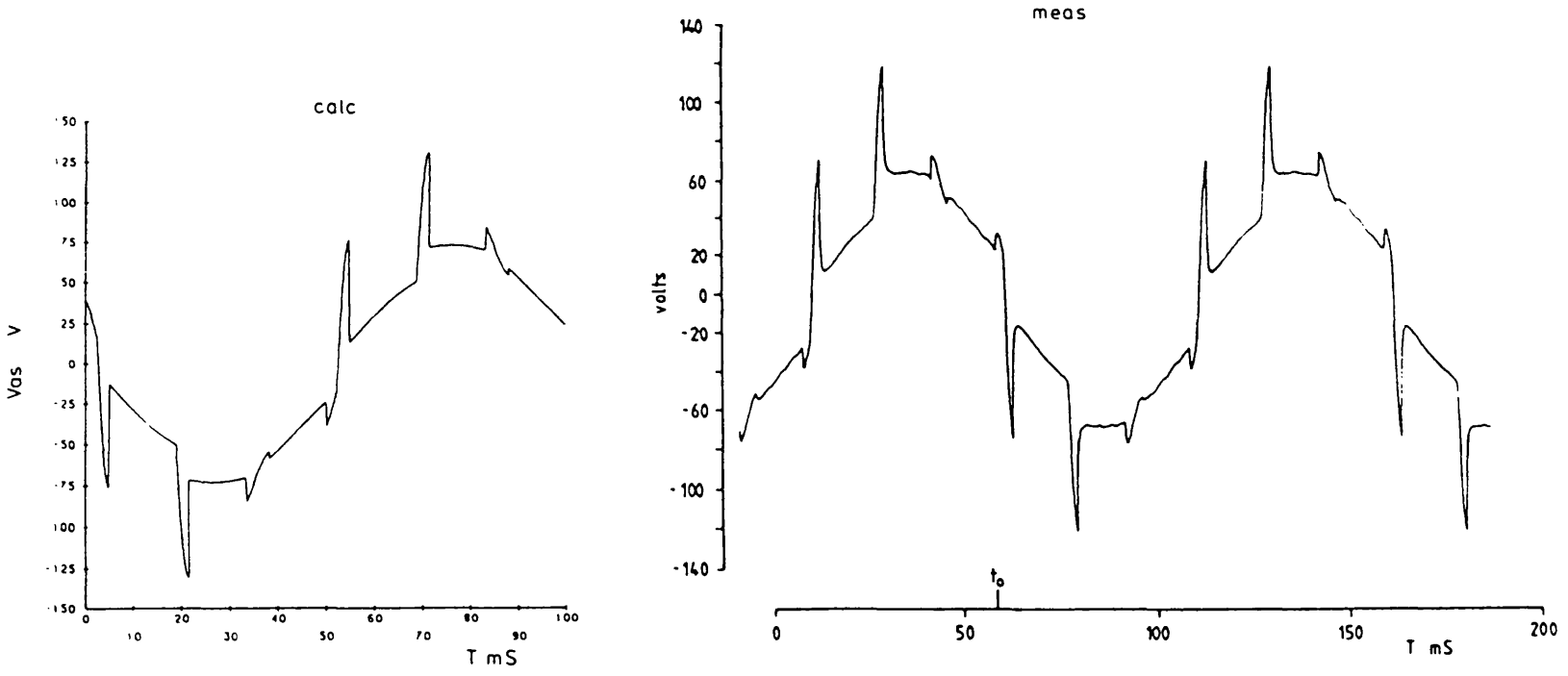

d) motor phase voltage Vas

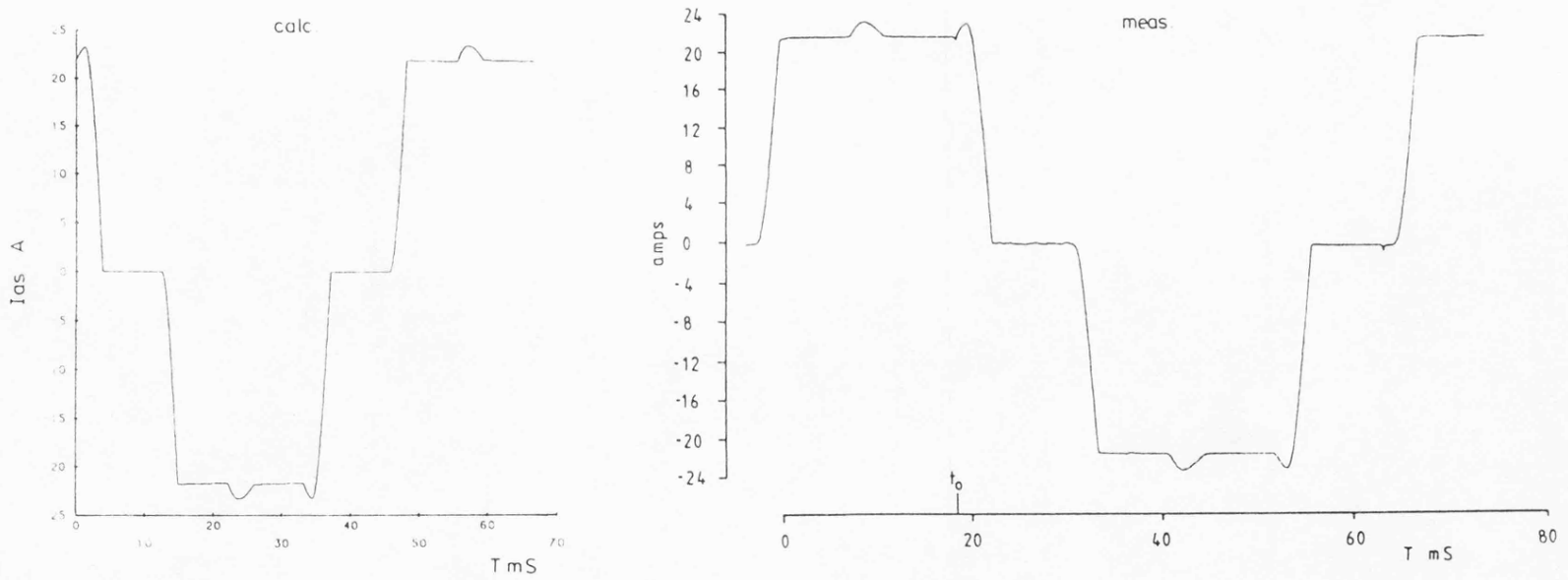

Fig 5.6 a) phase 'a' current, Ias freq = 15 Hz Vs = 71 volts $\sigma = 0{\cdot}775$ (101 rpm)

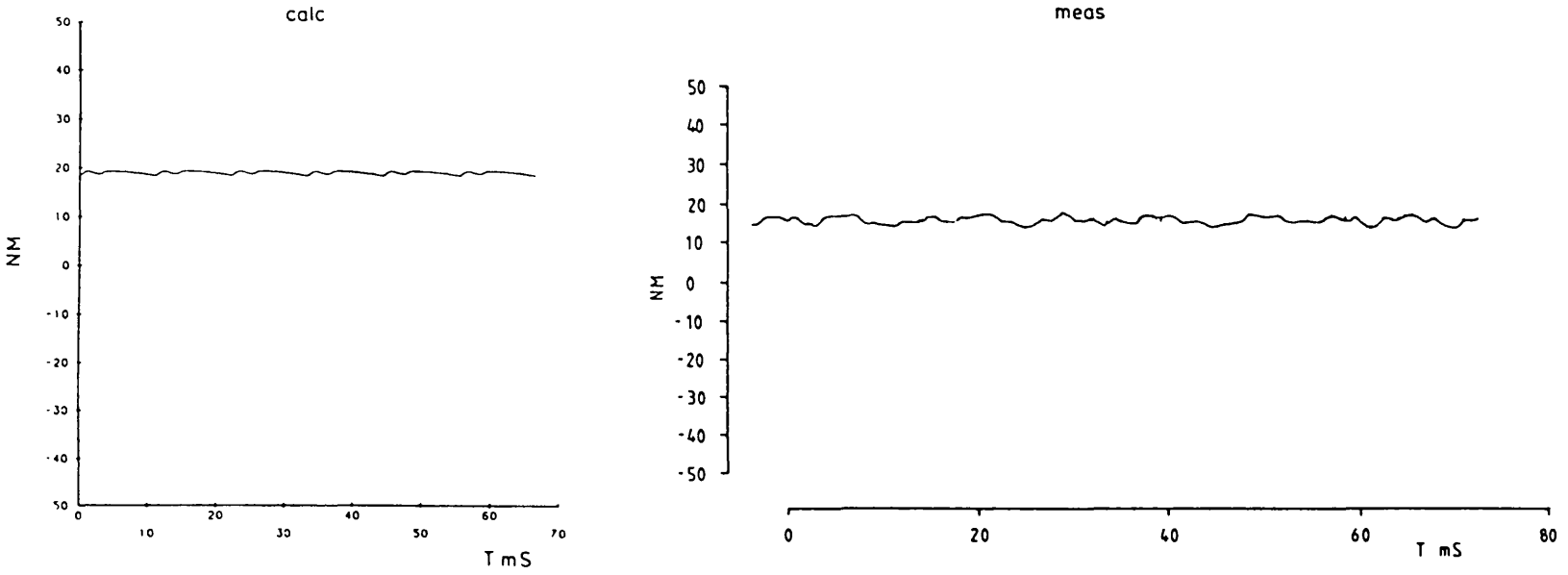
calc
meas
NM
T mS
50
40
30
20
10
0
-10
-20
-30
-40
-50
0
10
20
30
40
50
60
70
80

b) torque

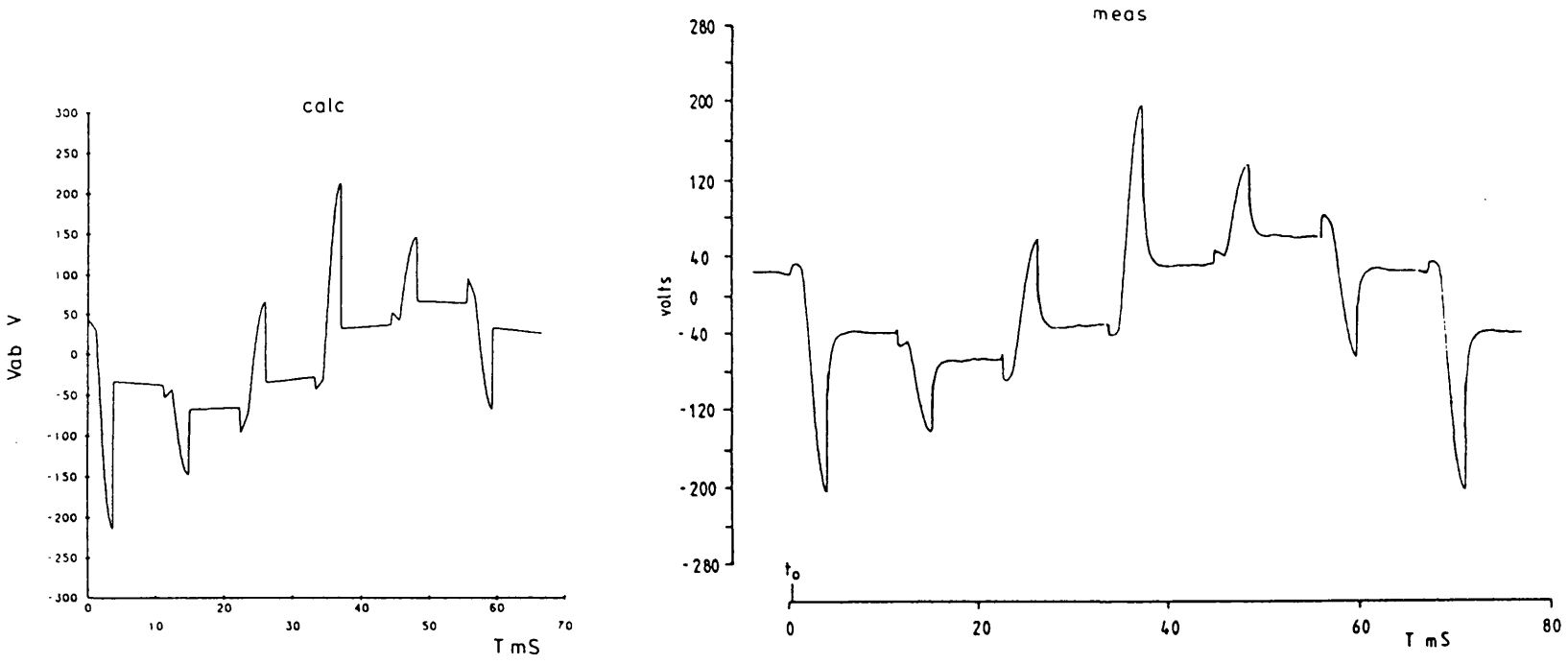

c) motor l-l voltage Vab

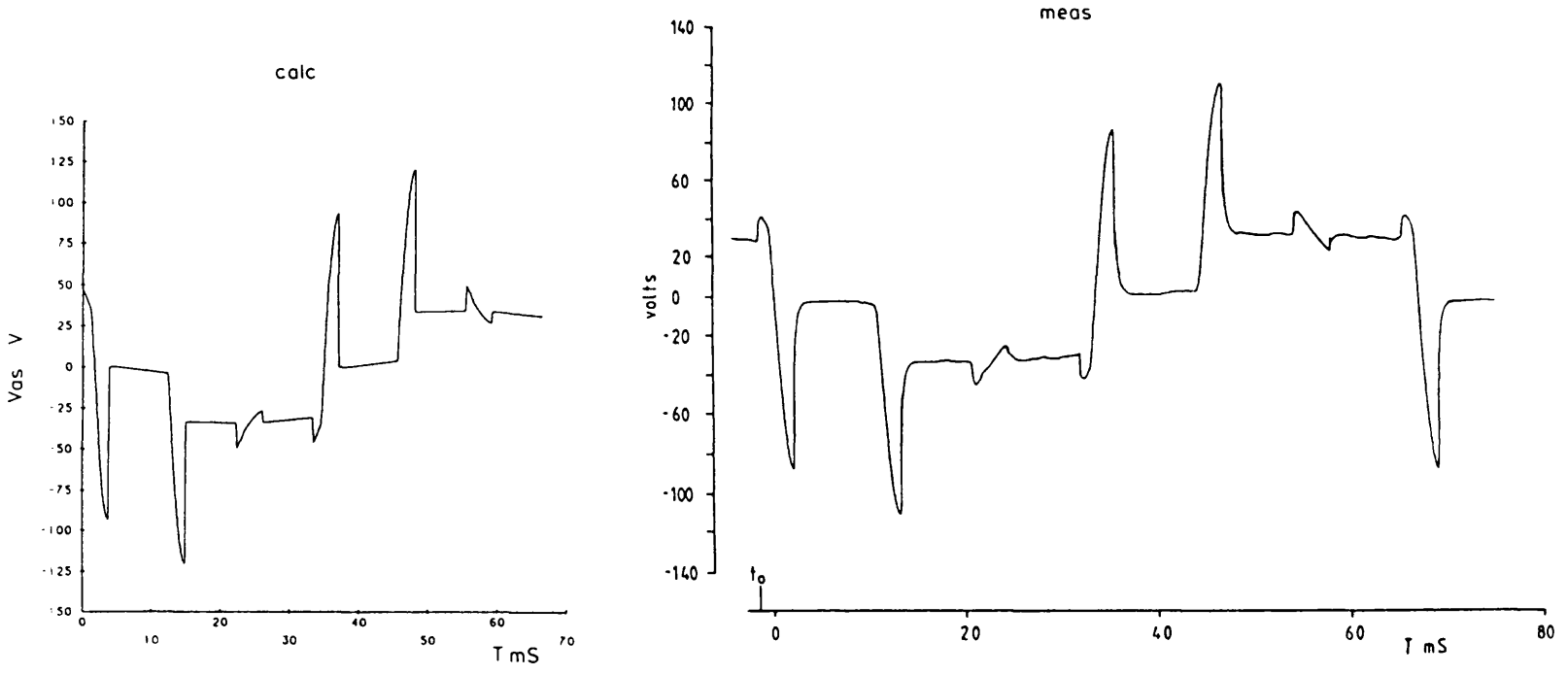

d) motor phase voltage Vas

currents, voltages and line to line voltages, the calculated values tending to be slightly higher, due to a probable inaccuracy in the value of motor leakage inductance used in the model.

Agreement between the magnitude and overall shape of the torque pulsations is good, although superimposed upon the waveform is a considerable amount of noise. The noise was generated by the DC machine, and because the force table and the load machine were rigidly mounted to the same supporting frame, was easily transmitted to the force transducers. Filtering of this vibrational noise was considered but because of its wide frequency spread, and the fact that the amplitude varied with motor speed, it proved difficult to provide a filter that would cope with these conditions. Also, as certain frequencies present within the noise tended to excite resonances within the induction motor - force table combination, which artificially increased the magnitude of the harmonics present within the torque waveform, it was difficult to remove these frequencies and still preserve the basic waveform shape.

A comparison of the calculated and measured harmonic torques present in the machine output, is shown in Table 5.2. In view of the limitations mentioned above there is a reasonable agreement between the calculated and measured results.

Harmonic torque Nm (rms)						
	6th		12th		18th	
frequency	calc.	meas.	calc.	meas.	calc.	meas.
5	27.5	22.1	15.9	11.0	10.6	8.8
10	5.79	4.86	2.39	2.59	1.39	-
15	0.21	0.331	0.051	0.106	-	-

Table 5.2 Harmonic torques in output

Ideally the force table and induction machine should be mechanically isolated from the load machine, the only coupling then being via the flexible drive between the rotor shafts. This should provide a more acceptable torque signal.

5.3 APPENDICES

5.3.1 Details of test machine

STATOR

Number of poles	4
Number of slots	48
Conductors per slot	20
(copper 0.092" LEWMEX)	
Pole pitch	0.1798 M
Coil pitch	0.1498 M (10 slots)
Air gap diameter	0.229 M
Core length	0.1016 M
Slot pitch	0.01498 M
Air gap length	0.001 M
Conductor overhang(lohs)	0.035 M

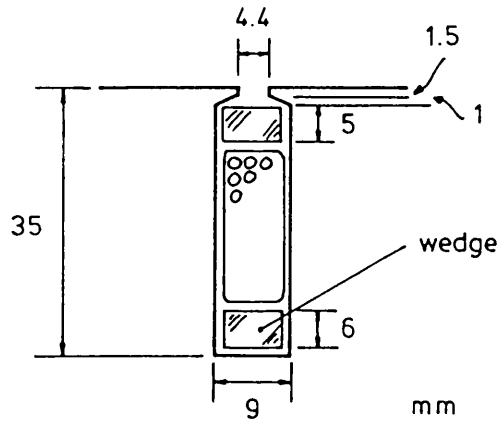

STATOR SLOT

ROTOR

Number of slots	37
Core length	0.105 M

End ring dimensions (brass)

Resistivity assumed approx.	0.75e-07 OhmM
Der	0.177 M
Aer	0.391E-03 M^2

Rotor bars located by wedging in end ring and securing with pegs

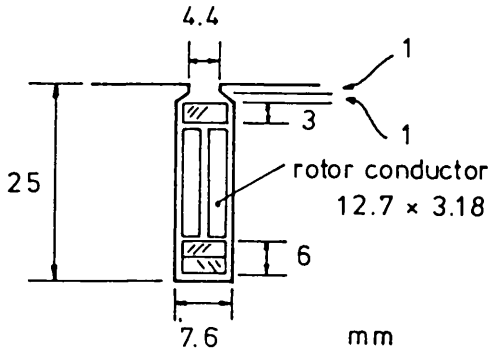

ROTOR SLOT

5.3.2 The current source inverter

The circuit diagram of the current source inverter used to obtain the experimental results described in this chapter is shown in Fig 4.9. The inverter was fed with a variable DC voltage supplied from a 3 phase variac and bridge rectifier via a series link inductor. The thyristors used in the inverter were International Rectifier type 81RK80 devices, and are rated at 125A rms, 800V. These are 'rectifier grade' thyristors, that is they have a relatively long turn off time compared to other devices available. The turn off time of these devices is typically 80 μS. The diodes used, are again I.R. type 25G80 and are rated at 95A rms.

A schematic diagram of the thyristor firing system is shown in Fig A5.1. The inverter thyristors are fired in the correct sequence by a shift register. The outputs of the shift register are turned into a burst of pulses by the firing pulse generators, Fig A5.2, and then amplified to a suitable level by the firing circuits, Fig A5.3. The firing circuits are isolated from the thyristors by transformer coupling.

To ensure reliable operation, multipulse firing is used in the pulse generators. The outputs of the shift register are used to gate 'on' an astable circuit, Fig A5.2. The main advantage of this type of circuit is that the first firing pulse occurs immediately on arrival of the gating signal. Schmitt NAND gates are used to provide a fast rising edge on the firing pulses. The firing pulses are then amplified by a Darlington pair, to drive a pulse transformer, Fig A5.3. To avoid damaging the thyristors the voltage , current and instantaneous power applied to the gate must fall within the limits specified by the manufacturer. The use of a 15 volt power

supply ensures the voltage constraint is met, whereas the current and hence the power is limited by R2. The diode D2 is a fast recovery diode and is provided to protect the gate from reverse bias, while R4 dissapates the firing pulses if the anode cathode junction is reversed biased. C1 and R5 constitute a snubber circuit to limit the voltage transients which occur during switching.

Prior to starting the inverter it is neccesary to set up the initial conditions both within the shift register and the inverter commutation paths. An external set switch is used to set up the logic pattern at the outputs of the shift register. When depressed, this enables the firing circuits for thyristors T1 and T2. Due to the time constant of the load there is insufficient time for the current in the inverter legs to reach the holding level of the thyristor before the end of the gate pulse. To overcome this problem a divert resistor is placed around thyristors T1 and T2 to establish the motor current. Once this has been achieved the resistors are able to be switched out, leaving the thyristors to take over the current path. The inverter is now ready to run. The shift register clock signal has to run at six times the desired inverter operating frequency, ie one puise for one thyristor commutation. No external methods are required to set up the required charge distribution on the commutation capacitors, as this is done automatically when current is established in the motor windings via thyristors T1 and T2.

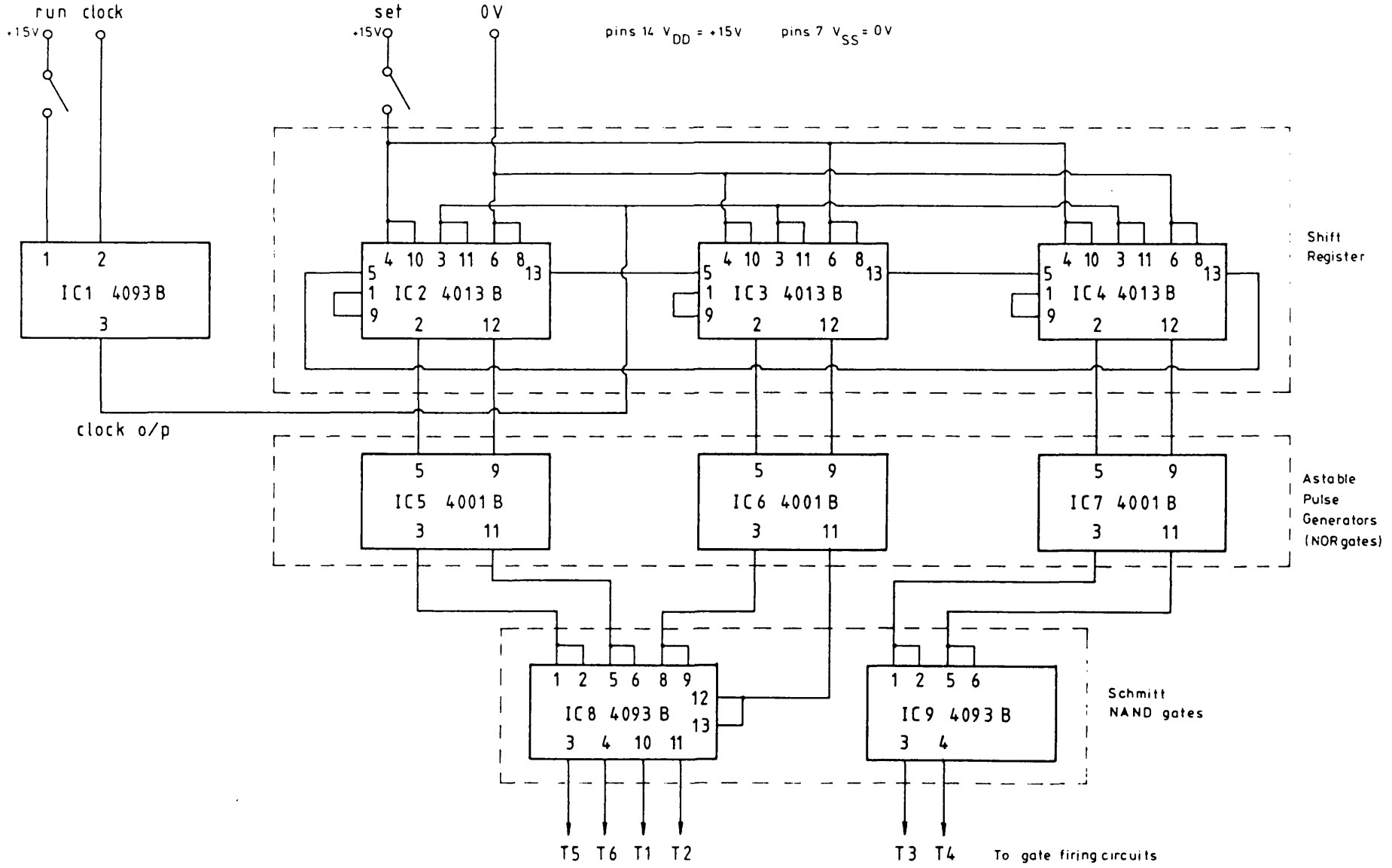

Fig A5.1 Thyristor firing scheme

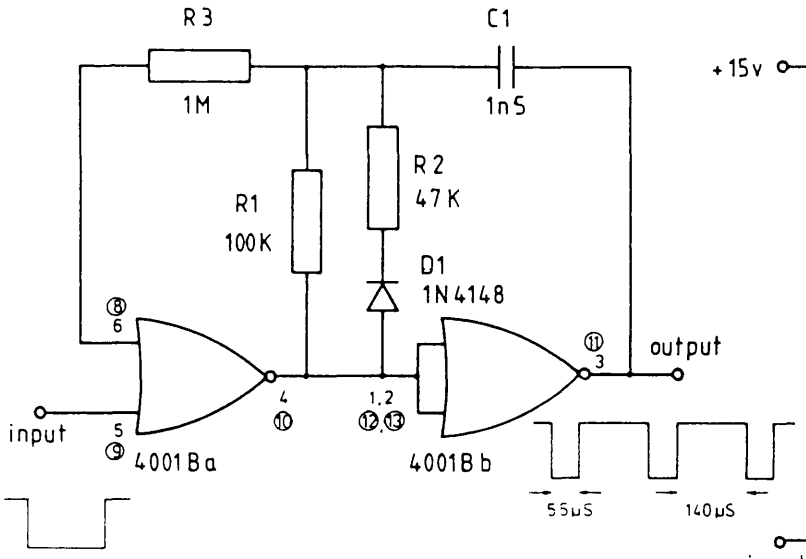

Fig A5.2 Astable pulse generator

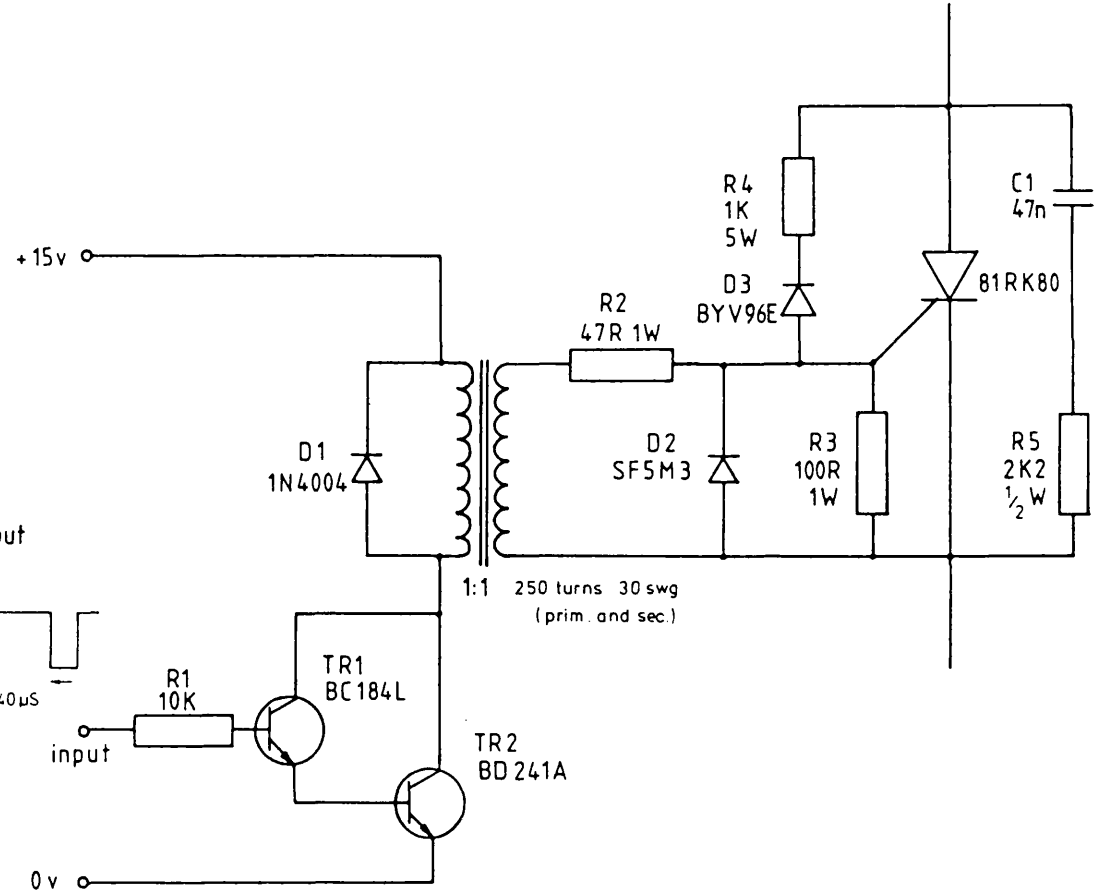

Fig A5.3 Gate firing circuit

CHAPTER 6

SUMMARY

It has been shown that even with a modest value of RMS current density, it is possible to design an induction or synchronous machine well within the weight specification of 1600 kg and of a size that will fit between the wheelset of a high speed locomotive. Of the three machine types studied on induction or salient pole synchronous machine operating under a 'rising voltage' control scheme, seems to be the most attractive, from a weight point of view, in this particular high speed traction application. The 'rising voltage' control scheme produces lighter designs but does incur the penalty of requiring a higher supply capacity. This point will have to be borne in mind when the overall economic and space requirements are considered.

The most suitable induction and synchronous machines are similar both in physical size and performance, and require supplies of a similar capacity. However, because of the large air gap, the salient pole synchronous machine is approximately 25% lighter than the induction machine. The synchronous machine does have the disadvantage of requiring slip rings and a separate field supply, but these difficulties should not discount its use for traction purposes, in view of the reduced track loading that would result from being lighter.

If a heat transfer study of these two machines were to be undertaken, and it proves that the use of higher current densities are feasible, a further reduction in machine weight would be possible.

Computer models have been presented for a voltage and current source inverter operating in the 120 degree conduction mode. An exact model of the current source inverter has been developed in which the effect of the DC link inductance is taken into account by considering the inverter to be fed from an ideal voltage source and setting up the inverter-machine equations accordingly.

An induction machine model has also been presented in which the rotor variables have been transformed to the stator. This type of machine representation has certain advantages when used to model inverter-machine systems. This is because, as the actual three phase voltages and currents are used, the charges of state within the inverter are easily observed. Also, as the stator and rotor currents are at the same frequency, the time taken to evaluate a steady state solution is reduced.

The inverter-machine models are used to predict the performance of the most suitable induction and salient pole traction designs. Voltage and current waveforms are shown, which allow the size of the inverter components to be accurately determined, and any areas of voltage stress to be identified. Torque waveforms are also predicted. These predictions make it possible to investigate the effect of harmonic torques on the power transmission system, and identify any source of mechanical resonance that they may induce.

Measured results are presented for a current source inverter fed laboratory induction machine. The agreement between the measured and predicted waveforms including torque pulsations is thought to be acceptable enough to verify the computer model.

CHAPTER 7

REFERENCES

[1] Saunders R M
'Digital computers as an aid in electrical machine design' Trans. AIEE 1954 Vol 73 Pt 1 pp189-192

[2] Veinott C G
'Induction machinery design being revolutionised by digital computer' Trans AIEE 1957 Vol 75 Pt 111 pp1509-1517

[3] Veinott C G
'Synthesis of induction motor designs on a digital computer' Trans AIEE 1960 Vol 79 Pt 111 pp12-18

[4] Anantha Pai M . Saunders R M
'Synchronous machine design using a digital computer' Trans AIEE April 1959 Vol 78 Pt 111 pp28-34

[5] Reece A B J . Chalmers B J
'The application of a digital computer to the design of induction motors ' Symposium at Queen Mary College . London 1958

[6] Herzog G W . Scimgeour J . Andersen O W and Chow W S
'The application of digital computers to rotating machine design' Trans AIEE Oct 1959 pp814-820

[7] Williams S B . Abetti P A . Magnusson E F
'Application of digital computers to transformer design' Trans AIEE Aug 1956 Vol 75 Pt 11 pp728-735

[8] Sharpley W A . Oldfield J V
'The digital computer applied to the design of large power transformers' Proc IEE 1958 105A pp112-121

[9] Middendorf W H
'An approach to induction motor synthesis' Trans AIEE April 1962 Vol 81 Pt 111 pp64-69

[10] Chalmers B J . Bennington B J
'Digital computer program for design synthesis of large squirrel-cage induction motors' Proc IEE Feb 1967 Vol 114 No 2

[11] Godwin G L
'Optimum machine design by digital computer ' Trans AIEE Aug 1959 Vol 78 Pt 111A pp478-488

[12] Erlicki M S and Appelbaum J
'Optimised parameter analysis of an induction machine' Trans AIEE Nov 1965 PAS 84 nos 11 pp1017-1024

[13] Rawle D L
'Recent developments in traction machines ' GEC Journal of Science and Technology 1977 Vol 43 Nos 3 pp99-106

[14] Siddall R B
'Development of an experimental inverter-induction motor drive for railway traction use ' IEE Conference Pub 179 .Electrical Variable-Speed Drives 1979 pp93-97

[15] Kielgas H . Nill R
'Converter propulsion systems with three phase induction motors for electric traction vehicles' Trans IEEE IA-16 No2 March/April 1980 pp222-233

[16] Brenneisen J . Futterlieb E . Muller E . Shultz M
'A new concept drive system for a diesel electric locomotive with asynchronous traction motors' Trans IEEE July/Aug Vol IA-9 Nos4

pp482-491 1973

[17] Barwell F T
'Traction Research' , Journal of the Institution of Locomotive Engineers Vol 56 (part2) 1966-67 pp158-195

[18] Stokes R W
'Three phase traction : problems and prospects' RGI November 1976 Vol 132 pp418-422

[19] Roffler M
'Class Am 6/6 and Class Ee 6/6 diesel and convertor locomotives of the Swiss Federal Railways' Brown Boveri Rev 12 1977

[20] Schaer R, Schmid A and Seger T
'Articulated Trams '2000 series' with three phase drive of the Zurich Municipal Transport Authority' Brown Boveri Rev 12 1983

[21] Ward E E , Kazi A and Farkas R
'Time - domain analysis of the inverter fed induction motor ' Proc IEE Vol 114 Nos 3 March 1967 pp361-369

[22] Charlton W
'Analytical methods for inverter fed induction motors' Proc IEE 1975 122(11) pp1273-1274

[23] Novotny D W
'Steady state performance of inverter fed induction machines by means of time domain complex variables' Trans IEEE PAS-95 1976 pp927-935

[24] Lipo T A and Turnbull F G
'Analysis and comparison of two types of square wave inverter drives ' IEEE Trans IAS Vol IA-11 Nos 2 March/April 1975 pp137-147

[25] Al-Nimma , Williams S
'Modelling a variable frequency induction motor drive' Proc IEE EPA Aug 1979 Vol 2 Nos 4 pp132-134

[26] Lockwood M
'Simulation of inverter / induction - machine system including discontinuous phase currents ' Proc IEE Nov 1978 EPA Vol 1 Nos 4 pp105-114

[27] Ward E E
'Inverter suitable for operation over a wide range of frequency' Proc IEE Vol 111 Aug 1964 nos 8 pp1423-1434

[28] Phillips K P
'Current Source converter for ac motor drives' IEEE Trans IA-8 Nov/Dec 1972 pp679-683

[29] Lipo T A, Cornell E P
'State variable steady state analysis of a current controlled induction motor drive ' IEEE IAS 1974 Annual Meeting Conf Record

[30] Slemon G R ,Dewan S B , Wilson J W A
'Synchronous motor drive with current source inverter ' Trans IEEE Vol IA-10 Nos 3 May/June 1974 pp412-416

[31] Farrer W, Miskin J D
'Quasi sine wave fully regenerative inverter ' Proc IEE Vol 120 Nos 9 Sept 1973 pp969-973

[32] Schwartz B
'Geometrical approach to the economical design of rotating electrical machines' Proc IEE Vol 113 Nos 3 March 1966 pp493-499

[33] Alger P L
'The nature of polyphase induction machines ' Wiley New York 1951

[34] Liwschitz - Garik M M , Whipple C C
'Alternating current machines' Von Nostrad ,New York 1961

[35] Say M G
'Alternating current machines ' Pitman 1976

[36] Lightband D A , Bicknell D A
'Direct current traction motor ' Business Books Ltd , London 1970

[37] Stanley H C
'An analysis of the induction machine' Trans AIEE vol 57 1938 pp751-757

[38] Asish K De Sarkar and Gunnar J Berg
'Digital simulation of three phase induction motors' Trans IEEE PAS Vol 89 Nos 6 July/Aug 1970 pp1031-1037

[39] Lipo T A , Krause P C and Jordan H E
'Harmonic torque and speed pulsations in a rectifier inverter induction motor drive ' Trans IEEE PAS-88 May 1969 pp579-587

[40] Adkins B , Harley R G
'The general theory of alternating current machines' Chapman and Hall 1975

[41] Gerald , Curtis F
'Applied numerical analysis Second Edition ' Addison - Wesley Pub Co May 1980

[42] Lienau W
'Torque oscillations in traction drives with current fed asynchronous machines' IEE Electrical Variable Speed Drives Conf 179 1979 pp102-107

[43] Tung hai Chin , Hideo Tomita
'The principles of eliminating pulsating torque in current source inverter induction motor systems' Trans IEEE IA-17 Nos2 March/April 1981 pp160-166

[44] Boocock D , King B L
'The development of the advanced passenger train' Proc Inst Mech Engrs 1982 Vol 196 Nos 6 pp35-45